BASE-CATALYZED DEPOLYMERIZATION OF LIGNIN AND HYDRODEOXYGENATION OF LIGNIN MODEL COMPOUNDS FOR ALTERNATIVE FUEL PRODUCTION

A Dissertation
Presented to
The Academic Faculty

by

Mariefel Valenzuela Olarte

In Partial Fulfillment
of the Requirements for the Degree
Doctor of Philosophy in the
School of Chemical & Biomolecular Engineering

Georgia Institute of Technology

May 2011

BASE-CATALYZED DEPOLYMERIZATION OF LIGNIN AND THE HYDRODEOXYGENATION OF LIGNIN MODEL COMPOUNDS FOR ALTERNATIVE FUEL PRODUCTION

Approved by:

Prof. Christopher W. Jones, Advisor
School of Chemical & Biomolecular Engineering
Georgia Institute of Technology

Prof. Pradeep K. Agrawal, Advisor
School of Chemical & Biomolecular Engineering
Georgia Institute of Technology

Prof. Sujit Banerjee
School of Chemical & Biomolecular Engineering
Georgia Institute of Technology

Prof. Charles Liotta
School of Chemical & Biomolecular Engineering
Georgia Institute of Technology

Prof. Arthur Ragauskas
School of Chemistry & Biochemistry
Georgia Institute of Technology

Date Approved: March 17, 2011

To my husband Ryan,
always

ACKNOWLEDGEMENTS

PhD was a very rewarding, though a very challenging time for me. There were many individuals throughout the years of my PhD research and study at GaTech that I am indebted to and without whom this endeavor will not be possible. First and foremost, my gratitude goes to my advisers, Prof. Pradeep K. Agrawal and Prof. Chris W. Jones. For their invaluable insights during discussions of the research, their patient mentoring and support as I navigated the nuances of being a researcher and surviving the challenges of the PhD process. They were both very generous with their time, expertise, encouragement and support. Next, I would like to thank my committee members, Prof. Sujit Banerjee, Prof. Charles Liotta and Prof. Art Ragauskas, who agreed to read and give comments on my dissertation and probe my knowledge of the subject matters involved in the research. Their comments and suggestions were very helpful in refining the dissertation. My gratitude also goes to Chevron Corporation for sponsoring the research and for Dr. Steve Miller for his helpful insights. I would also like to thank all the members of the Jones group who I had the chance to interact with throughout the years, especially to the original Chevron group: Teresita, Carsten, Henry and Travis. The times of brainstorming and discussions as well as overcoming the difficulties we faced individually and as a team, especially during the first year of the project, taught me the values of friendship and teamwork. Special thanks also go to the following individuals: Do-young for building the flow reactor system, his patient instruction on its complexities and for the company in Bunger-Henry at weird times of the night; Megan and Wei for running the TEM and XPS of my samples; and, Weiyin for shared experiences (fun) with

running continuous flow reactors. My thanks also go to the faculty of ChBE who became instructors, sharing their knowledge and passion for their respective fields. To the admin and facilities staff of both ES&T and Bunger Henry buildings, especially Gloria, Juanita, Kevin and Rod, who had made life a little bit easier. There were also special individuals to whom I am very much indebted. They were the ones who helped me in more ways than one during a personal tragedy, most remaining unnamed, and through their support and kindness, I was able to find inspiration and strength. I also want to thank my surrogate families and friends here in the US who had endeavored to give sound advices and a healthy dose of encouragement: to my best friends Yeny, Dewi and Gracy; Tito Lino and Tita Nene and family; the GT Catholic Center community led by Fr. Mario di Lella and Fr. Tim Hepburn; the CFC and CFC-SFC family. And through it all, I thank my families in the Philippines, Bayta-Valenzuela and Velasco-Olarte, who were always there through thick and thin – they will always be a constant source of love and inspiration and strength. Lastly to God, who is the source of all good things, to You be the glory.

To all of you who had made this endeavor possible: who lent a listening ear and gave sound advice, who gave moral support in times of stress and comfort in times of distress, who dished out sharp reminders (like shots of a stiff drink) and generously gave pearls of wisdom when the moment called for them, who provided intellectual stimulation and interesting insights, who shared the wow! yeah! and argh! times of this very challenging journey and who ultimately became instrumental to my holistic growth as a person throughout the years, I give you my deepest gratitude.

TABLE OF CONTENTS

LIST OF TABLES

LIST OF FIGURES

SUMMARY

The depleting amount of fossil fuel resources throughout the world has encouraged countries to expend research on alternative fuels. Biomass is considered as one of the most promising sources of alternative liquid fuels as well as of renewable chemical feedstock. The challenge lies in depolymerizing this very complex heterogeneous macropolymer and then upgrading the fragments into compounds that approximate crude oil properties. This characteristic would enable biomass-derived liquids to be compatible with the existing petroleum infrastructure.

This study considered the potential use of lignin as possible renewable fuel and chemical feedstock source. Among the various polymers present in lignocellulosic biomass, the polyaromatic lignin is the one component that is most chemically similar to petroleum. However, it still contains a much larger amount of oxygen compared to crude oil. As such, two strategies were employed in this study: (1) studying the lignin depolymerization in the presence of high temperature and base catalysts; and, (2) employing hydrodeoxygenation as a means to decrease the O/C ratio in lignin-derived model compounds. The results generated by this study can be divided into three parts: (a) the base-catalyzed depolymerization of organosolv lignin; (b) batch hydrodeoxygenation of syringaldehyde in the presence of bulk and supported nickel phosphide; and, (c) continuous flow hydrodeoxygenation/hydrogenation of phenol utilizing the bifunctional catalyst system of metal-acid active sites.

The base-catalyzed depolymerization of organosolv lignin was done in a 500-mL Monel Parr reactor at temperatures ranging from 165°C to 350°C. Water was used as a solvent while the base catalysts tested included NaOH, KOH and NH_4OH. Analyses by ^{13}C NMR, elemental analysis, gel permeation chromatography and GC analysis of dichloromethane solubles were done. Complete solubilization of lignin derivatives was possible in the presence of NaOH and KOH, except at 350°C. Identified and quantified DCM-soluble monomeric compounds were at most 6% of the starting material and included phenol, syrngaldehdye, catechols and guaiacols. NMR experiments revealed formation of carboxylic and alcoholic groups in these samples. On the other hand, the use of NH_4OH showed N incorporation. An interesting finding of this part of the study revealed the apparent susceptibility of syringyl units over guaiacyl units. This could in turn guide the choice of substrate on which base-catalyzed depolymerization could be applied.

Syringaldehyde was used as the starting material in the batch hydrodeoxygenation (HDO) part of this research. A 50-ml Parr reactor was used, pressurized by 1000 psig of H_2 and heated to 300°C. Nickel based catalysts (nickel phosphide, nickel oxide and nickel phosphate) as well as precious metals (Pt and Pd) were tested as HDO catalysts. Of the three O-containing functional groups of syringaldehyde, the aldehydic group was found to be the most susceptible. Additionally, the C-O bond in the methoxy substituents was seen to be labile at longer reaction times. These two reactions occur even in the presence of the bulk catalysts. In the presence of the Al_2O_3-supported catalysts, the methyl groups liberated were found to be incorporated back into the aromatic ring, forming alkylated compounds. Supported $Ni_{12}P_5/Al_2O_3$ showed preference over Pt/Al_2O_3 and Pd/Al_2O_3 for

the presence of these compounds in the product mixture. The average TOF for syringaldehyde conversion by $Ni_{12}P_5/Al_2O_3$ was higher compared to the supported noble metal catalysts though kinetic studies at lower conversions are necessary for direct activity comparisons between these catalysts.

In the last section of this dissertation, hydrothermally synthesized supported Ni on mesoporous silica (MCF) and acid catalysts (HY and H-Al-MCF) were used for probing the effect of bifunctional metal-acid catalysis on phenol hydrodeoxygenation/hydrogenation. Catalyst configurations were varied from the previously studied wet-impregnated Pt/HY catalyst. Based on a hypothesis that coking catalyzed by the acidic zeolite in the wet impregnated Pt/HY catalyst was the main cause of catalyst deactivation and decreased phenol conversion, separately synthesized metal and acid catalyst systems were tested. Complete phenol conversion was sustained for at least three times longer in a continuous flow reactor operated at 200°C and 0.79 MPa of flowing H_2. The separation of the metal and acid sites generated a tunable system capable of producing cyclohexanol, cyclohexane or cyclohexene at very high selectivities, even achieving 99% selectivities for cyclohexane.

CHAPTER 1

INTRODUCTION

1.1 Motivation

1.1.1 World petroleum demand and supply

Energy garnered the number one spot in the "Top Ten Problems of Humanity in the Next 50 Years", according to a list by 1996 Noble Prize winner Richard E. Smalley [1]. In a lecture given in 2003, he opined that having abundant energy may solve several of the foreseen water issue problems (second on the list) but the reverse is not necessarily true [1]. The main consideration in the energy problem is the depletion of petroleum. In the latest survey from the IEA, petroleum still occupied almost a third of all the world's energy resources [2]. Figure 1.1 shows that non-renewable sources comprised 81.3% of the world energy consumption in 2008 (oil 33.2%; coal and peat 27.0%; gas 21.1%). The oil fraction has been relatively reduced compared to 46.1% in 1976 [2]. However, the actual value increased from 2,819 million tons in 1973 to 4 073 million tons in 2008. This translates to an average increase of about 1.1% per year.

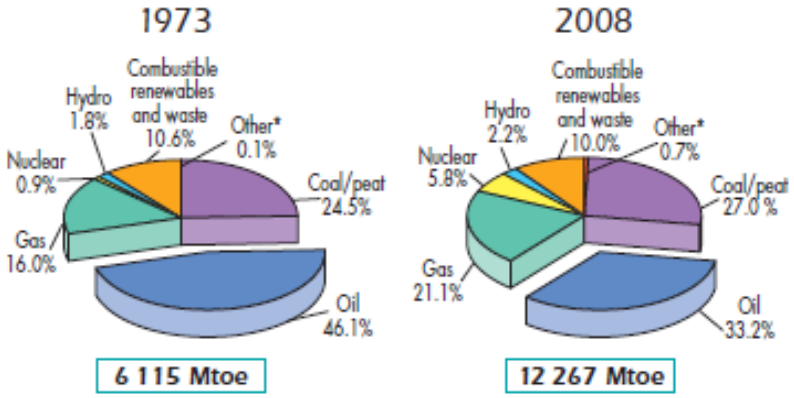

Figure 1.1 Total world consumption of primary energy in 1973 and 2008 [2]

On the other hand, the world supply of petroleum is considered depleting. Figure 1.2 summarizes the charted world oil consumption and discoveries from 1900 to 2007.

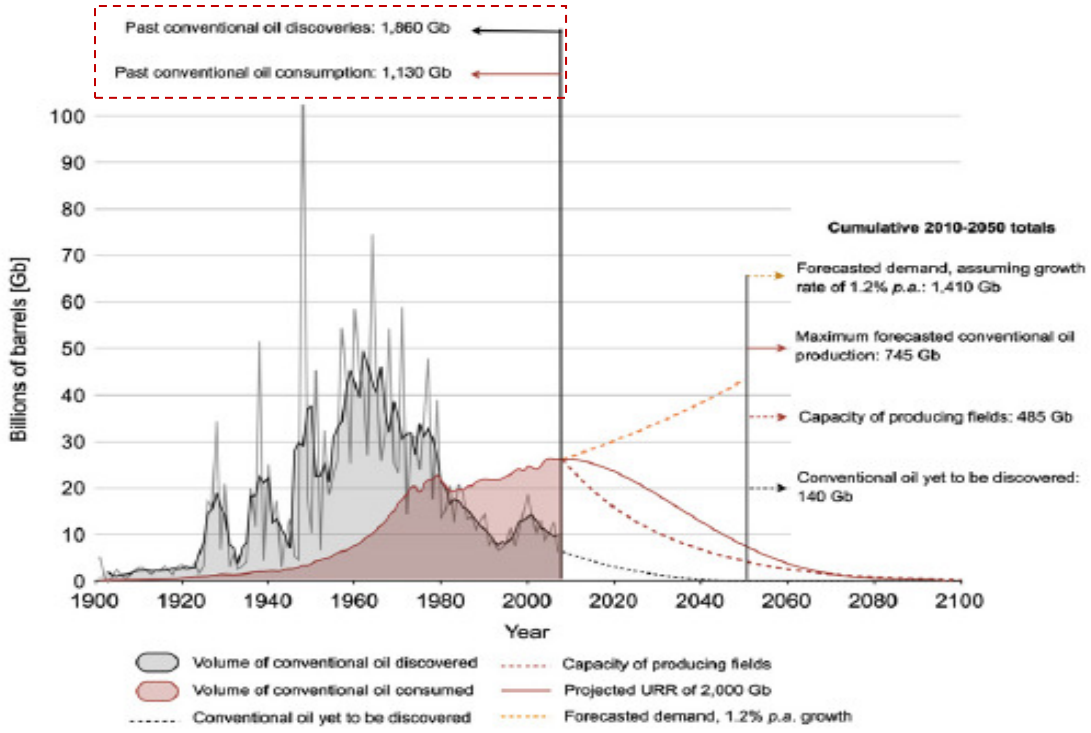

Figure 1.2 Annual proven+probable reserves (2P), backdated oil consumption, discoveries, forecasted consumption and forecasted production till 2100 [3]

It can be observed that the volume of discovered oil peaked around 1957. The authors noted that the past consumed volume of oil was about 61% of what had been previously discovered. However, from their model, assuming that world demand for oil would increase at an average of 1.2% per year, a time will come when the capacity of the producing fields plus the volume of oil that could still be discovered will be overtaken by the forecasted demand [3].

In view of this, it is thus imperative that alternative sources to crude oil be developed. This is reflected by the current trend in government policies all over the

world. These alternative resources should be renewable, readily available and would not contribute to the overall degradation of the environment – in a word, sustainable. Though the world coal reserves are much higher compared to petroleum [2, 4] and comprise the second most consumed fossil fuel next to petroleum, improvement in current technologies is required to make it sustainable [5-6]. Other resources that are currently being developed as alternatives include solar, nuclear, geothermal, wind and biomass.

1.1.2 US petroleum outlook and policies

From 2008 data, the United States was the world's largest net importer of crude oil [2]. This places the country in a susceptible position to changes in foreign oil trade, which impacts directly on fuel and commodity prices as well as the country's energy security[7]. Though the US is capable of producing oil, this has never been enough to satisfy internal demands. In the 1950s, M. Hubbert predicted that the US oil supply would start diminishing in the next 50 years [8-9]. He proposed a model which was reflective of the overall actual crude oil production in the US (Figure 1.3) [4]. The peak of highest production was achieved in 1972. Crude oil well productivity had been steadily decreasing since the late 1970s until it logged an increase in 2009. This may be attributed to expanded infrastructure and further investment in exploration and drilling.

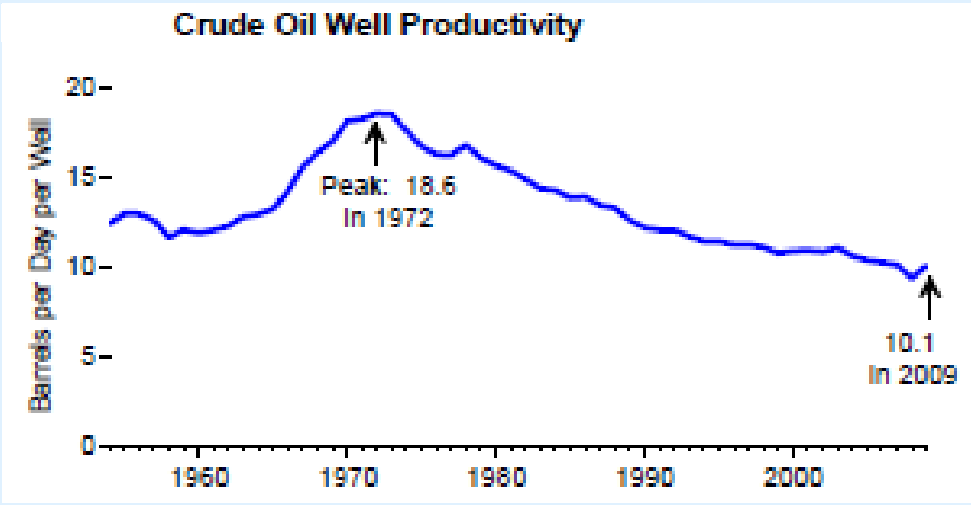

Figure 1.3 Crude oil well productivity in the US, 1949-2009 [4]

In 2007, the US General Accountabilities Office published a report which focused on the need to have a strategy to address the peaking of world oil production and subsequent sharp reduction in crude oil production, especially in terms of its immediate effect on the transportation sector [10]. Aside from enumerating strategies that directly enhance current oil production such as enhanced oil recovery, sourcing from deepwater and production from non-conventional sources such as oil shales, the report also evaluated the current state and possible mitigation effects of seven alternative fuel and advanced vehicle technologies such as corn ethanol, biomass gas-to-liquid, coal-gas-to-liquid and hydrogen-fuel-cell technologies. They noted that these technologies still require much development, both in technology and infrastructure, in order to absorb the effect of a petroleum shortage. The report pointed out the lack of a coordinated governmental strategy to address the impact of oil production peaking. It suggested several actions to minimize the uncertainty of when the production peak will occur as well as pointing out cost-effective areas where the government may assist the private sector in the development and adoption of alternative technologies.

In the same year, the Congress enacted the Energy Independence and Security Act of 2007 (EISA), the main reason for which was to reduce the US' dependence on foreign oil reserves [11]. It included four key provisions and one of them is the "Renewable Fuels Standard" that set a modified standard aiming to utilize 36 billion gallons of biofuels by 2022 in all US transportation fuels. This is equivalent to about 13.6 billion gallons of petroleum-based gasoline and diesel fuel [7]. At that time, 21 billion gallons were required to come from cellulosic ethanol and other advanced biofuels (vs. corn-based fuel) [12]. As such, the use of biofuels as an alternative to petroleum-based fuels is mandated by the US government as a means to further alleviate the country's dependence on foreign oil imports. In February 2010, the US Environmental Protection Agency (EPA) finalized the regulations relating to the National Renewable Fuel Standard Program for the year 2010 and onwards [7]. The EPA set volume standards for the first time for specific types of renewable biofuels including cellulosic, biomass-based diesel and total advanced biofuels.

1.1.3 Biomass as alternative fuel

Biomass has long been harnessed as an energy resource in the world. Wood has been harvested both in small and large quantities for energy generation through burning/combustion [13]. In the process, it has also been used as a chemical feedstock source, e.g. through wood distillation [14]. Biomass was a main source of fuel until the advent of fossil fuels.

Fuels from biomass have been divided into first-generation, second-generation and advanced biofuels [15]. First-generation biomass comprise of liquid biofuels sourced from starch, sugar and oil. The main agricultural crops associated with first-generation

biofuels are corn, sugarcane, soybean, oil palm and rapeseed [16]. Ethanol from corn is one of the most well-known of the first generation biofuels. Though first-generation technologies are the most mature ones currently, they have been deemed unsustainable mainly due to their direct competition with food use which causes the prices of these crops to increase as well as some ecological issues such as increased burden on water use [16].

Second-generation biomass includes lignocellulosic plants, agricultural and forest residues and non-food energy crops (e.g. switchgrass) [17-18]. The International Energy Agency forecasts in *World Energy Outlook 2010* that these fuels, together with advanced biofuels, would enter the market in 2020 [19]. Though ecological issues still exist with their use and these still need to be addressed [20], the use of second-generation biomass does not directly compete with use of crops for food consumption. Sims et al. commented that since technologies utilizing second-generation biomass are still currently immature, there is "potential for cost reductions and increased production efficiency levels as more experience is gained" [18].Typical routes for harnessing these types of biomass fall into two categories: biochemical and thermochemical processes [21].

Advanced biofuels can be sourced from either first- or second-generation biomass provided that the final fuel results in significant reduction of in life-cycle greenhouse gas (GHG) emissions [15]. Because of its ability to harness CO_2 from the atmosphere, algae-based biofuels are expected to be classified under advanced biofuels [22].

Biomass is a renewable, readily available resource. Because of its ability to use the CO_2 in the air, its utilization was reported to give a net positive change in emissions compared to fossil fuels, some feedstock more so than others [18]. In 2005, Oak Ridge

National Laboratory (ORNL) reported the availability of about a billion-ton of biomass for use as biofuel in the US [23]. This included biomass (crops and residues) from both forest and agricultural lands.

1.1.4 Biomass as alternative chemical feedstock source

The world consumption of petroleum by sectors is shown in Figure 1.4. As was noted, it was mainly used for transportation fuels – the amount of which increased by about 1,131 Mtoe from 1973 to 2008. Albeit at a much lower percentage, petroleum is next consumed in non-energy uses. Non-energy use was defined as "those fuels that are now used as raw materials in the different sectors and are not consumed as a fuel or transformed into another fuel" [2]. Chemical feedstocks for production of polymers and other derived chemicals fall under this category. Considering our society's heavy dependence on these products, the search for alternative sources for non-energy use is also very important.

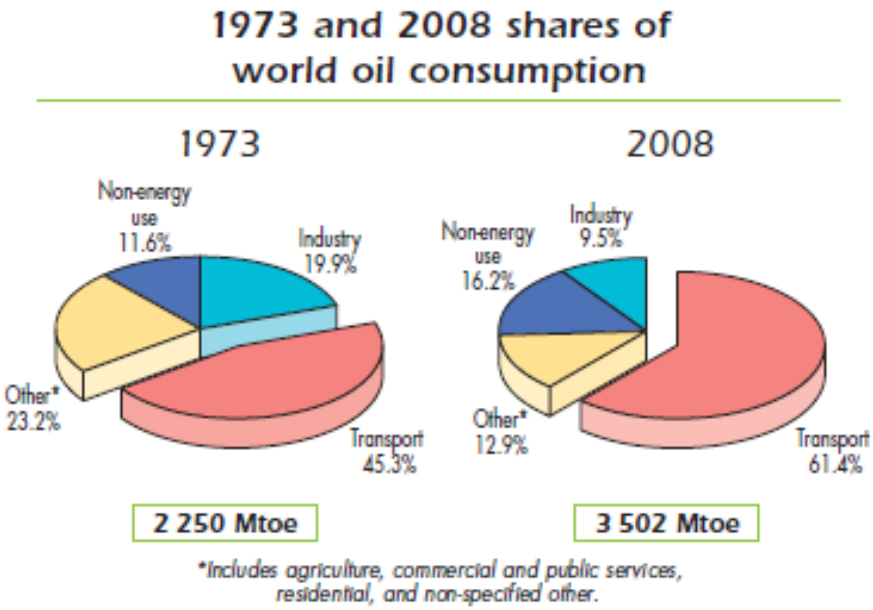

Figure 1.4 World total final oil consumption by sector, 1973 and 2008[1] [2]

Among all the possible sources of alternative energy, only biomass can be both a ready source of fuels and chemical feedstock. Through catalytic upgrading, high value products can be obtained from the products of biomass conversion [17, 24-25]. In 2004, the Pacific Northwest National Laboratory (PNNL) and National Renewable Energy Laboratory (NREL) published a list of top biomass value-added chemicals that can be generated from sugars as well as synthesis gas [26]. This was followed by a list of chemicals that can be sourced from lignin, including BTX (benzene, toluene and xylene) [27].

1.2 Lignocellulosic biomass

[1] These values only consider the "total final consumption" – i.e. the sum of consumption by the different end-use sectors, not including the backflows from the petrochemical industry . These were included in the calculations in Figure 1.1.

As previously mentioned, lignocellulosics are part of the second generation biomass currently being developed for biofuels. As the name implies, lignocellulosic biomass is composed of three major groups of polymers: cellulose, hemicelluloses, and lignin.

1.2.1 Cellulose and hemicellulose

Cellulose is a β-1→4 linked, linear chain of repeating units of cellobiose[2]. It comprises between 45-60% of biomass depending on the plant source [28]. It has both amorphous and crystalline constituents which affect its reactivity. Hemicelluloses, on the other hand, are polysaccharides that are amorphous in nature due to branching. Unlike cellulose, it is made up of different C5 and C6 sugars such as xylose, glucose, galactose, arabinose and mannose, linked together in different proportions depending on the type of plant it was sourced from. Figure 1.5 shows the representative structures of carbohydrates found in lignocellulosic biomass. Arabinoglucoronoxylans are the main hemicellulose groups from softwoods while galactoglucomannans are the majority of those found in softwoods [14].

[2] Cellobiose is composed of two glucose units that attached in a "staggered" fashion compared to the first unit.

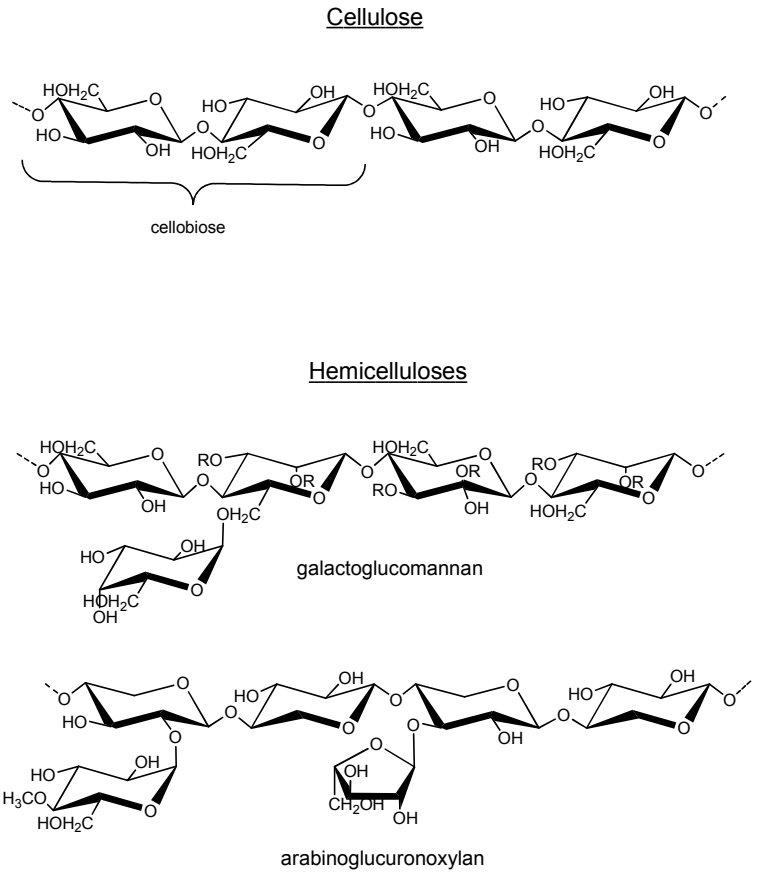

Figure 1. 5 Cellulose and hemicellulose structures

1.2.2 Lignin

The last of the macropolymers that make up lignocellulosic biomass is lignin, and it comprises 20-35% of biomass. Lignin has a vastly different chemical structure from the carbohydrates. It is amorphous and poly-aromatic in nature. At present, there is still no consensus as to what is its actual structure. One major hurdle is that its chemical make-up changes with the methods employed to extract it from the whole wood. Recently, Guerra, et al. [29-30] made some headway on lignin isolation protocols that they claimed were more representative of the native lignin structure. This process involved gentle milling and enzymatic treatment of the wood to extract the lignin.

A representative softwood structure is shown in Figure 1.6. Despite the ambiguity in its ultimate structure, it has been widely accepted that lignin resulted from the oxidative radical coupling of basic phenylpropanoid units (Figure 1.7) by the action of peroxidases and laccases in plants through the shikimic acid pathway [31-33]. Depending on the type of biomass, the proportions of these structures vary. Softwoods (gymnosperms) are mostly made up of coniferyl alcohol-derived constituents. On the other hand, hardwoods (angiosperms) would have a mixture of syringyl and coniferyl type structures. Grasses and other monocotyledons usually contain mainly p-coumaryl groups coupled with the other types [34]. The combinatorial-like coupling of monolignols gives rise to a vast and complicated network of inter-unit linkages, mainly of the C-C and C-O type. Figure 1.8 shows a general representation of the lignin monomer unit. Table 1.1 summarizes the types of linkages commonly found in lignin structures.

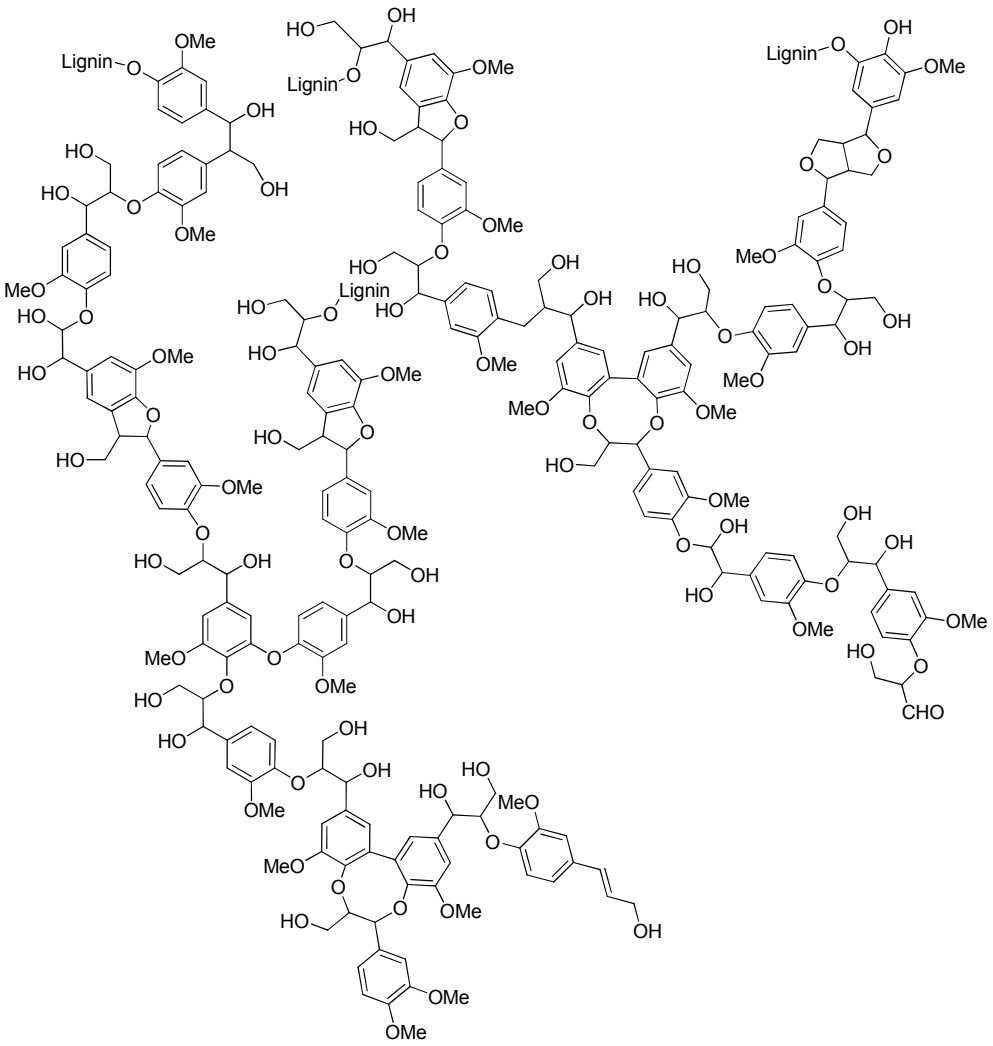

Figure 1.6 Proposed structure of lignin by Brunow, et al. [35]

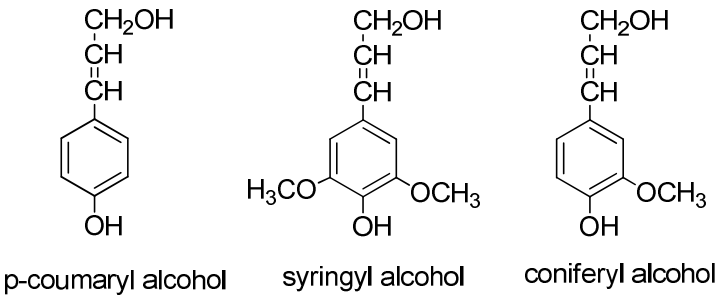

Figure 1.7 Lignin monomeric units

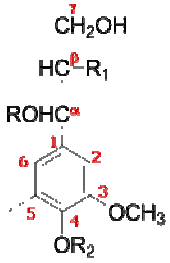

where R = H, alkyl, aryl, alkoxy or aryloxy

Figure 1.8 General formula for the phenylpropane unit

Table 1.1 Types and frequency of lignin inter-unit linkages in representative softwood and hardwood [36]

Linkages (per 100 C9-units)	**Softwood (spruce)**	**Hardwood (beech)**
β-O-4	49-51	65
α-O-4	6-8	--
β-5	9-15	6
β-1	2	15
5-5	9.5	2.3
4-O-5	3.5	1.5
β-β	3.5	1.5

Among the different biomass constituents, lignin has the structure most similar to petroleum. Indeed, fossil fuels are nothing but remains of ancient plants that have been acted upon by massive amounts of pressure and high temperature inside the earth. Considering their susceptibility to microbial degradation, typically it is the lignin constituent that gets left behind as ancient lignocellulosic remains [37]. Under these massive geologic processes, these remains become chemically transformed into what are being mined and drilled right now from the earth. The lowest form of coal is even called lignite, which is a brown, soft coal. This is in contrast to anthracite, the highest grade, which is hard-packed solid and black.

Since current biomass targeted for alternative fuels will not have the chance to be subjected to those tremendous geologic pressures and temperatures, the challenge lies in developing processes (thermal, chemical/catalytic, enzymatic or a combination of the three) that can convert them into molecules that have similar properties as crude oil. The important criteria that need to be met are summarized in the von Krevelen plot shown in Figure 1.9. These are the hydrogen-to-carbon (H/C) and oxygen-to-carbon (O/C) ratios. Crude oil has H/C ratio between about 1.60 and 2.10 and contains almost no oxygen at an O/C ratio between 0 and 0.03. On the other hand, wood, would typically have an O/C ratio higher than 0.61 and H/C higher than 1.4. As is obvious, oxygen removal is quite necessary. Additionally, it has been reported that the presence of oxygen-containing groups in bio-oils causes immiscibility with hydrocarbons, low heating values, increased liquid viscosities during storage, incomplete volatility and chemical instabilities, such as condensation and precipitation reactions [38-41].

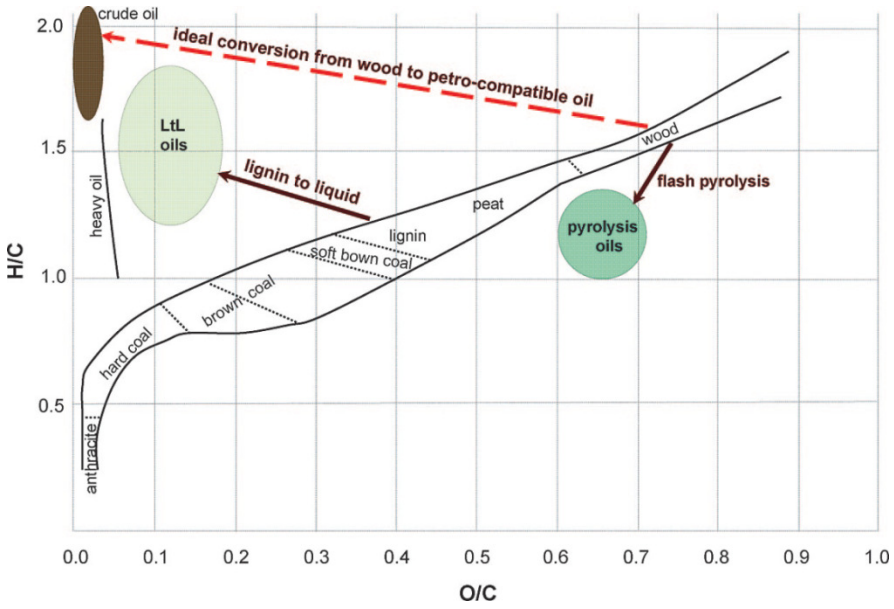

Figure 1.9 von Krevelen plot showing H/C and O/C of fossil fuels and different biomass-derived materials [42]

Lignin has a lower O/C ratio than wood at about $0.32 < O/C < 0.46$ and a lower H/C ratio between 1.1 and 1.3. It is quite an attractive starting material in that it already has lower oxygen content than the actual wood. During the removal of oxygen, hydrogen can be incorporated into the material (i.e. hydrodeoxygenation) thus creating a product that is more compatible with crude oil [43]. Recognizing this, it is suggested that deriving alternative fuels from the lignin fraction (rather than the carbohydrate fraction) of biomass maybe more attractive.

Utilization of biomass-derived materials would require some form of depolymerization or disintegration in order to access smaller fragments/compounds that are more amenable to subsequent processing. For lignin, depolymerization by thermo-chemical means would release monomeric aromatic compounds that can then be treated to produce chemicals compatible with existing petroleum-based fuels and chemicals [44]. Aside from the use as an alternative fuel source, lignin was also identified as an important chemical feedstock resource. In a report in 2007 published by Pacific Northwest National Laboratory (PNNL) [27] more than 15 chemicals and chemicals groups were identified to be possibly sourced from lignin. This includes hydrocarbons (BTX (benzene, toluene, xylenes), and cyclohexane), phenols, oxidized products (vanillin and quinones) and as macromolecules (carbon fibers and polymer fillers/extenders). The authors conclude that technologies still need to be developed in order to harness these chemicals from lignin in a more efficient manner.

1.3 Objectives and outline

The need for developing technologies to harness renewable resources to mitigate the effects of depleting worldwide petroleum resources, especially for the US, was discussed above. Biomass has been identified as a possible renewable alternative, both as a source of fuel and chemical feedstock. It is suggested that lignin be used as a feedstock considering that the carbohydrates have other present uses such as pulp for paper and ethanol feedstock while the lignin was typically considered as waste. Taking into account the polymeric nature of lignin, depolymerization is thus important. In this study, base-catalyzed depolymerization was applied to organosolv lignin. The second objective of this study was to catalytically upgrade lignin model compounds in order to lessen/remove the amount of oxygen present. This is important in order to produce feedstock that can be integrated into existing petroleum processing infrastructure. Different catalyst systems were evaluated in this study for their capacity in removing oxygen from these model compounds.

The outline of the thesis is as follows. Chapter 2 discusses the characterization of the starting material as well as the base-catalyzed depolymerization of organosolv lignin using NaOH, KOH and NH_4OH. The results of batch thermal treatments at temperatures higher than typical pulping conditions were analyzed using ^{13}C nuclear magnetic resonance (NMR) spectroscopy, quantification of extracted monomeric units using GC/FID and determining the effect of depolymerization using gel permeation chromatography (GPC).

In Chapter 3, the batch hydrodeoxygenation of syringaldehyde using nickel phosphides and other catalysts is described. Syringaldehyde was identified as a product in

the base-catalyzed depolymerization of lignin. It is an interesting lignin-derived model compound because it contains three oxygen-bearing functional groups, namely phenolic, aldehydic and methoxy groups. The action of the relatively novel, non-precious metal containing catalyst, nickel phosphide, was compared with supported commercial Pt- and Pd-based catalysts. Synthesis and characterization of nickel phosphide along with its catalytic performance are discussed in this chapter.

The hydrodeoxygenation of phenol, a ubiquitous lignin-derived compound, was studied using a continuous flow reactor in the presence of non-precious metal bi-functional catalyst systems. A previous study in the group had shown that supported noble metals on zeolitic supports were capable of producing deoxygenated products from an aqueous phenol feed. However, declining phenol conversion was shown to occur after some time on stream. Chapter 4 describes the efforts to modify this bifunctional catalyst system with a cheaper active metal. Variation in catalytic configurations also resulted in identifying more robust systems capable of fully converting phenol at longer time-on-streams. Specific compounds were formed at high selectivities (>90%).

Lastly, Chapter 5 summarizes the different learnings obtained from these studies. Recommendations for further studies are also enumerated.

CHAPTER 2

BASE-CATALYZED DEPOLYMERIZATION OF LIGNIN

In the previous chapter, the motivations behind using lignin as an alternative feedstock for fuel and chemical generation were given. This chapter deals with the base-catalyzed depolymerization of lignin. A background on the topic discussing key concepts and previous studies related to lignin depolymerization is given. The goals for this study are listed as well as the experiments and analyses done to accomplish them. A discussion of the results is loosely divided into two parts: (a) characterization of the starting lignin material, and (2) base-catalyzed depolymerization studies done on a commercially available organosolv lignin. Three bases were used in the study, namely NaOH, KOH and NH_4OH.

^{13}C NMR analyses of the products show the possibility of mechanisms similar to a combination of alkaline and oxidative reactions. This functional analysis by ^{13}C NMR was not reported in previous BCD studies. Analysis by gel permeation chromatography shows the fragmentation of the starting material though the actual amount of identifiable and quantifiable monomers derived from dichloromethane extractions by this process was very small.

2.1 INTRODUCTION

2.1.1 ^{13}C NMR of lignin

Nuclear magnetic resonance spectroscopy analysis is a non-destructive, highly sensitive technique and is thus a very useful analytical tool. It works on the principle of

measuring the decay of the magnetic moment of a group of specific nuclei back to their inherently relaxed state following their excitation by an external RF pulse [45]. The free induction decay (fid) signal is then converted through Fourier transform into a spectrum showing "peaks" or "shifts" corresponding to the nucleus of interest in the sample. The signal from a specific nucleus is affected by the environment in which the nucleus is found and the atoms that are bound to it, up to two bond distances. As such, different functional groups give different signals and can thus be identified. ^{1}H NMR is quantitative, i.e. integration of a sample's spectrum should yield the expected moles of protons in the sample. Quantitative measurements are also possible for other nuclei but several considerations (outlined next) must be addressed. For lignin, the most common nuclei that have been used include ^{1}H, ^{13}C and ^{31}P. Ralph et al. have compiled an NMR database for lignin structures and cell wall constituents in different deuterated solvents, such as d_6-acetone and $CDCl_3$ [46]. The list for the more common ^{13}C chemical shifts assigned to lignin is presented in Table 2.1.

Table 2.1 Frequency ranges in ^{13}C NMR for lignin functional groups [46]

Structure or functional group	Frequency range, ppm
Aromatic C total	102-162
Aromatic C-H	102-127
Aliphatic-COR	58-95
Methoxy	54.5-56.5
C-3/C-5 in β-O-4 S	150.8-153.3
$C_\gamma H_2OH$[a]	58.4-64
C-2/C-6[b] in S	102.3-107.5
C_β in β-β and β-5	53.4-54
Acetyl carboxyl carbons:	
Primary hydroxyl groups	170.4-171.6
Secondary hydroxyl groups	169.5-170.4
Phenolic groups	168.5-169.5

[a] Except in Cγ in β-β units found at 71.2 ppm.
[b] Except in C-2/C-6 in p-hydroxyphenyl units.

Both solution and solid-state ^{13}C NMR have been used in the study of lignin (for example, [46-50]. ^{13}C has 1.108% natural abundance of the ^{1}H nuclei but the development of stronger magnets allowed its use as a research tool for functional group identification [51]. However, regular ^{13}C NMR is not quantitative. Different types of ^{13}C nuclei, that is, primary, secondary, tertiary and quaternary carbons, require different relaxation times. The relaxation time is very much affected by the atoms surrounding the nuclei in question such that the more hydrogen atoms bonded to the nuclei of interest, the faster it relaxes. Quaternary carbons require much longer relaxation times than primary carbons. This puts proper relaxation delay time as a very important parameter in quantitative analysis. Insufficient delay times will cause incomplete ^{13}C nuclei relaxation back to their equilibrium Boltzmann distribution and will thus skew the intensity of the resulting spectrum [45].

Another issue for quantitative ^{13}C NMR is the presence of the nuclear Overhauser enhancement (NOE). NOE occurs when two different but coupled nuclei are irradiated, for example, ^{1}H and ^{13}C. When the number of ^{1}H nuclei in the higher level is increased, the carbon atoms attached to these protons adjust their equilibrium distribution to increase the population of carbon nuclei in the lower energy state [50]. Overall, NOE artificially increases the signal of carbon nuclei that are in an environment that has more protons in close proximity compared to that which does not have any nearby protons. Again, this will cause the spectra to not reflect the correct intensity of some shifts in the NMR spectrum.

Lastly, a sufficient number of data points or scans needs to be taken to minimize noise in the data. The relationship between noise and number of scans has been described

as follows: the reciprocal of noise in the data is related to the square root of the total number of scans made. A shorter experiment time with insufficient number of scans may not be able to record the proper shape and area of the peak [45] thus giving incorrect integration.

To summarize, issues that need to be considered in order to gain quantitative ^{13}C NMR spectra are as follows: (a) proper relaxation delay time; (b) presence of NOE effects; and, (c) proper amount of scans. To address these issues, the following strategies were implemented: (1) the use of inverse-gated decoupling protocol to eliminate NOE effects; (2) the use of a relaxant (chromium (III) acetylacetonate) for faster nuclei relaxation which translates to shorter relaxation delay times (d1) times; and, (3) the optimization of the number of scans required.

2.1.2 Methods of lignin isolation

Lignin isolation was divided by Browning (1967) into three categories: (1) isolation by extraction; (2) isolation as a residue; and, (3) isolation as derivatives [52]. The first and the third typically cause the dissolution of the lignin component. However, according to Browning, the main differences lie in using neutral solvents which do not react with the lignin for the first type of isolation while in the third, several reagents (singly or in tandem) can react with the lignin in the biomass which produces soluble derivatives [52]. Brauns, in1939, was the first to isolate a purified fraction of lignin through extraction using ethanol and showed that it is similar to the major components of lignin in wood [52-53]. Milled wood lignin (MWL) is considered as being representative of the original lignin (protolignin) in plants, and is typically produced by extensive milling of the wood sample followed by extraction with dioxane-water [54].

Analysis of whole biomass typically involves the quantification of the acid-insoluble lignin or the so-called Klason lignin [54-55]. The extractive-free wood sawdust sample is treated with 72% H_2SO_4 diluted to 4% at 110°C, a condition that hydrolyzes the carbohydrate and leaves most of the lignin intact. This lignin is typically more cross-linked than other isolated lignins [14]. However, this method was found to be problematic for previously-treated substrates as the residue produced was found to be not exclusively lignin structures only [56]. Other acids such as hydrochloric acid and phosphoric acid have also been used to isolate lignin[52]. More recently, enzymatic mild acidolysis lignin (EMAL) was developed by treating the whole wood with enzyme (cellulases), liberating an intermediate fraction, which then undergoes further treatment with mild acid to further purify the lignin [30].

In the isolation of holocellulose (cellulose + hemicellulose) from wood, $NaClO_2$ is typically used to cause delignification to solubilize the lignin [57].Several solvents, such as phenol, thioglycolic acid and acetic acid have been used to extract lignin [52]. Other procedures used either pure solvent or combination of the solvent and co-solvent such dioxane [52, 58-59], and, dimethylsulfoxide (DMSO) [52, 60-61] in the presence of NaOH. For pulping in papermaking, several chemical processes using inorganic chemicals have been developed which typically dissolve most of the lignin and also some of the carbohydrates [14, 62-63]. The most well-known of these processes is Kraft pulping. It employs both NaOH and Na_2S, producing soluble lignins that are commonly referred to as lignosulfonates. On the other hand, soda pulping only relies on the action of OH^- from NaOH. Pulping temperatures are typically between 165 – 170°C [62]. Pulping can also use organic solvents instead of water [64]. Delignification using acidic ethanol is

an example of these organosolv processes. Lastly, removal of residual lignin to improve pulp brightness also relies on the dissolution of lignin with little or no effect on the pulp [65]. In these mentioned procedures, the lignin produced were typically modified by the extraction procedure used and will thus have distinctive properties apart from another lignin extracted in a different method. This has made the identification of the true native structure of lignin challenging over the years.

2.1.3 Isolation of lignin using alkali

Base-catalyzed depolymerization (BCD) of lignin was the route chosen to decompose the lignin starting material in this study. As previously mentioned, alkalis have been used to cause lignin dissolution in both the Kraft and soda pulping. Though pulping is done at much lower reaction temperatures, it would be useful to review the reactions that have been attributed to occur in the presence of hydroxyl species which are expected to be present in BCD as well.

Most of the chemistry that occurs in alkaline pulping has been addressed by Gierer [63, 66]. Lignin reactivity depends on the type of linkage present as well as the moieties that were joined together (e.g. phenolic or non-phenolic). α-Aryl ether bonds of the phenylcoumaran type (A_1 in Figure 2.1) are extensively cleaved during the alkaline process. Formaldehyde may be liberated by the cleavage of the Cγ. However, α-aryl ether bonds in non-phenolic moieties (A_2 or B_2) are more stable in alkali because the methylene quinone intermediate will not be formed.

As previously noted, β-aryl ether linkages comprise the majority of the lignin linkages in biomass (see Table 1.1). Schemes 2.1 and 2.3 show the possible reactions that can be undergone by this type of linkage during alkaline processing. For units that have

free phenolic hydroxyl groups *para* to the side chain, styryl aryl ether units can form. These are stable in alkali at pulping conditions and will thus not be capable of further depolymerization. This route, which includes proton elimination from the β-carbon, does not result in the cleavage of the ether linkage. However, another route may cause depolymerization if the nucleophilic "neighboring-group" mechanism occurs. Scheme 2.1 summarizes these reactions. In another route, a hydroxymethyl group attached to the β-carbon can be released as formaldehyde (Scheme 2.2). On the other hand, β-aryl ether linkages connected to non-phenolic moieties undergo elimination of the aryl group attached to the β-carbon in the fashion shown in Scheme 2.3. This liberates phenolic groups and forms glycol groups [63].

Accessibility of the reactive groups is an important consideration in the above-mentioned depolymerization reactions. Lapierre and Rolando [67] quantified the presence of these accessible groups in pine compression and of poplar woods. The authors reported that in these samples, about 30% of the guaiacyl (G-) moieties having β-aryl ether linkages were terminal while only 6% were accessible for syringyl (S-) moieties.

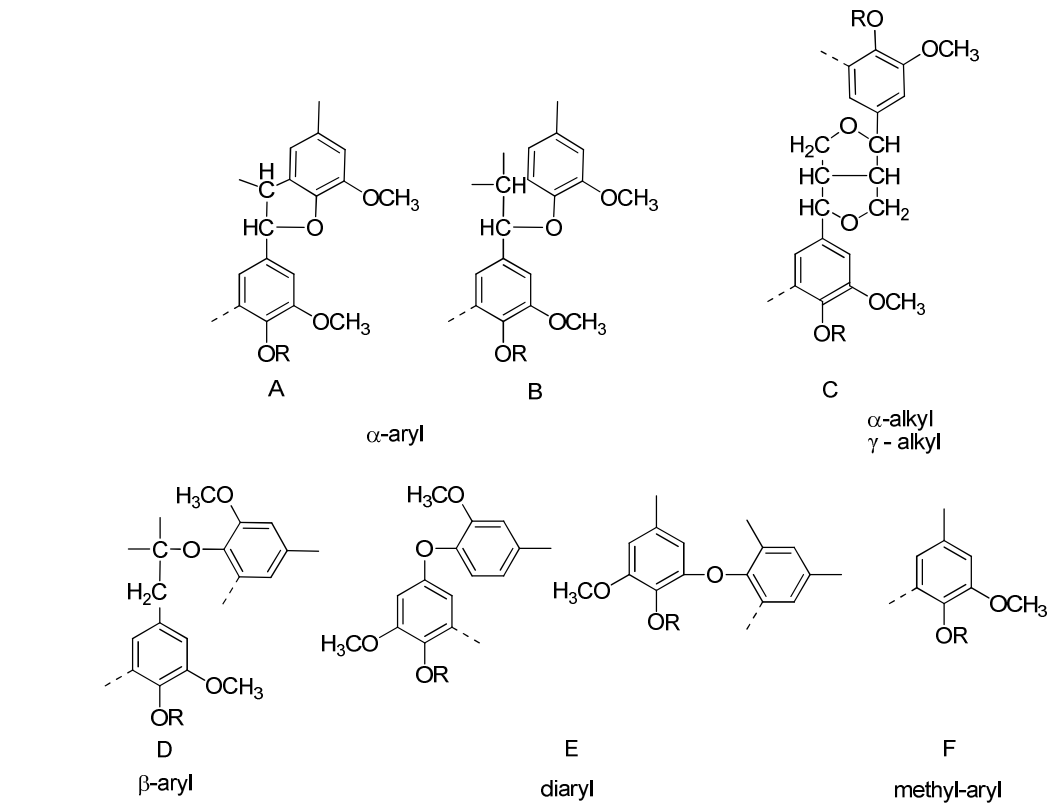

$A_1 – F_1$: R = H (phenolic)
$A_2 – F_2$: R = Aryl (non-phenolic)

Figure 2.1 Main ether linkages in lignin [63]

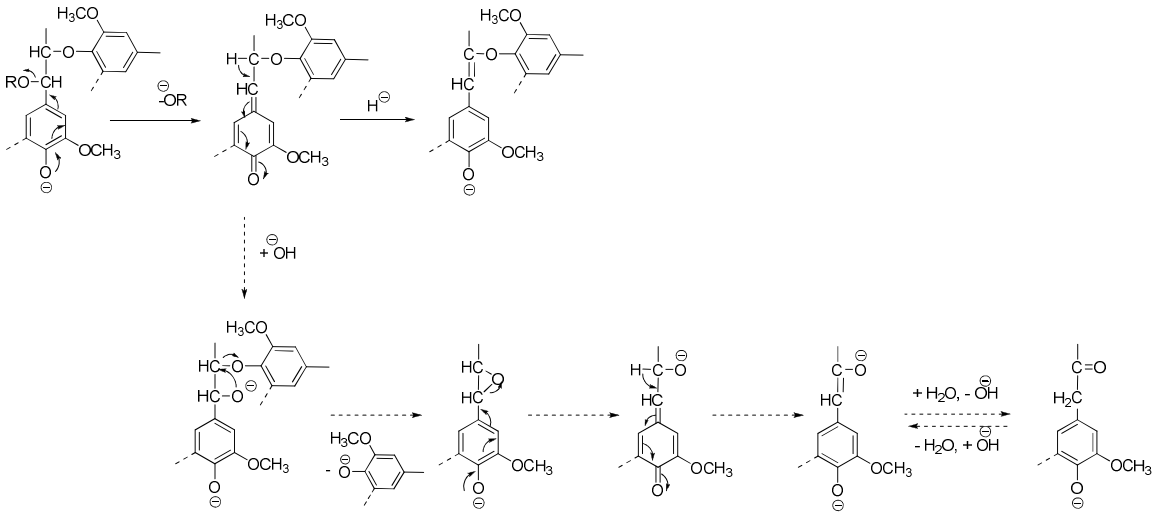

Scheme 2.1 Reactions of phenolic β-aryl ether linkages in alkali [63]

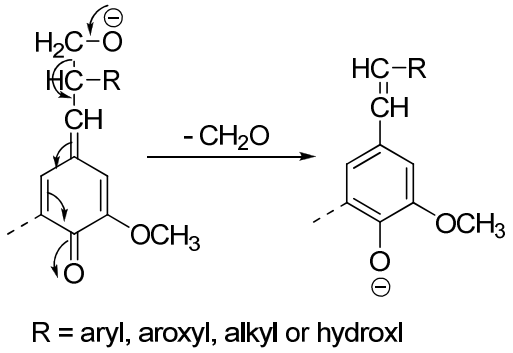

Scheme 2.2 Generation of formaldehyde [63]

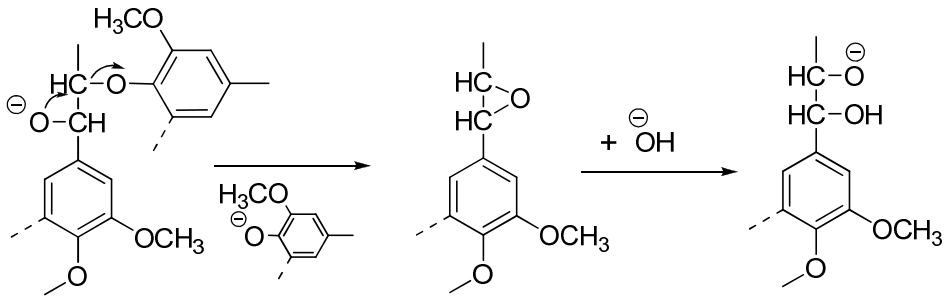

Scheme 2.3 Reaction of non-phenolic (etherified) β-aryl ether linkages in alkali [63]

As can be gleaned from the previous discussions, β-O-4 linkages typically get broken during alkali treatment of lignin, though the product may still contain some β-O-4 linkages [63, 68]. On the other hand, organosolv lignin is supposed to contain relatively more oxidized functionalities, compared to alkali lignin. The organosolv lignin process mainly attacks the α-O linkages and thus retains relatively larger amounts of β-O-4 linkages [65, 68].

2.1.4 Previous BCD studies

After an overview of some alkali reactions of lignin, a brief review of some previous base-catalyzed depolymerization studies is discussed in this section. In 1994, Thring published a study on the alkaline degradation of Alcell lignin, a type of organosolv lignin [69]. He used a 500 ml stainless steel reactor lined with Inconel 900 and ran reactions from 200°-340°C for 15 to 90 minutes. The concentrations of NaOH solutions (both in water and in ethanol) that were used ranged from 0.5 wt% to 6 wt%. Results showed that temperature was more important than the reaction time. Maximum yield of DCM-solubles was noted to be at 10% of the lignin fed, with a maximum of 4 wt% identified and quantified monomeric products [69].

Kadangode and Shabtai from the University of Utah finished a series of studies on the base-catalyzed depolymerization (BCD) of lignin in the presence of alcoholic base [70]. They used several types of lignin, including kraft (Indulin) and organosolv (Repap) lignins. Ethanolic or methanolic KOH at 10% base concentration was typically used. The BCD process was considered as a first stage to a complete process that included hydrodeoxygenation as a second stage to produce reformulated gasoline [70]. This complete system was proposed in previous patents by the group [71-72]. Kadangode showed through GC-MS analysis that drastic changes in the lignin were found to start at 270°C, but became more pronounced at 290°C. Alkylation of the aromatic ring through reaction with the solvent was considered to be ideal. Partial oxygen removal occurred through the expulsion of methoxy groups [70]. Also part of the project was the catalytic upgrading of the BCD products through hydrogenation with supported metal catalysts, such as NiMo/Al_2O_3, Pt/C and Pt/Al_2O_3, in a subsequent hydroprocessing step. Two

more patents were obtained by Shabtai, et al. in 2003 [73-74]. The highest temperature they tested for BCD was 310°C.

Sandia National Laboratories published reports on BCD studies done using microreactors (~14 cm^3) [75-76]. The first one was an extension of the studies done by Shabtai, et al. in the base-catalyzed depolymerization of lignin using alcohol solvents [76]. The second one used water as solvent [75]. For the first study, several bases were tested, including, CsOH, NaOH, LiOH, $Ca(OH)_2$ and Na_2CO_3. Aside from gravimetric quantification, simulated distillation was also used for analysis. They reported that (a) strong bases (i.e. NaOH, KOH and CsOH) resulted in the least amount of insolubles at 290°C for 1 hour of reaction as well as that (b) excess base was required for effective dissolution. Combinations of sub-stoichiometric amounts of NaOH and KOH with $Ca(OH)_2$ were also seen to have synergistic effects and improved the dissolution brought about by $Ca(OH)_2$ alone [76].

The combination of bases was also tested in aqueous media. Though using NaOH on its own as the base was more successful than $Ca(OH)_2$, $Mg(OH)_2$, CaO, Na_2CO_3 and MgO, a combination of Na_2CO_3 and CaO was proposed to be an economically successful alternative [76]. Methyl group migration and loss of methyl/methoxy groups were probed by model compounds studies.

2.1.5 Objectives

The general objectives of this chapter combine the characterization of the starting organosolv lignin material as well as the treatment of the lignin with base in order to affect depolymerization. Specifically, the objectives were as follows:

(1) evaluate the use of different bases, that is, NaOH, KOH and NH_4OH in the base-catalyzed depolymerization of lignin;

(2) probe the effect of reaction time and reaction temperatures;

(3) analyze the BCD products without further work-up using ^{13}C NMR;

(4) identify and quantify monomeric products produced; and,

(5) determine the extent of depolymerization using GPC.

2.2 EXPERIMENTAL METHODS

2.2.1 Screening of starting materials

Three types of lignin were first screened for the experiments. These were (a) commercial hydrolytic lignin (Sigma-Aldrich); (b) commercial organosolv lignin (Sigma-Aldrich); and, (c) laboratory prepared hydrolytic residue [77]. Both the organosolv and the hydrolytic lignins were procured from Sigma-Aldrich and used without further purification. Two types of laboratory-synthesized acid hydrolysis residues were used. One was the by-product of acid hydrolysis with trifluoroacetic acid (TFA) and sulfuric acid (SA). These were by-products of the batch hydrolysis treatment of loblolly pine at 200°C for 1 hour with a $pH_{25°C}$ = 1.65 [77]. Several solvents for these lignins were screened including acetone, ethanol, tetrahydrofuran, p-dioxane and dimethylsulfoxide (DMSO), a solvent commonly used to dissolve lignin for analysis [36]. Organosolv lignin was found soluble in all solvents tested, except water. The ^{13}C NMR protocol used for the preliminary screening of lignin starting material was not carried out using quantitative methods at this stage.

2.2.2 Elemental Analysis

Some samples of the four lignins were sent out to an outside vendor, Atlantic Microlab Inc., for elemental analysis.

2.2.3 Acetylation

Acetylation of lignin and lignin product solid samples is a technique usually done to improve the solubility of lignin in organic solvents [29, 45, 47], such as THF and DMSO. The method used in this study was modified from Glasser et al. [78]. In a typical process, 40 ml of 50% pyridine-50% acetic anhydride solution per gram of lignin starting material was used. The mixture was allowed to react for 24 hours while mixing. The solids were re-precipitated using 150 ml of HCl solution (pH = 1.0). The solids were then collected using a vacuum filtration set-up. They were washed with some HCl solution and then with copious amounts of deionized (dI) water. The collected solids were vacuum-dried at 40°C and stored in vials for further analysis.

In order to analyze the aqueous products using an organic GPC, derivatization by acetylation was done. A 25-ml portion of the liquid product was dried in the oven overnight. The solids formed were gathered and used for acetylation using a similar procedure as outlined above.

2.2.4 ^{13}C NMR

For the characterization of the starting material, both the acetylated and commercial, non-acetylated organosolv lignins were analyzed. They both were found to be soluble in dimethylsulfoxide (DMSO). Thus, d_6-DMSO was used as the NMR solvent. The recommended sample concentration for lignin analysis with ^{13}C NMR is between 80-150 mg lignin per ml of deuterated solvent [46]. As such, about 100 mg of organosolv

lignin was used. However, as mentioned before, other lignins have portions that were not soluble. In order to increase the amount of solubilized samples for analysis, more than 150 mg were used for the commercially available hydrolytic lignin and laboratory prepared acid hydrolysis lignin.

Typical delay times used for quantitative NMR are about d1 = 10-12 seconds [46, 79]. In an effort to reduce the subsequent analysis machine time, chromium (III) acetylacetonate (Cr (acac)$_3$) was added as a relaxant [79-80]. A saturated Cr(acac)$_3$ solution was made by dissolving enough of the crystals into d_6-DMSO until some solids remain undissolved. This was stored in a vial and was constantly checked for saturation.

To determine whether the amount of relaxant has an effect on the lignin sample, the amounts of the saturated Cr(acac)$_3$ in d_6-DMSO solution added into the dissolved lignin were varied. Several delay times, decreasing from d1 = 10 seconds to d1 = 1 second were applied to the NMR analysis. The number of scans made was also varied. The integration of the resulting spectra for specific ranges (i.e. carbonyl group, $I_{166\text{-}172}$ and methoxy group, $I_{56\text{-}58}$) were then compared to that expected from a sample run with longer delay time without the Cr(acac)$_3$.

On the other hand, BCD products typically contain solubilized lignin in aqueous alkali. For ^{13}C NMR analysis, this whole mixture was analyzed, making the aqueous alkali the designated solvent by virtue of its larger amount. As an example, if all the lignin starting material dissolved after the reaction, only 10% of the resulting liquid comprised the lignin, the rest, being the aqueous alkaline solution. Analysis of this whole product with ^{13}C NMR was done by mixing 1 ml of the liquid with 100 µL of d_6-DMSO saturated with Cr(acac)$_3$. The d_6-DMSO was used for spin-locking and the Cr(acac)$_3$ as

the relaxation agent. A glass pipette was used to transfer the liquid through another cotton-plugged pipette into a 5-mm Wilmad NMR tube. Analysis was done with a Bruker AMX-400 spectrometer operating at 100.04 MHz using Bruker XWIN 3.1 software. However, analysis of the data off-line was done using the free version Mestre-C 2.3. Inverse-gated ^{1}H decoupling (zgig protocol) with d1 = 1 sec and 20000 scans was used. A Gaussian line broadening equivalent to 10 Hz was applied.

Aside from inverse-gated ^{1}H decoupled ^{13}C NMR, distortionless enhancement polarization transfer (DEPT) experiments were also done for some samples to further characterize the products. DEPT was used to distinguish between the type of carbons present in the sample during the identification of functional groups present in the BCD products.

^{1}H NMR was also run for most of the samples. However, due to the large amount of water present, a large water peak that dominated most of the field was typically present in all samples. Though water suppression protocol was used, this was found to be insufficient and still removed an integral part of the peaks for the samples. Evaporating the water, drying the residue and re-dissolution in D_2O was tried but was not successful because the resulting solid was not readily re-dissolved.

All the ^{13}C NMR experiments were done using a Bruker AMX 400 machine with 5 mm broadband probehead of the Nuclear Magnetic Resonance Spectroscopy Center at GaTech. Inversely-gated ^{13}C NMR pulse program was used to screen out the nuclear Overhauser effect (NOE) in order to obtain quantitative ^{13}C spectra.

2.2.5 Analysis of DCM-soluble compounds

Inasmuch as analysis of the whole product was prioritized, fractionation of the products based on solubility was found to be inevitable. The mainly aqueous products in the presence of alkali salts were not amenable to analysis by GC-FID (Shimadzu QP 2010) directly. Problems encountered included turning off of the flame during analysis as well as possible wear of the inlet parts and the column due to salt encrustation. Eventually, it was confirmed that complete solubility of the BCD product did not readily mean extensive depolymerization. As such, direct injection of the sample may also cause contamination if not all of the injected sample was gasified. Silylation was also employed to minimize the possible inclusion of acids in their protonic form; both polar and nonpolar silylating agents were used. In the end, extraction was done on the samples. Ethyl acetate was initially used for extraction but was found to degrade in the presence of base. As a recourse, acidification was used before the extraction with dichloromethane (DCM) [69].

The DCM solubles were eventually analyzed in the GC-FID. In a typical product work-up, about 3 ml of the liquid was transferred into a 45-ml centrifuge tube. It was then acidified to about pH = 2 with concentrated HCl that was added drop-wise. A pH meter monitored the pH change. The mixture was shaken vigorously after each acid addition. After the desired pH was reached, about 15 mL of DCM was added into the centrifuge tube. The mixture was then centrifuged for 3 minutes and allowed to stand for 15 minutes. The clear bottom part was recovered using a glass pipette. At least two more 15-ml portions of DCM were used to extract the soluble products from the mixture. Extraction was judged complete once the extract was judged clear by eyesight. All the

extracts were combined and the solvent partially removed by rotavap. An aliquot was added to a vial containing acetone and analyzed using the GC-FID. External standards for identified compounds were done separately using standard chemicals procured from Sigma-Aldrich.

2.2.6 Gel permeation chromatography

Analysis of the resulting molecular weight of the base-catalyzed product was done using a Polymerlabs Chromatograph (PL-GPC-50 Plus) equipped with a refractive index detector (RID) and a viscometer for universal calibration using the Cirrus Multi software. THF was used as eluent. A filtered injected sample (~5 mg/mL) passed through three identical columns in series (PLgel Mixed-E, 3 µm, 300 x 7.3 mm, MW up to 30 000 Da) for molecular weight separation before reaching the detectors.

2.2.7 Reactor set-up

A 500-mL stirred autoclave was specifically procured from Parr Instruments (Moline, Illinois) for the base catalyzed experiments. It was made of Monel which is a nickel alloy that can withstand the highly corrosive conditions of high pH, high temperatures and relatively high pressures. Autoclave seal was accomplished through the application of 35 ft-lb_f of torque on hex screws that keep in place a graphite O-ring in between the split-ring connections. The reactor is equipped with a thermocouple, a pressure gauge and a magnetic drive stirrer. The sheer weight of the reactor, especially when fully assembled, required the use of a cart for safe handling during transfer from one place to another.

2.2.8 Base-catalyzed experiments

In a typical experiment, 12 grams of organosolv lignin was transferred into the reactor. About 120 grams of alkali solution was then poured into the reactor. The alkali solution was made with deionized water (dI) and the required amount of NaOH or KOH pellets to make 2.78 M of solution. For the NH_4OH, 12 grams of the solution from the reagent bottle were mixed with 108 grams of dI water. The reactor was then sealed. The atmosphere above the mixture was replaced by purging with N_2 for 1 minute. This was followed by closing the gas outlet valve and allowing the reactor to be pressurized with 15 psig of N_2 for about 30 seconds and was then vented. The sequence from purging to venting was repeated two more times. After the last venting, the reactor was finally pressurized with 15 psig of N_2. After allowing a few minutes to check for the presence of leaks, the reactor was finally heated to its target temperature. The heat up time varied with the target reaction temperature. Because of the bulk of the reactor, heat up typically took between 45 to 60 minutes depending on the target temperature. Reaction time was considered only once the reactor reached the target temperature. After the required reaction time, the reactor was submerged in an ice-water bath that was constantly replenished with fresh ice until the temperature in the reactor reached below 20°C. It was then allowed to vent out the remaining pressure by opening the gas outlet valve before attempting to loosen the split-ring.

Parameters tested for the base-catalyzed depolymerization of organosolv lignin are summarized in Table 2.2 below.

Table 2.2 Summary of conditions tested

Base	Temperature, (°C)	Reaction Time @ T_{rxn}, (mins)
NaOH	**165**	**15**
	210	**15**
	290	**15**
	290	**60**
	350	**15**
KOH	**165**	**15**
	290	**15**
	350	**15**
NH_4OH	**165**	**15**
	290	**15**
	350	**15**

As mentioned, variables included the type of alkali used (NaOH, KOH and NH_4OH) , reaction time (15 and 60 minutes) and temperature (165°C, 210°C, 290°C and 350°C for NaOH and 165°C, 290°C and 350°C for the other two) . No distinct difference was seen between 15 minutes and 60 minutes at reaction temperature. As such, 15 minutes of reaction was typically used for the subsequent depolymerization experiments.

2.3 RESULTS AND DISCUSSION

2.3.1 Elemental analysis of lignins

Several lignins were screened. Two were obtained commercially while two were by-products of acid hydrolysis experiments previously done in our lab [77]. Some

qualitative descriptions are summarized in Table 2.3. These samples were all sent out for elemental analysis. The results are summarized in Table 2.4.

Table 2.3 Properties of analyzed lignin samples

	Organosolv Lignin	**Hydrolytic Lignin**	**TFA-6**	**SA-4**
Notes on sourcing	Commercially available from Sigma-Aldrich; from hardwood mix	Commercially available from Sigma-Aldrich; from sugarcane bagasse	Laboratory-prepared; from loblolly pine	Laboratory-prepared; from loblolly pine
Solvent/Catalyst	Aqueous ethanol	Not available	TFA; pH 1.65	H_2SO_4; pH 1.63
Reaction temperature	Not available	Not available	200°C	200°C
Time at reaction temperature	Not available	Not available	60 mins	60 mins

Table 2.4 Elemental analysis of the different lignins (ash-free basis)

	Organosolv	**Hydrolytic**	**TFA-6**	**SA-4**
C	65.7	60.5	66.4	58.0
H	6.0	5.7	5.3	5.7
O	28.2	31.5	28.1	36.0
N	0.0	0.6	0.0	0.0
O/C	0.3	0.4	0.3	0.5
H/C	1.1	1.1	0.9	1.2

Based on elemental analysis alone, there is not much difference among these lignins. As expected, C is the major element present, followed by O. If we refer to the von Krevelen chart (Figure 1.9) and compare the O/C and H/C ratios with the target for crude oil-like properties ($1.60 < H/C < 2.10$ and $0 < O/C < 0.03$), all of these samples require incorporation of H and reduction of O content. In the presence of different solvents, these lignins also exhibited different solubility characteristics, suggesting the presence of different types of linkages present, of different extent of cross-linking present

and of the presence of carbohydrate impurities [14, 64]. Further characterization of the different lignins using ^{13}C NMR is discussed in the next section.

2.3.2 ^{13}C NMR of lignins

Lignin that has undergone processing is expected to have different characteristics compared to its starting material. It is one of the objectives of this project to characterize the lignin samples as well as possible. Techniques that could be employed include elemental analysis, ^{13}C NMR, GPC, functional group analysis (i.e. methoxy and hydroxyl content of lignin) as well as other degradative methods such as potassium permanganate oxidation and alkaline nitrobenzene oxidation. Solution ^{13}C NMR spectra in d_6-DMSO of four lignins are shown in Figure 2.2. These comprise two commercially available samples and two by-products of the acid hydrolysis experiments from fractionation of biomass. Analysis by ^{13}C NMR of another laboratory prepared sample, Klason lignin (acid insoluble lignin after treating wood with 72% H_2SO_4 for 2 hours and boiling at 3% H_2SO_4 for 4 hours), was attempted. However, it was very sparingly soluble in the solvent and not enough lignin was dissolved for analysis. As such, only the commercial organosolv and hydrolytic lignins and the laboratory-prepared TFA-6 and SA-4 were analyzed by NMR.

Robert [46] recommended 20 – 40% (w/w) (400 to 600 mg in 1.8 mL d_6-DMSO) for NMR analysis, though he noted that concentrations as low as 100mg sample/1.8mL solvent can be analyzed if the number of scans is increased. For these samples, about 100mg/mL solvent was the target concentration used.

The commercial lignins were more soluble in DMSO than the acid-insoluble ones. Organosolv lignin readily dissolved in the solvent while some particles remained

insoluble for the hydrolytic lignin. Anticipating that the laboratory-prepared samples will have much lower solubility due to the presence of non-lignin components, the amount of solid samples for these were doubled. However, a comparable concentration with the commercial samples was still not achieved. It must be noted that the temperature was not increased nor was sonication applied to these samples to avoid possible damage to the starting material. However, the poor solubility translated to both TFA-treated and sulfuric acid-treated samples having spectra with much lower signal-to-noise ratio despite similar acquisition parameters for all the samples. It may be speculated that the possible presence of carbohydrates or other carbohydrate–derived by-products hampered lignin dissolution. An experiment wherein cellulose fibers were immersed into DMSO overnight only resulted in the swelling and not in the dissolution of the cellulose.

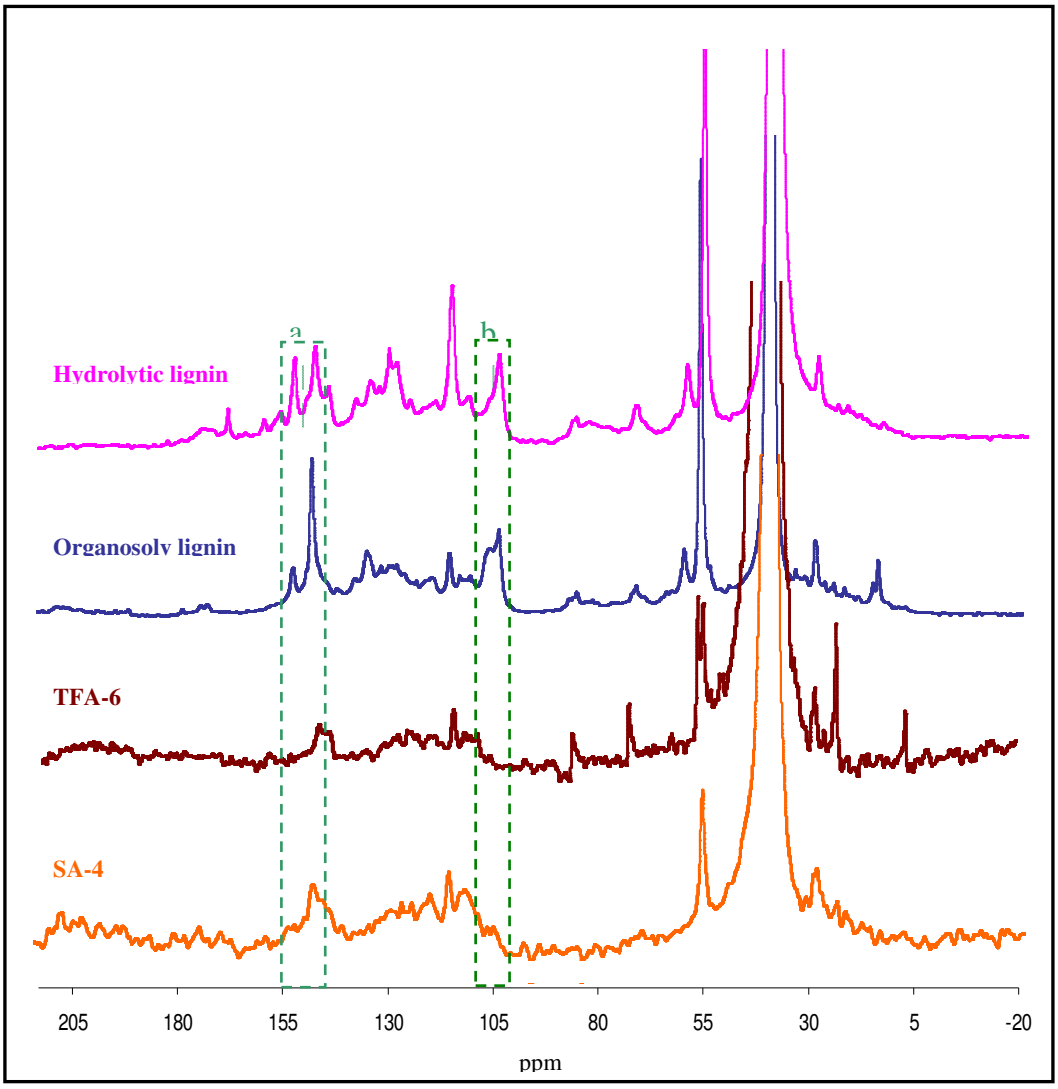

Figure 2.2 ^{13}C NMR spectra of different lignins in d_6-DMSO

A total of 11000 scans were taken for each sample except for organosolv lignin which only had 10714 scans. Quantitative comparisons among the four spectra would be difficult because of the difference in the actual lignin content that were in the NMR solutions. Aside from functional group information, ^{13}C NMR can also be used as a tool to characterize the structural components of the lignin sample. However, some resonances are worth noting. Lignins with S units (hardwoods and grass) would give a signal between 150.8-155 ppm. This is evident in the spectra of the commercial lignins

(Figure 2.2 a). However, since the laboratory-prepared samples were derived from softwoods which do not contain S units (if any, only a small amount), the characteristic peak for S was not found in these samples. Another S resonance is around 104-106 ppm which is from the C2/C6 aromatic carbons (Figure 2.2 b). Again, the laboratory-synthesized lignins did not have this shift. In all the samples, the methoxy resonance at around 56 ppm was quite sharp. With respect to carbohydrate impurities, the resonance signal of the C1 carbohydrate around 90-100 ppm is very small and can thus be considered to be negligible (Figure 2.2 b) [79].

With the difficulty encountered in dissolving the laboratory-synthesized hydrolytic lignins and its effect on their subsequent ^{13}C NMR analysis, organosolv lignin was chosen to be the starting material for the BCD study.

The following section describes the efforts undertaken to make the ^{13}C NMR analysis quantitative.

2.3.2.1 Quantitative ^{13}C NMR

Inversely gated decoupling pulse program was used in gathering quantitative ^{13}C NMR data. A cartoon depicting this protocol is shown in Figure 2.3. In here, the ^{1}H decoupling is on during acquisition and during the RF pulse but is turned off during the relaxation delay to avoid NOE build up [81]. Assuming that sufficient relaxation delay time is allowed (d1), the FID should only then reflect the quantitative intensities of the carbon nuclei present.

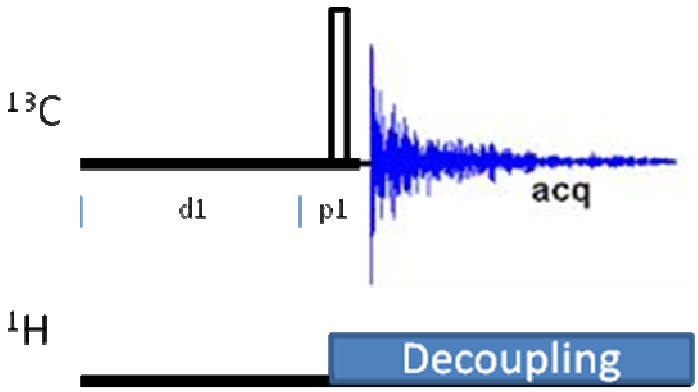

Figure 2. 3 Inverse-gated decoupling

As mentioned, a delay time of 10 to 12 seconds was recommended for lignins to achieve quantitative ^{13}C NMR data [38]. With 10000 scans, this will amount to about 33 hours of machine time. Considering the cost and time availability of the machine, a shorter analysis time would be very attractive. By adding sufficient amount of relaxant, shorter delay times of the ^{13}C nuclei without losing quantitative accuracy can be achieved [79]. For the relaxant $Cr(acac)_3$, the paramagnetic Cr^{3+} shortens the relaxation time of the ^{13}C nuclei, thus making complete relaxation for all carbon nuclei possible at a shorter delay time.

In order to arrive at an optimum set of conditions, the amount of relaxant and the length of relaxation delay times were varied. The intensities of the regions from around 56-57 ppm (methoxy group attached to C_3 and C_5) and those between 166-172 ppm (carbonyl group) were noted and their ratio calculated as $I_{56\text{-}57}/I_{166\text{-}172}$. These regions were expected to contain carbon nuclei with the most different relaxation times. With more protons attached to the carbon nucleus, the carbon in a methoxy group would have a much lower relaxation delay time compared to a carbonyl carbon. As such, at conditions when

insufficient relaxation was allowed for the carbonyl carbon nuclei, their intensities were expected to be lower than if they were allowed to fully relax. This will translate to a higher $I_{56\text{-}57}/I_{166\text{-}172}$ ratio than is quantitative. The results of these experiments are summarized in Table 2.5.

Table 2.5 Summary of relaxation delay experiments of acetyl-brominated commercial organosolv lignin

Amount of relaxant, $Cr(acac)_3$ in DMSO (μL)	30			100	
Relaxation delay time, d1 (s)	1	5	10	**1**	2
Number of scans	20000	20000	10000	**20000**	20000
Number of machine-hours	12.5	34.7	31.3	**12.5**	18.1
$I_{56\text{-}57}/I_{166\text{-}172}$	0.886	0.702	0.833	**0.700**	0.700

As can be seen, all three parameters tested (i.e. d1, amount of relaxant and number of scans) had an effect in the optimization of the NMR spectra. Using a relaxant solution of 30 μL, the required number of scans was halved from 20000 to 10000 with a d1 = 10 seconds, the $I_{56\text{-}57}/I_{166\text{-}172}$ ratio was about 0.883. Adjusting the d1 to 1 second showed that the relaxation time, despite the doubling of the number of scans to improve resolution was grossly insufficient since the ratio went up. Increasing the d1 to 5 seconds showed an improvement in the ratio, actually much lower than the run with 10 seconds but only 10000 scans. However, a machine time of 34.7 hours was far from being attractive. Hence, the amount of relaxant was increased to a total of 100 μL. As shown in the table, the ratio between d1 = 1 second and d1 = 2 seconds did not have any difference. With close to 6 hour difference in their analysis time, a d1 equivalent to 1second and 20000 scans was chosen for analysis of samples with 100 μL of the $Cr(acac)_3$-d_6-DMSO solution.

2.3.2.2 Empirical formula of organosolv lignin

Combining the information from the quantitative ^{13}C NMR of lignin and that of the elemental analysis, an empirical formula for the organosolv lignin can be determined based on C_9 or the monomeric units of lignin. Integration of the organosolv lignin spectra gives the percentage of methoxy groups in all the carbons present in the sample. This value was calculated at 16.97%. The empirical formula calculated for the organosolv lignin becomes $C_9H_{6.35}O_{1.65}(OCH_3)_{1.84}$.

2.3.3 ^{13}C NMR analysis of base-catalyzed depolymerization products

2.3.3.1 Solubility of starting material in alkali

In the previous section, the complete dissolution of organosolv lignin in d_6-DMSO allowed its analysis by ^{13}C NMR. In pure water, organosolv lignin was insoluble. However, it was found to be quite soluble in alkali medium, as noted by other authors as well [68, 70].

Figure 2.4 shows the spectra of the lignin dissolved in d_6-DMSO as well as in 10% NaOH. $Cr(acac)_3$ dissolved in d_6-DMSO (100 µL/ml of product) was added in both samples as a relaxant ($Cr(acac)_3$) and as an internal standard (d_6-DMSO). It must be noted that the shifts in the spectrum of the organosolv showed some differences in each of the solvents. The different shifts in the NaOH dissolved sample could be attributed to the ionization effect of the high pH of the medium [68, 82].

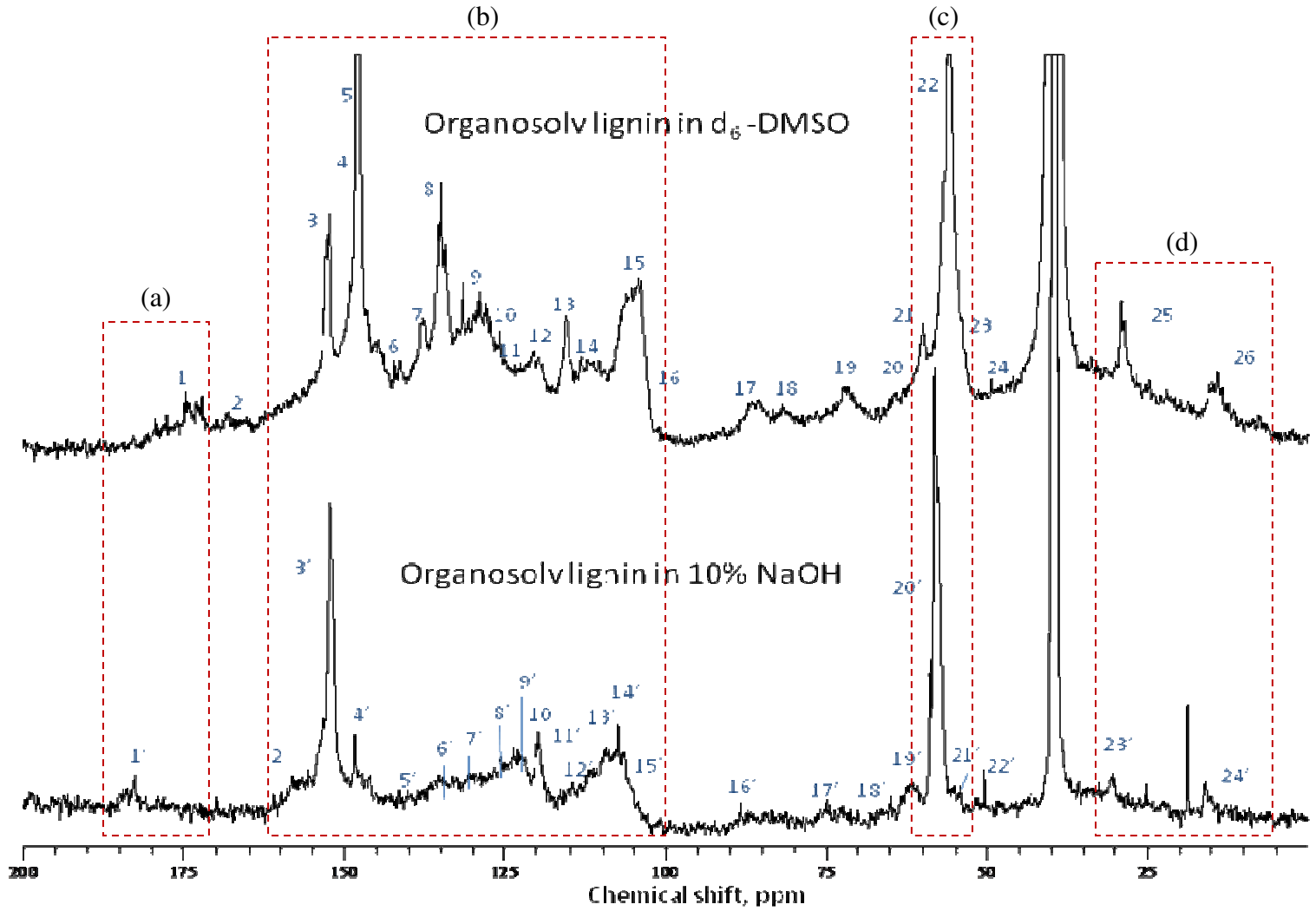

Figure 2.4 ^{13}C NMR spectra of organosolv lignin in different solvents: (a) d_6-DMSO and (b) 10% NaOH

Table 2.6 Chemical shift assignments (ppm) of organosolv lignin ^{13}C NMR spectra in d_6-DMSO and in 10% NaOH (2.76 M)

	Spectrum in d_6-DMSO			Spectrum in 10% NaOH	
#	CS, ppm		#	CS, ppm	
1	172.4-174.4	β- , and γ-COOH , non-conjugated	1'	182.6-184.9	β- , and γ-COOH , non-conjugated
2	164.9-169.0	γ- COOR	2'	153.4-155.6	C-3 in Gne; C-3,5 in Se
3	152.2-152.7	C-3,5 in Se	3'	152.2	C-3,5 in Sne; C-3 in Ge
4	148.1	C-4 in Ge	4'	148.5	C-4 in Sne; C-4 in Ge
5	147.6-148.0	C-3 in Ge	5'	137.7-138.5	C-1 in Se
6	144.0-144.8	C-4 in Gne; α- in FA e	6'	134.7-136.7	C-4 in Se; C-1 in Ge
7	137.6-138.1	C-1 in Se; C-4 in Se	7'	128.8-130.7	C-5 in Ge subst
8	134.2-135.2	C-4 in Sne and Se; C-1 in Sne; C-1 in Ge	8'	125.5-125.9	C-1 in Sne
9	128.9-131.5	C-1 in Gne; C-1 in S with α-COOH; C-5 in G subs	9'	121.9-123.7	C-6 in Ge; C-5 in Gne
10	125.8	C-1 in pCA e	10'	120.1	C-6 in Gne
11	122.3	C-6 in FA e	11'	119.7	C-5 in Ge
12	119.9-120.6	C-6 in Ge and Gne	12'	114.4	C-2 in Gne and Ge
13	114.5-116.0	C-5 in Ge and Gne	13'	108.6-112.1	C-2,6 in Se
14	109.5-114.0	C-2 in Ge and Gne	14'	107.4	C-2,6 in Sne
15	104.3-107.0	C-2,6 in Se and Sne	15'	106.4	unknown (carbohydrates?)
16	103.7	unknown (carbohydrates?)	16'	85.6-88.3	β- in β-O-4, α- in β-5
17	85.2-87.0	β- in β-O-4, α- in β-5	17'	74.0-75.8	α- in β-O-4
18	81.2-82.5	unknown (aliphatic side-chains?)	18'	64.8	CH_2OH
19	72.2	α- in β-O-4	19'	61.5	γ-CH_2OH
20	64.4	CH_2OH	20'	57.5-58.7	OCH_3
21	60.0	γ-CH_2OH	21'	54.1	β in β-5 e
22	56.0-58.3	OCH_3	22'	50.3	β in β-5 ne
23	53.8	β in β-5 e	23'	23.5-37.0	-CH_2-
24	49.5	β in β-5 ne	24'	10.0-21.8	-CH_3
25	23.0-33.9	-CH_2-			
26	5.6-22.4	-CH_3			

G = guaiacyl; S = syringyl; e = etherified; ne = non-etherified; FA = ferulic acid (3-(4-hydroxy-3-methoxyphenyl)-2-propenoic acid); pCA = p-coumaric acid (3-(4-hydroxyphenyl)-2-propenoic acid)

Table 2.6 summarizes the assignments for the organosolv lignin shifts. References used in these assignments include [46, 68, 82-84]. The main differences between them are mainly seen in (a) carboxylic shifts found between 172 and 185 ppm (**1** and **1'**), and (b) the range for aromatic region 100 to 165 ppm (**3 – 16** and **2' – 15'**). These main differences can be attributed to the ionization chemical shifting due to the presence of ionizable groups in the sample which are ionized in a given solvent/medium [82]. In lignin, these would be the carboxylic and the phenolic functionalities. The changes in the methoxy and aliphatic regions, (c) and (d) respectively, are indirect effects of these ionizations.

2.3.3.2 Ionization chemical shifts

As mentioned, the solvent used in the medium can affect the expected shifts of a specific compound. For example, the chemical shift of dissolved water in different deuterated solvents was found to change as follows: d_3-chloroform, 1.5 ppm; d_6-benzene, 0.4 ppm ; d_6-acetone, 2.75 ppm; d_5-pyridine, 5.0 ppm and d_2-water, ~4.75 ppm [51]. The change in the peaks may be attributed to the interactions of the compound with the solvent. From the work of Schaefer et al. [85], the interactions of specific functional groups with the solvent of choice, e.g. through π-electron or ionic interactions, have been studied by other researchers as well.

Akim et al. studied the chemical shifts brought about by ionization in the alkali medium using aromatic model compounds and milled wood lignins [82] as well as different types of technical lignins [68]. For various model compounds dissolved in 1 N NaOH, the ionization of phenolic hydroxyl groups in the aromatic ring as well as the conjugation of the aromatic ring with the substituents in the aliphatic side chain were found to be the main contributors to the resulting differences in shifts of these compounds [82]. Dissolution in a high pH medium results in the loss of protons of phenolic and carboxylic groups. This makes the hydroxyl groups of phenol stronger electron donors while making the erstwhile strong acceptor carboxyl group into a weak donor carboxylate group [86]. Typically, the main carbons affected are the aromatic C-1 and C-4 nuclei. Akim et al. also assigned peaks for actual technical lignins, such as organosolv, ozone-treated and kraft lignins dissolved in 1 N NaOH [68]. The assignments in Table 2.7 were based on the shifts given for organosolv lignin dissolved in 1 N NaOH.

Because of the ionizing effect of the solvent, the difference between the etherified and non-etherified (C-4) moieties became more obvious. Referring to Figure 2.4, one main difference between the spectra occurred in the downfield region between 145-165 ppm. The C-3, C-5 in the non-etherified S group as well as the C-3 in etherified G were now shifted to about 152.2 ppm (**3'**). The C-3 in non-etherified G as well as the C-3 and C-5 in etherified S units appear as a shoulder between 153.5 and 155.6 ppm (**2'**).

Other aromatic ^{13}C nuclei were also shifted in the NaOH as compared to the DMSO dissolved lignin. This shifting of the peaks in the region between 102 and 145 ppm was also seen in the reported spectra of Akim, et al. [68]. The prominent broad peak around 135 ppm that was found in the d_6-DMSO dissolved lignin was typically assigned to several groups: C-4 in both etherified and non-etherified S, C-1 of non-etherified S and C-1 of etherified G (**6**). In the alkali-dissolved lignin, this region was only attributed to the presence of C-4 in etherified S and C-1 in etherified G (**6'**) and can thus explain the difference in intensities.

One of the dominant regions in both spectra, the methoxy groups of the organosolv lignin were seen at a more downfield shift in the alkali medium compared to the d_6-DMSO (**20'**: 57.5, 58.0, 58.7 ppm vs. **22:** 56.0, 56.7, 58.3 ppm). A zoomed-in view of this region is shown in Figure 2.5. This suggests that these groups were attached to aromatic rings that were affected by ionization, possibly due either to the presence of phenoxy groups or the conjugation effect of an ionized carboxylic group in the aliphatic side chain or a combination of both. According to Akim [82], an ionized phenolic group would have more impact on the shifts compared to conjugation from the side chain. This was also verified by an experiment which compared the methoxy group shifts of veratric

acid (*3,4-dimethoxybenzoic acid*) and syringic acid (*4-hydroxy-3,5-dimethoxybenzoic acid*) (Figure 2.6). As shown, the methoxy groups in the syringic acid, which has an ionizable phenolic group, gave a more downfield shift. On the other hand, the spectrum of the methoxy groups in veratric acid showed the presence of two distinct peaks because the ^{13}C nuclei in the two methoxy groups were not equivalent.

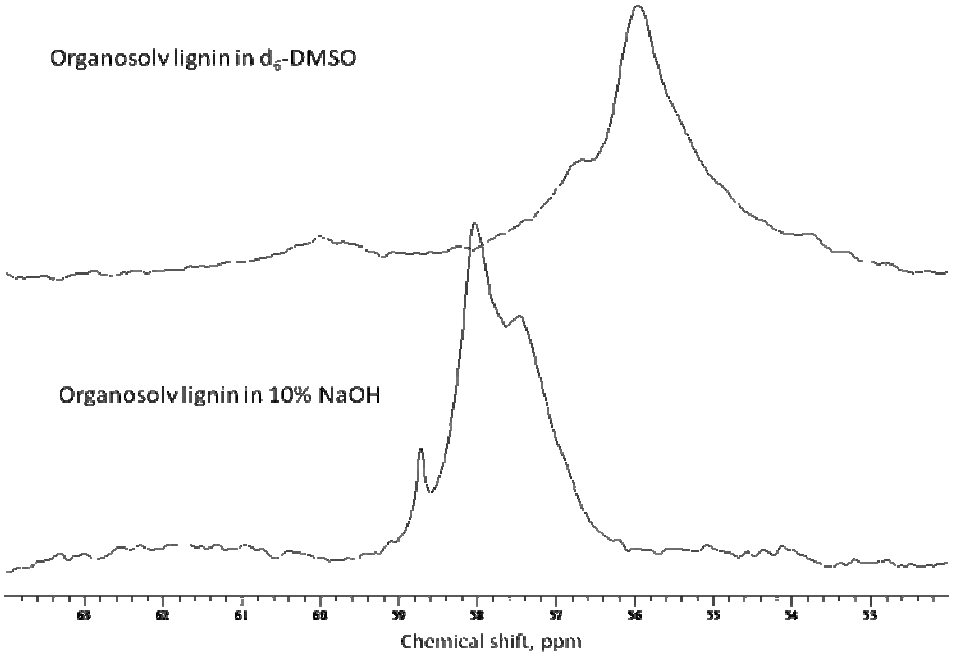

Figure 2.5 Methoxy groups of commercial organosolv lignin in d_6-DMSO (top) and 10% NaOH (bottom)

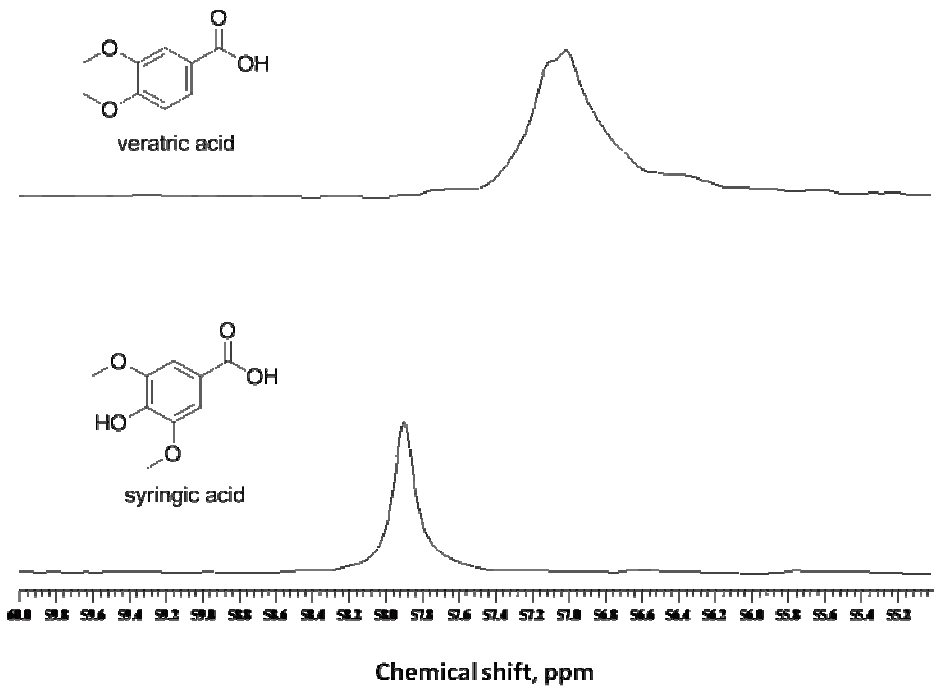

Figure 2.6 Effect of phenoxy group vs. carboxylic group in the shift caused by ionization in the methoxy groups of model compounds

2.3.3.3 Effect of reaction time

In a study done by Kadangode on the base-catalyzed depolymerization of organosolv lignin using 10% methanolic solution of KOH, a major difference in the GC-MS profile of the resulting BCD products (appearance of methylated aromatics) was observed at 290°C compared to lower reaction temperatures [70]. As such, 290°C was first used to test the BCD in this study. Since the batch autoclave system used required some time to reach the target temperature (heat-up time), reaction time was considered to begin only after the target temperature was reached. However, it is also considered that some reactions would have already occurred before the reaction temperature was reached. Heat up time from room temperature to 290°C was about 60 minutes.

Since NaOH is cheaper and more readily available than KOH, this base was tested first. Two reaction times, 15 and 60 minutes, were used.

Both reactions yielded a homogenous liquid product. Vacuum filtration using a qualitative-grade filter paper did not reveal any residue. (Though the starting material was fully soluble in the alkali medium, subsequent treatments at very high temperature and NH_4OH showed the presence of residue). ^{13}C NMR spectra of the liquid products of these two reactions are shown below, together with the starting material in Figure 2.7. As can be seen, no substantial difference was observed at the longer reaction time of 60 minutes. This lack of significant difference may be attributed to the amount of time at that it took to heat up the 500-mL reactor (60 minutes). During this time, the main reactions relevant to these two reaction times seem to have already occurred. Hence, 15 minutes was the reaction time used for further screening with other alkalis.

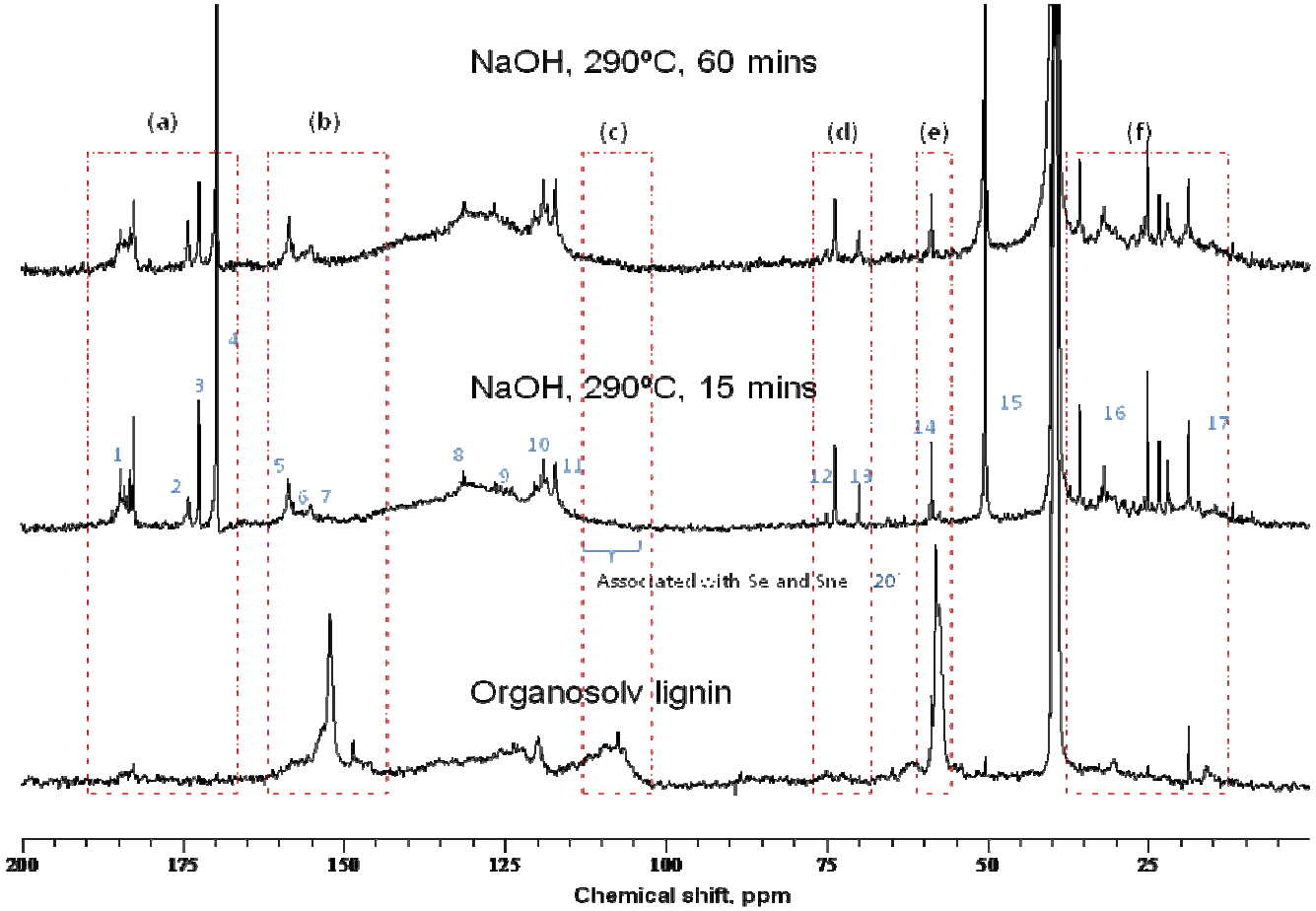

Figure 2.7 Spectra of NaOH-treated organosolv lignin at 290°C: BCD after 60 mins, BCD after 15 mins and starting material

Comparison of the spectra of the organosolv starting material and the BCD products at 290°C shows the following differences (Figure 2.7, a section denoted by a letter): (a) increased presence of peaks downfield of 168 ppm, primarily denoting the presence of more oxidized functional groups; (b) drastic reduction in the aromatic carbons associated with methoxy groups (144 to 162 ppm), particularly that of non-etherified syringyl carbons, causing peaks, associated with C-4 Gne to be more prominent; (c) drastic reduction of chemical shifts associated with C-2 and C-6 syringyl carbons; (d) marginal decrease of the methoxy groups (56-58 ppm), which used to be the 2nd most abundant functional group and formation of other alcohol functional groups, possibly aliphatic; (e) appearance of the peak at around 50 ppm which was assigned to methanol; and, (f) formation of more aliphatic functionalities. A more detailed assignment of the spectra is presented in Table 2.7. The chemical shifts listed for organosolv lignin in Table 2.6 are also included for comparison.

It is interesting to note that most of the peaks associated with syringyl functionalities seem to have been drastically reduced. Most notably reduced were the shifts from 107 to 112 ppm, which were previously exclusively assigned to C-2,6 in Se and Sne and from 152 to 156 ppm, which also contain the shifts for both C-3,5 in Se and Sne. This suggests that syringaldehyde groups were more susceptible to the BCD reactions than their guaiacyl counterparts. The results of a study by Sun et al. on the reactivity of bagasse syringaldehyde and guaiacyl structures to alkali and alkaline peroxide delignification prompted the authors to suggest a similar conclusion [83].

Table 2.7 ^{13}C shift assignments for NaOH-treated organosolv lignin at 290°C for 15 minutes [68]

Spectrum in 10% NaOH		Spectrum in 10% NaOH, 290°C, 15 minutes		
CS, ppm		#	CS, ppm	
182.6-184.9	β- , and γ-COOH , non-conjugated	1	182.6-184.9	β- , and γ-COOH , non-conjugated
		2	174.2	COOH in muconic acid structures
153.4-155.6	C-3 in Gne; C-3,5 in Se	3	172.5	β- OH, conjugated
152.2	C-3,5 in Sne; C-3 in Ge	4	169.8	C-4 in Gne with α-C=O
148.5	C-4 in Sne; C-4 in Ge	5	158.0-158.2	C-4 in Gne
137.7-138.5	C-1 in Se	6	154.8-155.6	C-3 in Gne; C-3,5 in Se
134.7-136.7	C-4 in Se; C-1 in Ge	7	152.40	C-3,5 in Sne; C-3 in Ge
128.8-130.7	C-5 in Ge subst	8	126.5-131.4	C-1 in Ge cond; C-1 in Ge with α-C=O; C-6 in G with α-C=O
125.5-125.9	C-1 in Sne	9	123.7-125.7	C-1 in Ge with α-COOH; C-6 in Ge
121.9-123.7	C-6 in Ge; C-5 in Gne	10	118.7-120.4	C-5 in Gne
120.1	C-6 in Gne	11	117.2	C-5 in Ge
119.7	C-5 in Ge	12	73.7	α- CH_2OH/$CH(CH_3)OH$
114.4	C-2 in Gne and Ge	13	70.0	unknown
108.6-110.1	C-2,6 in Se	14	58.8	OCH_3
107.4	C-2,6 in Sne	15	50.4	methanol
106.4	unknown (carbohydrates?)	16	23.5-37.0	-CH_2-
85.6-88.3	β- in β-O-4, α- in β-5	17	10.0-21.8	-CH_3
74.0-75.8	α- in β-O-4			
64.8	CH_2OH			
61.5	γ-CH_2OH			
57.5-58.7	OCH_3			
54.1	β in β-5 e			
50.3	β in β-5 ne			
23.5-37.0	-CH_2-			
10.0-21.8	-CH_3			

The following sections attempt to discuss in detail the effect on each of the specific functionalities formed or lost in the lignin BCD product at 290°C.

2.3.3.3.1 Carbonyl groups

Not too many functional groups have chemical shifts downfield of 168 ppm. A quick look at the ^{13}C NMR list of shifts revealed that this region typically involves the presence of carbonyl groups: aldehydes, ketones, carboxylic groups and their salts as well as some esters[3] [45]. The presence of these groups in the product mixture then suggests that oxidation of some bonds occurred, thus forming the carbonyl functionalities. Re-

[3] DEPT studies revealed that the shift at 172.4 ppm is actually a methine group that is possibly attached to a hydroxyl.

examining the reactions proposed by Gierer et al. [63] for reactions in alkali systems[4], carbonyls were suggested to be formed in the reaction of phenolic β-O-4 structures as quinone structures or β carbonyls (See Scheme 2.1). Aldehydes and ketones typically have shifts downfield of 190 ppm though conjugated systems with α, β unsaturation (R-C=C-CH=O or R-C=C-C=O) may be found downfield of 175 ppm. The range of 168 to 175 ppm is typically assigned to carboxylic acids and possibly some esters. Akim et al. [68] assigned 180.6 to 182.0 ppm to β- and γ-COOH in non-conjugated systems in 1 N NaOH and 172.7-174.5 ppm in d_6-DMSO. Aside from the non-conjugated carboxylic groups, reactions similar to lignin auto-oxidation at alkaline pH [87-88] or through the reaction with oxygen-derived radicals may have given way to muconic acid structures. Shown in Scheme 2.4 is the mechanism suggested by Ji, et al. [89] (adapted from Chang and Gratzl [90]). This would have involved a ring-opening reaction of the aromatic structure.

The formation of the peroxy anion can give way to formation of either (a) the muconic acid structure resulting from a ring-opening reaction or (b) the orthoquinone structure. In both pathways, methanol is a by-product through the removal of the methoxy groups (demethoxylation) from the aromatic ring. These could account for both the drastic reduction in the methoxy signals between 54-58 ppm and formation of methanol peaks at around 50 ppm. However, the absence of signals for C-3 and C-4 downfield suggests in the dienone species (~196 ppm) in most resulting BCD-spectra points to the formation of the of the muconic acid type moieties instead. Formation of

[4] Note that the reactions in [47] were originally suggested for pulping reactions which typically occur at temperatures around 165 – 170°C and has biomass as a starting material. Still, organosolv lignin was said to have relatively frequent amount of β-O-4 linkages since mostly α-O-C cleavages occur in acidic ethanol extraction.

these structures could also explain the reduction of the aromatic carbon nuclei between 148 to 160 ppm since these shifts were attributed to C-3and C-5 that are typically methoxylated [34, 68] .

On the other hand, formation of muconic acid structures have been reported even at room temperature in the autoxidation of t-butylsyringol and t-butylguaiacol in a span of 12 days [87]. Its formation was found to be pH dependent. Significant quantities were formed at about pH 11.65, relatively very small at ~ pH 10.4-10.6 and quite negligible at ~ pH 9.6-9.8 [87]. It must be noted that the pH of the BCD reaction products in the presence of NaOH and KOH ranges from pH 13.5 to 14.0.

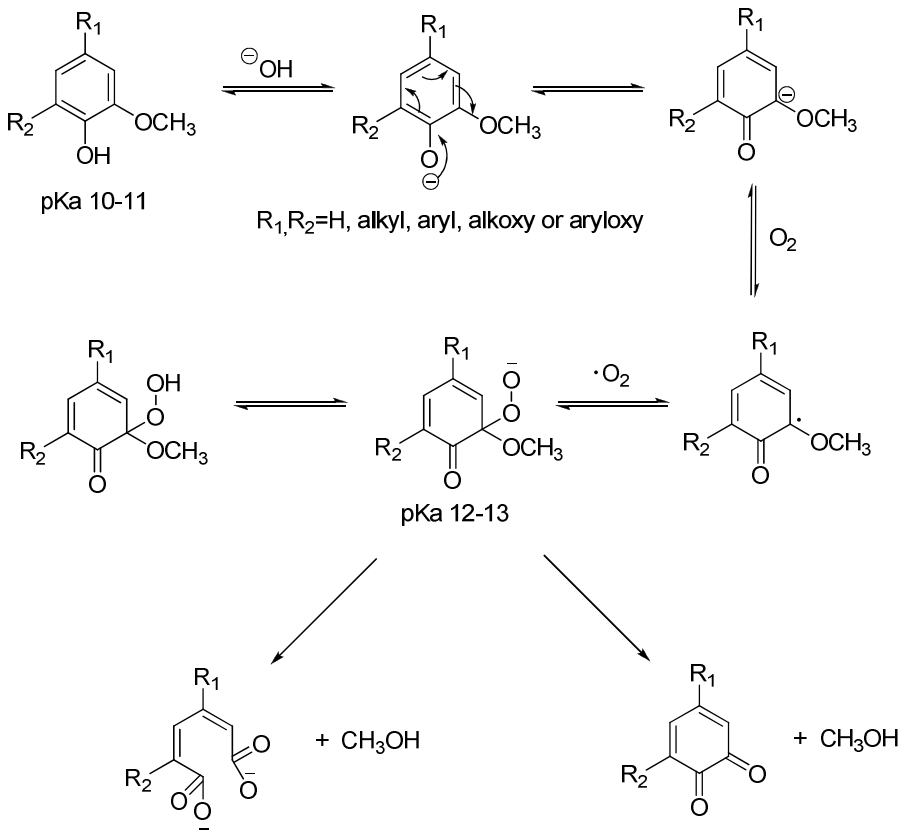

Scheme 2.4 Reaction of phenolic lignin in the presence of oxygen in alkali medium [89]

2.3.3.3.3 Demethylation

Alkali can also cause the demethylation of the methyl-aryl ether bonds to form methanol and a phenolate ion, as shown in Scheme 2.5. However, Gierer noted that at alkali pulping conditions (165°C), this reaction occurs only to a minor extent [63]. Since the methoxy shifts in the spectra were much reduced, it is possible that this reaction occurred to a much larger extent at higher temperatures. Indeed, the presence of large amounts of methanol (50 ppm) seems to agree with this assumption. This mechanism may also explain the formation of catechols as isolated products after the DCM extraction of the acidified BCD products.

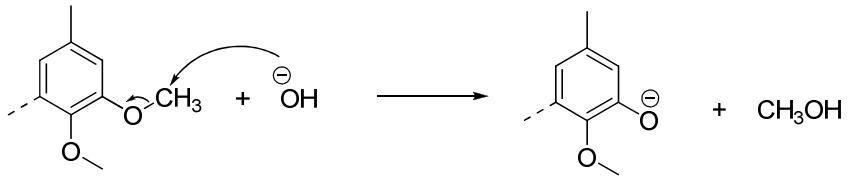

Scheme 2.5 Cleavage of methoxy groups during alkali pulping [63]

2.3.3.3.4 Aliphatic groups

Figure 2.7 showed the formation of alcohols at shifts around 70 and 74 ppm. This could be attributed to the cleavage of non-phenolic β-aryl ethers that result in the formation of hydroxyls in both C_α and C_β (see Scheme 2.3) [63]. The aliphatic range between 10 – 30 ppm also showed an increase in peaks. It has been reported that the amount of saturated CH_2 and CH_3 increase during oxidative delignification though there are no clear mechanisms yet for this phenomena [91]. Lastly, comparing DEPT spectra at 90° and 135° pulse angles revealed that the peak at about 172.4 ppm was a methine carbon, probably attached to an O-containing functional group.

2.3.3.4 Effect of reaction temperature

To determine the effect of reaction temperature on the BCD of organosolv lignin, four temperatures (165°, 210°, 290° and 350° C) were tested in the presence of 10% NaOH. The lowest temperature, 165°C, was tested because this is typically used for Kraft pulping [62] . The intermediate temperature, 290°C was chosen because it showed more than 90% yield of ether solubles based on Kadangode's work [70]. The highest temperature used in this study, 350°C was higher than the highest (310°C) used by Kadangode [70].

Figure 2.8 shows the ^{13}C NMR spectra of the liquid products of the 10% NaOH-catalyzed depolymerization products of organosolv lignin. All of these were run in batch for 15 minutes at the target reaction temperature. Changes in regions to note as temperature was increased were as follows: (a) formation of carbonyl groups; (b) reduction of aromatic carbons associated with shifts, typically associated with syringyls; (c) shifting of the aromatic peaks downfield, suggesting the nuclei were relatively more deshielded, probably because of the presence of more electronegative (i.e. O) atoms; (d) drastic reduction of the C-2 and C-6 S and Sne groups, suggesting higher susceptibility of the syringaldehyde groups to BCD; (e) drastic reduction of attached methoxy groups and formation and decrease of C nuclei associated with alkyl –OH groups; (f) formation of methanol, probably as by-product of the demethoxylation as well as the C-γ cleavage; and, (g) formation of more alkyl groups.

Comparison between the starting material and the resulting BCD product at 165°C (typical Kraft pulping temperature [62]) showed that most of the structural features of the lignin remained intact, though some differences do exist. The amount of

oxidized groups (carboxylic and hydroxyl groups) have slightly increased as evidenced by the appearance of the peaks between 168 – 175 ppm as well as the more noticeable carboxylic group shifts around 182 – 187 ppm. Formation of some muconic acid type structures seemed to have occurred already. There was minimal difference in the aromatic region as well as in the methoxy groups. A slightly higher intensity peak at around 50 ppm hinted at the possibility that some demethoxylation process had occurred as well.

BCD at 210°C showed further increase in shifts in the regions downfield of 168 ppm. The intensity of the shift attributed to methanol also increased. Additionally, more noticeable peaks appeared in the aliphatic region between 10 – 37 ppm.

Major differences were noticeable at 290°C and 350°C. Kadangode commented that a "profound change" in the composition of the BCD products was seen starting at 270°C in a KOH-ethanol system and was even more pronounced at 290°C [70]. Most of the changes previously mentioned occurred around this temperature. As already mentioned, more carbonyl groups seemed to have been formed at this temperature. Because of the addition of oxygen groups, it is suggested that the aromatic nuclei became more deshielded such that there were relatively more shifts downfield. Additionally, the large shifts between 152 to 156 ppm that were a feature from the starting material up to 210°C all but vanished. These shifts were attributed to C-3 in Ge and Gne as well as C-3 and C-5 in S and Sne units. However, it seems more logical to suggest that it was the syringyl units that were more affected as this will be compatible with the drastic reduction/disappearance of the peaks between 105 – 112 ppm. These peaks were associated with lignin C-2 and C-6 Se and Sne units. As previously mentioned, this

suggests that syringyl units seem to be more susceptible to BCD than their guaiacyl counterpart. This insight might be used to evaluate which lignin starting material will be more suited for base depolymerization as compared to other biomass feedstock (i.e. hardwood and non-woody sources with more syringaldehyde groups versus softwoods). Also at 290°C, the most drastic reduction in the methoxy groups occurred, accompanied by an increase in the shift associated with methanol. Other changes include formation of alkyl alcohol units and more alkyl groups. Possible reactions that caused the formation and presence of these structures have been discussed earlier in other sections of this chapter.

Features of the spectrum of the liquid product following BCD at 350°C for 15 minutes showed similarities with the 290°C spectrum. However, some shifts have vanished, suggesting that further reactions occurred at this temperature. These include removal of the (a) hydroxyl shifts at 70, 74, 75 and 172.5 ppm which suggested reactions involving these aliphatic alcohol side chains; (b) the methoxy groups had decreased further in tandem with a noticeable decrease in aromatic signal around 156 to 158 ppm; and, (c) methanol shift became smaller. Reduction of the aliphatic alcohols in the course of delignification has been reported to be probably due to the progressive elimination of the C_α hydroxyl groups as well as the elimination of the γ carbons to release formaldehyde, forming condensed β-guiacoxy styrene structures [92].

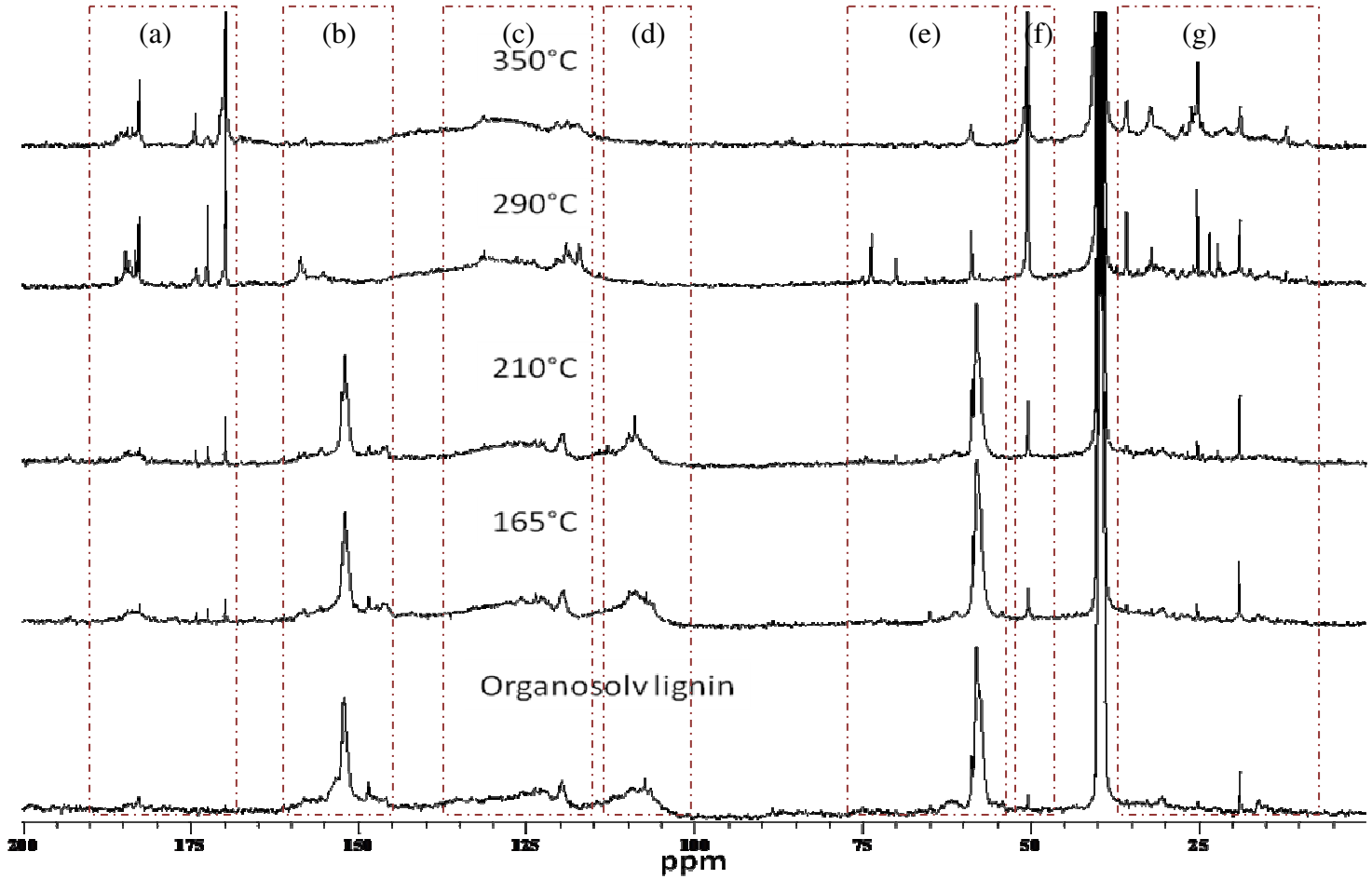

Figure 2.8 ^{13}C NMR spectra of NaOH-catalyzed organosolv lignin depolymerization at various temperatures, for 15 minutes

Figure 2.9 shows the relative percentage components of the different functionalities identified in the ^{13}C NMR spectra of NaOH-catalyzed BCD products at different temperatures. The integration values taken out of the spectra in Figure 2.8 were corrected for insufficient delay time by comparing the integration of the spectra of a BCD product without $Cr(acac)_3$ using d_1 = 10 sec and 10 000 scans for 33 hours machine time ([46, 79]) and one using the typical procedure (100 µL saturated $Cr(acac)_3$ in d_6-DMSO per 1 ml of liquid product, d_1 = 1 sec, 20 000 scans and 12.5 hours machine time). The loss of quantitativeness of the procedure optimized for the starting material dissolved in d_6-DMSO may be due to the much lowered amount of relaxant present in the analyzed sample due to crashing out of solution of the $Cr(acac)_3$ in the mainly aqueous alkaline medium. However, by compensating with correction factors for underestimation or overestimation of the different shift ranges, a semi-quantitative approximation of the functional group percentage can be presented and trends can be followed, as in Figure 2.9.

As previously discussed, an increase in temperature from 165°C to 290°C showed increasing carboxylic groups (188-192 ppm, 168-176 ppm) as well as methanol (50-51 ppm) and aliphatic groups (10-37 ppm). The drastic disappearance of the methoxy groups at 290°C can also be seen (55-60 ppm). At this temperature, there was also a sudden reduction in the amount of carbon nuclei attributed to C-2 and C-6 of the syringyl units (102-112), leading to the conclusion that syringyl groups were more susceptible to BCD than guaiacyl groups. Lastly, Figure 2.9 also reflects the formation and then degradation of alkyl alcohol groups (60-95 ppm).

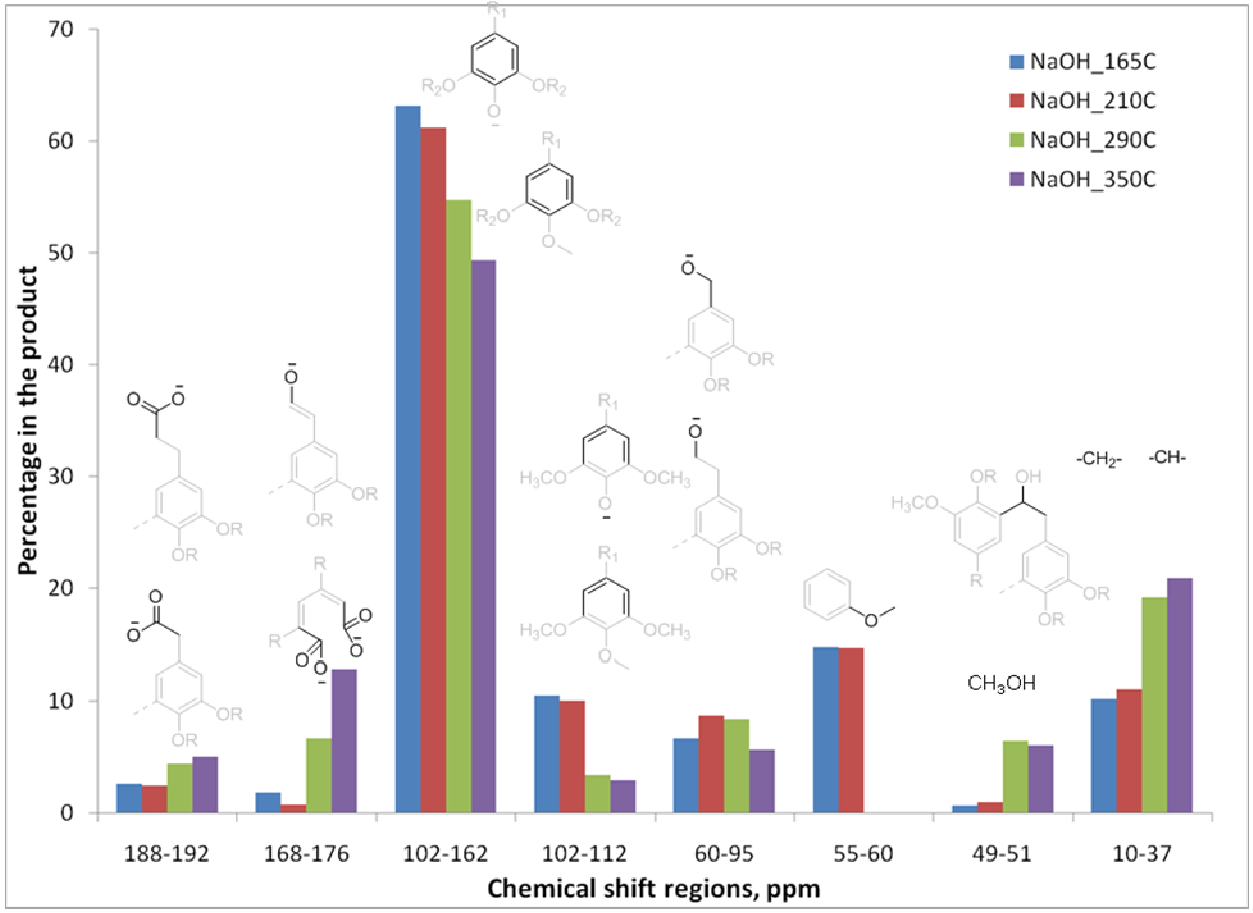

Figure 2.9 Relative functional group composition of NaOH-catalyzed BCD at different temperatures

Aside from changes in the liquid product NMR spectrum, some solids were recovered at the end of the 350°C experiment, amounting to about 6.3% of the lignin fed. This was unlike the previous runs at lower temperatures which were typically fully soluble. The formation of these solids can be possibly explained by condensation and repolymerization reactions. A similar observation, i.e. increased formation of solids at temperatures higher than 300°C, was noted by Cheng, et al. during the liquefaction of woody biomass in the presence of alcohol-water co-solvents [93]. XRD analysis of the residue formed showed the diffraction pattern associated with turbostratic carbon. It must be noted though that in this instance, there were other compounds present that could have contributed to the solid formation such as furfurals, etc. [93].

For lignin itself, formation of solids at higher temperatures has been reported for pyrolysis [94], in the presence of water-phenol solvent and supercritical water [95] as well as in repolymerizations that occur at higher temperatures in alkali and kraft pulping [62]. Alkaline condensations typically involve the activation of the unsubstituted aromatic C-5 position. Formaldehyde, formed as by-product of the cleavage of the C_γ, may participate in the reaction, as shown in Scheme 2.6.

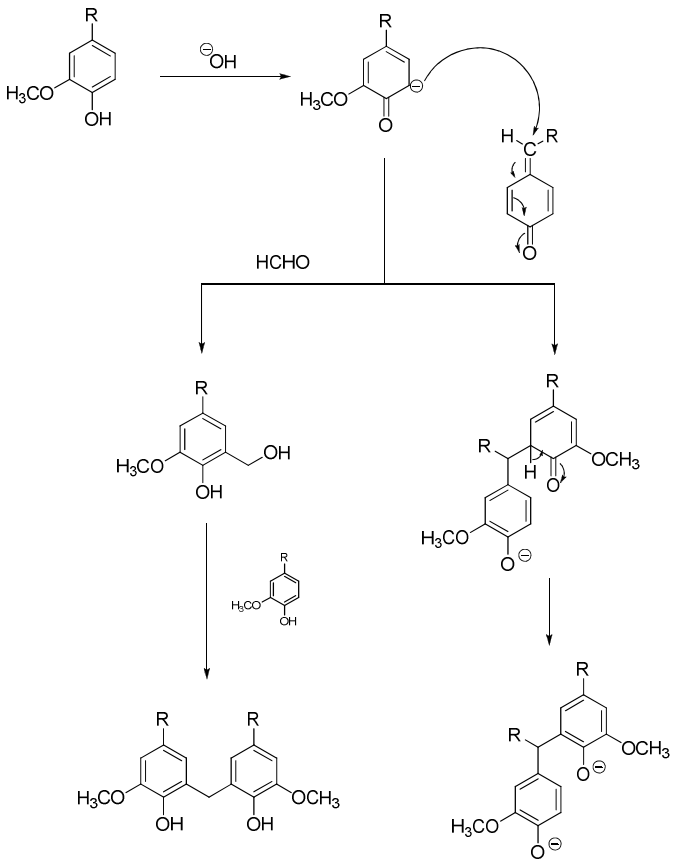

Scheme 2.6 Condensation reactions of phenolic units in alkaline reactions [89, 96]

2.3.3.5 BCD with KOH

Aside from NaOH, KOH was also used as a catalyst. KOH was used in the BCD study done by the University of Utah, in collaboration with National Renewable Energy Laboratory (NREL) as well as in the studies done by Sandia National Laboratories. They were typically in the presence of alcoholic solvent, mainly methanol and ethanol [70, 73, 75]. In this study, only aqueous KOH was tested. Results of the ^{13}C NMR of these runs, compared with the NaOH-catalyzed products are shown in Figures 2.10 – 2.12. As

shown, the spectra of NaOH and KOH-catalyzed products gave similar shifts suggesting similar pathways undergone by the organosolv lignin. The previous studies mentioned did not report any ^{13}C NMR spectra.

Figure 2.13 gives the relative composition of the functional groups present in the KOH liquid product. The trends seen in this graph are similar to those seen with NaOH (Figure 2.9), as expected from their similar ^{13}C NMR spectra.

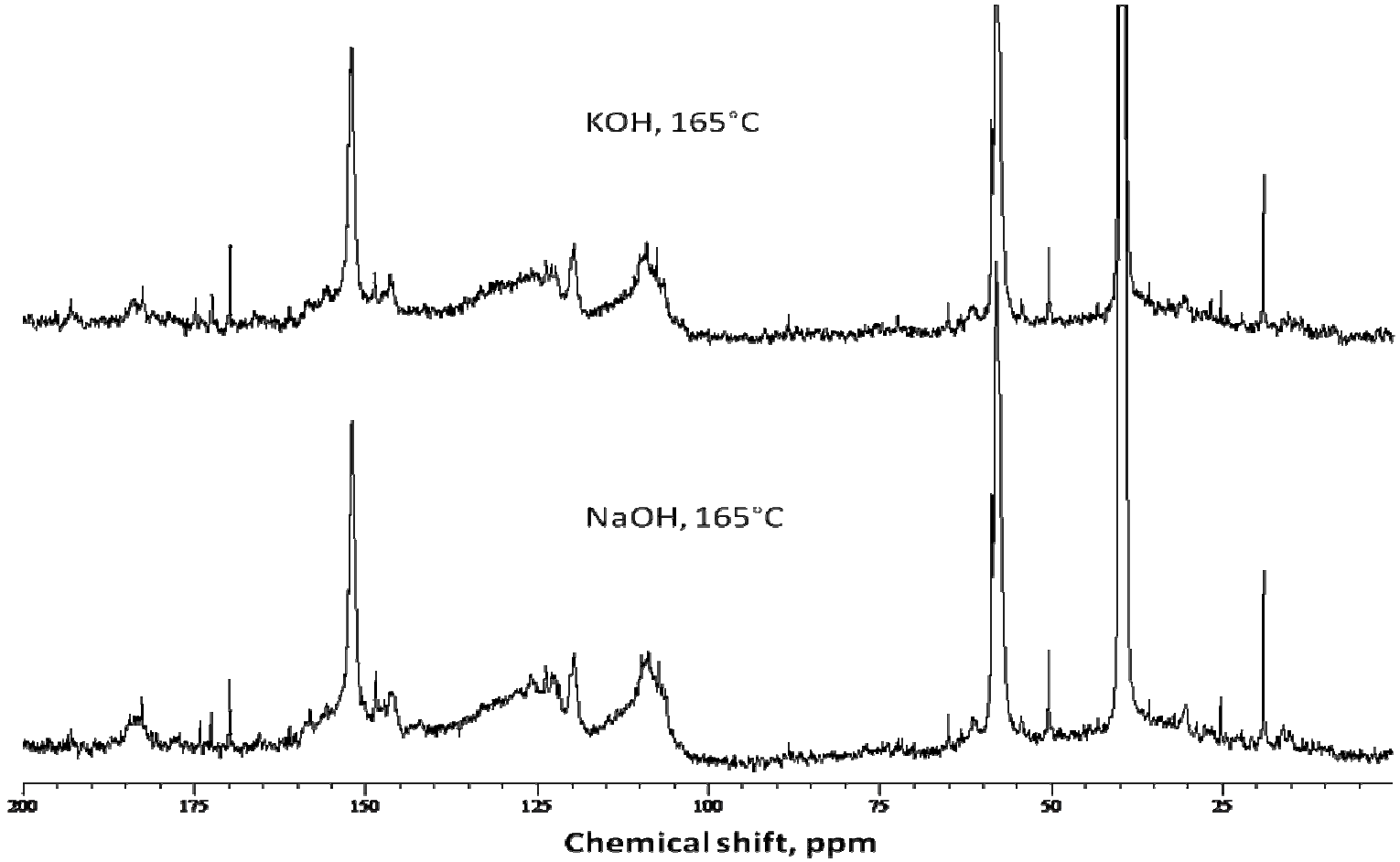

Figure 2.10 ^{13}C NMR spectra of KOH- and NaOH- catalyzed reactions at 165°C

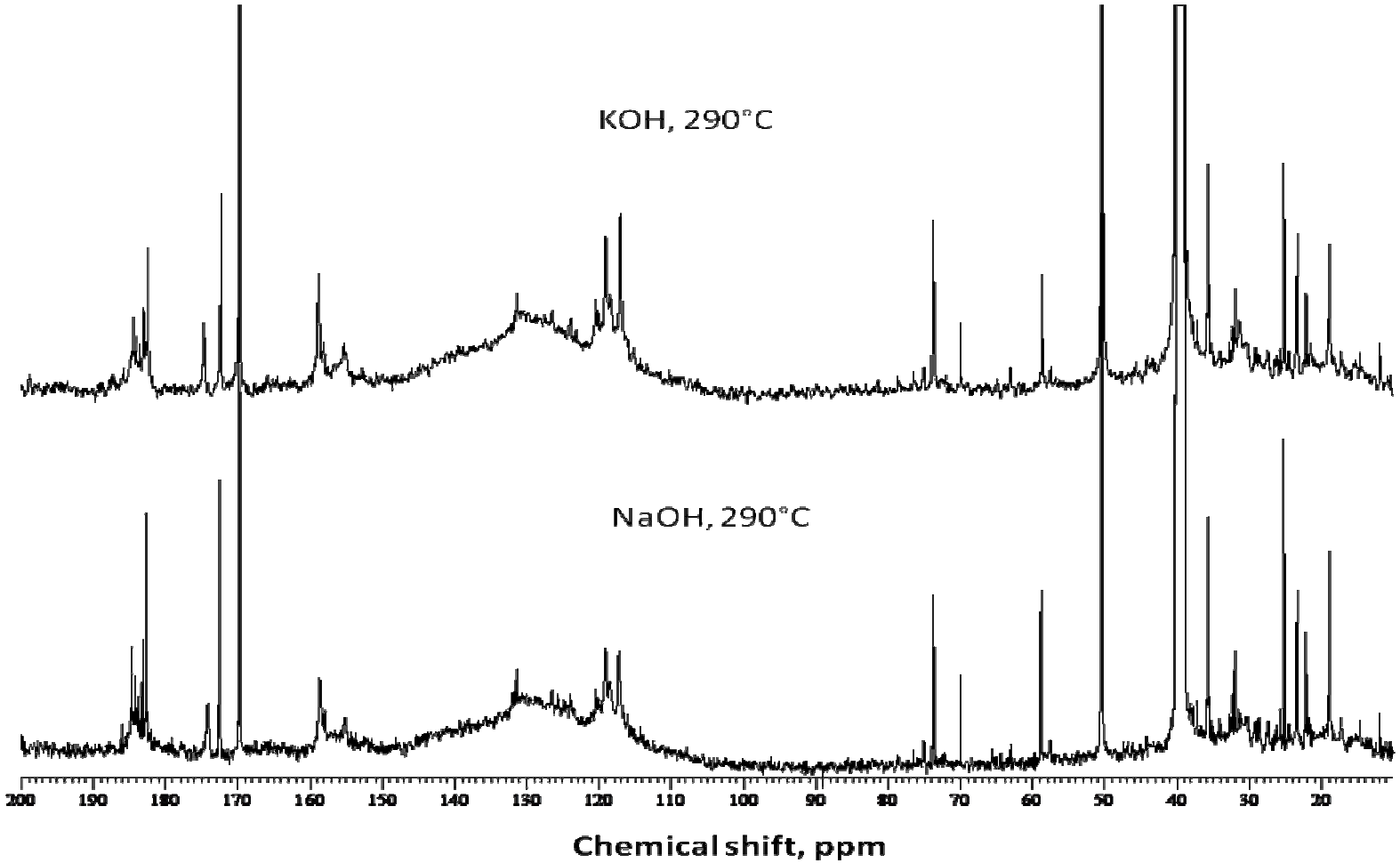

Figure 2.11 ^{13}C NMR spectra of KOH- and NaOH- catalyzed reactions at 290°C

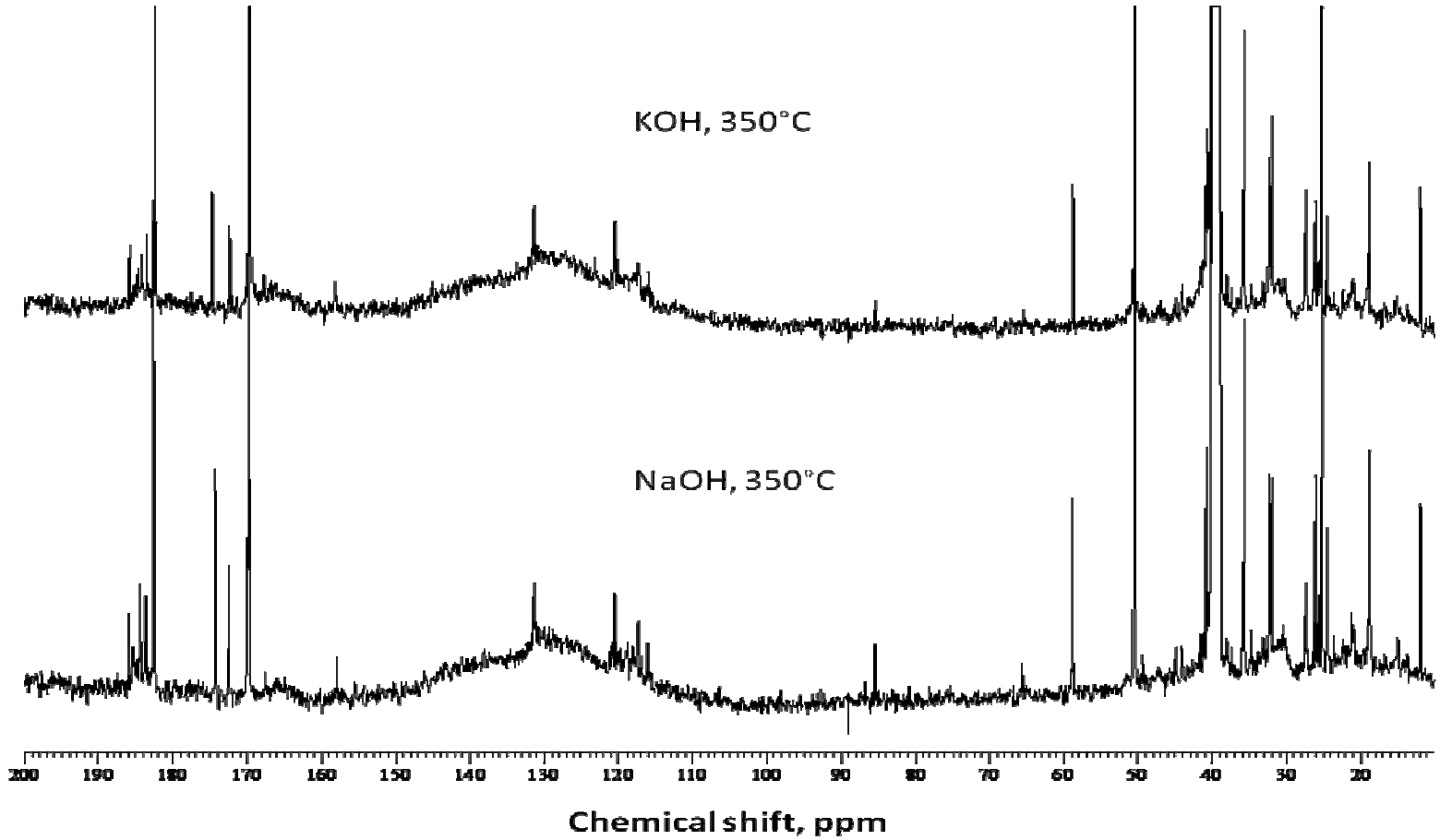

Figure 2.12 ^{13}C NMR spectra of KOH- and NaOH- catalyzed reactions at 350°C

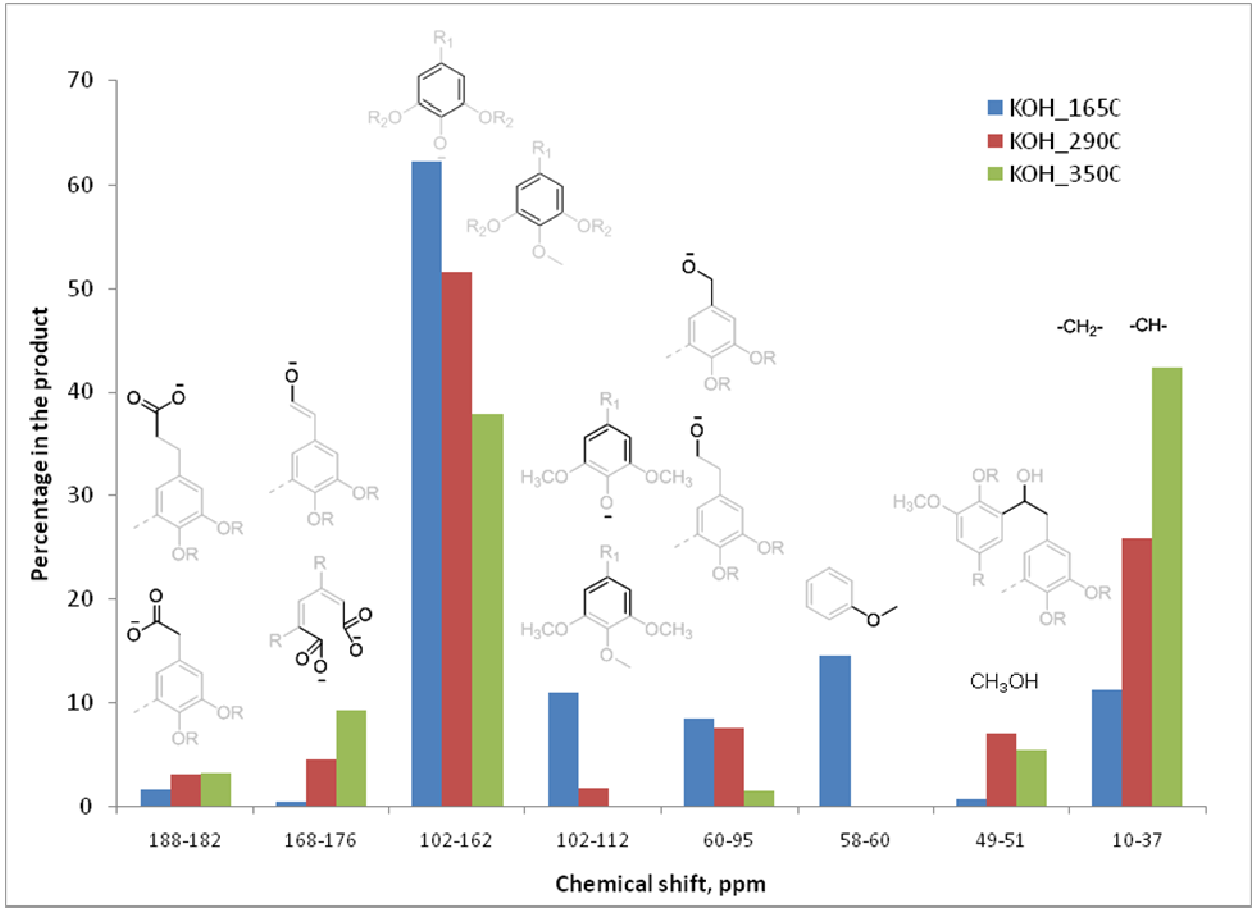

Figure 2.13 Relative functional group composition of KOH-catalyzed BCD at different temperatures

2.3.3.6 BCD with NH_4OH

Ammonium hydroxide was used as another base for the depolymerization of lignin. One reason was that NH_4OH may be converted to NH_3 gas and it was hypothesized that this might be a good route for separation downstream. Figure 2.15 summarizes the ^{13}C NMR spectra comparing the products of the NH_4OH- catalyzed experiments at different temperatures and will be discussed shortly.

Figure 2.14 shows a comparison between the spectra of the organosolv lignin, NaOH- and NH_4OH-catalyzed reactions at 290°C. As shown, the NH_4OH- catalyzed spectra showed distinctly different features especially at 290°C and 350°C. The main expected shifts were still present in the NH_4OH products: (1) aromatic carbons (105–162 ppm) **(b)** ; (2) aromatic shifts attributed to carbons with methoxy groups (148–156 ppm) **(b)**; (3) methoxy groups (56–58 ppm) **(d)**; (4) methanol (50 ppm) **(e)**; and, (5) aliphatic groups (37 – 10 ppm) **(f)**. However, comparison with the NaOH-product and NH_4OH-products shows different shifts in the carbonyl region (**a)** and in the aliphatic alcohol region **(d)** and **(e).** The reasons for this may be: (1) different reaction mechanisms that incorporate $–NH_2$ instead of –OH into the lignin; and (2) NH_4OH-catalyzed BCD yielded solids, which may actually contain the "missing" functional groups. At 165°C, about 60.6% solids were collected. For 290°C, this amount decreased to 37.2 %, while at 365°C, the amount of solids was about 51% of the original lignin fed.

At 165°C, the insolubility of most of the lignin was manifested in the weak intensity of the signals (Figure 2.14). However, at 290°C, the shifts became sharper, suggesting monomeric, or at most small oligomeric groups. (Broad shifts are typically associated with NMR spectra of polymers because of possible overlaps of shifts [45].)

The 290°C spectrum still showed the distinct presence of methoxy groups and the aromatic carbons associated with them, though more methanol as well as carbonyl groups were present **(a')**, as compared to the experiment done at 165°C. The carbonyl groups in **(a')** are expected to be attached to $–NH_2$ functionalities, to exist as an amide.

As previously stated, the presence of ammonia also seemed to introduce N-groups into the products **(a'** and **d')**. This is in line with what Capanema, et al. reported with respect to oxidative ammonolysis of lignin at lower temperatures (70°, 100°, and 130°C) but elevated oxygen pressures [97-100]. In the spectra presented in Figure 2.14, the distinct peaks associated with N-containing groups include the shift at 46.5 ppm which was assigned to a benzylic carbon attached to an amine, as well as the peaks between 166 and 167 ppm which were attributed to terminal carbonyl carbons attached to an amine [45]. Possible mechanism of N incorporation into the lignin is shown in Scheme 2.7. This is a modification of Scheme 2.3 which shows the β-O-4 cleavage of non-phenolic groups through the action of a hydroxyl moiety. Competing reactions between OH- and NH-incorporation were also noted by Capanema, et al. empirically by charting the elemental analysis ratio of C/N and C/O of their resulting products [98-99].

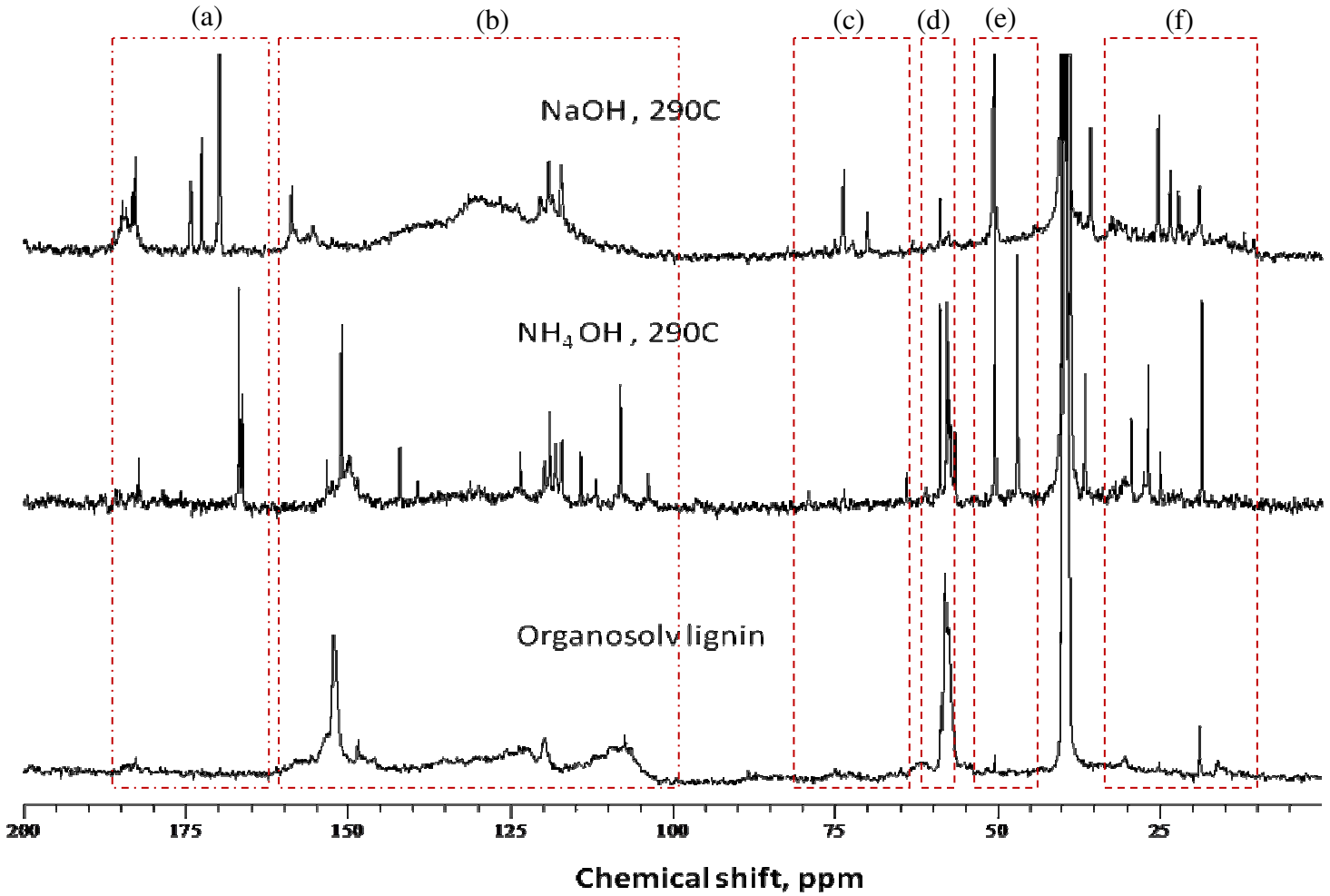

Figure 2.14 Comparison between the ^{13}C NMR spectra of the starting material and the liquid product of NaOH and NH_4OH BCD

The ^{13}C NMR spectrum of the NH_4OH-catalyzed reaction at 350°C showed the same general features as that of the 290°C spectrum. It can be noted that the distinctive carbonyl shifts in the stronger base catalyzed reactions were only minimally present (~182 ppm) **(a')**. This can be considered as indirect evidence of the competing reactions between O- and N- incorporation. It is also possible that these carboxyl groups were present in the solids that crashed out of the solution and were thus not accounted for. Due to the lower pH after NH_4OH reactions (pH ~10 – 10.5 (NH_4OH) vs. pH ~13.5 – 14 (NaOH)), there is a possibility that these acidic groups were no longer ionized and thus, insoluble in water.

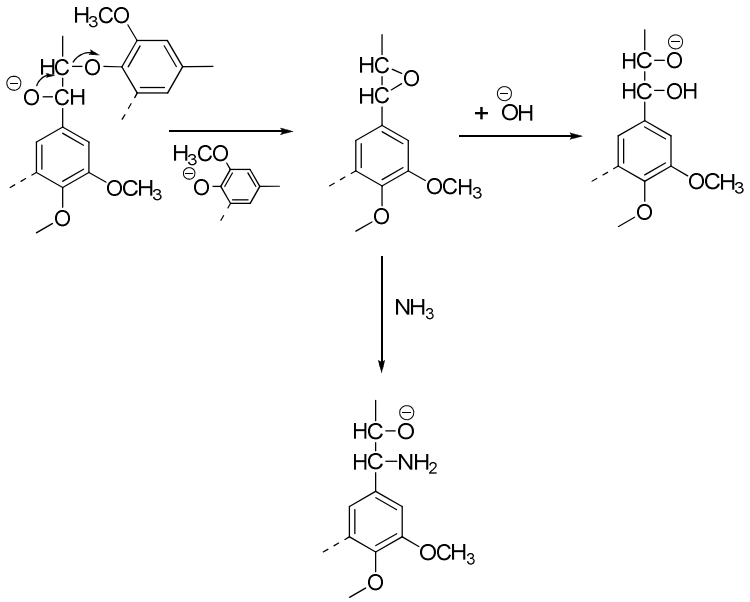

Scheme 2.7 Mechanism of N-incorporation during β-O-4 cleavage showing competing reaction with O-incorporation, modified from [63]

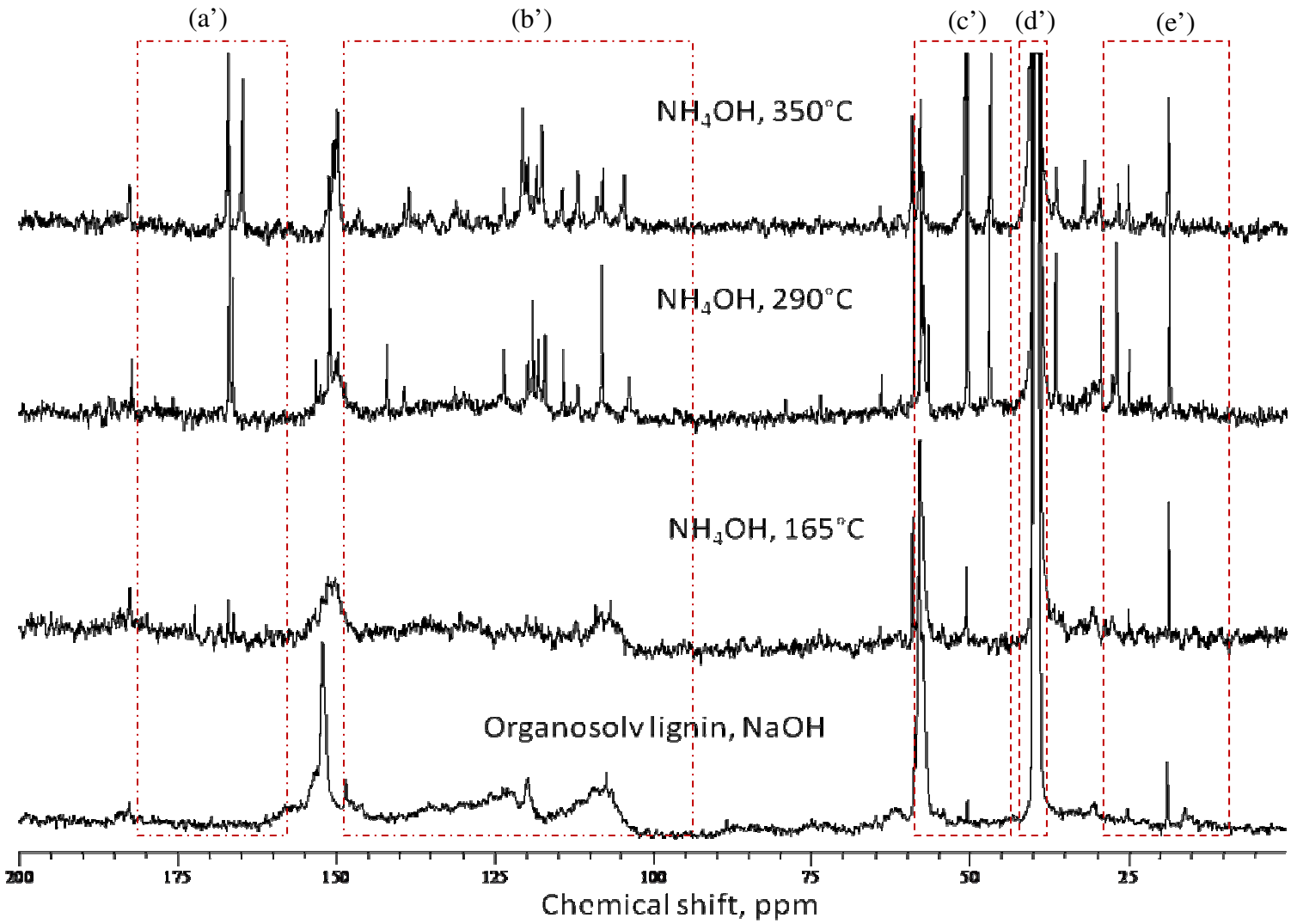

Figure 2.15 ^{13}C NMR spectra of NH_4OH-catalyzed reactions at different temperatures

Figure 2.16 shows the relative composition of the NH_4OH-catalyzed BCD reactions. The most notable trends lay in the increase of the amide containing groups (164-176 ppm) as well as of the alkyl groups, though with a less dramatic increase compared to the other bases (10-37 ppm). The decrease in methoxy groups (58-60 ppm) was accompanied by an increase in the methanol signal at 49-51 ppm.

2.3.4 Gel permeation chromatography

Since depolymerization was the goal of this study, the resulting molecular weights of the resulting BCD product need to be determined. Gel permeation chromatography (GPC) is the most commonly used technique in measuring molecular weights. Another name for this type of chromatography is size exclusion chromatography. The mechanics are similar to HPLC where a liquid solvent (eluent) carries the sample from the injection port through a column that has the capacity to segregate compounds, based on chemical property (HPLC) or size of the molecules (GPC). Polymer standards with narrow polydispersities, such as poly(styrene) (typical for organic) or poly(ethylene glycol) (PEG, for aqueous-phase) were used to calibrate elution times with actual molecular weights. The sample needs to be fully soluble in the eluent, or the values derived will not be representative of the actual molecular weight of the sample.

GPC has been used in the analysis of lignin. Baumberger, et al. published a paper summarizing GPC parameters that have been used and determined the best conditions for aqueous and organic phase GPCs [101]. They recommended the use of 0.5M NaOH/TSK Toyopearl HW-55 (F), with the eluent flowing at 1ml/min at 25°C. According to them, the Toyopearl gel was stable, adsorption of lignin onto the column was low, and interlaboratory reproducibility was high. Results were found to correspond with the

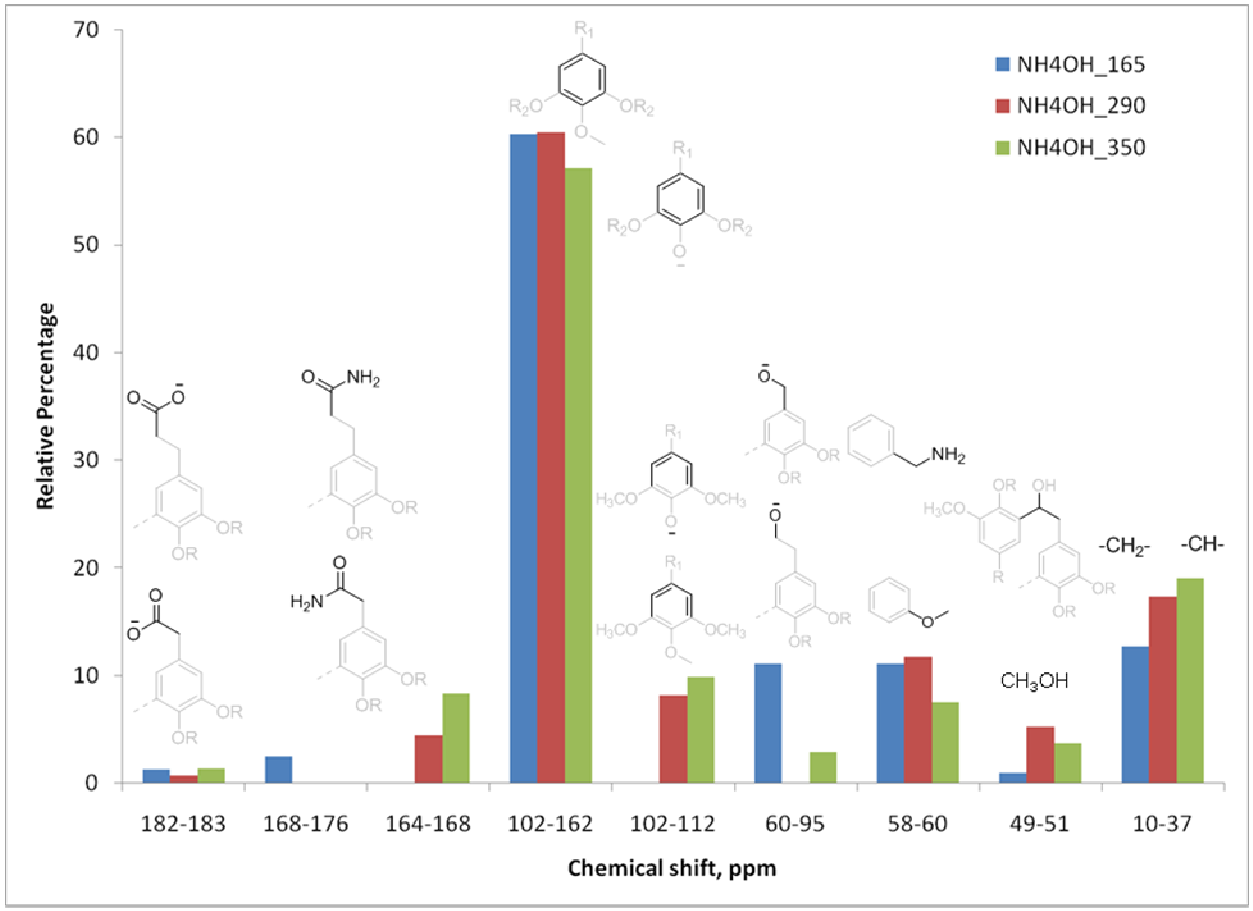

Figure 2.16 Relative functional group composition of NH_4OH-catalyzed BCD at different temperatures

DMSO and DMAc- data gathered previously. For organic GPC, the authors recommended the use of THF/SDVB PL Gel, flowing at 1 ml/min at 25°C [101].

Chen and Li used aqueous GPC for their study of lignosulfonates and alkali lignins [102]. They noted that in aqueous GPC, secondary effects, such as ion exclusion, ion-inclusion, ion adsorption and adsorption of elutes could affect the retention volume of the solutes, aside from its hydrodynamic volume. In the presence of carboxyl, phenolic, hydroxyl, and sulfonated groups in lignins, secondary effects will be present – thus showing erroneous results. To counteract this, pH and ionic strength can be tuned [102] . Similar to the conditions recommended by Baumberger et al. [102], the eluent used should be at high pH (~pH 12) and in the presence of salts (0.1M $NaNO_3$).

On the other hand, association of lignin in DMF has also been reported [103] . In order to remove association forces, LiCl was added. Current procedures for analyzing lignin in organic solvent, usually THF, include acetylation of the sample to insure complete solubility [29-30, 104]. Acetylation will also cap most of the functional groups that cause secondary interactions, as mentioned in [102].

Owing to the variability in the structure of lignin, we attempted to use universal calibration instead of the typical conventional calibration that assumes that the standard is the same chemically as the sample [105]. The universal calibration requires two detectors: one for measuring the intrinsic viscosity and another for the concentration of the polymer. This was possible in a viscometer-refractive index (RI) detector tandem in a Polymer Labs GPC. However, this GPC uses an organic eluent, THF, thus requiring acetylation of the evaporated samples.

Ideally, an aqueous GPC set at very high pH with the viscometer-RID capability would have been better choice because this means that no modification would be necessary to be done on the alkali-soluble product. However, due to the absence of this instrument, acetylation was done. Acetylation was said to give good results compared to the as-is lignin starting material [101] but it is conceivable that processed samples might have different response to the process.

Figures 2.17 to 2.19 show the MW distributions of the BCD products with the actual traces as insets. These samples were generated from the evaporated liquid product fractions which were then acetylated following the procedure previously indicated. For the NH_4OH-BCD generated solids, solubility was not much an issue. For the NaOH and KOH products, some solids were not completely solubilized during the acetylation, though these fractions were at most about a tenth of the solids initially used for acetylation. The results reported here reflect the trends in the soluble components of the acetylated products. It is possible that the insoluble solids were higher molecular weight fractions. In general, the traces showed increasing amounts of smaller molecular weight fractions with respect to the original lignin. However, due to possible repolymerization reactions at 350°C, the MW of the KOH- and NaOH-BCD samples slightly increased compared to the MW at 290°C. This was more apparent in the NH_4OH-catalyzed experiments. However, it must be noted that only the soluble products were analyzed here. As mentioned, NH_4OH-BCD at increasing temperatures formed more insoluble solids.

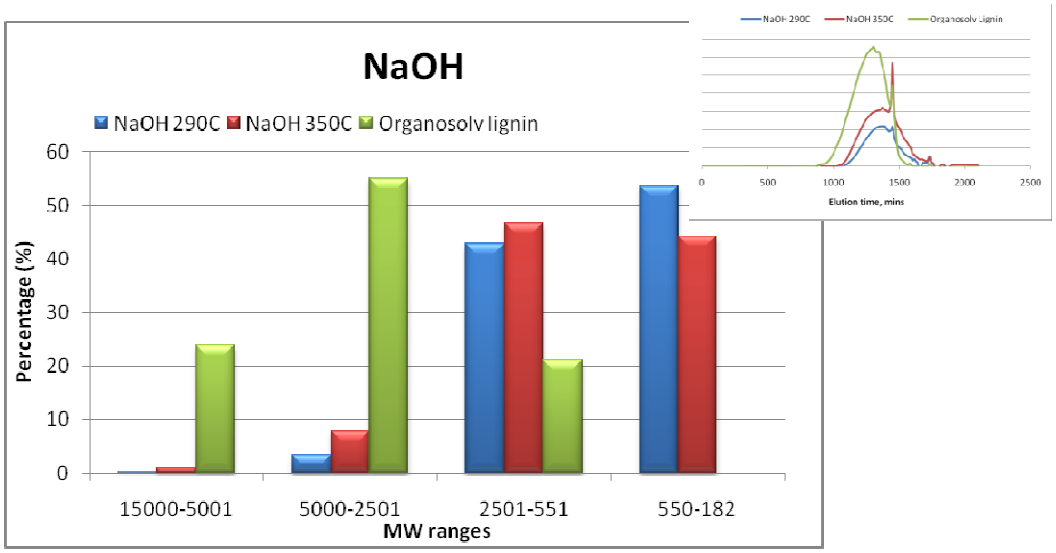

Figure 2.17 THF GPC traces and MW distribution of acetylated NaOH-BCD products at 290°C and 350°C

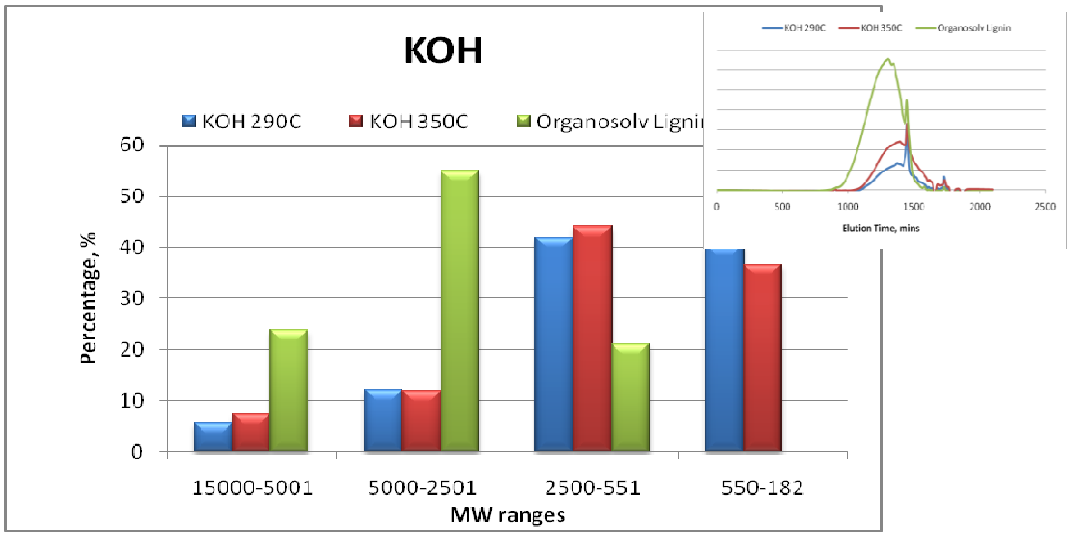

Figure 2.18 THF GPC traces of acetylated KOH-BCD products at 290°C and 350°C

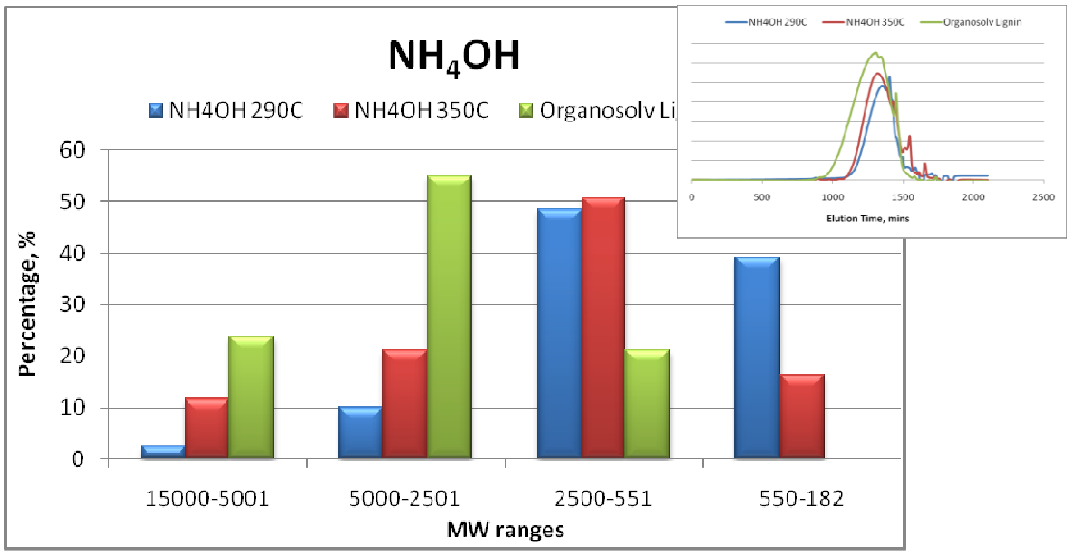

Figure 2. 19 THF GPC traces of acetylated NH_4OH-BCD products at 290°C and 350°C

2.3.5 Monomeric products of BCD reactions

Identification and quantification of monomeric products were done on the dichloromethane (DCM) extract of acidified (pH = 2) liquid products using a Shimadzu QP 2010 GC-MS/FID system. External calibrations of specific compounds were done without an internal standard. Compounds that were quantified include the following (Figure 2.20):

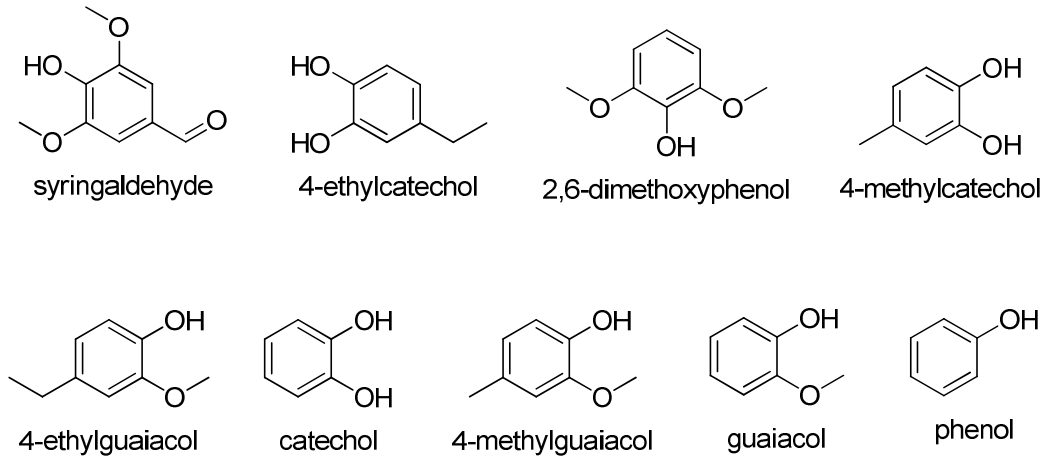

Figure 2.20 Identified and quantified compounds from DCM-extracted BCD products

Figure 2.21 summarizes the amount of monomeric products isolated and produced at different temperatures using NaOH as the base catalyst while Figure 2.22 presents the same information for KOH as base catalyst. Both bases show similar overall trends in the monomer product formation. Catechol, which was not isolated at 165°C was the major product at 290°C. Its amount dropped down at 350°C which may be attributed to further oxidation reactions [106]. Increased oxidation at higher temperatures was also reflected in the results of the ^{13}CNMR analysis. Syringaldehyde and 2,6-dimethoxyphenol were also identified as products in relatively large quantities in these experiments. Phenol was shown to continuously increase with increasing temperatures. Both KOH and NaOH are similar in that the amount of the identified products was at a maximum at 290°C.

Such was not the case for the NH_4OH-catalyzed experiments (Figure 2.23). As the temperature was increased, the total amount of the isolated compounds also increased. Another difference was the lower number of identified compounds such that phenol together with guaiacol and 4-methylguaiacol were not identified. The amount of the

monomeric products identified in all the reactions did not exceed 5% of the starting material (KOH at 290°C), suggesting that most of the products, though soluble were actually soluble oligomers or polymers or were not identified.

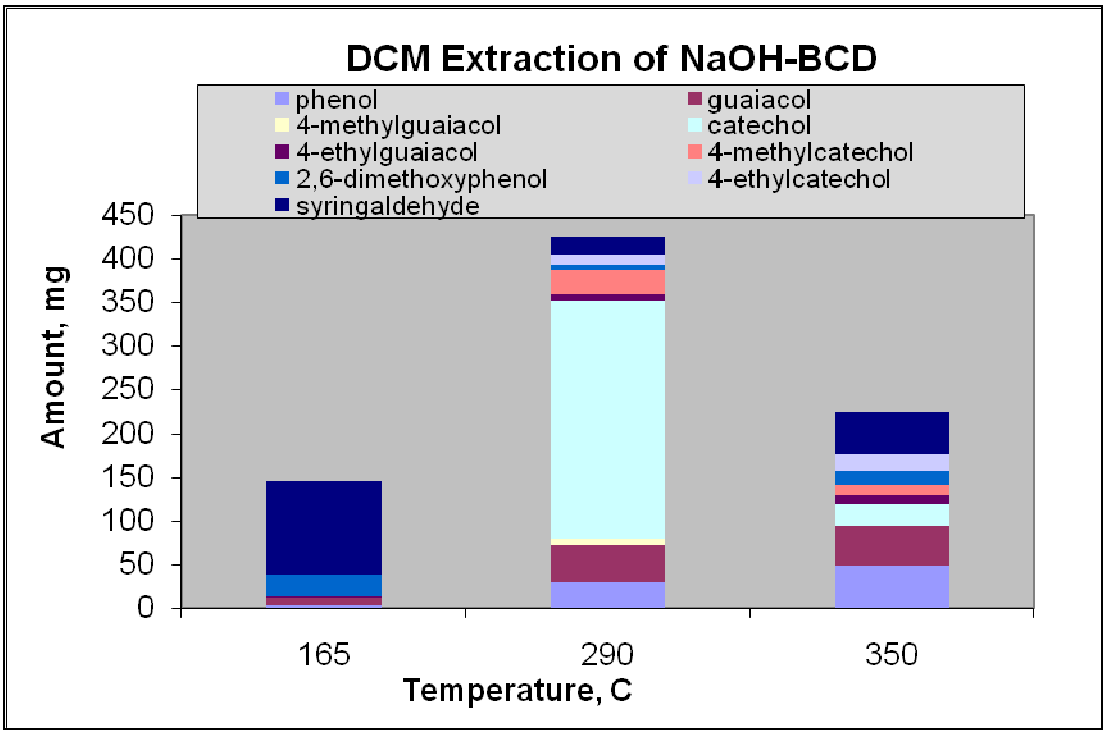

Figure 2.21 DCM extraction product of NaOH-catalyzed experiments

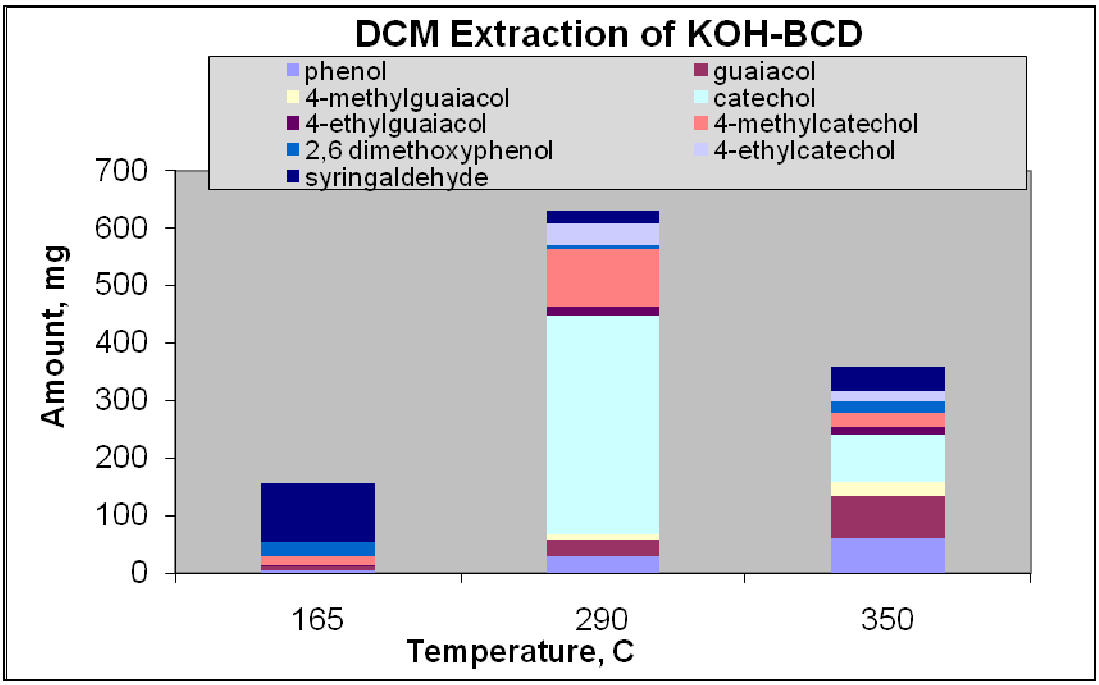

Figure 2.22 DCM extraction product of KOH-catalyzed experiments

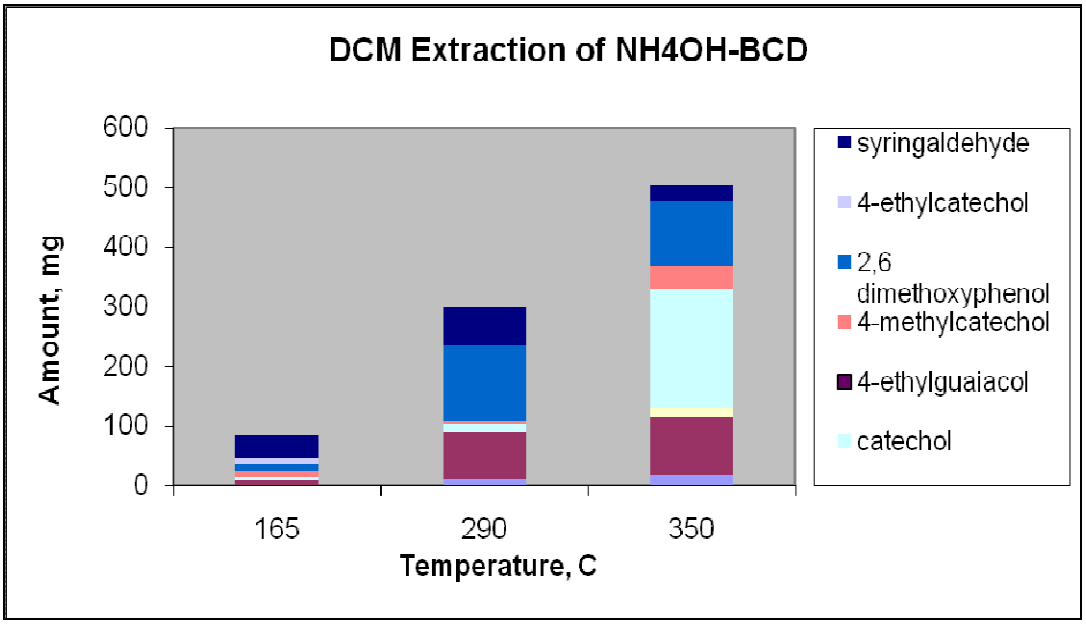

Figure 2.23 DCM extraction product of NH_4OH-catalyzed experiments

2.4. CONCLUSIONS

This chapter dealt with the characterization of the starting lignin material as well as the products formed from base catalyzed depolymerization of this lignin. ^{13}C NMR was used extensively in order to get insights into the changes that occur in the different functional groups present in lignin at different conditions during BCD. A protocol for quantitative analysis of the starting material was developed through the use of inverse-gated decoupling protocol and the use of relaxant. The amount of relaxant, number of scans and the length of d1 (delay time) were optimized by calculating the ratio of the integrals between the methoxy and the carbonyls ($I_{56-57}/I_{166-172}$) until a minimum converged. From 33 hours of analysis time, this was successfully reduced to about 12.5 hours.

The results of the base-catalyzed depolymerization of commercial organosolv lignin using three different bases (NaOH, KOH and NH_4OH) were also reported. Except for runs at 350°C, both NaOH and KOH yielded fully soluble products at the end of the experiments, although less than 5 wt% of the starting lignin material were identified as the monomeric products. Gel permeation chromatography results point to the presence of larger species that may contain up to 10 monomer units. Whether this is the result of oligomerization or reploymerization is unclear at this time. However, NH_4OH-catalyzed depolymerization produced solids even at all temperatures. This might be attributed to the lower pH recorded at the end of the experiments as well as in the possible different reaction pathways due to the presence of NH_3 in the solution.

^{13}C NMR revealed changes in the functional groups of the lignin as temperature was increased. Oxidative reactions in the presence of high pH were considered to be the

main cause for the formation of the hydroxyl and carboxyl groups responsible for the solubility of the resulting products. Results also show that syringyl units seem to be more susceptible to BCD-reactions as evidenced by the loss of shifts (102-112 ppm). This insight will be valuable in deciding the feedstock to use to which staring material to use for possible BCD applications. However, for the conditions used, GC-FID quantification as well as GPC studies showed that the solubility of the BCD products did not readily translate to isolated monomers. The formation of carboxylic acids may have just facilitated dissolution but may not have translated to bond breaking. Furthermore, repolymerization and condensation reactions might have occurred as well.

Monomeric units identified include phenols, cathecols, guaiacols and syringaldehyde. Syringaldehyde, which contains three oxygen containing functional groups was used as a model compounds for the next study.

2.5 RECOMMENDATIONS

Analysis of the type and number of bonds of the starting material may prove to be a good screening tool to determine whether a lignin source will be successfully depolymerized. This can be determined through wet chemistry methods [34, 83, 107] or through spectroscopic means [51, 79, 108]. Another possibility is to use conditions that have the capability of quenching repolymerization reactions. This may include the use of hydrogen-donating solvents [109] or the presence of added hydrogen in the reactor. Inclusion of or replacement by metal-based catalysts capable of breaking the lignin linkages may also be used to produce more effective bond-breaking. A catalyst with high activity and recyclability may off-set the initial higher cost associated with the catalyst.

Lastly, elimination of the residual oxygen in the mixture may prove to be important and may thus be explored.

CHAPTER 3

BATCH HYDRODEOXYGENATION OF SYRINGALDEHYDE

Removal of oxygen from biomass-derived compounds is a critical step in order to produce a fuel or chemical feedstock resource that can be easily "dropped" into our existing petroleum-based infrastructure. One way of accomplishing this is through hydrodeoxygenation. This chapter discusses the hydrotreatment of syringaldehyde, a multi-functional lignin-derived model compound. A relatively novel hydrodeoxygenation catalyst, nickel phosphide, was used both as a bulk and as a supported catalyst. Other catalysts were also tested as a point of comparison with nickel phosphide; these included bulk nickel oxide and nickel phosphate as well as commercially available supported Pt/Al_2O_3 and Pd/Al_2O_3. The overarching goal of this study was to determine the hydrodeoxygenation reaction pathway of syringaldehyde, considering that it has aldehyde, methoxy and phenolic functional groups.

3.1 INTRODUCTION

3.1.1 The need for hydrodeoxygenation (HDO)

For years, biomass has been seriously considered as an alternative fuel and a chemical feedstock source [23]. The impetus for this is the now generally acknowledged dwindling capacity of fossil fuel supplies, which was foreseen by M. King Hubbert for the US in the 1950s [8-9], though others might agree to varying degrees with his prediction [110-113]. Petroleum, which had been and still is the major source of transportation fuels as well as chemical feedstock [2], is becoming scarcer and more

concentrated in areas associated with political turmoil or civil unrest. By creating and developing sustainable technologies based on biomass, important governmental considerations such as fuel security, stability and renewability will be addressed [12, 114]. Historically, these fossil fuels were derived from ancient biomass that have been buried in the earth for millions of years and have been acted upon by massive heat and pressure. However, the chemical make-up of current biomass sources is very much different from that of the fossil fuels from the ground. Therefore, technologies need to be developed for biomass-derived fuels to be efficiently integrated into existing petroleum infrastructure.

Huber et al. [115] summarized existing thermochemical biomass technologies into three categories: (a) gasification; (b) hydrolysis; and, (c) pyrolysis or liquefaction. Gasification produces syngas (mainly H_2 and CO, along with other gases [116]) at relatively high temperatures. With Fisher-Tropsch chemisty and other reactions such as the water-gas shift and methanation reactions, alkanes, methanol, and subsequently, liquid fuel blends can be formed. On the other hand, the variation in the chemical composition of the major polymeric groups in biomass allows fractionation through the action of hydrolysis. Acid catalyzes the dissolution mostly of the sugars though some portion of the lignin is soluble as well [77]. The soluble components can be fermented, dehydrated or treated with reforming catalyst to form ethanol, aromatic hydrocarbons, liquid alkanes and/or hydrogen. The mainly lignin fraction that remains undissolved can be upgraded to liquid fuels. This would require the depolymerization of the lignin polymer to smaller molecules which can then be upgraded catalytically (hydrodeoxygenation). Lastly, pyrolysis and liquefaction can form liquid products

through two proposed ways: (a) zeolite upgrading and (b) hydrodeoxygenation. These processes are summarized in Figure 3.1.

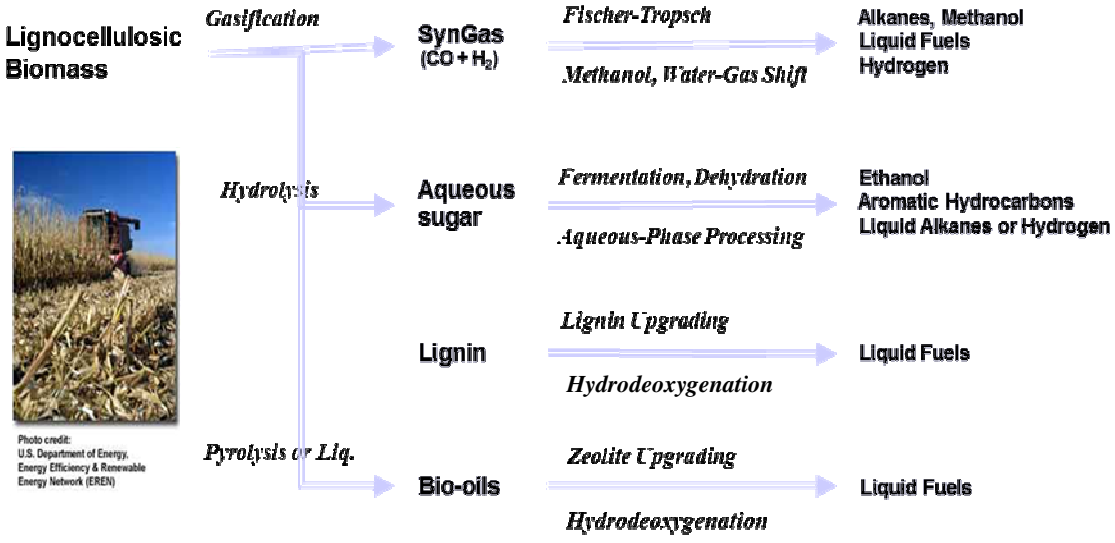

Figure 3.1 Suggested routes to alternative fuel from biomass [115]

Hydrodeoxygenation (HDO) is the catalytic removal of oxygen in the presence of H_2 at elevated temperatures. It is one of the processes collectively known as hydrotreatment which includes hydrodemetallation, hydrodesulfurization and hydrodenitrogenation. Though the other catalytic treatments have been traditionally used already in petroleum refining to remove compounds that can have debilitating effects on the downstream processing catalysts, hydrodeoxygenation was typically not of high importance. This is mainly because oxygen is not a major component of fossil fuels. However, considering that biomass contains more than 40% oxygen [40, 117], hydrodeoxygenation becomes a necessity in order to produce petroleum-compatible bio-derived alternatives [38, 118].

Several reasons have been identified why oxygen removal is necessary. Oxygen-containing groups in pyrolysis oils cause low heating values, increased liquid viscosities during storage and other chemical instabilities [38-40]. Typically, oxygen removal through HDO is accompanied by hydrogen incorporation into the fuel. Kleinert, et al. [42], presented a von Krevelen chart illustrating the ideal levels of H/C and O/C ratios: for crude oil, about $1.60 < H/C < 2.10$ and $0 < O/C < 0.03$ (Figure 1.2). Wood would have upwards of about O/C = 0.61 and H/C = 1.4. Lignin, a major wood constituent, came in at about $0.32 < O/C < 0.46$ and $1.1 < H/C < 1.3$. Pyrolysis oil would typically have about $0.60 < O/C < 0.71$ and $1.0 < H/C < 1.35$. HDO offers a catalytic pathway to improve the H/C and O/C ratios.

3.1.2 Nickel phosphides

Traditonal HDO catalysts consist of sulfided CoMo and NiMo supported on γ-Al_2O_3. The group of Delmon used these catalysts in the hydrotreatment of pyrolysis oils and model compounds [119-125]. However, these catalysts require sulfidation to be active. Since sulfur is a known poison for catalysts being used for downstream processing of petroleum and that biomass already contains much smaller amounts of sulfur compared to petroleum (if any, depending on such parameters such as species, location of planting, age, etc.), it makes more sense to use catalysts that do not require sulfur to be active.

This study involved the use of both nickel phosphide catalysts for the hydrodeoxygenation of syringaldehyde. These family of catalysts have been found to be sulfur-tolerant [126] and showed activities higher than commercially available hydrotreating catalysts (NiMo and CoMo on alumina) for hydrodesulfurization. This

group of catalysts does not require sulfur to be active. Overall, nickel phosphides have been shown to have good activity in hydrotreatment, such as hydrodesulfurization, hydrodenitrogenation and more recently, hydrodeoxygenation [126-127].

Several phases of nickel phosphides exist and have been presented in the literature. Ni_3P has been identified as a catalyst for the synthesis of carbon nanostructures [128-130]. Ni_2P and $Ni_{12}P_5$ have been used for hydrotreatment [127, 131-134]. Formation of a specific nickel phosphide phase has been reported to be affected by preparation method, precursor compounds, precursor ratio, reduction temperature and the support used [133, 135-136]. Oyama et al. [136], showed that increasing reduction temperature may convert $Ni_{12}P_5$ into Ni_2P, depending on the precursor ratio used. On a support, Sawhill et al. suggested that the phosphate decorates the surface of the Ni metal during reduction (~400°C). As the temperature was increased, P was thought to bind with the metallic Ni to form $Ni_{12}P_5$, which can be converted to Ni_2P at higher temperatures [133]. PO_4^{3-} precursor may also interact with the support itself. For SiO_2 support, it is more likely that phosphorus oxides will form while the phosphates may interact with the alumina to form $AlPO_4$ [133]. Figure 3.2 illustrates these processes. On the other hand, Berhault et al. [137] completely reduced a precursor, $NiNH_4PO_4{\bullet}H_2O$[138], to produce Ni_2P without going through $Ni_{12}P_5$. In this study, formation of the desired nickel phosphide phases was mainly confirmed by X-ray diffraction.

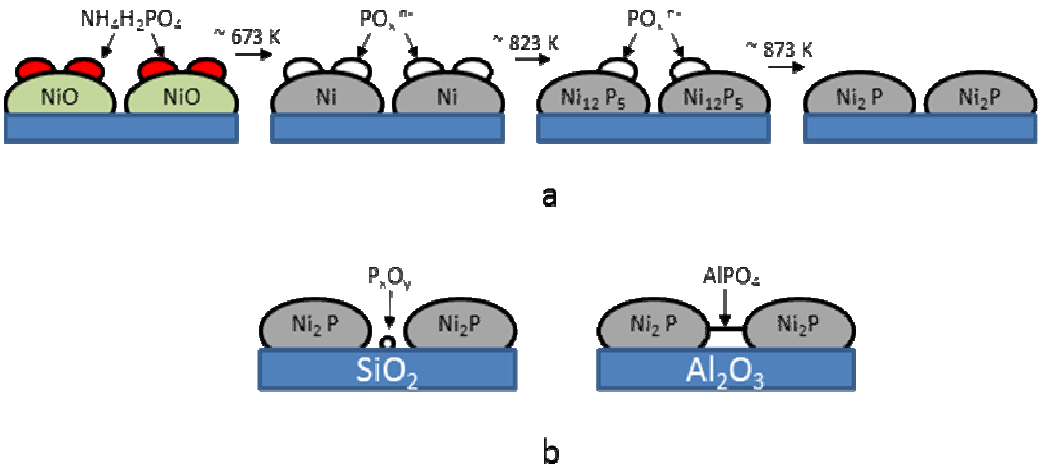

Figure 3.2 Schematic of Ni_2P formation from precursors [133]. (a) Proposed transformation occurring as a function of increasing temperature in the presence of H_2; (b) Formation of support-phosphate species: phosphorus oxides on SiO_2 and $AlPO_4$ on alumina

3.1.3 Syringaldehyde

Previous studies with nickel phosphide have used benzofuran [126-127, 136] under sulfided conditions, cinnamaldehyde [134] though O removal was not the primary objective in that study and more recently, guaiacol [130]. In this study, we used nickel phosphides for the HDO of syringaldehyde. Syringaldehyde was identified as a monomeric product in our base-catalyzed depolymerization experiments. As a model compound, syringaldehyde (Figure 3.3a) is of interest in that it contains three oxygen-containing functional groups. These groups are typically found in pyrolysis oils, namely, aldehydic, phenolic and methoxy groups. It must be noted that aldehydes have been considered as main culprits in the formation of condensation products in stored pyrolysis oils [40]. As a source of chemical feedstock, one of syringaldehyde's HDO by-products, 2,6-dimethoxy-4-methylphenol (Figure 3.3b), was identified as a component in fragrance manufacture [139]. Additionally, the alkylated, hydroxylated aromatics that were found

to be produced in the presence of supported nickel phosphide are becoming a major and growing constituent of biomass-derived liquid fuels that can be converted to jet fuels and gasoline [140]. This is because in general, aromatics have higher energy density than paraffinic compounds [141].

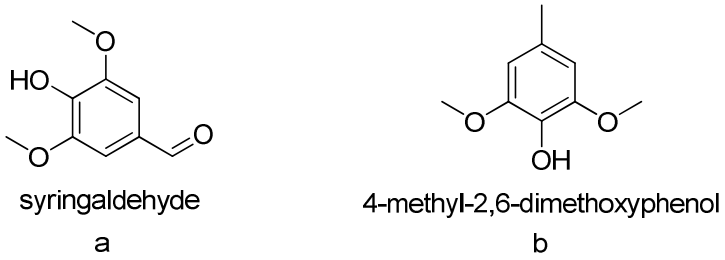

syringaldehyde
a

4-methyl-2,6-dimethoxyphenol
b

Figure 3.3 Model compound feed and primary HDO by-product

3.1.4 Objectives

The main objective of the study discussed in this chapter was to use nickel phosphide in the batch HDO of syringaldehyde. Specifically, the goals were:

(1) synthesize nickel phosphide, both bulk and supported on alumina;

(2) compare the product profile of bulk nickel phosphide with unreduced nickel solids such as nickel oxide (NiO) and nickel phosphate ($Ni_3(PO_4)_2$;

(3) compare the product profile using supported nickel phosphide with noble metal catalysts, namely Pd/Al_2O_3 and Pt/Al_2O_3; and,

(4) understand the reaction pathway in the HDO of syringaldehyde.

3.2 EXPERIMENTAL METHODS

3.2.1 Materials

The chemicals for this study were obtained from Sigma-Aldrich and were used without further purification. Syringaldehyde (MW = 182 g/mol, 97%), anhydrous octane (99%), pentadecane (99.8%), 2,6-dimethoxy-4-methylphenol (97%), Pt/Al_2O_3 (Degussa, 5 wt%), Pd/Al_2O_3 (Degussa, 5 wt%), nickel nitrate ($Ni(NO_3)_2 \bullet 6H_2O$), and ammonium phosphate dibasic ($(NH_4)_2HPO_4$).

3.2.2 Catalyst synthesis

3.2.2.1 Bulk $Ni_{12}P_5$

For the synthesis of bulk $Ni_{12}P_5$, a measured amount of $(NH_4)_2HPO_4$ (1.7 g) was dissolved in about 40 ml of dI water, followed by $Ni(NO_3)_2 \bullet 6H_2O$ (7.3 g); these starting materials amounted to a Ni/P atomic ratio of 2 [132]. Phosphorus had been reported to be lost as phosphine during reduction. Drops of concentrated HNO_3 were added to the milky white mixture until a clear green solution was formed. This was dried overnight at 85°C, followed by 4 hours at 100°C. Calcination was done by increasing the furnace temperature at a rate of 1.2°C/min from room temperature to 120°C (soaked for 2 hours), followed by an increase to 500°C (soaked for 4 hours) using the same temperature ramp.

Reduction of the calcined precursor was done in-situ in the Parr reactor. The reactor was first flushed with He, followed by H_2 before the reactor heat-up. Reduction was done under flowing H_2 while heating the reactor from room temperature to 300°C over one hour. The reactor was then pressurized with 1000 psig of H_2 before being sealed. Reduction was continued at 300°C for 1 hr. The reactor was then allowed to cool down using an ice bath. Once the temperature was below 20°C, the residual pressure was

released until about 50 psig remained. The gas outlet valve was closed, and the reactor was placed inside the glove box for octane loading.

3.2.2.2 $Ni_{12}P_5/Al_2O_3$

Supported nickel phosphide catalysts were synthesized through wet impregnation of γ-Al_2O_3 with a dissolved solution of ($Ni(NO_3)_2 \bullet 6H_2O$) and $(NH_4)_2HPO_4$. The γ-Al_2O_3 support used was first activated by calcination at 400°C for 4 hours, using a ramp rate of 1.2 °C/min, with an intermediate soaking at 120°C for 2 hours.

The precursor solution was typically made by mixing 2.73 g of $Ni(NO_3)_2 \bullet 6H_2O$ and 1.24 g $(NH_4)_2HPO_4$ in 2.5 ml dI H_2O for every 5 g of γ-Al_2O_3. Several Ni/P ratios were tested in this study but the Ni/P atomic ratio of 1 was able to form the $Ni_{12}P_5$ phase. As mentioned previously, P can be lost either as phosphine during reduction or as a phosphate phase interacting with the support. A few drops of concentrated HNO_3 were added to ensure the formation of a clear green solution. The resulting precursor solution was then added drop-wise to the support. To ensure complete homogeneity, the mixture was stirred with a spatula. After this, the impregnated solids were dried at 85°C and calcined using the same protocol that was used for the bulk $Ni_{12}P_5$ catalyst as described previously.

Since the temperature required for the reduction of the supported catalyst was higher than the maximum allowable in the Parr reactor, ex-situ reduction was done. Typically, about 250 mg of the calcined catalyst was loaded into a ½" diameter quartz U-tube reactor equipped with ball valves at each end for sealing the reactor. The catalyst solids were supported on quartz wool. A mixture of 4% H_2/Ar was allowed to flow through the system for about one minute at 65 cc/min. The temperature was then allowed

to increase from room temperature to 650°C at a heat ramp of 1.6 °C/min and allowed to soak for 2 hours. The set-up was then cooled down to room temperature. The H_2/Ar flow was closed, ball valves were closed. Then, the quartz reactor assembly was transferred into the glove box and the reduced contents transferred into a vial for storage.

3.2.3 Characterization

3.2.3.1 X-ray Diffraction (XRD)

X-ray powder diffraction (XRD) patterns of the synthesized catalysts were used to confirm the presence of nickel phosphide phases. Data were taken using PANalytical X'pert Pro Diffractometer with a Cu-Kα source (λ = 1.5418740 Å) from 2θ = 5° – 85° with a step size of 0.017° and scan time of 60 s. The nickel phosphide phase was confirmed by comparing with installed reference patterns as well as values available in the literature [133, 142-144]. The reduced catalysts were passivated at room temperature under flowing He for 8 hours (O_2 content ~1ppm according to vendor) before exposure to air during the XRD analysis.

3.2.3.2 Temperature-programmed reduction (TPR)

Temperature-programmed reduction (TPR) of the catalysts was performed using the Micromeritics AutoChem II equipped with a thermal conductivity detector (TCD). About 50 mg of sample was weighed and transferred into a quartz sample holder. The sample was first heated and soaked at 200°C under argon for 1 hour to remove water. After allowing it to cool down to room temperature, reduction under flowing 10% H_2/Ar was achieved by heating the sample tube with an electric furnace using a heating ramp rate of 5 K/min from 50°C to 950°C at which the temperature was held constant for 30

minutes. The temperature ramp was measured using a thermocouple situated inside the sample tube and measuring the actual temperature of the sample. A coiled trap cooled by a liquid N_2-isopropanol mixture placed downstream to the quartz sample holder was used to freeze condensable impurities (i.e. water) that may interfere with the TCD analysis.

3.2.3.3 H_2-O_2-H_2 Chemisorption

Pulsed hydrogen-oxygen chemisorption of the commercially available supported Pt and Pd on alumina catalysts were also done using the same equipment as used for TPR. About 100 mg of the catalyst powder was weighed and transferred into the quartz sample holder. The first part of the experiment involved the TPR of the catalyst using the same procedure as above but at a lower temperature of 300°C. After cooling to room temperature under H_2/Ar , H_2 titration using 10% H_2/Ar was done with 20 injections. This was followed by an O_2 titration using 10% O_2/He. Another round of H_2-O_2-H_2 titrations followed. The absorbed amount of gas was measured as the cumulative difference between the injection volume and the volume corresponding to the amount that the TCD recorded for each injection.

3.2.4 Reactor set-up

A 50-ml Parr autoclave was used in the batch HDO of syringaldehyde. The top cover was retrofitted by machining three pin spanner holes (on non-sealing surfaces) to allow application of torque to properly seal the reactor. This allowed the use of a Teflon O-ring rather than the original Kalrez O-ring which had a temperature limitation of 275°C. The former, if properly torqued, was resistant to extrusion during reaction conditions, which was frequently encountered when Kalrez O-rings were used (both the standard 4079 compound and the specialty 7090 compound). For experiments requiring

$Ni_{12}P_5/Al_2O_3$, the catalyst was loaded inside a dry glove box since the catalyst was already pre-reduced. For experiments with bulk $Ni_{12}P_5$, commercial Pt/Al_2O_3 and commercial Pd/Al_2O_3, the unreduced catalyst was loaded outside the glove box and subsequently reduced in-situ. However, loading of the solvent was done inside the glove box. Bulk NiO and $Ni_3(PO_4)_2$ were not reduced before the experiments and were put in the reactor after the addition of the solvent.

As mentioned, 16 ml of anhydrous octane (solvent) was added inside the glove box. Since the solvent acted as a barrier from oxygen contacting the reduced catalysts, syringaldehyde (1.328 g) and pentadecane (internal standard) (0.75 µL) were added outside the glove box. The autoclave was then capped and tightened with a pin spanner wrench and using a bench vise for proper application of torque to the PTFE gasket. A bench vise with smooth jaws was used to avoid wear on the circular surface of the reactor. It was purged with He for 3 minutes followed by H_2 for 5 minutes. The reactor was pressurized with 1000 psig of H_2 and the gas inlet valve was closed. The heater was set to 300°C. This was the highest working temperature recommended by the manufacturer. Reaction was considered "started", once the reaction temperature (300°C) was reached. Typically, heat-up time was about 60 minutes.

3.2.5 Liquid product work-up and analysis

The liquid products formed by the reaction were typically in two phases. The liquid phase was diluted and the reactor washed with DCM to generate a single phase for the GC-FID (Shimadzu QP-2010) analysis. Quantification was done based on a series of calibrations of known compounds with respect to the internal standard (pentadecane).

The catalysts were recovered through a filter using a vacuum-filtration set-up and further washed with DCM.

3.2.6 Hydrodeoxygenation experiments

Several bulk catalysts ($Ni_{12}P_5$, unreduced commercial NiO and $Ni_3(PO_4)_2$) were tested. NiO and $Ni_3(PO_4)_2$ were used unreduced in order to determine how unreduced Ni species will perform at the HDO conditions. $Ni_{12}P_5$ supported on alumina was used in comparison to the bulk $Ni_{12}P_5$ as well as to two supported noble metal catalysts: Pt/Al_2O_3 and Pd/Al_2O_3. 0.5 grams of the catalysts were typically loaded in the reactor for each experiment. The mole ratio of the feed was 26:380:1 (syringaldehyde: octane: pentadecane). Samples were only analyzed at the end of each run. Yield was calculated as moles of compound per mole of syringaldehyde x 100%, assuming each identified product was formed from a single syringaldehyde molecule. The amounts of other by-products such as water and methane were not quantified.

3.3 RESULTS AND DISCUSSION

3.3.1 Catalyst synthesis and characterization

X-ray diffraction was used to identify the phase of the nickel phosphide formed in both the bulk and supported catalyst. Figure 3.4 shows the diffraction patterns for the supported $Ni_{12}P_5/Al_2O_3$ and bulk $Ni_{12}P_5$. The main diffraction peaks associated with the $Ni_{12}P_5$ phase are as follows: $2\theta = 38.5°$, 41.2°, 44.2°, 46.6° and 48.6° [144]. However, as seen from the reference pattern taken from the database included in the program used (X'Pert High Score) (Figure 3.5), small peaks at different 2θ were also present. All these peaks were readily identifiable in the diffraction pattern of the bulk catalyst.

For the supported catalyst, peaks associated with the γ-Al_2O_3 support (2θ = 37°, 46° and 67°[145]) overlapped with the diffraction pattern of the nickel phosphide. However, these mainly appear as broad peaks, as expected of amorphous materials. The sharp peaks that were apparent in the pattern can be attributed to the major peaks associated with $Ni_{12}P_5$.

The absence of a peak at 2θ = 51.8° rules out the presence of bulk Ni metal [143] though its presence as nanoparticles may not be completely discounted. Phosphorus is typically expected to be released during the reduction as phosphines as evidenced by studies with online GC-MS after the reduction chamber [127, 136]. However, others found that it may also react with the support to form $AlPO_4$ or crystalline oxides such as P_2O_5 or P_4O_7 (2θ = 21.2°, 25.6°, 26.7°, 28.4°, 30.0°, 31.6°, 35.1°, 38.2°, and 43.5°) [133]. These peaks were not observed. However, since the support used was Al_2O_3, the former form of phosphate may be more expected, according to the suggestion by Sawhill, et al. [133] (see also Figure 3.2b).

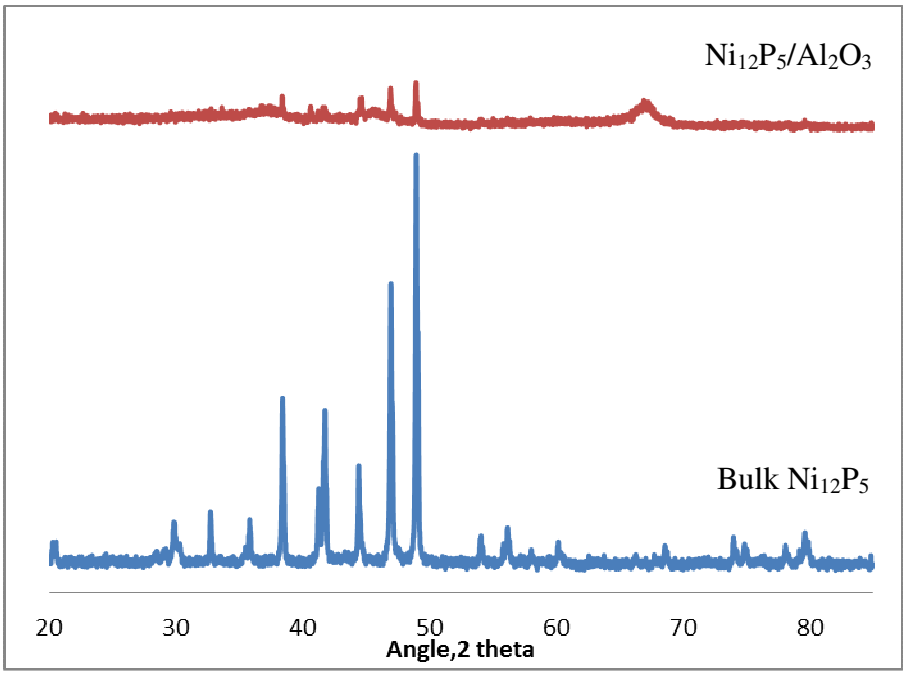

Figure 3.4 X-ray diffraction pattern of synthesized catalysts: from top, supported $Ni_{12}P_5$ and bulk $Ni_{12}P_5$

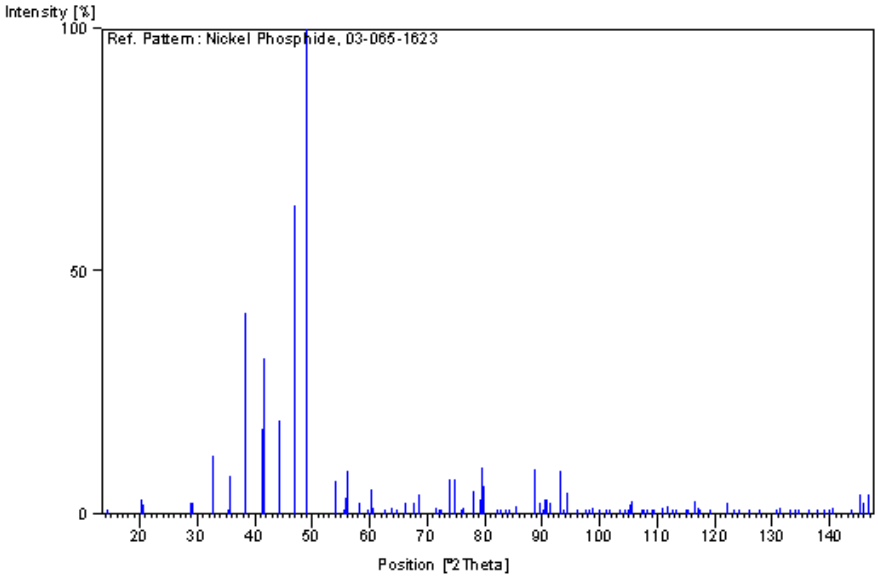

Figure 3.5 X-ray diffraction of $Ni_{12}P_5$ reference (sourced from X'Pert High Score database)

Elemental analysis of the synthesized catalysts yielded Ni/P ratios of 2.2 for $Ni_{12}P_5$ and 0.8 for the supported $Ni_{12}P_5/Al_2O_3$. The theoretical ratio for $Ni_{12}P_5$ is 2.4. These catalysts were phosphorus-rich, containing more phosphorus than what was warranted by the stoichiometry of their identified phases. Similar results were also reported by previous researchers [134, 146-147]. The higher amount of P in the supported catalyst suggests its incorporation into the support even though the diffraction pattern for other phases, aside from the alumina and the $Ni_{12}P_5$, were not noted by XRD, probably due to the size of these phases.

The Scherrer equation ($\tau = \kappa\lambda/\beta\cos\theta$) was used to determine crystallite sizes of the nickel phosphides. κ is the shape factor (value taken as 0.9), λ is the incident X-ray wavelength (λ = 1.5418740 Å), β is the line broadening at half the maximum intensity (FWHM) in radians and θ is the Bragg angle. Considering the inherent error of this method, the derived values surprisingly did not show distinct differences: 43 nm for the bulk $Ni_{12}P_5$ and 45 nm for the $Ni_{12}P_5/Al_2O_3$. Typically, it should be expected that increasing the surface area of the support should result in a smaller crystallite size, as was shown by previous studies with supported nickel phosphide on silica [147-148]. However, we purposefully increased the reduction temperature in order to gain a good signal from the XRD in order to be able to determine the dominant nickel phosphide phase present in our catalyst. The large crystallite size of our supported catalyst may be attributed to the sintering of the particles on the surface due to the reduction temperature as well as the length of time that this catalyst was exposed to. Sintering at increased temperature is particularly true in the case of the widely studied supported nickel catalysts [143, 149].

The temperature-programmed reduction profiles of the different catalysts under 10% H_2/Ar are shown in Figure 3.6. It must be noted that TPR was done only to characterize the catalyst. Actual reduction protocols for use of catalysts in reactor studies were done using pure H_2.

Several parameters affect the full reduction of a sample. This includes the reduction temperature at which the reduction rate is at maximum, the hydrogen gas concentration at this temperature, the heating rate and the kinetics of the reactions. For first order kinetics, Monti and Baiker [150] derived the Equation (3-1).

$$\ln \frac{T_m^{\,2} \overline{C}_m}{\beta} = \frac{E}{RT_m} + \ln \frac{E}{RA} \qquad (3\text{-}1)$$

where T_m = reduction temperature at maximum rate
$\overline{C}_m$ = mean H_2 concentration at T_m
β = reduction rate
E = activation energy
R = universal gas constant
A = pre-exponential factor

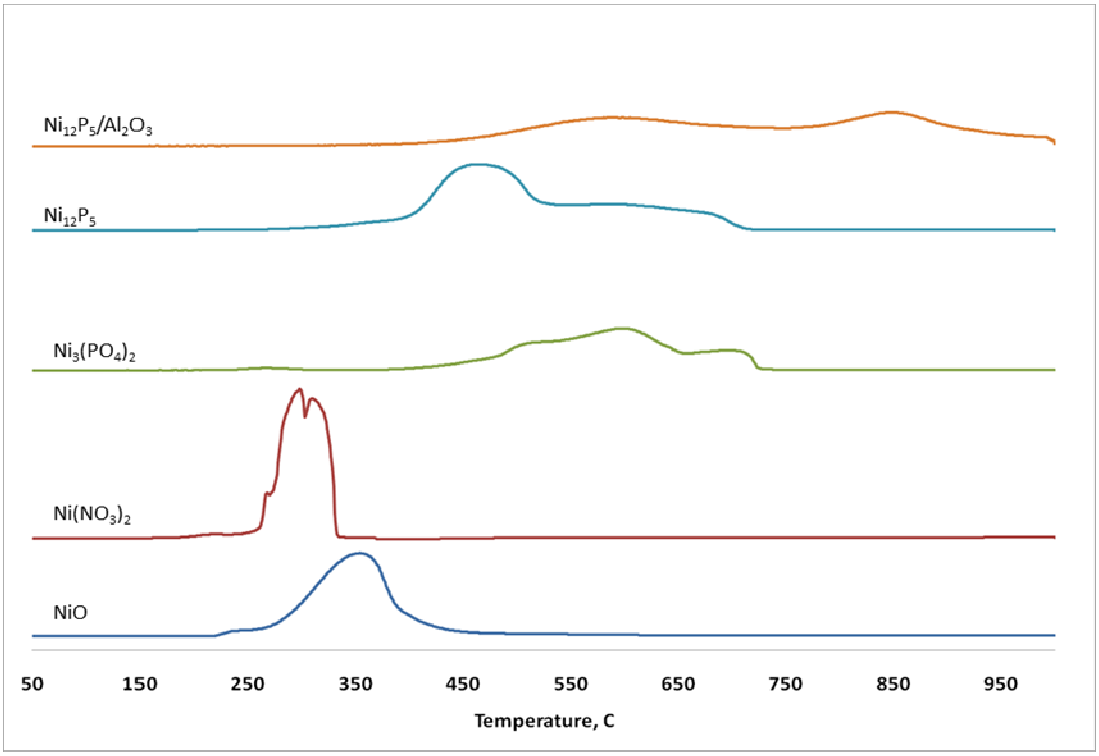

Figure 3.6 TPR profiles of different nickel phosphide precursors and some reference catalysts (heating rate = 5 K/min)

The addition of P into the Ni metal caused a much higher reduction temperature requirement for the phosphides than the typical Ni oxide to Ni metal reduction [133] and will thus cause an increase in the reduction temperature for the nickel phosphide catalyst. Commercial bulk nickel oxide can be fully reduced by ~450°C under our TPR conditions (10% H_2/Ar, 5 K/min) while the commercial bulk nickel phosphate required a much higher temperature of ~725°C. The nickel phosphate showed a slight peak around 250°C which can be attributed to easily reducible NiO species. Both the bulk phosphate and nitrate TPR profiles showed multiple peaks which may be attributed to the presence of different reducible species present. Reduction of the $Ni_{12}P_5$ precursor showed the same temperature range as the nickel phosphate. However, the proportions of the peaks were

different. This may be attributed to the differences in the chemical compositions of these two samples. Lastly, among all the synthesized catalyst precursors, the supported catalyst required the highest reduction temperature. The increased temperature requirement can be attributed to nickel phosphide interactions with the Al_2O_3 support [133, 151] as well as the presence of the phosphate and its interaction with the Ni in the formation of the nickel phosphide phase.

The amounts of Ni and P in the precursor supported catalyst affect the shape of the TPR profiles. Figure 3.7 shows the TPR profiles of four supported catalysts as well as the already mentioned commercial bulk catalysts included in Figure 3.6. From the top: (a) supported NiO/Al_2O_3; (b) supported Ni_xP_y/Al_2O_3 at Ni wt% = 3 and Ni/P ratio = 2; (c) supported Ni_xP_y/Al_2O_3 at Ni wt% = 9 and Ni/P ratio = 1; (d) supported Ni_xP_y/Al_2O_3 at Ni wt% = 9 and Ni/P ratio = 2; (e) commercial $Ni_3(PO_4)_2$; (f) commercial NiO; and, (g) commercial $Ni(NO_3)_2$. As shown, supporting the $Ni(NO_3)_2$ on the Al_2O_3 catalyst dramatically increased the required reduction temperature as compared to the reduction of bulk $Ni(NO_3)_2$, supporting the presence of metal-support interactions. Additionally, the presence of P caused the formation of another phase that required a much higher temperature for reduction, that is, (b) vs. (a), as was already noted. Comparing curves (b) and (d) showed that the amount of Ni directly affected the first broad reduction peak. However, increasing the amount of P from a Ni/P = 2 to Ni/P = 1 did not show a distinct difference in the reduction temperature requirement if (b) and (c) were compared.

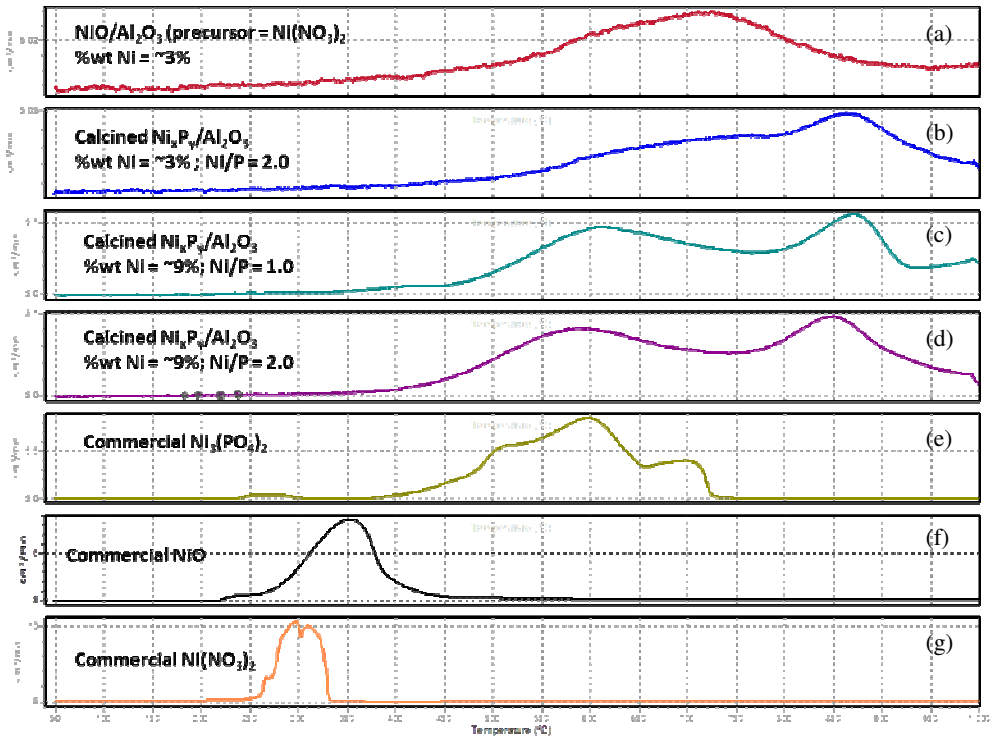

Figure 3. 7 TPR profiles of supported Ni_xP_y precursor catalysts with different Ni and P contents as well as some bulk catalysts. (a) NiO/Al_2O_3; (b) supported Ni_xP_y/Al_2O_3 at Ni wt% = 3 and Ni/P ratio = 2; (c) supported Ni_xP_y/Al_2O_3 at Ni wt% = 9 and Ni/P ratio = 1; (d) supported Ni_xP_y/Al_2O_3 at Ni wt% = 9 and Ni/P ratio = 2; (e) commercial $Ni_3(PO_4)_2$; (f) commercial NiO; and, (g) commercial $Ni(NO_3)_2$

3.3.2 Hydrodeoxygenation of syringaldehyde

3.3.2.1 Bulk catalysts

Nickel phosphides were used to catalyze the hydrodeoxygenation of syringaldehyde in batch mode at 300°C. Inherent to the system is the presence of a heat up time from room temperature to 300°C, which typically took 1 hour. As previously mentioned, reaction time was considered to start once 300°C was reached by the reactor. Figure 3.8 shows the syringaldehyde conversion of the nickel-based catalysts used in this study. It was apparent that syringaldehyde conversion had occurred even during the heat-up of the reactor from room temperature to 300°C. A separate blank run showed that in

the absence of any catalyst, conversion of syringaldehyde due to thermal effect was ~ 2.5%. At the end of this run, a solid lump was recovered from the reaction – unlike the typically more viscous liquid that was formed in the presence of catalysts.

Experiments catalyzed by NiO showed almost complete conversion of syringaldehyde (comparable to the supported catalyst) even at the onset of the reaction temperature. Considering that the NiO was the most easily reducible catalyst used in this study, it is very possible that part, if not all, of the loaded NiO became converted to active Ni metal under the conditions of the reactor heat-up (initial H_2 pressure of 1000 psig) despite the presence of the solvent.

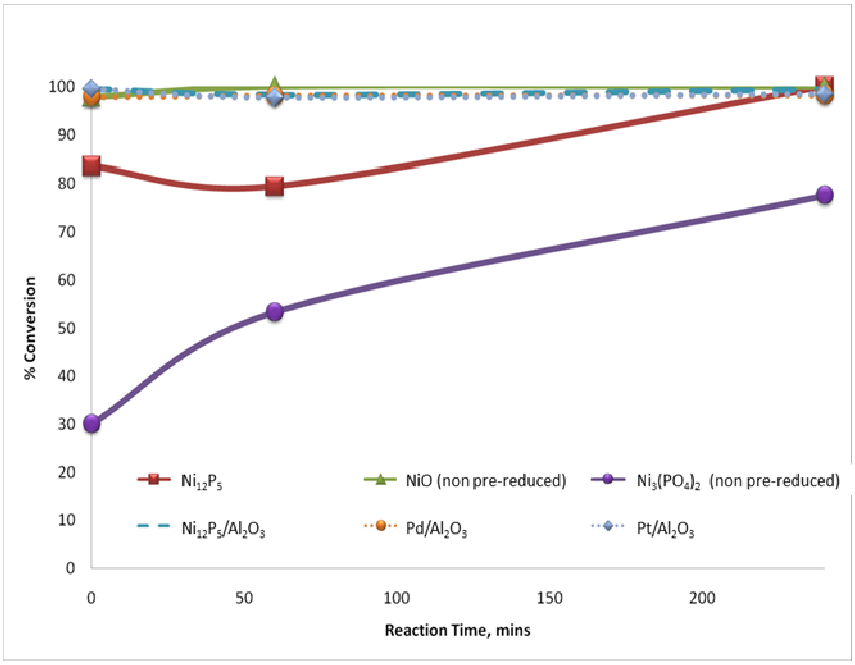

Figure 3.8 Syringaldehyde conversion using different catalysts

Syringaldehyde conversion for the other bulk catalysts improved at increased reaction time. $Ni_{12}P_5$ eventually gave complete conversion after 240 minutes while the unreduced bulk $Ni_3(PO_4)_2$ only reached ~80% conversion even after 240 minutes. The

possibility of partial reduction of the $Ni_3(PO_4)_2$ at longer exposure to the H_2-rich atmosphere was also not discounted in this instance.

3.3.2.1.1 2,6-dimethoxy-4-methylphenol (4-MDP)

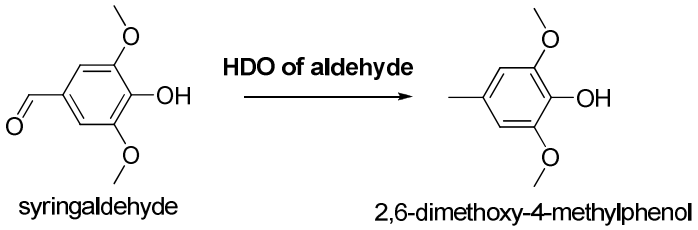

Figure 3. 9 Main conversion route of syringaldehyde HDO

The most abundant compound identified in the resulting product mixtures was 4-MDP through the deoxygenation of the aldehyde group. This is the main HDO product directly from the starting material (Figure 3.9). As previously mentioned, this compound finds use in the flavor and scent industry and thus can have added value [139]. Though both the aromatic ring and the carbonyl group have unsaturated bonds, it has been suggested that the double bond of the carbonyl group would have more affinity to the surface of the catalyst due to its polar nature [121].

Figure 3.10 shows the amount of 4-MDP (solid lines) in the resulting liquid product at different reaction times using various bulk catalysts. $Ni_3(PO_4)_2$ showed an increase of 4-MDP from 0 to 60 minutes at 300°C from 12 to 37%, after which the yield leveled off. A very slight decrease in 4-MDP yield for the whole period of 4 hours was noted with NiO. Lastly, a more pronounced decrease in the 4-MDP yield was noted for the batch experiments with $Ni_{12}P_5$. This can be explained by the formation of 3,4-dihydroxy-5-methoxytoluene, as discussed in the next section.

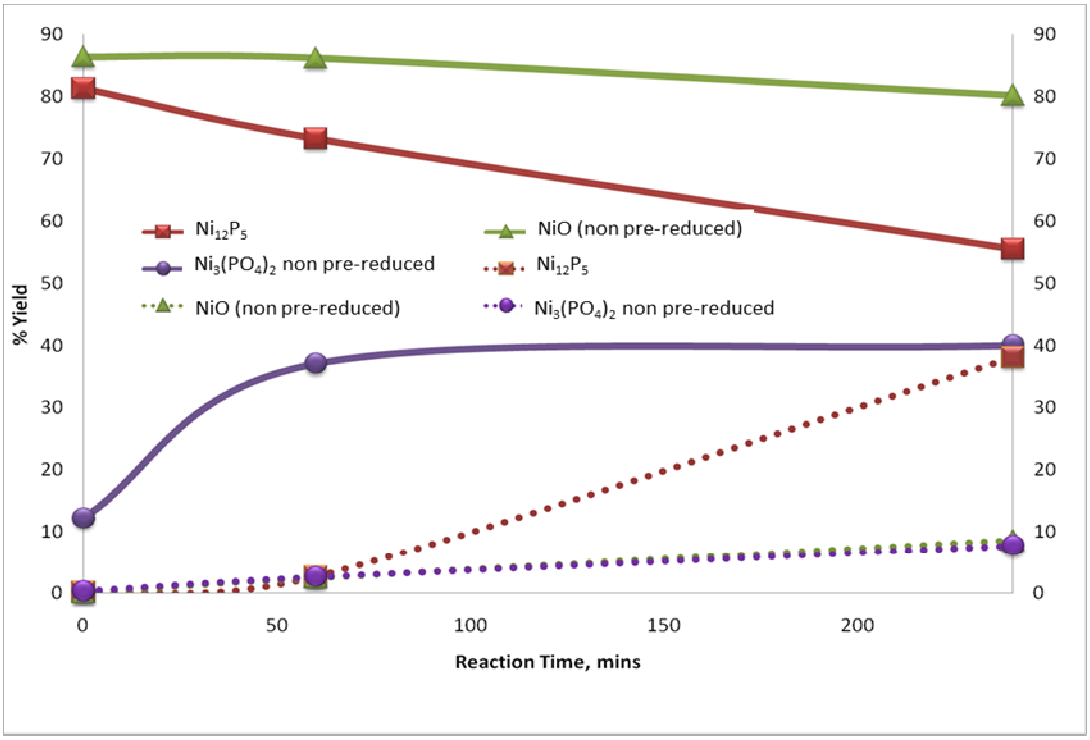

Figure 3.10 Yield of 2,6-dimethoxy-4-methylphenol (4-DMP) (solid lines) and 3,4-dihydroxy-5-methoxytoluene (5-MDT) (broken lines) in the presence of different bulk catalysts at different reaction times

3.3.2.1.2. 3,4-dihydroxy-5-methoxytoluene (5-MDT)

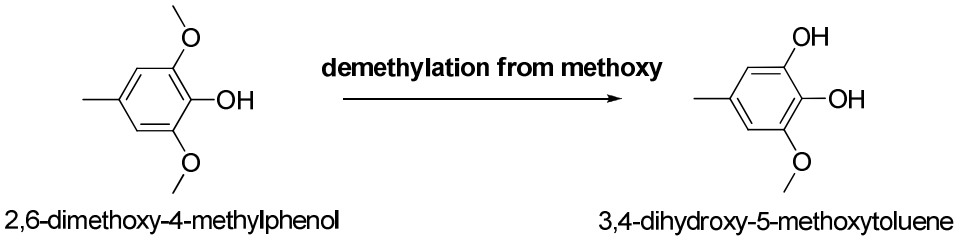

Figure 3.11 Demethylation of 2,6-dimethoxy-4-methylphenol (4-DMP) to 3,4-dihydroxy-5-methoxytoluene (5-MDT)

3,4-dihydroxy-5-methoxytoluene (5-MDT) is the second most abundant product in the product stream of syringaldehyde HDO with bulk catalysts. It is formed from 4-DMP through demethylation of one of the methoxy groups (Figure 3.11). The yield of 5-MDT in the presence of bulk catalysts was shown in Figure 3.10 (dashed lines). For both NiO and $Ni_3(PO_4)_2$, the increase in 5-MDT was just slight as the reaction time was increased. Except for the $Ni_{12}P_5$, the quantified 5-MDT amounts were in similar range - less than 10% within 4 hours. On the other hand, the $Ni_{12}P_5$ yielded close to 37% of 5-MDT over the same time span. The decrease in the amount of 4-MDP at 100% syringaldehyde conversion ($Ni_{12}P_5$, 240 minutes, 300°C), mirrored the increase in 5-MDT yield for the nickel phosphide.

Formation of 5-MDT from 4-DMP may be explained by the O-C scission of one of the two methoxy substituents. Bredenberg, et al. [152], in their study of anisole hydrogenolysis in the presence of $NiMo/SiO_2$-Al_2O_3 at 300°C, suggested that a weak coordinative bond can be formed between the free electron pairs of the oxygen atom and the catalyst through vacancies in the metal catalyst surface. A phenoxide and a methyl radical are subsequently formed by the homolytic dissociation on the metal. These species can then be further hydrogenated to form 5-MDT and methane. If this mechanism is considered, it can be suggested that vacant (active) metal sites seem not to be as available on the NiO and $Ni_3(PO_4)_2$ as on the nickel phosphide catalyst.

3.3.2.1.3. 2,6-dimethoxyphenol (2,6-DMP)

Figure 3.12 Decarbonylation reaction of syringaldehyde

The presence of a decarbonylated derivative of syringaldehyde, 2,6-DMP, was also detected in the products (Figure 3.12). Yields of 2,6-DMP at different reaction times in the presence of different bulk catalysts were shown in Figure 3.13. NiO seems to be particularly active for this reaction. As can be seen, the amount of product typically increased from 0 to 60 minutes, regardless of the catalyst used. However, yield seemed to go down for $Ni_{12}P_5$ while it plateaued off for NiO. An important thing to note is that the formation of 2,6-DMP translates to a net loss in C to CO formation which may not be very attractive for the C efficiency of the process.

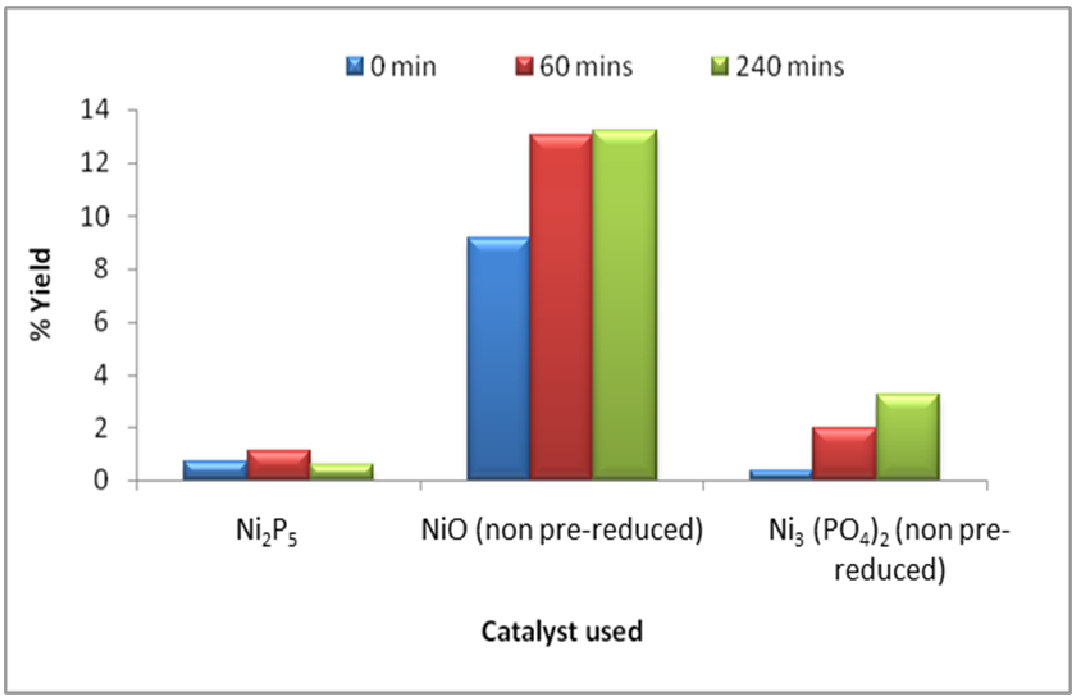

Figure 3.13 Yield of 2,6-dimethoxyphenol in the presence of different bulk catalysts at different reaction times

3.3.2.2. Supported catalysts

In comparison with the bulk catalysts, syringaldehyde conversions over different supported catalysts (wet-impregnated $Ni_{12}P_5/Al_2O_3$, commercial Pt/Al_2O_3 and commercial Pd/Al_2O_3) appeared to be 100% during the heating of the reactor to 300 ^oC. (Figure 3.8, dashed lines). With these catalysts, aldehyde conversion to the methyl substituent seemed to have mainly occurred during the heat up process. Incorporating a correction for the amount of syringaldehyde thermal degradation (2.5%) and considering that the reaction only occurred for 40 minutes of the 60 minutes of the heat-up process, Table 3.1 summarizes the averaged TOF for the supported catalysts. Though the TOF of the supported $Ni_{12}P_5$ was an order of magnitude higher than the other two, comparison of

the relative activities of these catalysts would require kinetic studies at lower syringaldehyde conversions (e.g. lower temperature).

Table 3.1 Turnover frequencies for the supported catalysts determined from an average reactivity over the whole reaction time.

Catalyst	Wt. of metal (%)	Crystallite size (nm)	Dispersion (%)	TOF[c] (x 10^{-2} s^{-1})
$Ni_{12}P_5/Al_2O_3$	12.1	45[a,d]	1.5[d]	> 20.3[d]
Pd/Al_2O_3	3.8	1.3[b]	86.5	> 1.8
Pt/Al_2O_3	3.5	1.4[b]	82.1	> 3.8

[a] by XRD[153]

[b] by H_2 chemisorption

[c] $TOF = \frac{molecules\ of\ syringaldehyde}{metal\ surface\ atoms \cdot time}$

[d] Properties approximated based on nickel.

It must be noted that in the calculation of crystallite size, the stoichiometric ratio between Pt and H_2 molecule was considered as 1 in this calculation instead of the typical value of 2, i.e. Pt atom to H atom ratio equals 1. Assumption of the stoichiometric ratio of 2 would have arrived at a dispersion that was more than 100%. The situation typically arises in the presence of very small metal particles (crystallite size ≈ 1 nm) [153] or in the presence of hydrogen spillover onto the support [154]. On the other hand, for the supported Pd catalyst, a stoichiometric ratio of 2 was used. If it was assumed to equal 1, a dispersion of 43.3% would be calculated with a crystallite size of 2.59 nm. The assumption would then not be valid, considering that the crystallite size would be much bigger than 1 nm.

3.3.2.2.2. 4-MDP and 5-MDT

Figure 3.14 shows the yields for 4-MDP and 5-MDT in the presence of supported catalysts. As the reaction time was lengthened, the yield for these two major components decreased to below 10% after 240 minutes at 300°C. Considering the high activity for syringaldehyde conversion exhibited by these supported catalysts and the results shown in Figure 3.10, it can be argued that 4-MDP is the primary reaction product of syringaldehyde HDO formed during the reactor heat-up, and 5-MDT could be the series product formed from 4-MDP. Unlike in the bulk catalyst experiments, both compounds seemed to be rapidly consumed by other subsequent reactions. Both the supported metal as well as γ-Al_2O_3 support could catalyze such reactions as hydrogenolysis, hydrogenation and alkylation [124, 152, 155-156]. It can be noted that Pt/Al_2O_2 seemed to be not as efficient in converting 4-MDP as the other two catalysts. This was suggested by the higher amounts of this compound still present in the product compared to the other supported catalysts. However, in experiments using 4-MDP as the starting material, Pt/Al_2O_3 also showed about the same yield as Pd/Al_2O_3 (300°C, 60 minutes, 4-MDP: 11.5% and 11.7% respectively).

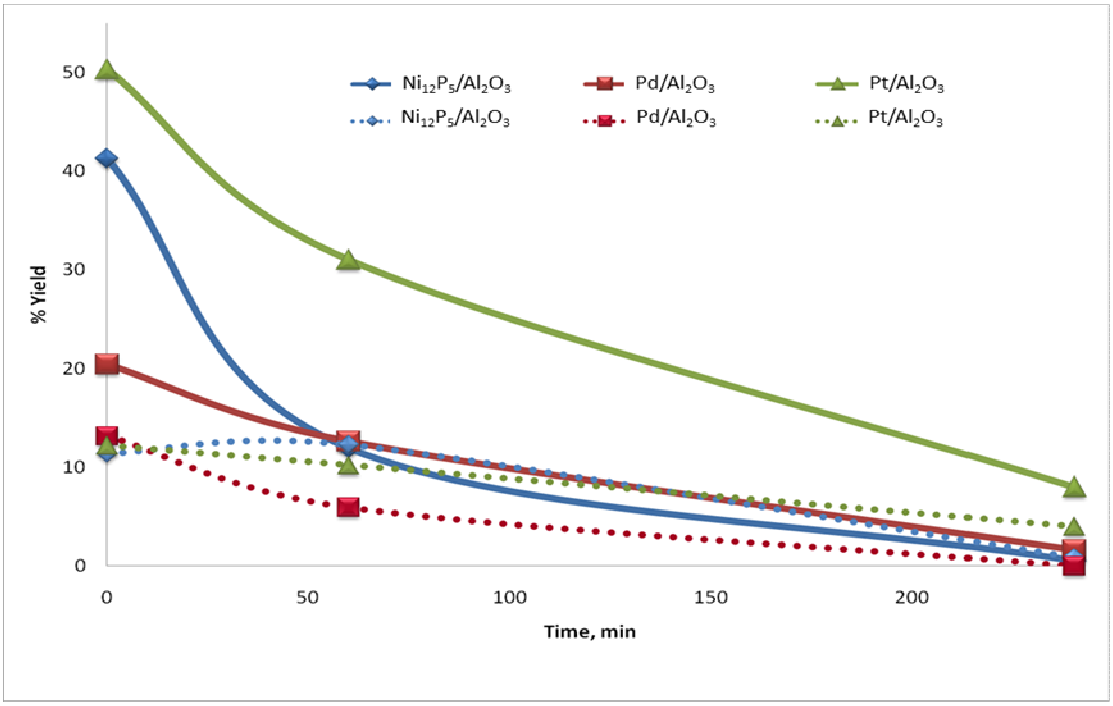

Figure 3.14 Yield of 2,6-dimethoxy-4-methylphenol (solid lines) and 5-methyl-3,4-dihydroxytoluene (dotted lines) using supported catalysts

3.3.2.2.3. Aromatic isomers and oxygenated saturated cyclics

Unlike the bulk catalysts, the combined yields of 4-MDP and 5-MDT were less than 50% in all experiments using the supported catalysts after 60 minutes at 300°C suggesting the higher activity of these supported catalysts for subsequent conversion of these compounds (Figure 3.14). The yields of 2,6-dimethoxyphenol at these reaction times were also minimal. Indeed, the GC/MS analysis of the rotavapped liquid product identified the presence of aromatic compounds with molecular weights ranging from that of phenol (94 g/mol) to 4-MDT (168 g/mol). These molecules seem to be the alkylated, demethoxylated and dehydroxylated products of syringaldehyde and of the other intermediate products. Alkylation was most probably catalyzed by the support, γ-Al_2O_3 [121, 157].

Possible structures of the isomeric compounds based on their mass fragmentation patterns were shown in Figure 3.15a. The presence of identifying mass fragments (m/z) for lignin-derived molecules (which syringaldehyde is) based on previous studies was confirmed to be present for each compound [158]. These aromatic isomers are typically not available commercially for comparison. The small oxygenated cyclic compounds (Figure 3.15b) were identified directly by the GC-MS. Based on the time at which these isomers eluted, two fractions of peaks were identified and quantified: (a) small oxygenated cyclohexyls and the small aromatic compounds, catechol, guaiacol and p-cresol; and, (b) the rest of the aromatic isomers (not including 4-DMP and 5-MDT). Figure 3.16 summarizes the yields of the aromatic isomers and small oxygenated compounds present in the products. The relative compositions of these two groups at different reaction times are also plotted.

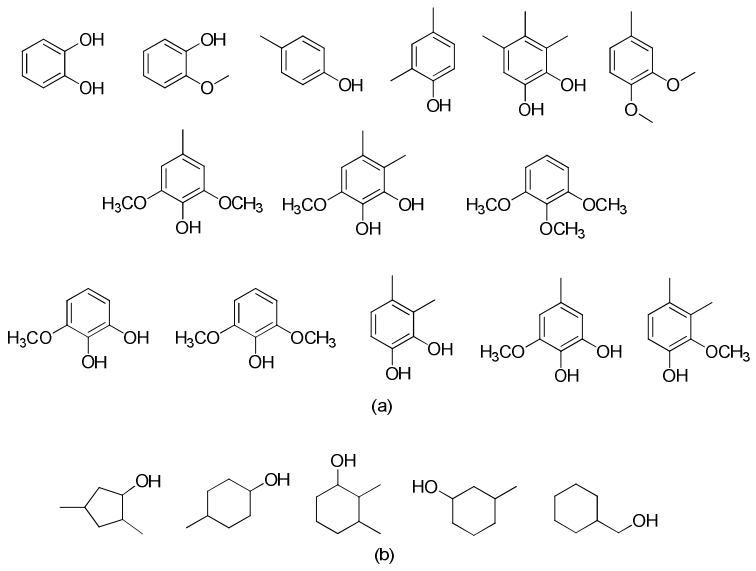

Figure 3.15 Possible aromatic isomers and cyclic oxygenated compounds based on GC/MS

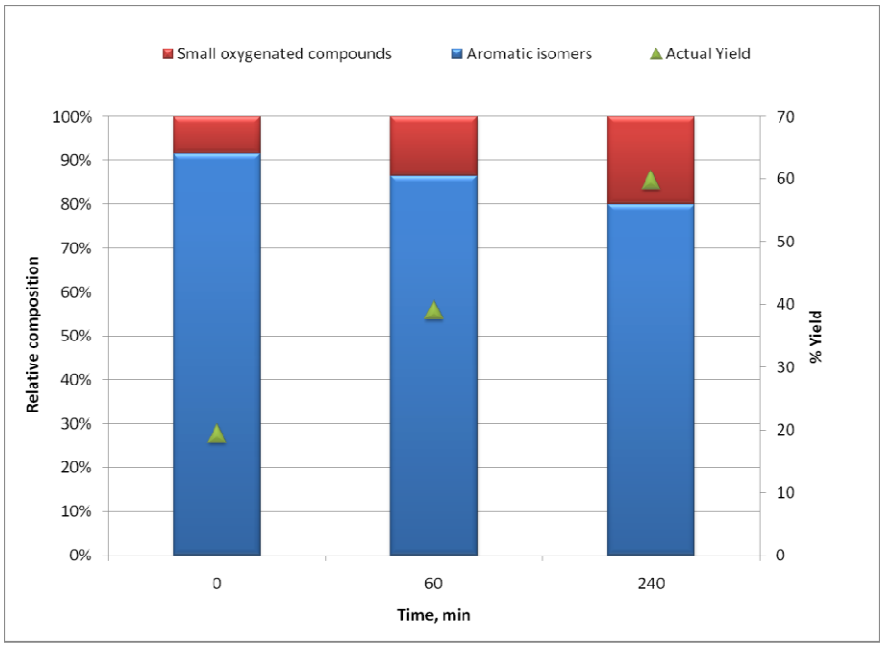
Small oxygenated compounds
Aromatic isomers
Actual Yield
100%
90%
80%
70%
60%
50%
40%
30%
20%
10%
0%
Relative composition
70
60
50
40
30
20
10
0
% Yield
0
60
240
Time, min

(a)

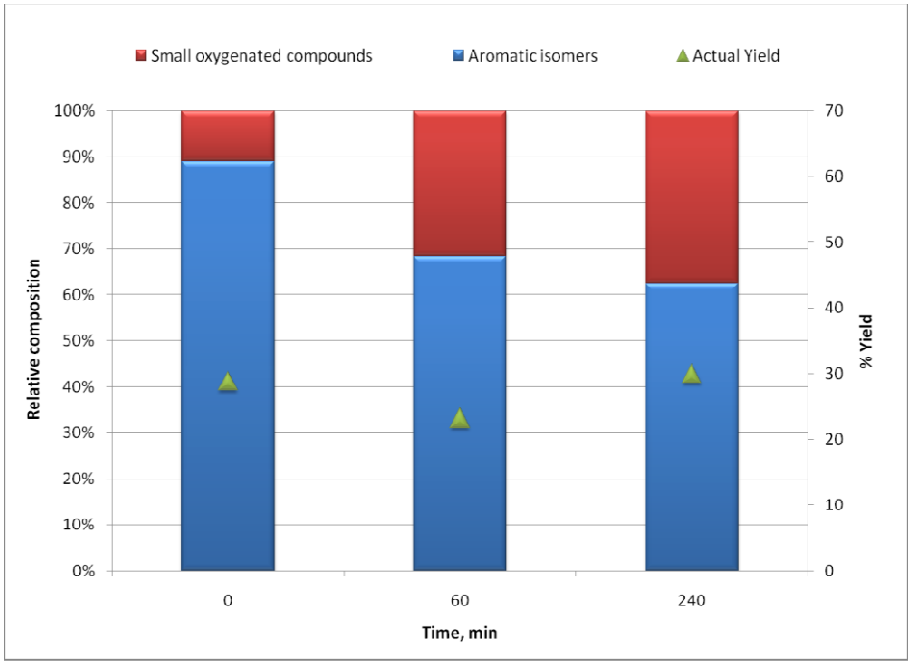
Small oxygenated compounds
Aromatic isomers
Actual Yield
100%
90%
80%
70%
60%
50%
40%
30%
20%
10%
0%
Relative composition
70
60
50
40
30
20
10
0
% Yield
0
60
240
Time, min

(b)

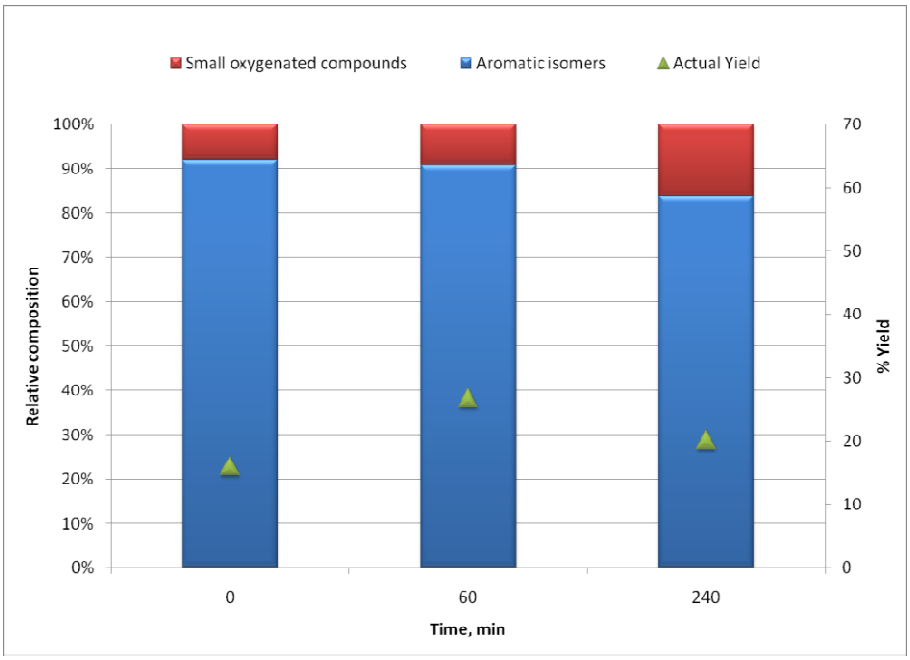

(c)

Figure 3.16 Yields and relative compositions of small oxygenated compounds and alkylated aromatic isomers: (a) $Ni_{12}P_5/Al_2O_3$; (b) Pd/Al_2O_3; and, (c) Pt/Al_2O_3

The yields of these by-product compounds were different for each catalyst. $Ni_{12}P_5/Al_2O_3$ showed the highest yield of the alkylated aromatic groups which can be quite attractive as feedstocks for fuel applications [141]. In general, as the percentage of the aromatics decreases with increasing reaction time, the relative amount of the smaller compounds increased. It can be suggested that the smaller compounds were formed from the action of the catalysts on some of these aromatics. From the relative percentages of these compounds in Figure 3.16, Pd/Al_2O_3 was better at catalyzing the hydrogenation and hydrodeoxygenation of the aromatics than both the supported $Ni_{12}P_5/Al_2O_3$ and Pt/Al_2O_3. A maximum for the combined yield of these types of compounds seem to have occurred

for Pt/Al_2O_3 after 60 minutes at 300°C while a steady increase was seen for the $Ni_{12}P_5/Al_2O_3$.

3.3.2.3. Mass balance

The yields for the identified and quantified products of the experiments using supported catalysts are summarized in Table 3.2. As shown, the fraction of the unknown compounds tended to increase with increasing reaction time. It can also be noted that the fraction of accounted for products for the supported nickel phosphide tended to be higher than the supported noble metals. As mentioned previously, the tri-hydroxy compounds tend not to be measurable in the GC-FID and these may account for the discrepancy. Another limitation was the overlap of the hydrocarbons, i.e. cyclohexane and cyclohexene, with the solvents in the GC-FID chromatograms. The much larger areas associated with the solvents may introduce large errors in the computed values. Aside from monocyclic products, small amounts of condensed products were also observed, typically at t = 0 minutes. These were probably formed from the condensation of the aldehyde feed [159]. Lastly, the incomplete balance may also be due to the formation of coke which has been reported in previous studies [121, 125]. From our own TGA measurement, organics on the catalysts did not exceed 15% by weight of catalyst. As another aside, X-ray photoelectron spectroscopy (XPS) was used to analyze the spent catalysts. This revealed different types of carbon present [160].

Table 3.2 Summary of HDO product yields

	$Ni_{12}P_5/Al_2O_3$			Pd/Al_2O_3			Pt/Al_2O_3		
	0 min	**60 min**	**240 min**	**0 min**	**60 min**	**240 min**	**0 min**	**60 min**	**240 min**
Small hydrogenated cyclics	1.7	5.3	12.0	15.4	11.7	9.9	1.3	2.5	3.3
Aromatic Isomers	17.8	33.8	47.9	13.4	11.5	20.1	14.8	24.4	16.9
5-MDT	11.4	12.9	0.8	13.1	5.9	1.3	12.2	10.2	4.0
4-MDP	41.1	12.1	0.5	20.4	12.6	1.6	50.3	31.0	8.0
SUM	**71.9**	**64.1**	**61.3**	**62.4**	**41.7**	**32.9**	**78.6**	**68.0**	**32.2**

3.3.2.4. Products and reaction pathway

Based on our results, a proposed reaction pathway for the HDO of syringaldehyde is shown in Figure 3.17. Analysis of the liquid product by gas chromatography showed the presence of two major products in the HDO of syringaldehyde. These were not readily identified, by the MS libraries available to our group (NIST, 2005 and Wiley, 1985). They were later identified as 4-methy-2,6-dimethoxyphenol (4-MDP) through injection of a commercially available pure compound, and 3,4-dihydroxy-5-methoxytoluene (5-MDT) through synthesis [161], purification and eventual analysis of the pure compound. We propose that the route for the formation of these compounds to be the dominant route for both bulk and supported catalysts. The aldehydic O was more labile than the other functional groups (i.e., methoxy and phenolic) and was attacked first. This supported the findings reported by Delmon et al. using sulfided supported CoMo and NiMo [121-122, 124-125]. The carbonyl group was reported to have a much lower activation energy at a lower temperatures (12 kcal/mol at 203°C) compared to a

carboxylic group (26 kcal/mol at 283°C) or an alkyl phenol (*para-:* 33.6 kcal/mol at 340°C, and *ortho-*: 35.8 kcal/mol at 367°C) [122].

In the formation of 5-MDT from 4-MDP, demethylation of one of the methoxy groups occurred. The sequential formation of 5-MDT from 4-DMP was confirmed by experiments with 4-MDP as feed. Cleavage of the $–CH_3$ within the methoxy group was also reported for HDO of guaiacols [121, 124-125, 130, 162-165] and anisole [166-168] in the presence of hydrotreating catalysts. As previously mentioned, the homolytic scission between the methyl and O may have occurred on specific sites on the catalyst. In the course of the reaction, it was expected that the other methoxy group should be demethylated as well. This would have formed 5-methylbenzene-1,2,3-triol. However, as mentioned previously, this product was not amenable to analysis in the procedure used in this study. Silylation may improve the quantification of these types of compounds in the product as this process tends to lower the boiling point of the compound in question.

In the presence of the acidic alumina support, another mechanism may explain the breaking of the C-O bond of the methoxy groups. Bredenberg et al.[152] cited that a heterolytic scission on the support may occur between the C-O bond because of the presence of Brønsted acid sites from octahedral alumina. The methyl carbonium ion that was formed may then attack the aromatic ring. This mechanism could very well explain the presence of the alkylated aromatics in the product when the supported catalysts were used.

HDO of syringaldehyde with the non pre-reduced NiO and $Ni_3(PO_4)_2$ produced the most quantified amounts of 2,6-dimethoxyphenol (2,6-DMP). It is probable that the formation of this compound came from the hydrodealkylation of 4-DMP due to the

possible formation of reduced Ni metal in these catalysts during the course of the experiment. In the hydrodealkylation of toluene at 380°C in the presence of different supported Group VII-B and VIII metals, Ni was found to have the highest relative specific activity for benzene formation from toluene [169]. This same mechanism could very well play an important role in the NiO-catalyzed HDO.

Lastly, another pathway for the formation of 2,6-DMP may also be present through the decarbonylation of syringaldehyde in the presence of extra-framework alumina in the support. In the deoxygenation of benzaldehyde in the presence of GaZSM-5, similar competing pathways forming benzene and toluene from benzaldehyde were also observed [159]. The selectivity to benzene formation was closely associated with the availability of Brønsted acidity in the catalyst [159].

3.4 CONCLUSIONS

Both bulk $Ni_{12}P_5$ and supported $Ni_{12}P_5/Al_2O_3$ were successfully synthesized by temperature reduction, as confirmed by XRD measurements. These were used in the HDO of syringaldehyde, a lignin-derived compound which contains aldehydic, methoxy and phenolic groups. Experiments showed that the aldehydic group was the most susceptible among the three.

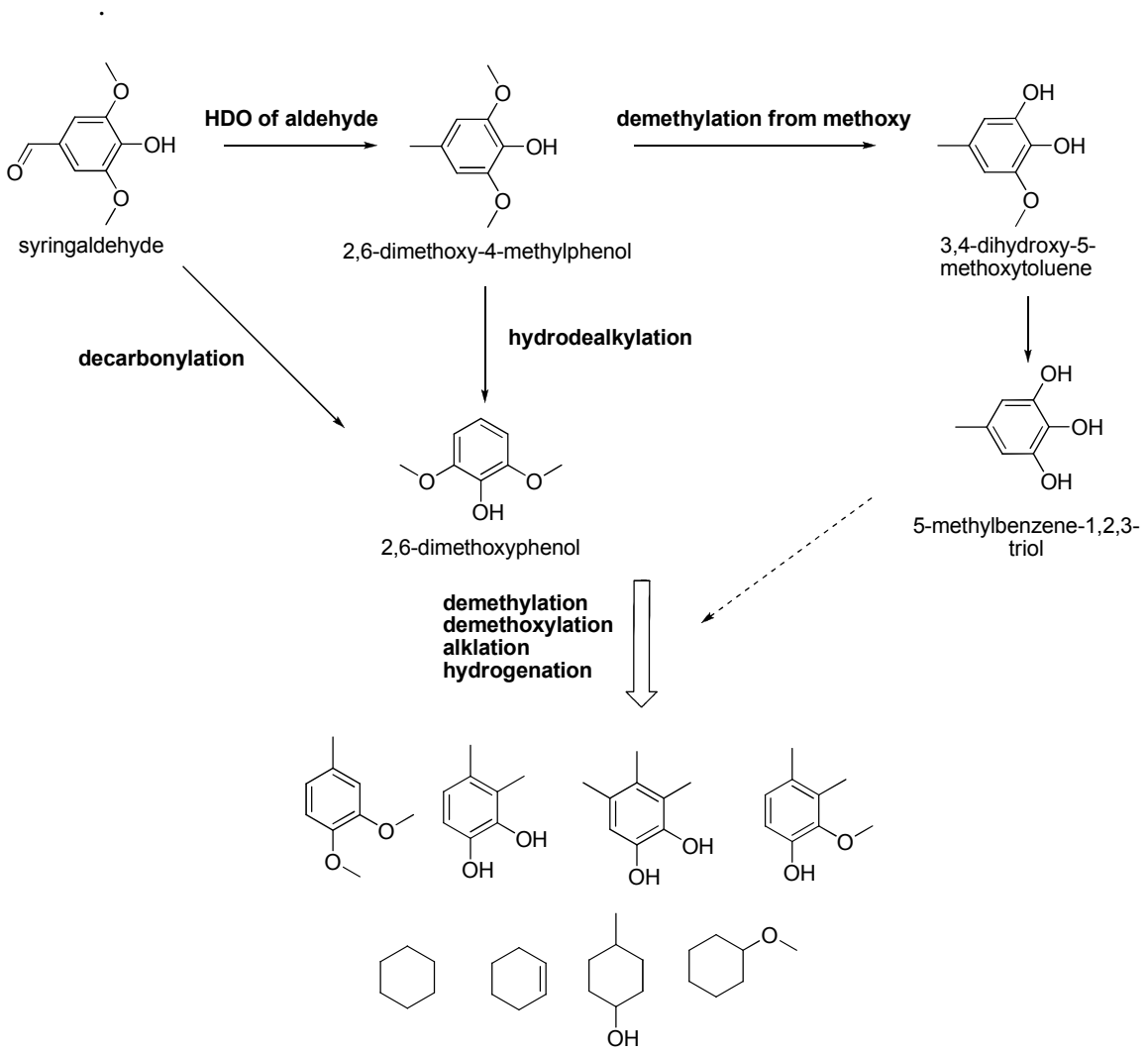

Figure 3.17 Proposed reaction pathway for the hydrodeoxygenation of syringaldehyde

The bulk $Ni_{12}P_5$ yielded ~80% conversion at the start (during the reactor heat-up phase) and showed complete conversion of syringaldehyde after 4 hours at 300°C. Comparatively, non-reduced NiO showed almost complete conversion even at the beginning of 300°C while $Ni_3(PO_4)$ did not reach complete conversion even in 4 hours. $Ni_{12}P_5$ was more capable of demethylation of the methoxy substituent, compared to the other bulk catalysts, thus forming 5-methyl-3,4-dihydroxytoluene (5-MDT). On the other

hand, NiO produced the decarbonylated compound, 2,6-dimethoxyphenol (2,6-DMP) at relatively much higher quantities.

The main reaction pathway of syringaldehyde to 4-MDP to 5-MDT was still followed by the supported catalysts. However, the presence of the γ-Al_2O_3 support caused the alkylation of the aromatic ring, thus forming alkylated compounds. In the conditions used in this study, Pt/Al_2O_3 showed the least conversion of 4-MDP to other by-products. On the other hand, Pd/Al_2O_3 yielded the most hydrogenated small molecules. Lastly, $Ni_{12}P_5/Al_2O_3$ gave an order of magnitude higher average TOF compared to the other two supported catalysts (commercially available Pt/Al_2O_3 and Pd/Al_2O_3.). However, kinetic studies with low syringaldehyde conversions are necessary (possibly at lower temperature) are necessary to compare their relative activities.

3.5 RECOMMENDATIONS

This study was focused more on understanding the pathway for the hydrodeoxygenation of syringaldehyde using different catalysts. The experiments showed that the aldehydic group of syringaldehyde is the most susceptible to hydrodeoxygenation in the presence of the supported $Ni_{12}P_5/Al_2O_3$ as well as that of the commercially supported noble metals. It is thus suggested that using a lower temperature step for the sole purpose of stabilizing the aldehydic group may be explored. In this study, this step seemed to occur during the reactor heat-up. Since the goal at this stage is the removal of one oxygen molecule (that associated with the aldehyde), the amount of H_2 needed for this reaction should be lower than what is currently applied and thus, can be optimized.

For further removal of the remaining oxygen, reactions at a higher temperature may be necessary. The main limitation for attempting a higher temperature in this study was the reactor. Though it was already modified in order to accommodate the more stable PTFE at higher temperature than original Kalrez O-ring, the use of a reactor with graphite as an O-ring might allow for higher temperature testing. However, the amount of torque applied to sealing the O-ring is more critical for the graphite. Thus, a different reactor closure design may be required.

Alkylation of the aromatic group is favorable in increasing the octane number of the product. Since methylation was seen to occur in this system with the only source most probably as the methyl removed from the methoxy group, it can thus be conceived that addition of some amount of methanol and/or other alcohol in the feed may lead to higher degree of alkylation. However, since addition of the alcohol would definitely increase the vapor pressure of the system, a more robust reactor seal is necessary more than ever especially at high temperatures.

Better catalyst understanding may be done through kinetic studies as well as recyclability studies. Using different loadings of $Ni_{12}P_5$ may also be tested.

Lastly, a mixture of different starting materials approximating pyrolysis oils may be used as feed instead of only one model compound with different functionalities. This would give a better metric of the performance of the catalysts used in this study in the presence of actual biomass pyrolysis oil.

CHAPTER 4

PHENOL HYRODEOXYGENATION/HYDROGENATION

Chapter 3 focused on batch hydrodeoxygenation for a lignin model compound, syringaldehyde using nickel phosphide, nickel- and noble metal-based catalysts. In this chapter, the continuous mode hydrodeoxygenation of yet another lignin-derived compound, phenol, is presented. The goal of this part of the study was to probe the hydrodeoxygenation/hydrogenation of phenol by bifunctional catalysis. Instead of the previously tested Pt/HY catalyst [170] nickel-based supported catalysts were used in the present study. Three supports were utilized: mesocellular silica (MCF), aluminated mesocellular silica (Al-MCF) and zeolite HY. Aside from the wet-impregnated metal-acidic support catalysts, several catalyst bed configurations were also screened: (a) Ni on silica (MCF) alone, (b) sequential beds of Ni-MCF followed by acidic catalyst (either HY or Al-MCF) and (c) a physical mixture of the Ni-MCF and the acidic catalysts. A solution of phenol and water was fed into a stainless steel reactor, heated at 200°C. Phenol conversion was found to be complete and stable in systems with the metal and acidic sites on separate catalysts. Depending on catalyst configuration, the main product that was formed can be tuned and produced at high selectivities, yielding cyclohexanol, cyclohexene and cyclohexane as main products at more than 90% selectivities. Aside from the catalyst configuration, hydrogen to phenol ratio was found to play an important role in the product selectivities as well.

4.1 INTRODUCTION

4.1.1 Motivation

Aside from its familiar use as the most ubiquitous energy source, fossil fuels also find importance as a chemical feedstock. The International Energy Agency [2] reported that "non-energy use" of fossil fuels, consumed as raw material (petrochemical feedstock), comprised the second biggest use for oil in 2008. Together with transportation, these two sectors comprise a total of ~77% of crude oil consumption, with ~16% attributed to non-energy use [2]. Today, significant efforts focus on identifying alternative sources to supplement petroleum as a fuel and as a chemical feedstock. Lignocellulosic biomass is a most promising feedstock for both applications. However, the O/C ratio of biomass-derived products needs to be reduced while its H/C ratio needs to be increased, in order for the alternative products to be compatible with the existing petroleum processing infrastructure [42].

Lignocellulosic biomass consists mainly of carbohydrate fractions (cellulose and hemicellulose), poly(aromatic) groups (lignin), inorganic compounds (ash) as well as proteins and other organic compounds (pectin and resins). The three main macropolymers, (cellulose, hemicellulose and lignin) make up ~90 wt.% of the biomass. This value also considers non-wood feedstocks which tend to have higher amounts of extractives and ash than woody biomass does [28].

Cellulose and hemicelluloses are currently tapped for production of paper, industrial polymers (e.g. cellulose acetate) and bio-ethanol. This process leaves lignin as a by-product. Considering that lignin is typically close to about one third of the mass of the starting material, this is a renewable resource that must be utilized efficiently. Among

the three biomass-derived polymers, lignin most closely resembles petroleum chemically. In comparison, carbohydrates have higher O/C and lower H/C ratios. Routes to chemically transform lignin to useful fuels or chemicals have attracted significant research for decades and are gaining more momentum [44, 171-173].

Fast pyrolysis is one of the biomass-conversion processes that are currently being tapped to produce liquefied products. This process produces bio-oils that usually contain large amounts of phenolic compounds from lignin and lignin-carbohydrate reaction products [170]. It has been reported that phenols in these oils could reach as high as 45% of the organic phase product [174]. In view of Furimsky's note that together with furans, phenols could be recalcitrant to hydrodeoxygenation [38], there is a need for new or improved technologies in order to harness phenolic compounds for alternative fuel or chemical feedstock use.

4.1.2 Removal of oxygen from phenol

In a proposed multistage HDO processing of bio-oils, it has been suggested that methoxyphenols, biphenols and ethers be treated in a so-called stabilization stage in the presence of H_2 at temperatures less than 573 K [38]. These primary reactants would then be converted to phenol which would probably require processing protocols similar to coal-derived liquid processing conditions, e.g. at 623 K, for second stage treatment [38]. The hydrodeoxygenation/hydrogenation of phenol gives way to the formation of benzene, cyclohexanone, cyclohexanol, cyclohexene and cyclohexane in the presence of a catalyst. In the presence of acid sites, methylcyclopentane can also be formed through cyclohexane isomerization [156]. Formation of products with enhanced molecular mass

through ring-coupling reactions in the presence of bifunctional catalysts (strong acid sites and hydrogenation sites) has been reported [170].

In a previous studies, benzene production from phenol had been suggested to be formed through a pathway different from the one involved in the formation of other products[170, 175]. Phenol can also be converted into the very reactive intermediate, cyclohexen-1-ol, which could be converted to either cyclohexanol or cyclohexanone. The competing pathways both produce cyclohexene and then cyclohexane. From recent experiments, we have found that cyclohexanol and cyclohexanone can be easily inter-converted under certain reaction conditions, which was is in agreement with previously published literature [176]. This is reflected in the inclusion of the cyclohexanol to cyclohexanone pathway into the scheme described in Scheme 4.1.

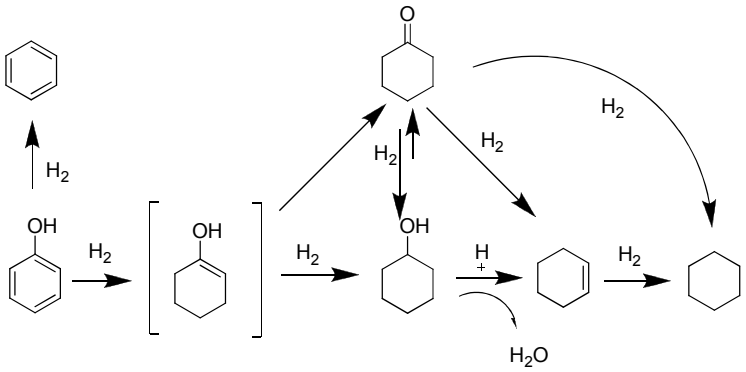

Scheme 4.1 Modified hydrogenation pathway of aqueous phenol

Hong et al. also reported the formation of bicyclics and tricyclics. These compounds were postulated to be acid-catalyzed products of phenol with the intermediate products, cyclohexanone and cyclohexanol [170].

Of the array of products described above, the fully hydrogenated products cyclohexane and bicyclohexyl have properties that make them useful fuels. The ring-

saturated but oxygen-containing products, cyclohexanol and cyclohexanone, are important chemicals used in the production of nylon 6,6 [177]. Cyclohexene derivatives have been used for polymer synthesis [178-179] and cyclohexane is also used as a solvent or as the feedstock for cyclohexanol and cyclohexanone production [180]. Considering the various by-products resulting from the hydrotreatment of phenol, it would be beneficial to tune the reaction selectivity of phenol in order to produce either chemicals or fuels.

4.1.3 Previous phenol hydrogenation studies

Catalytic treatment of phenol had been studied both as a model compound for biomass-derived (specifically, lignin-derived) products or as a means of remediation treatment for the environment, using different catalysts and different temperatures (to name a few: [170, 175-176, 181-189]). Noble metal catalysts such as Pd have been used as well as Ni, which is a cheaper non-precious metal. A quick look at spot prices places Pt at $ 26,500/lb, Pd at $ 11,900/lb and Ni at $ 12/lb [190], with Ni being three orders of magnitude cheaper.

Several groups have used Ni in the study of oxygen removal from phenol [175, 181-182, 191], most notable of which were done by Keane and coworkers [175-176, 181-182]. They used wet impregnated Ni on commercially available Cab-O-Sil silica catalysts, at different Ni loadings. This variation of metal content on SiO_2 (1 – 20.3% wt/wt) translated to different metal particle sizes and activities. Using a glass-flow reactor and under flowing H_2, reactions temperatures (423 – 573 K), flow rates and solvents were varied. Cyclohexanol was formed as the main product (selectivity > 50%) up to ~540K (267°C, with 1.4 nm), followed by benzene and cyclohexanone. Benzene was favored at

bigger particle sizes (2.5 – 3.1 nm vs. 1.4 nm, W/F = 69 g/mol h), becoming the major product at 473 K (200°C) with the catalysts having 3.1 nm particles. However, in the presence of water at 473 K and using the catalyst with 3.1 nm particles, cyclohexanol was the main product [175]. Under the same conditions, with cyclohexanol as the feed, cyclohexane and benzene were shown to be mostly in the product stream with a negligible amount of cyclohexanone. On the other hand, with cyclohexanone as feed, cyclohexane was formed at about 70% selectivity with benzene and cyclohexanol having about the same selectivity. Analyzing the trend in cyclohexane production showed similar profiles between cyclohexanone and phenol, rather than cyclohexanol, leading the authors to suggest that cyclohexane most probably was formed through the cyclohexanone route [175].

Hong et al. [170] reported the HDO of aqueous phenol (10 wt% water) at elevated pressures (40 bars) at 200°C using Pt supported on different supports, but mainly on zeolite HY (0.5 wt% Pt/HY). Due to the presence of the acidic support, the main product in these experiments was cyclohexane. Hong et al. also reported the formation of bicyclics and tricyclics formed as aldol condensation reactions through acid-catalyzed reactions [170]. Additionally, they varied the weight hourly space velocity (WHSV) to obtain different phenol conversions and found out that selectivities for cyclohexanol and cyclohexanone reversed at about 25% phenol conversion, confirming the competing pathways forming these products [189]. However, unlike selectivity for cyclohexanol and cyclohexanone, selectivity for benzene was quite impervious to changes in phenol flowrates. This prompted the authors to conclude that a separate pathway for the hydrodeoxygenation of phenol directly to benzene exists. From further experiments, it

was noted though that the zeolite supported catalyst deactivates after only 5 hours. Considering that industrial operations of these types of reactions require much longer catalyst lifetimes, it would be interesting to determine if this system can be improved, such that phenol conversion can be maintained at much longer time-on-stream.

4.1.4 Objectives

The main objective of this study was to develop a Ni-based catalyst system for the hydrodeoxygenation of phenol capable of sustained phenol conversion for extended period of time. Specifically, the goals included:

(1) synthesis and characterization of supported Ni catalysts though wet impregnation and through hydrothermal synthesis on mesoporous silica, mesoporous aluminosilicate and zeolite HY supports;

(2) probing the role of bifunctional catalysis on the removal of oxygen from phenol in the presence of Ni and an acidic catalyst;

(3) systematically vary catalyst configuration and determine its effect on product selectivity; and,

(4) determine the effect of H_2/phenol ratio on product selectivity and catalyst deactivation.

4.2 EXPERIMENTAL METHODS

4.2.1. Materials

The chemicals used in this study, including the precursor compounds for the catalysts and pure compounds for GC-FID calibration were obtained from Sigma-Aldrich and used without further purification: nickel (II) nitrate hexahydrate ($Ni(NO_3)_2 \bullet 6H_2O$,

99.999%), tetraethylorthosilicate (TEOS, 98%), poly(ethylene oxide)-block-poly(propylene oxide)-block-poly(ethylene oxide) (PEO-PPO-PEO, avg M_n = 5800), 1,3,5-trimethylbenzene (1,3,5-TMB, (≥99.0%), hydrochloric acid (HCl, 37%), ammonium hydroxide (NH_4OH, 30%), ammonium phosphate dibasic ($NH_4H_2PO_4$, ACS reagent), aluminum nitrate nonahydrate ($Al(NO_3)_3 \cdot 9H_2O$, ≥98%), phenol (≥99%), cyclohexanone (≥99.5%), cyclohexanol (99%), benzene (≥99.5%), cyclohexane (≥99%), cyclohexene (≥99%), methylcyclopentane (≥99.5%) and silicon carbide (SiC, - 200 mesh, ≥97.5%). Zeolite NH_4Y was obtained from Zeolyst International (CBY712), with a SiO_2/Al_2O_3 = 12. The gases used (helium, He and hydrogen, H_2) were of ultra-high purity grade obtained from Air Gas.

4.2.2. Synthesis of Ni-MCF

Ni-MCF was synthesized by hydrothermal synthesis method using $Ni(NO_3)_2 \cdot 6H_2O$ and TEOS as the nickel and silicon sources, respectively. As with typical MCF syntheses [192], the triblock surfactant, PEO-PPO-PEO, was used as structure-directing agent with 1,3,5-trimethylbenzene as the pore expander. The target ratio for the nickel loading was Si/Ni = 12. In a typical synthesis, two mixtures, A and B, were prepared. Mixture A consisted of 5 g of PEO-PPO-PEO transferred into an Erlenmeyer flask, to which 2.5 g of 1,3,5-TMB and 187.5 g of aqueous HCl (pH = 1.5) were added. The mixture was stirred using a magnetic stir bar at 40°C for about 4 hours, at which point, Mixture B was poured in. Mixture B, which contained the nickel and silica source, was prepared by dissolving about 0.123 g $Ni(NO_3)_2 \cdot 6H_2O$ in a stirred flask of 12.5 g of aqueous HCl solution (pH = 1.5). About 10.625 g of TEOS was then added. Mixture B was stirred for about 2 hours at room temperature before being added to Mixture A. The

resulting combination of Mixture A and B was then vigorously mixed for 20 hours at 40°C to age it. After this, the mixture was cooled and neutralized by carefully adding drops of NH_4OH (30 wt% NH_3) solution. The sol was then transferred into the Teflon lined bombs (*Parr Instruments*, 45 ml) and rotated in the oven for 24 hours at 100°C. After quenching in an ice bath, the solid contents of the reaction bombs were filtered and washed with copious amounts of water. The solids were then dried overnight in an oven at 85°C. After transferring into porcelain dishes, the solids were calcined to burn off the surfactant template. The calcination protocol consisted of drying the solids under flowing air for 4 hours at 120°C followed by a heating ramp of 1.2 °C/min to 550°C and keeping at 550 ^{o}C for 8 hours under flowing air. The solids were then cooled and stored in vials. Before an experiment, the catalyst was pelletized, crushed and sieved. The -35 +70 fraction (average sieve opening = 460 μm) was recovered for the catalytic experiments.

4.2.3. Synthesis of H-Al-MCF

A similar procedure was followed for the synthesis of H-Al-MCF [193]. The target theoretical Si/Al ratio was 6, which is similar to the Si/Al ratio of the zeolite used in this study. $Al(NO_3)_3 \bullet 9H_2O$ was used as the aluminum source. In a typical synthesis, Mixture A was prepared the same way as in the Ni-MCF synthesis. However, instead of adding the Ni precursor to make Mixture B, 1.594 g of $Al(NO_3)_3 \bullet 9H_2O$ was added to the aqueous HCl. When Mixture B was added to Mixture A, another portion of 1.594 g of $Al(NO_3)_3 \bullet 9H_2O$ was added to the combined mixtures. The work-up was similar to what was described above.

4.2.4. Wet impregnation of HY and H-Al-MCF

Zeolite HY was obtained from Zeolyst (CBY712), with Si/Al = 6. The acid catalyst was activated and transformed to the H^+ form by increasing the temperature of the calcination oven to 120°C (soak for 4 hours) at a ramp rate of 1.2 °C/min followed by calcination at 500°C for 8 hours (heat ramp: 1.2 K/min, soak at 120°C for 4 hours) before use. $Ni(NO_3)_2 \bullet 6H_2O$ was dissolved in 7 ml of water. This was then added to 5.640 g of pre-activated HY. The resulting wet solids were dried at 85°C overnight and then calcined at 500°C for 8 hours.

For the synthesis of Ni-Al-MCF, about 2 g of calcined H-Al-MCF was impregnated with $Ni(NO_3)_2 \bullet 6H_2O$ solution composed of 0.6383 g $Ni(NO_3)_2 \bullet 6H_2O$ dissolved in 2.4 ml of water. It was also dried overnight and calcined at 550°C. The theoretical Si/Ni ratio for both impregnated catalysts was 12.

4.2.5. Catalyst Characterization

4.2.5.1 Elemental analysis

Elemental analysis of the catalysts was done by an outside laboratory (Columbia Analytical Services, Arizona) using ICP analysis. As previously mentioned, target Si/Ni ratio for the catalysts was 12, and Si/Al ratio was 6.

4.2.5.2 Temperature-programmed reduction (TPR)

Temperature-programmed reduction (TPR) was performed in flowing 10% H_2/Ar with a heating rate of 5 K/min after pre-treating the sample at 200°C in flowing Ar for an hour. This was done using a Micromeritics Autochem II system equipped with a TCD

detector. Typically, about 0.050g of catalyst was loaded into the quartz U-tube sample holder.

4.2.5.3 Temperature-programmed desorption (TPD)

Temperature-programmed desorption (TPD) of NH_3 of the catalysts was monitored by first drying 50-100 mg of catalyst in a quartz U-tube at 200°C in flowing He for 1 hr. After cooling the sample down to room temperature, 2000 ppm NH_3/He (Air Gas) was passed over the sample for 2 hours. Then, He was flowed over the sample for 1hr to remove physically adsorbed NH_3. The temperature was then increased from 40°C to 750°C and the amount of NH_3 desorbed was monitored. TPD of pre-reduced catalysts at 500°C under 10% H_2/Ar was also performed. TPD was also done using the Micromeritics Autochem II.

4.2.5.4 Nitrogen physisorption

Nitrogen physisorption experiments at 77 K were carried out using Micromeritics ASAP 2000 and ASAP 2020 for the MCFs and the zeolite Y-based supports, respectively. Prior to the analysis, the samples (~100 mg) were first degassed overnight at 180°C under 5 mm Hg of vacuum. Surface area was calculated using the Brunauer-Emmett-Teller (BET) equation. The pore size was calculated using Frenkel–Halsey–Hill-modified Broekhof–de Boer method (BdBFHH).

4.2.5.5 X-ray absorption spectroscopy

Extended X-ray Absorption Fine Structure (EXAFS) and X-ray Absorption Near Edge Structure (XANES) measurements of the hydrothermally synthesized and wet-impregnated Ni-AlMCF were carried out at the bending magnet beamline of the MR

CAT at the Advance Photon Source, Argonne National Laboratory by Dr. Jeff Miller and Dr. Tianpin Wu. The spectra were obtained in about 10 min in step-scan, transition mode. Ni foil for energy calibration was taken simultaneously with the samples. About 8 mg of each sample was pressed into a 4 mm self-supporting wafer. The sample holders could hold 6 samples allowing samples to be pre-treated under identical conditions.

The reactor was a 30 cm x 2.5 cm cylindrical quartz reactor, equipped with Cajon fittings and shut off valves and sealed by O-rings. The 0.5 x 0.5 mm X-ray beam went through Kapton windows at the end of the reactor. Each sample was positioned such that the beam would pass through the center of each sample.

Samples were run in air and then reduced ex-situ at 500 °C, with 50 cc/min of flowing 100% H_2 or 4% H_2 within 30 minutes to an hour. The temperature was measured at the sample by an internal thermocouple. After reduction, the reactor was cooled to room temperature under He and was properly sealed. The set-up allowed data to be collected for the reduced catalysts without its exposure to air.

The data were fit using the WinXAS 3.1 software. Experimental Ni-O and Ni-Ni phase and amplitude functions were obtained from NiO and Ni foil, respectively, as standards. XANES fits were obtained by a linear combination of the starting catalysts and Ni foil. The edge position was also compared to the XANES of NiO.

4.2.5.6 Fixed bed reactor

The diagram for the flow reactor system used is shown in Figure 4.1. The flow system consisted of the liquid delivery module, the gas delivery module, the down-flow reactor, and the analysis unit. Liquid feed (10 wt% water- phenol) was pumped through the system using a Shimadzu HPLC pump. Flow rates ranged from 0.0008 ml/min to

0.0078 ml/min. Pump pressure ranged between 5.0 and 8.0 MPa. Pressure readings outside this range for extended periods signaled that a check of the pump for blockages, or obstructions was needed.

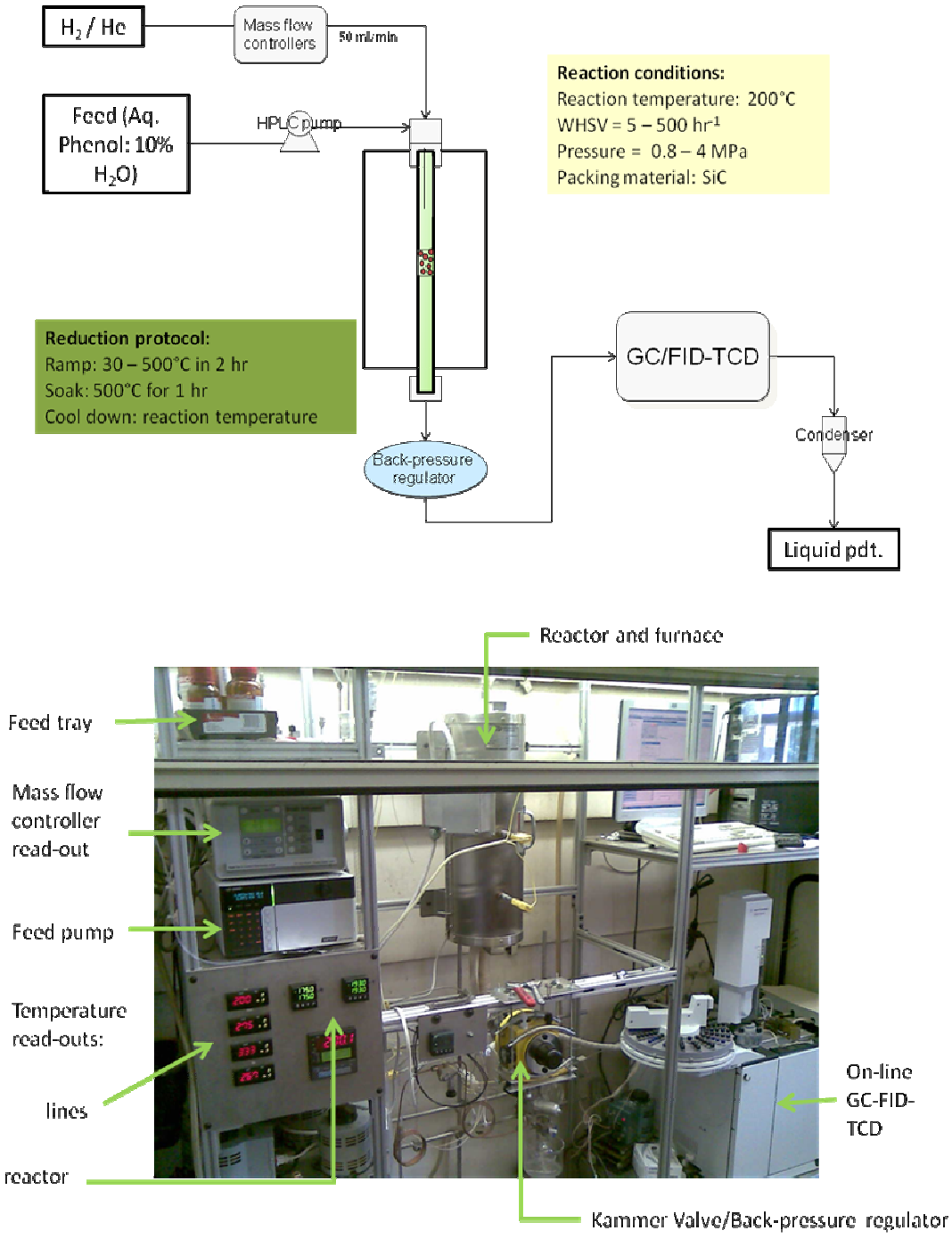

Figure 4.1 Flow reactor set-up

Ultra-high purity (UHP-grade) He and H_2 gases were metered into the system using Brooks mass flow controllers. During a typical reaction, about 50 ml/min of H_2 was allowed to flow through the system. At the end of a reaction, He was used as a purge gas for 30 minutes. The reactor and furnace were then allowed to cool down.

The reactor was a downflow packed bed column consisting of ¼" stainless steel tube with an internal diameter of 0.152" and length of 24". At both ends, VCR fittings were welded for connections to the rest of the system. Silicon carbide was used to disperse the catalyst as well as to promote temperature homogeneity throughout the reactor. The catalyst bed was prepared by mixing the pre-weighed catalyst pellets (-35 +75 fraction) with SiC to obtain a 1 ml mixture. The reactor was brought to the target temperature by an electric furnace. The furnace had three heating zones in order to allow better temperature control. Temperatures were measured by K-thermocouples, which are then connected to Omega DPCNi16 PID temperature controllers.

Depending on the required experimental condition, single- and dual- catalyst bed systems were run. The first catalyst bed was located at about 14.5" from the top of the reactor, while the second bed was 20" below the reactor top. The pressure in the reactor was controlled by a back-pressure regulator (either an air-actuated Kammer valve or a modified Tescom 44-2300 manual back pressure regulator).

Heated 1/16" lines from the reactor led into an online dual detector GC (Agilent 7890A) for analysis of the reaction products. Six-port valves with 0.25 ml sampling loops introduced the products into parallel columns: (1) HP-1ms column to the flame ionization detector (FID); and, (2) HP-PLOT S column to the thermal conductivity detector (TCD). Standard compounds were injected to identify elution times and generate calibration

curves for quantification. The excess gas products were constantly passed through a condenser (0°C) with an attached collector. Thus, condensed liquid samples could be collected and analyzed in an off-line GC-MS (Shimadzu QP-2010) for the identification of products.

4.2.5.7 Reaction conditions

Flow experiments were typically done at 200°C and at 7.8 bars (100 psig) of H_2. Some preliminary experiments were done at 40 bars to compare with a previous study by Hong et al. that used 0.5 wt% Pt/HY catalyst [170]. The H_2 flow was set at 50 ml/min, and the WHSV of aqueous phenol solution was typically 5 hr^{-1}. WHSVs as high as 500 hr^{-1} were run in some cases.

The following catalyst configurations were tested: (a.1) Ni-MCF; (a.2) Ni-impregnated acidic catalysts; (b) Ni-MCF followed by a downstream bed of acid catalysts (dual bed experiment); and, (c) a physical mixture of the Ni-MCF and acidic catalyst in the same bed. These configurations are illustrated in Figure 4.2. For a typical experiment, the amount of Ni was held constant at 6 mg (6% by wt, 100 mg supported catalyst) with constant aqueous phenol flow of 0.0078 ml/min.

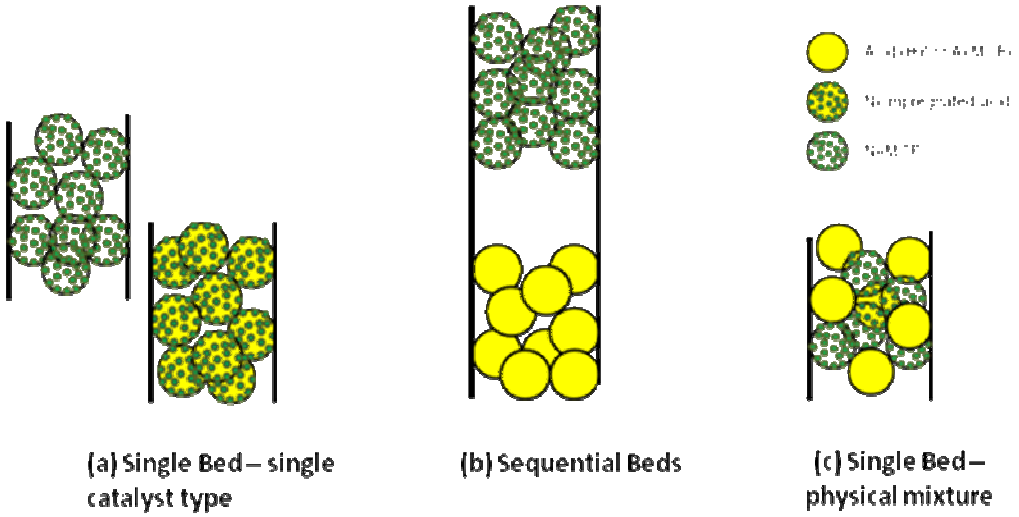

Figure 4.2 Various catalyst configurations used in the study

4.3. RESULTS AND DISCUSSION

4.3.1. Catalyst Characterization

4.3.1.1. Textural properties

The role of Ni and acid catalytic sites for the hydrogenation of phenol was probed by using different combinations of the following catalysts: (a) hydrothermally synthesized Ni-MCF, (b) acidic supports (HY and Al-MCF) and (c) bifunctional catalysts: Ni-impregnated on acidic supports. The composition of the Ni-containing catalysts, surface areas, and pore volumes are summarized in Table 4.1. All three Ni-based catalysts had similar Si/Al and Si/Ni ratios. As expected, the zeolite-supported catalyst, Ni-Y, had the highest surface area but the smallest pore volume. The MCF supported catalysts had about three times the pore volume of the zeolite catalyst and about an order of magnitude bigger pore size. As such, it may be able to handle the more branched or larger bio-based molecules such as alkylphenols and fatty acids required in

the processing of real biomass without significant pore blocking and mass diffusion problems [194].

As expected, the addition of Al into MCF reduced the surface area and pore volume of the catalyst. Liu *et al.* reported similar values for surface area and pore volumes for H-Al-MCF materials [193]; using $Al(NO_3)$ as the aluminum source (same as in the present study) produced the smallest surface area in all their synthesized catalysts [193].

Table 4.1 Textural properties of the nickel-based catalysts

Catalyst	Si/Al	Si/Ni	BET SA Capacity (m^2/g)	Pore volume capacity (cm^3/g)
Ni-MCF	-	11.8	451	1.31
Ni-H-Al-MCF	5.1	11.2	403	1.07
Ni-Y	6.0	11.4	755	0.42

4.3.1.2 Temperature-programmed Reduction (TPR)

Temperature programmed reduction experiments were used to elucidate the reducibility of the catalysts used in these experiments. Figure 4.3 shows the summary of the TPR profiles of the array of catalysts used here; also included are TPR profiles of commercial $Ni(NO_3)_2$ (precursor) and NiO, for comparison.

As expected, the bulk commercial compounds had lower reduction temperatures. Commercial NiO showed two distinct reduction peaks: at about 240°C and 350°C. The low temperature peak is typically assigned to non-stoichiometric nickel oxide, i.e., Ni_2O_3 [151]. The Ni^{3+} species typically contribute to the black color in the otherwise generally green NiO [151]. The peak at 350°C would correspond to the majority Ni^{2+} species. In

supported catalysts, this range has been assigned to the reduction of large NiO crystallites that have minimal or no interaction at all with the support [195-196]. On the other hand, the commercial bulk $Ni(NO_3)_2$ TPR curve showed reduction peaks that are much lower than those of NiO. This might be attributed to the presence of the nitrates. According to Miguel-Garcia et al., the direct reduction of NO_x starts around 230°C and peaks at 280°C by a coupled TGA-MS analysis of cerium nitrate under an H_2/N_2 atmosphere [197]. The TPR ramp rate used by these authors was twice the temperature ramp (10 K/min) used in this study (5 K/min).

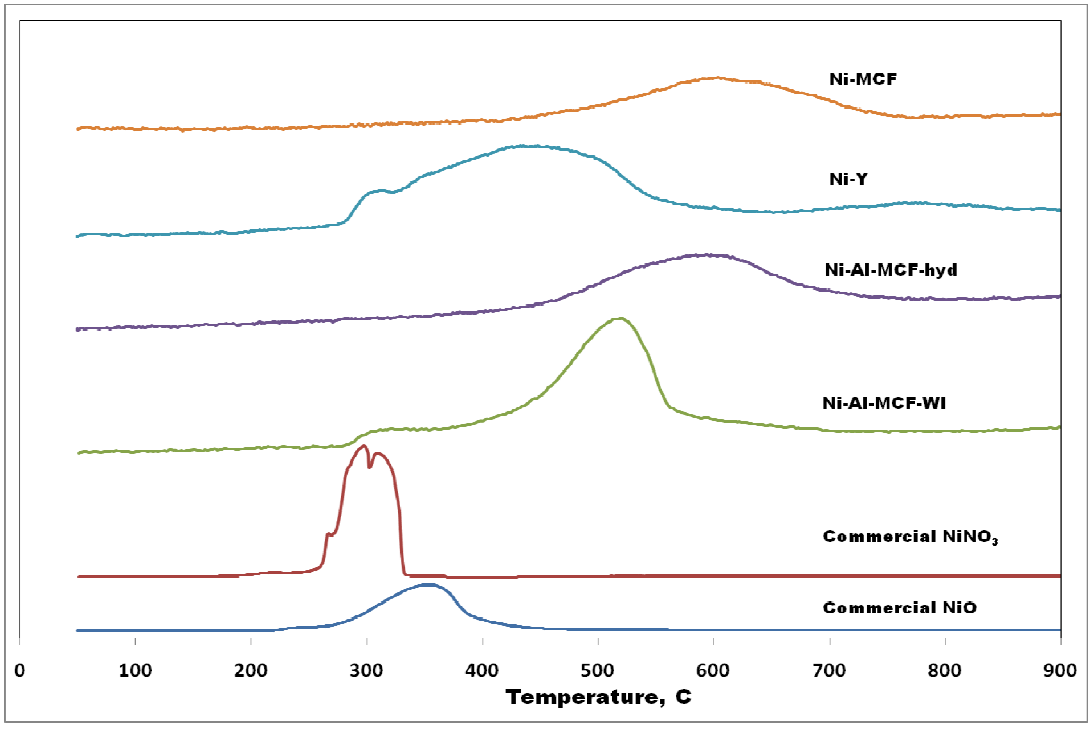

Figure 4.3 Temperature-programmed reduction (TPR) profiles of different catalysts and standards (heating rate 5 K/min)

The TPR curves of the synthesized catalysts showed that complete reduction for these bifunctional catalysts occurred at much higher temperatures than the bulk samples.

This increase in reduction temperature may be attributed to (a) metal oxide/support interactions; (b) metal oxide particle size; and, (c) location of the metal on/in the support [151, 196, 198]. Wet-impregnated zeolite Y (Ni-Y) showed a broad TPR curve consisting of at least two peaks (the peak associated with Ni^{3+} was negligible). Compared to the commercial NiO, most of the Ni species required a higher reduction temperature. This suggests the presence of metal-support interactions, as expected for this zeolite. The breadth of the peaks is consistent with the presence of Ni^{2+} species that are more dispersed and in the supercage and sodalite sites of the zeolite [199]. The reduction in the pore volume of the impregnated catalysts compared to the bare HY zeolite supports this assumption. On the other hand, the wet–impregnated Ni-Al-MCF, had a higher fraction of Ni^{2+} requiring a higher reduction temperature as compared to the Ni-Y. This suggests the presence of smaller Ni^{2+} crystallites that are more difficult to reduce. Other possible reasons for a higher reduction temperature may be the strength of the metal-support interactions. The metallic species present in Ni-MCF have a reduction temperature of around 600°C. This high temperature is similar to what has been reported in the literature for the reduction of nickel silicates [200-203], suggesting incorporation of nickel in the framework for hydrothermally synthesized nickel catalysts.

To compare the effect of synthesis procedure (hydrothermal synthesis vs. wet impregnation) on the reducibility of the catalyst, hydrothermally-synthesized Ni-Al-MCF was also reduced using the same temperature program as the wet-impregnated Ni-Al-MCF. As can be seen in Figure 4.3, some overlap does exist in their respective TPR curves. Overall though, the shapes of their profiles were quite different. The hydrothermally synthesized Ni-Al-MCF required much higher temperatures to be fully

reduced, consistent with the hypothesis that nickel atoms were partly incorporated into the silicate framework or Ni crystallites are of much smaller in size than the wet-impregnated one.

4.3.1.3 Temperature-programmed Desorption (TPD) with NH_3

Figure 4.4 shows the NH_3 TPD curves for the various catalysts.

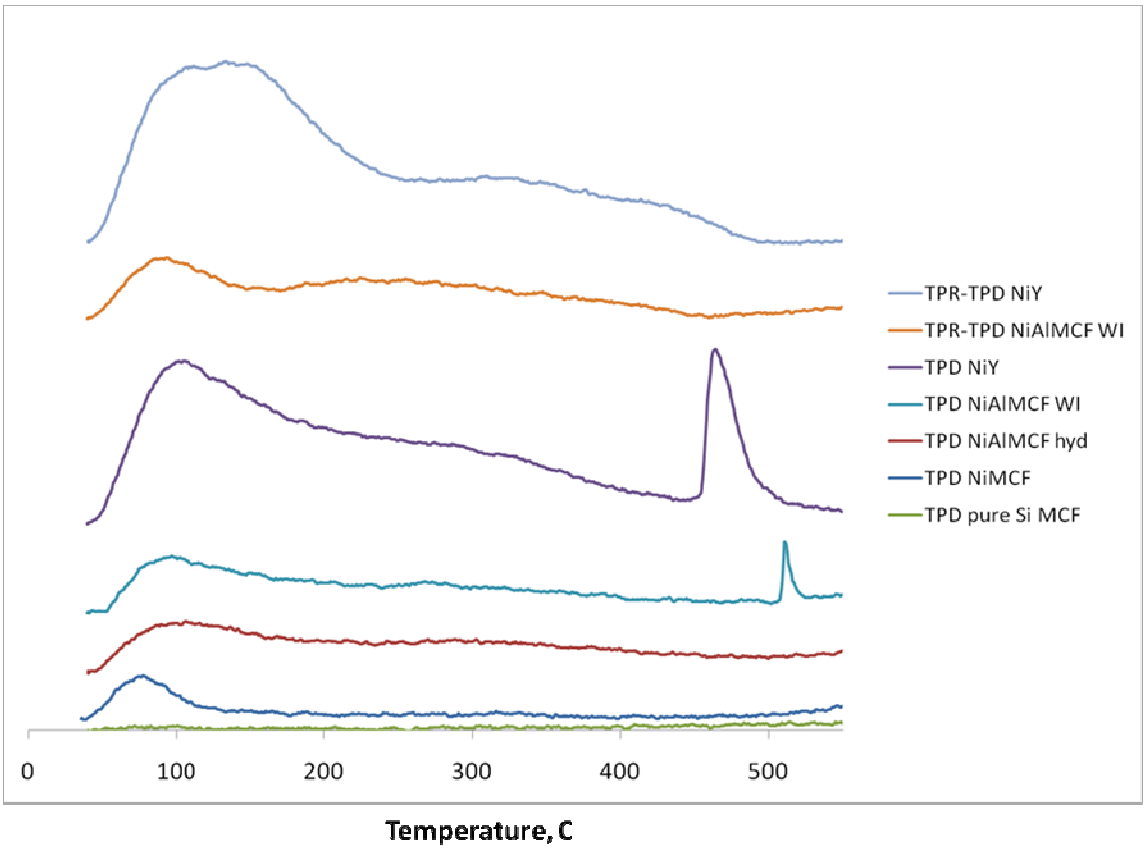

Figure 4.4 NH_3-TPD profile of different catalysts (heating rate: 4K/min)

As expected, the acidic catalytic supports HY and H-Al-MCF showed the presence of significant NH_3-adsorbing sites. For NH_3-TPD, microcalorimetry has been used to classify acid sites that interact with NH_3 [204]. Peak maxima between 142°C –

183°C have been associated with weak acid sites while peaks between 297°C and 322°C were considered intermediate acid sites. Peaks higher than 400°C were considered as strong acid sites [204-205].

The catalysts used in this study have largely weak and medium strength acid sites [204]. Table 4.2 reports the quantity of acid sites in different catalysts in terms of mmol of NH_3 adsorbed per g of catalyst. As expected, the HY-based catalysts had stronger acid sites than the H-Al-MCF-based ones. On the other hand, the Ni-MCF TPD showed the presence of weak acid sites that were originally not present in the siliceous MCF. Generation of acid sites on silica due to the addition of Ni [206] and other metal cations [207-208] has been previously reported in the literature.

Table 4.2 Adsorbed NH_3 in TPD of the different catalyst

Catalyst	Acidic site (mmol/g)
HY	0.68
Ni-Y (WI)	0.67 (0.09)*
H-Al-MCF	0.29
Ni-Al-MCF (WI)	0.27 (0.01)*
Ni-MCF	0.14

* Numbers in parentheses represent additional strong acid sites found in wet impregnated catalysts

Aside from the weak and medium strength acid sites found in all samples, both wet impregnated catalysts showed the presence of peaks indicative of strong acid sites. These peaks were between 450-550°C in the Ni-Y and Ni-Al-MCF profiles (Figure 4.4). Peaks at similar high temperatures have also been previously observed and reported in conjunction with addition of metal onto zeolites [209-211].

To further characterize the source of these strong peaks, a tandem experiment consisting of TPR pretreatment followed by NH_3 adsorption and TPD of the wet impregnated catalysts was used. Results showed (Figure 4.4, first two peaks) that the high temperature peaks were not present in the TPD profiles of both pre-reduced Ni-Y and Ni-Al-MCF. This result strongly points to the importance of unreduced Ni species (i.e. NiO) and their interaction with NH_3 as the strong acid sites. Once these species have been reduced from Ni^{2+} to Ni^0, these strong NH_3 adsorbing sites vanished. Interaction of NH_3 with metal oxides has been documented in the literature [199, 212].

In the case of the hydrothermally synthesized Ni-MCF, the oxide-NH_3 interaction only resulted in resolving the formation of weak acid sites. As the support itself did not respond to the NH_3 (see MCF curve, Figure 4.4), the weak acid site can only be attributed to the presence of Ni. It is further suggested that the method of its synthesis, i.e. hydrothermally, could possibly cause different species of Ni^{2+} to exist. For wet impregnation, one species contribute to strong NH_3 adsorption. In the hydrothermal synthesis, with its possibility of metal incorporation into the framework, only weak interaction with NH_3 seems possible. The effect of Ni incorporation into the framework which may affect their accessibility has been suggested in the literature [213-214]. This seemed to be further reinforced by our TPR result, in which hydrothermally synthesized catalysts require higher reduction temperature than the wet impregnated one.

4.3.1.4 X-ray Absorption Spectroscopy (XAS)

4.3.1.4.1 Hydrothermal synthesis vs. Wet-impregnation

To further probe the effect of hydrothermal synthesis vs. wet impregnation on the Ni species formed and their interaction with the support, wet-impregnated Ni-Al-MCF

and hydrothermally synthesized Ni-Al-MCF (Ni-Al-MCF-hyd) were sent to Argonne National Lab for XAS. Both TPR and TPD profiles of the Ni-Al-MCF hydrothermal catalyst show more similarity with the hydrothermally synthesized Ni-MCF rather than the wet impregnated Ni-Al-MCF.

After taking scans of the calcined catalysts in air, the samples were reduced at the beamline at 500°C for 30 minutes. As expected from the TPR (Figure 4.3), the wet-impregnated Ni-Al-MCF was found to be more reducible than the Ni-Al-MCF-hyd under these experimental conditions. However, neither sample was fully reduced. The Fourier transform of the EXAFS experiments are shown in Figures 4.5– 4.7.

The EXAFS transforms show a good correspondence between the reference NiO and the Ni-Al-MCF catalysts, including the high coordination shells. Their imaginary parts were well-matched as well (data not shown). On the other hand, the Ni-Al-MCF-hyd spectrum showed very different high shell peaks. The Ni-O-Ni bond distance in the Ni-Al-MCF-hyd was slightly longer than the other two, with the higher shells significantly different. The lower peak amplitudes also indicate better dispersed Ni^{2+} than the Ni-Al-MCF. Upon reduction, 60% of the nickel in Ni-Al-MCF was reduced while only 30% was reduced for the Ni-Al-MCF-hyd sample.

Figures 4.6-4.7 show the profiles of the reduced catalysts with the calcined and reference samples. It is clear from Figure 4.6 that the Ni-Al-MCF peaks corresponding to Ni-O and Ni-O-Ni were very much decreased while the Ni-Ni peak of the catalyst matched that of the Ni foil reference. On the other hand, the lower amount of reduced Ni^{2+} in the sample made it difficult to model the Ni^{0} in the partially reduced Ni-Al-MCF-hyd catalyst, though the Ni-Ni peak was noticeable in Figure 4.7. Overall, these results

reinforced the differences in the state of the Ni species present in these two catalysts. This data supports what has been elucidated in the TPR and TPD experiments previously. The significant difference in the higher shells, the different Ni-O bond distances, and the higher resistance to reduction shown by Ni-Al-MCF-hyd suggests that the Ni^{2+} were incorporated at least partly in the support, forming silicates or aluminosilicates.

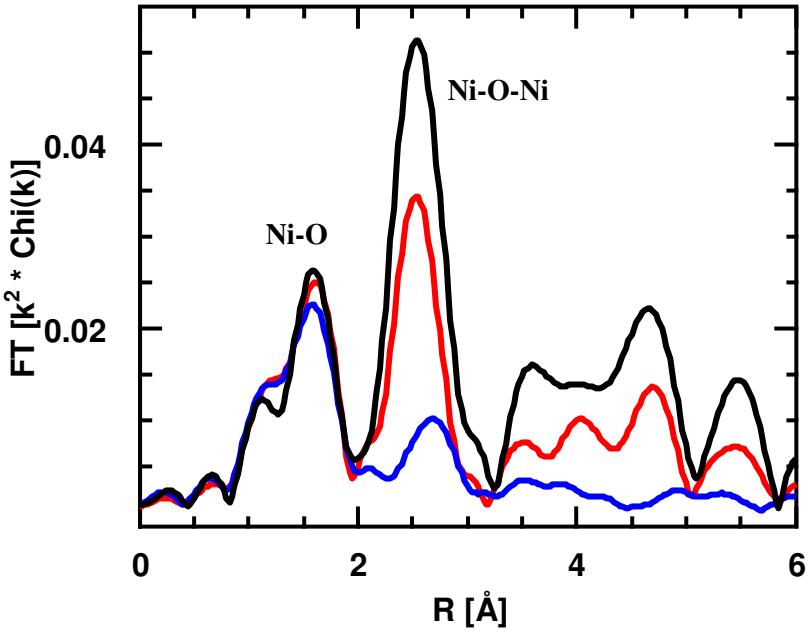

Figure 4.5 Fourier transform of calcined hydrothermally synthesized (blue) and wet-impregnated (red) Ni-Al-MCF with the NiO reference (black)

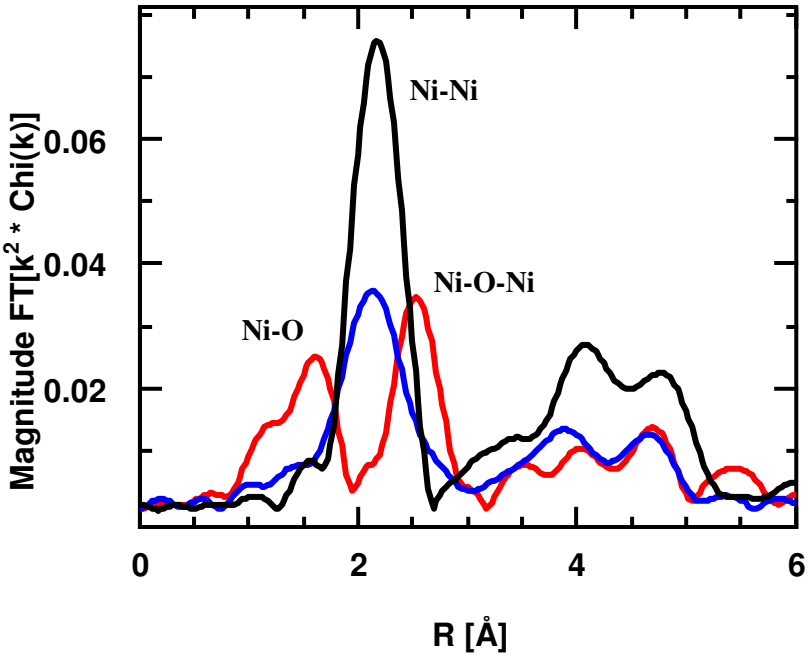

Figure 4.6 Fourier transform of calcined (blue) and partially reduced (red) hydrothermally synthesized Ni-Al-MCF with the Ni foil reference (black)

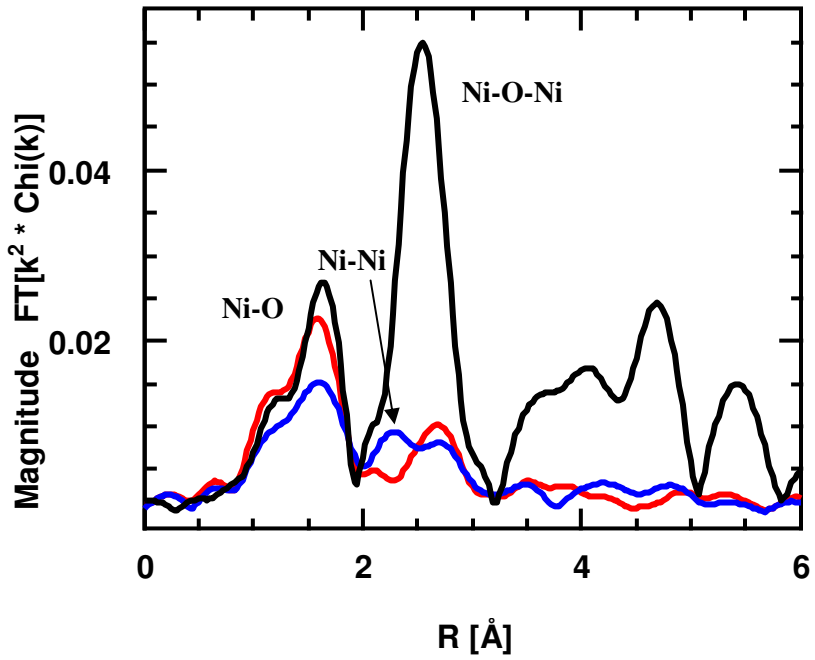

Figure 4. 7 Fourier transform of calcined (blue) and partially reduced (red) hydrothermally synthesized Ni-Al-MCF-hyd with the NiO reference (black)

4.3.2.1 Overview of previous study

In a previous study [170], both the metallic (Pt or Pd) and acidic functionalities utilized for the conversion of phenol to reduced compounds were situated in one bifunctional catalyst - synthesized through wet impregnation of a metal precursor onto zeolite supports. Scheme 4.1 showed the modified proposed reaction pathway of phenol conversion. As shown, two sites are involved in the conversion of phenol: metallic and acidic sites. In the complete deoxygenation/hydrogenation route from phenol to cyclohexane, the metallic site was considered responsible for the activation of the phenol and most of the catalytic conversions. In the suggested pathway, a route through cyclohexanone would only need the metallic sites. On the other hand, acid sites were required if the formation of cyclohexane is through the cyclohexanol route. The acid sites catalyze the dehydration of cyclohexanol to cyclohexene [170, 188, 215] . The acidic functionality also catalyzes the formation of the bicyclics [170] as well as some possible cracking reactions [216]. In the previous study, several bicylics were formed. The pathway for bicyclic formation was proposed to be through the reaction of phenol and either cyclohexanol or cyclohexanone, as shown in Scheme 4.2.

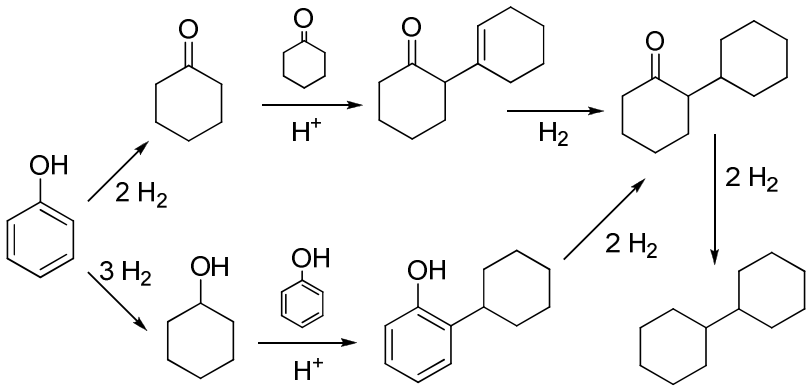

Scheme 4.2 Suggested reaction routes for the formation of several bicyclic compounds found in the treatment of aqueous phenol with Pt-HY[170]

Figure 4.8 shows the products of a phenol conversion catalyzed with the 0.5 wt% Pt/HY catalyst. Hong et al. [170] varied the WHSV of experiments from 5-20 hr^{-1} to arrive at different phenol conversions. As shown, cyclohexane was found to be the major product and was shown to be increasing as the phenol conversion reached completion. However, for a typical run at WHSV = 5 hr^{-1} with 4 MPa of H_2 at 200°C, the lowest WHSV tested, it was found out that phenol conversion was not maintained. As shown in Figure 4.9, it started decreasing after 5 hours on stream. Considering that this will be unattractive in an industrial setting, improvement to the system had to be made.

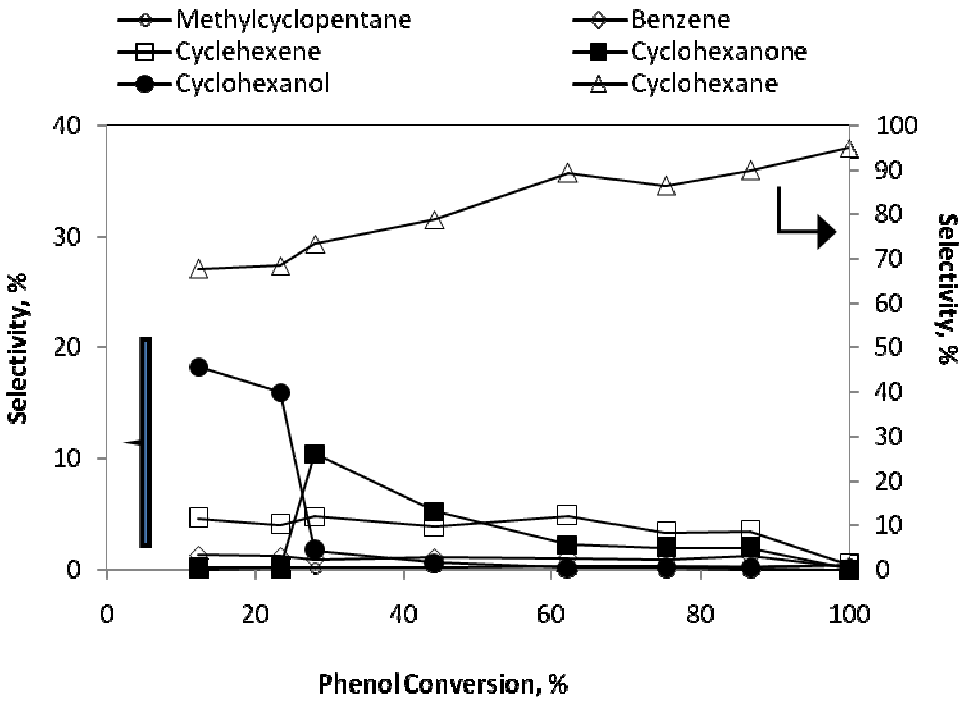

Figure 4.8 Monocyclic product selectivities at varying phenol conversions. Reaction conditions: temperature, 200°C; H_2 pressure, 4 MPa; catalyst loading, 100 mg; catalyst, 0.5 wt% Pt-Y (SiO_2/Al_2O_3 = 12); WHSV, 5-20 hr^{-1}; H_2O content, 5 wt% [170].

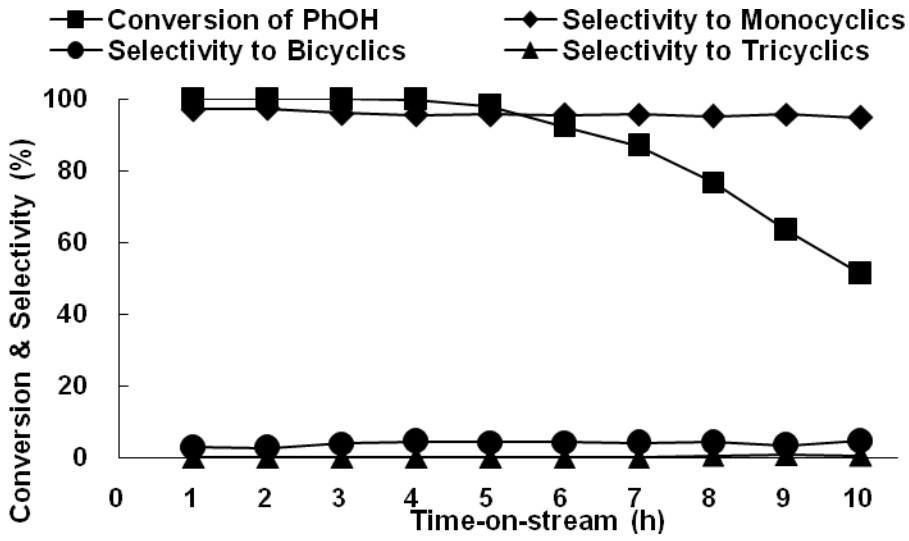

Figure 4.9 Phenol conversion and selectivities to monocyclic, bicyclic and tricyclic products. Reaction conditions: temperature, 200°C; H_2 pressure, 4 MPa; catalyst loading, 100 mg; catalyst, 0.5wt% Pt/HY (SiO_2/Al_2O_3 = 12); WHSV, 5 hr^{-1}; H_2O content, 10 wt%.

Deactivation due to coking is a common pathway for zeolites, especially acidic ones [217-218]. Though the bicyclics and tricyclics formed were interesting as molecular weight enhancement products, it was hypothesized that these structures were actually coke precursors which eventually choked out the activity of the catalyst [219]. In an industrial setting, this very short lifespan for the catalysts would be undesirable. As the possible coke precursors were acid-catalyzed, it was further hypothesized that it could be more advantageous for the system if the metal sites could be separated from the acidic sites. As such, it was proposed to support the active metal on a less reactive support, i.e. silica and the acid sites to be on a separate catalyst. In a continuous flow packed bed reactor setting, this would translate to a sequential bed system where the metal catalyst was upstream of the acid catalyst. The implication is that by separating the active sites, the life of the catalysts may be prolonged.

4.3.2.2 Phenol conversion in the presence of Ni-MCF

For the proposed sequential bed system, Ni was chosen instead of either Pt or Pd. Ni was previously shown to have very good activity for phenol conversion [175-176]. Another important reason for choosing nickel over the noble metal catalysts was the cost. In a recent market price research, Ni was priced at $ 12/lb [220] while Pt was at $ 26,500/lb [221]. Considering this three orders of magnitude advantage of nickel in terms of cost, it is very attractive to develop a cheaper catalyst capable of a more sustained phenol conversion.

At the time when this project was started, hydrothermal incorporation of metal onto silica mesocellular foams (MCF) by hydrothermal synthesis was not yet reported in the literature. MCF was the support chosen because of two reasons: (a) it has a relatively large pore opening such that it might be possible to process large molecules such as fatty acids [193-194] and lignin in the future; and, (b) it can be synthesized as pure silica and as aluminosilicates.

Ni-MCF (Si/Ni = 12, ~5 wt%) was tested in the continuous flow reactor using the same operating conditions as those used by Hong et al. [170] temperature of 200°C, H_2 pressure of 4 MPa, catalyst loading of 100 mg, WHSV of 5 hr^{-1} and H_2O content, 10 wt%. From Scheme 4.1, it was suggested that phenol activation/conversion only requires the metal site. As such, only Ni-MCF was used in the experiment, and the results are shown in Figure 4.10. This graph shows the complete conversion of phenol for 15 hours. Compared to Figure 4.9, 100% phenol conversion with Ni-MCF was shown to last at least 3x of the phenol conversion with the 0.5 wt. % Pt/HY. This preliminary result was very encouraging.

Though phenol conversion was 100%, it cannot be claimed that there was no deactivation occurring since product selectivity varied during the run. Figure 4.11 shows the product selectivity trends for this run. In the presence of Ni-MCF, cyclohexanol was the main product. However, as time on-stream increased, the amount of cyclohexane was shown to increase with a decrease in the cyclohexanol selectivity.

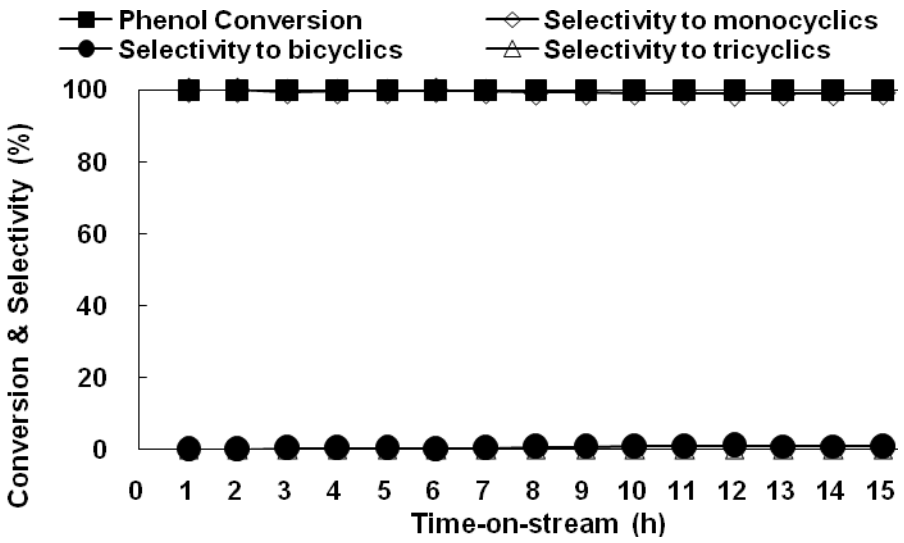

Figure 4.10 Phenol conversion and selectivities to monocyclic, bicyclic and tricyclic products. Reaction conditions: temperature, 200°C; H_2 pressure, 4 MPa; catalyst loading, 100 mg; catalyst, Ni-MCF (Si/Ni = 12); WHSV, 5 hr $^{-1}$; H_2O content, 10 wt%.

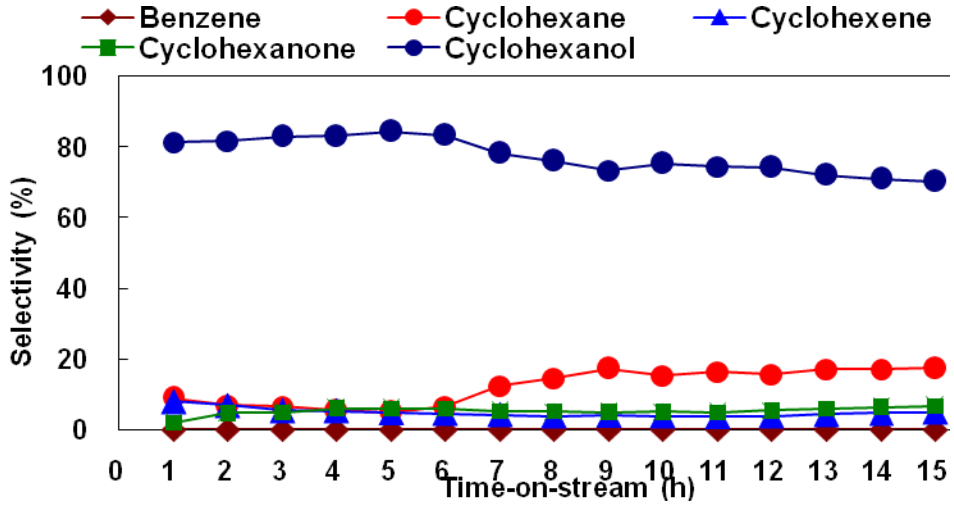

Figure 4.11 Product selectivities. Reaction conditions: temperature, 200°C; H_2 pressure, 4 MPa; catalyst loading, 100 mg; catalyst, Ni-MCF (Si/Ni = 12); WHSV, 5 hr $^{-1}$; H_2O content, 10 wt%.

4.3.2.3. Experiments at 0.79 MPa

H_2 in itself holds promise as a renewable energy carrier. The US Dept. of Energy considers its "potential for a clean, reliable and affordable energy supply" an integral part of America's bid to become fossil fuel independent [222]. However, there are still technological challenges that hinder its becoming a reality. Because it is an expensive resource, conserving its use in any process is highly desirable. With this in mind, a lower H_2 pressure was tested to see if conversion of phenol as well as maintaining its complete conversion was still possible. A lower pressure of 100 psig was chosen.

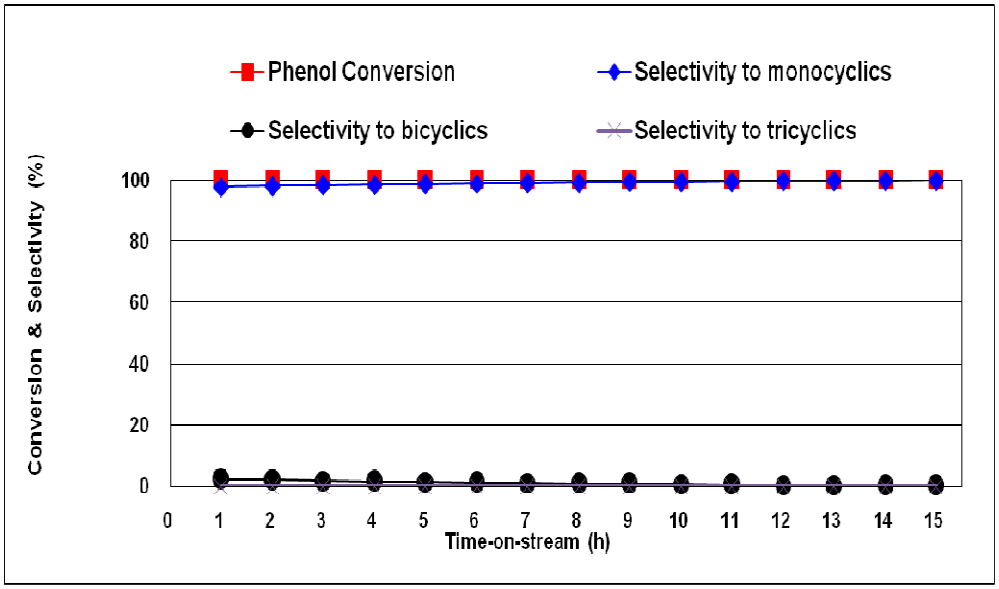

Figure 4.12 Phenol conversion and selectivities to monocyclic, bicyclic and tricyclic products. Reaction conditions: temperature, 200°C; H_2 pressure, 0.78 MPa; catalyst loading, 100 mg; catalyst, Ni-MCF (Si/Ni = 12); WHSV, 5 hr $^{-1}$; H_2O content, 10 wt%.

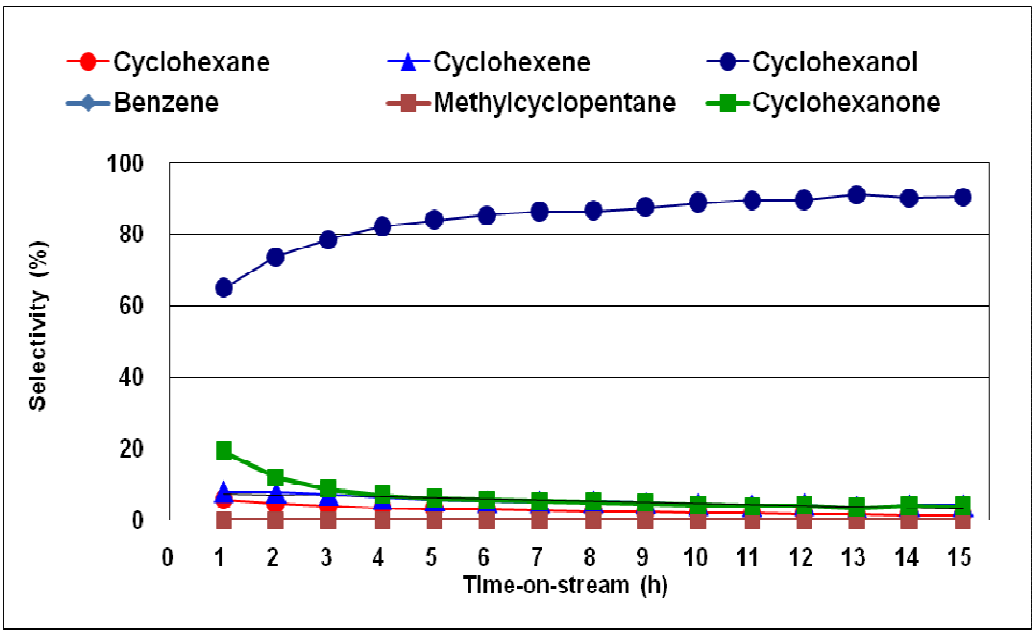

Figure 4.13 Product selectivities of monocyclics produced from phenol conversion. Reaction conditions: temperature, 200°C; H_2 pressure, 0.78 MPa; catalyst loading, 100 mg; catalyst, Ni-MCF (Si/Ni = 12); WHSV, 5 hr $^{-1}$; H_2O content, 10 wt%.

Lowering the H_2 pressure, from 4 MPa to 0.79 MPa (100 psig), still showed a complete conversion of phenol for 15 hours (Figure 4.12). This was encouraging, considering that there was about 80% decrease in the process H_2 pressure supplied, the phenol conversion was sustained at 100%, again at about 3x longer than a similar run using 0.5 wt% Pt/HY. It must be noted that by elemental analysis, the amount of nickel in the Ni-MCF catalyst used was about 10x the weight that of the supported Pt/HY catalyst. However, since as mentioned, the Pt is about 3 orders of magnitude higher in price than the Ni. As such, the larger amount of the Ni used at these reactions does not put it at a disadvantage. Using the same Ni-MCF catalyst, all subsequent experiments were done at this lower reactor pressure. Though it was already hinted at in these reactions, the effect of H_2 available for the reaction will be further discussed in a subsequent section.

4.3.2.3.1 Effect of varying WHSV

The weight hourly space velocity is the amount of feed allowed into the reactor per unit time per unit weight of the catalyst. This was tuned by varying the amount of Ni-MCF catalyst while feeding the same amount of aqueous phenol into the reactor. H_2 pressure (0.79 MPa) and temperature (200°C) were maintained. Figure 4.14 illustrates the relationship between phenol conversion and the WHSV. Phenol conversions lower than 99% were only seen at WHSV higher than 50 hr^{-1}. Consider that industrial WHSV are typically much lower than the ones used in these studies that resulted in at least 99% phenol conversion. At much higher WHSV, phenol conversion became much lower: with the 15 hour conversion lower than the 4 hour one. Two reasons may be suggested for the decreased conversion: (1) deactivation of the catalyst due to coking; and, (2) channeling of the feed through the catalyst bed due to the comparatively much smaller amount of catalyst particles present. In the second instance, even if the loaded catalysts were still active, by-pass of the phenol to the reactor exit without contacting the catalyst will result in a very small, almost negligible over-all conversion.

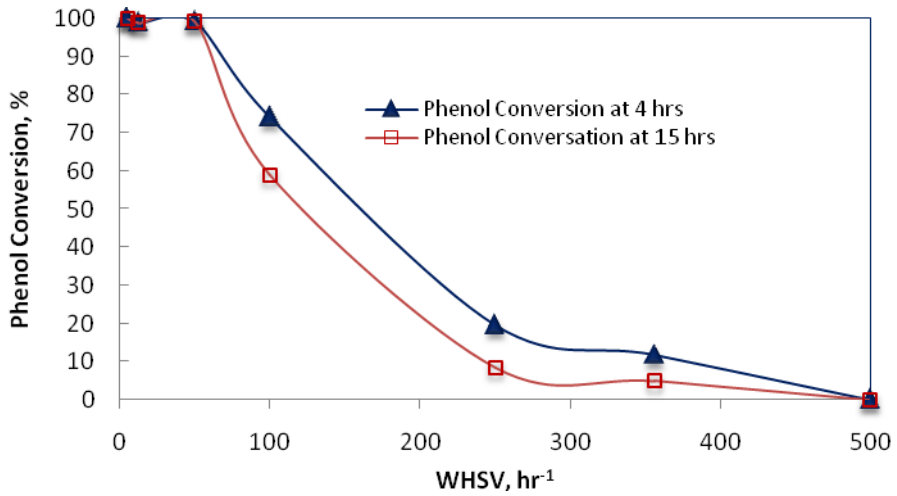

Figure 4.14 Phenol conversion vs. WHSV

4.3.2.3.2 Effect of varying H_2/phenol ratio

The WHSV (5 hr^{-1}) of several experiments were maintained by changing both the phenol flowrate (0.0078, 0.0028 and 0.0008 ml/min) and the catalyst amount (100, 35.5, 10 mg). The H_2 flowrate was maintained at 50 ml/min and the reactor pressure at 100 psig. In effect, the ratio of H_2/phenol was being varied. Results are summarized in Table 4.3.

Table 4.3 Reactions at varying aqueous phenol feed flowrate and catalyst at constant WHSV = 5 hr^{-1} and constant H_2 pressure

Amount of Catalyst (mg)	Feed Flowrate (ml/min)	Ratio H_2/Phol	Major Product	Selectivity to Major Product		Phenol Conversion	
				after 4 hrs	after 15 hrs	after 4 hrs	after 15 hrs
100	0.0078	37	Cyclohexanol	82	91	100	100
35.5	0.0028	104	Cyclohexanol	60	80	100	100
10	0.0008	369	**Cyclohexene**	56	45	100	100

At 200°C and 100 psig, in all of the presented experiments in Table 4.3, the apparent phenol conversion remained complete and was maintained at 100% for 15 hours, as was observed previously. However, the product selectivity changed as the amount of catalyst and amount of aqueous phenol became smaller. Since the amount of H_2 was maintained, decreasing aqueous phenol feed in effect increases the H_2/phenol ratio. At the H_2/phenol ratio of 37, cyclohexanol was the main product. At the highest ratio, cyclohexene became the main product. This was not initially expected as cyclohexanol was the usual main product of aqueous phenol with Ni-MCF. As Scheme 4.1 suggested, cyclohexene can only be produced from cyclohexanol in the presence of

an acid. However, since the amount of acid was not increased during these two runs, another reason may exist. It may be suggested that in the presence of higher amounts of hydrogen, the other route of cyclohexene production, passing through cyclohexanone, may have become more favored.

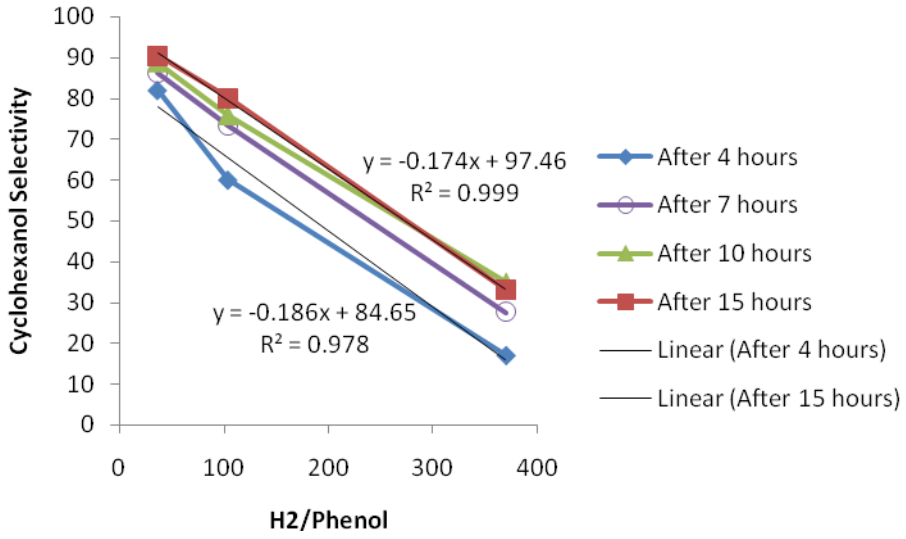

Figure 4.15 Cyclohexanol selectivity vs. H_2/phenol ratio

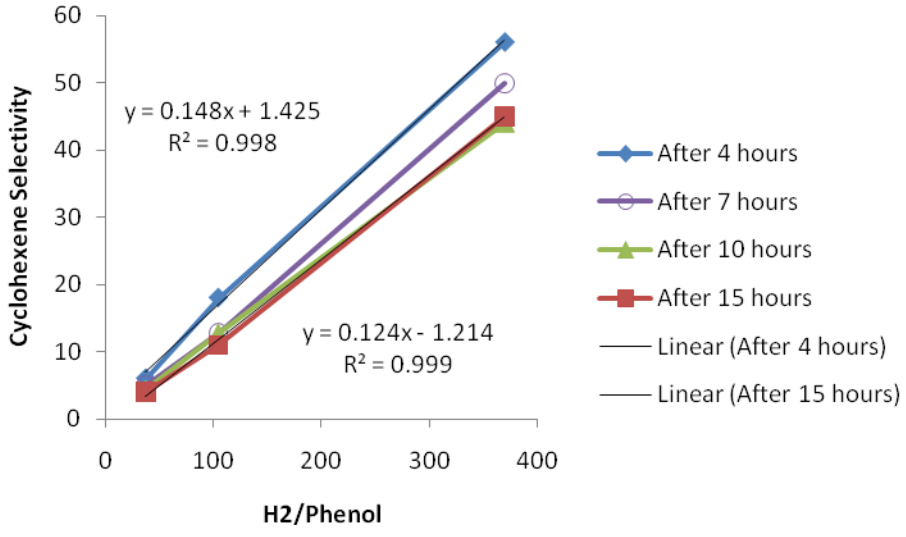

Figure 4.16 Cyclohexene selectivity vs. H_2/phenol ratio

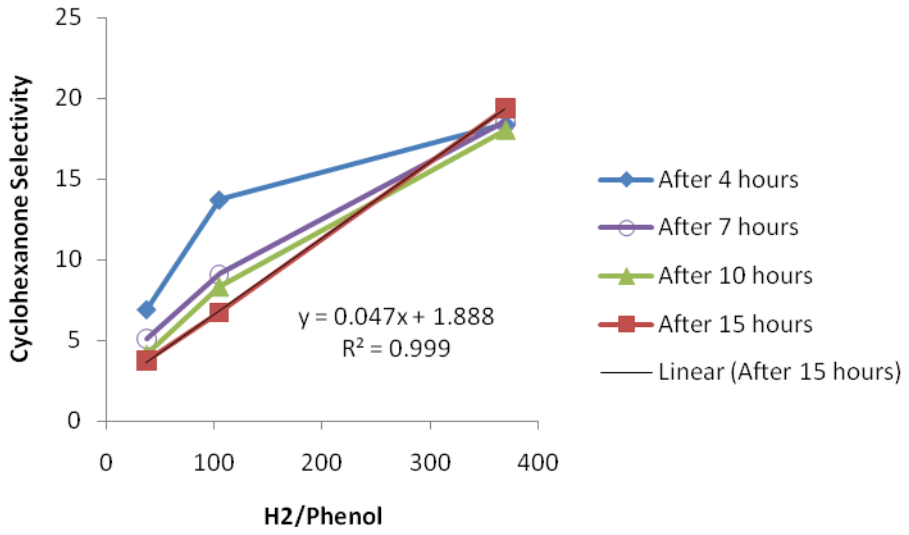

Figure 4.17 Cyclohexanone selectivity vs. H_2/phenol ratio

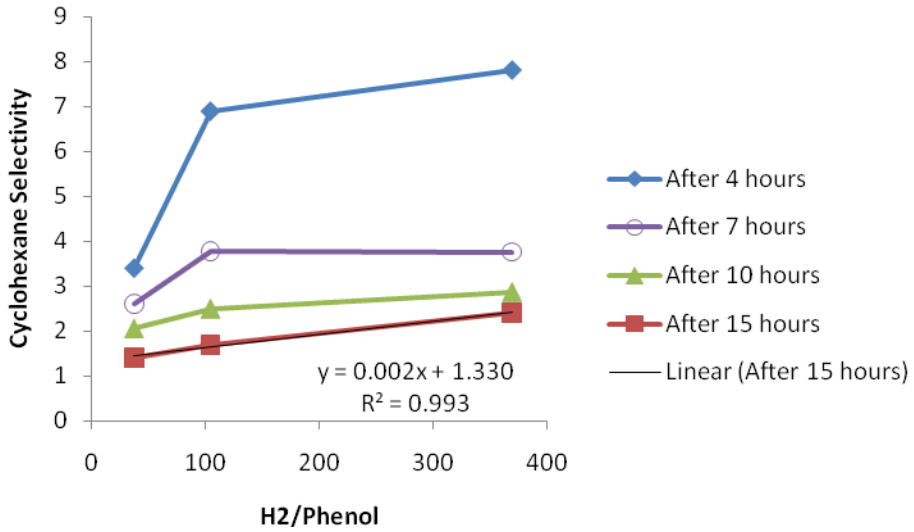

Figure 4.18 Cyclohexane selectivity vs. H_2/phenol ratio

Figures 4.15 – 4.18 present the effect of H_2/phenol ratio on the selectivities of each product. What was apparent was the increasing linearity of the relationship between these two parameters at higher time-on-streams in all cases. Cyclohexanol was the only one that had an inverse relationship with the H_2/phenol ratio, suggesting that higher cyclohexanol selectivities will be achieved at lower H_2 pressures. Corollary, these figures suggest that the other compounds could be formed at higher concentrations in the product stream at increased H_2/phenol ratio in the presence of Ni-MCF.

4.3.2.3.2.1 Cyclohexanone as feed

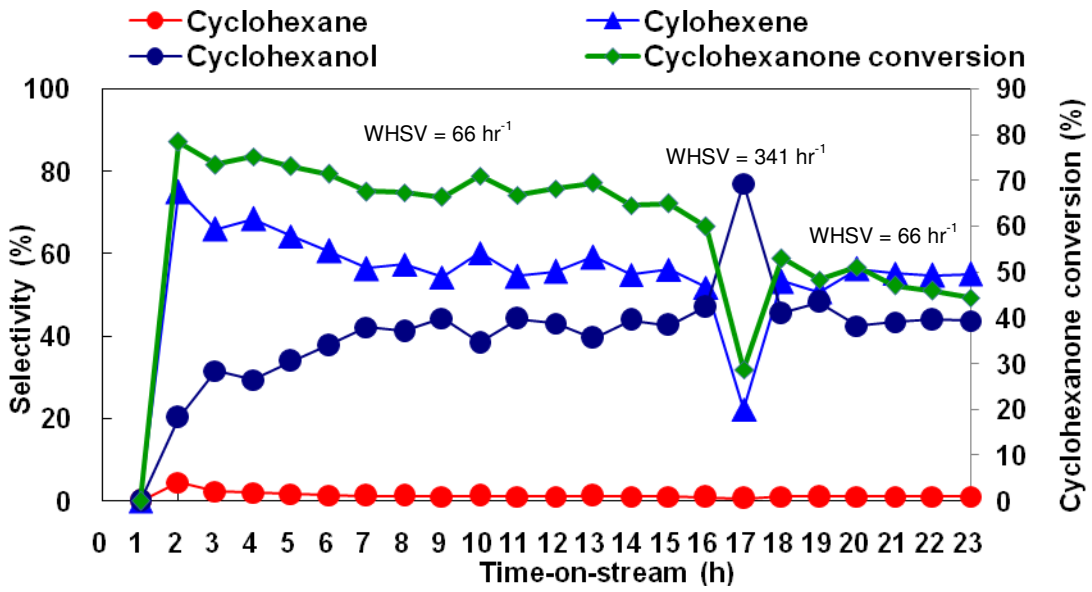

Figure 4.19 Cyclohexanone conversion and resulting products. Reaction conditions: temperature, 200°C; H_2 pressure, 0.78 MPa; catalyst loading, 1.3 mg; catalyst, Ni-MCF (Si/Ni = 12); WHSV, 66hr $^{-1}$ and 341 hr^{-1}; H_2/cyclohexanone, 154 and 30; H_2O content, 10 wt%.

Figure 4.19 shows the conversion of cyclohexanone to cyclohexanol, cyclohexene, and cyclohexane. Two WHSVs were tested for this reaction, 66 hr^{-1} and

341 hr^{-1}. Changing the WHSV was shown to affect the selectivities between cyclohex**ene** and cyclohexanol. The variation was accomplished by controlling the amount of cyclohexanone fed into the system. At the beginning, WHSV = 66 hr^{-1} was used for the first16 hours. The equivalent H_2/cyclohexanone ratio for this was 154. As shown, the main product for this reaction was cyclohex**ene** followed by cyclohexanol and lastly, cyclohexane. Reduction in cyclohexanone conversion was definitely apparent at increasing time-on-stream. After the sampling at 16 hours, the feed flowrate was switched to a faster flowrate, i.e. WHSV = 341 hr^{-1} and a lower H_2/cyclohexanone of 30. This resulted in an expected sharp decrease in the cyclohexanone conversion. Also, it caused a switch in the main product of the reaction, such that cyclohexanol became the product with the higher selectivity, now followed by cyclohexene. Cyclohexane, because of its very small presence only showed very negligible effect at this transition. After sampling at the end of the 17^{th} hour, the feed flowrate was turned back to the slower flowrate and the previous trend of slowly decreasing cyclohexanone conversion was again seen.

In the previous experiment, the pressure of the H_2 fed was not changed. As shown, the decrease in WHSV affected the H_2/feed ratio and resulted in a switching effect between the selectivities of cyclohexanol and cyclohex**ene** in the product stream**.** This correlates with the observation noted from the experiments tabulated in Table 4.3. The amount of catalyst used in this reaction corresponded to the amount used for the phenol conversion at WHSV = 356 hr^{-1}. The reason for doing so was to ensure that the conversion of the starting material will not be complete. As the results show, such was the case here.

4.3.2.3.2.2 Cyclohexanol as feed

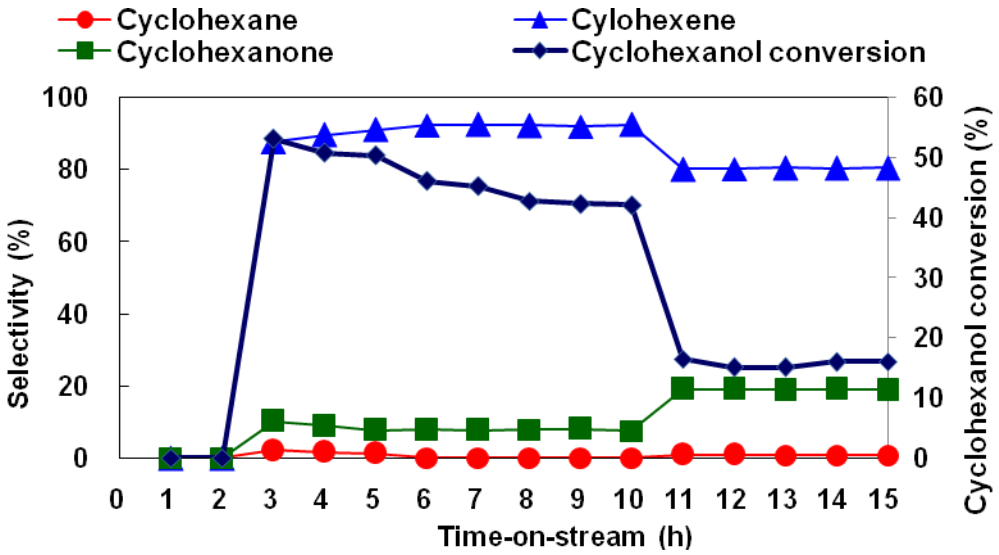

Figure 4.20 Cyclohexanol conversion and resulting products. Reaction conditions: temperature, 200°C; H_2 pressure, 0.78 MPa; catalyst loading, 1.3 mg; catalyst, Ni-MCF (Si/Ni = 12); WHSV, 67hr $^{-1}$ and 347 hr^{-1}; H_2/cyclohexanol, 155 and 30; H_2O content, 10 wt%.

Figure 4.20 shows the effect of changing feed flowrates, resulting to H_2/feed ratio, for a cyclohexanol-fed experiment. One important finding of this experiment is that cyclohexanone was a product from cyclohexanol. Previous studies did not mention this reversibility between cyclohexanol and cyclohexanone at these reaction conditions. Second, though the formation of cyclohex**ene** from cyclohexanol was supposed to require acid functionality, it was still the main product for cyclohexanol conversion in the presence of the Ni-MCF. Lastly, a switch between cyclohexanone and cyclohex**ene** did not occur when the feed flowrate was varied, unlike when cyclohexanone was the feed, though a lessening in the cyclohex**ene** selectivity did translate to an increase in cyclohexanone selectivity. This suggests that the inter-conversion between

cyclohexanone and cyclohexanol was more favored from cyclohexanone to the alcohol, rather than the other way around.

4.3.3 Bifunctional catalyst reactions

4.3.3.1 Sequential beds

As mentioned at the beginning of this chapter, the main objective of this portion of study was to develop a catalyst configuration that would enable a more prolonged complete phenol conversion based on the understanding of the suggested mechanism. The main hypothesis was that the separation of the metal and the acidic catalyst would solve this problem thus implying that coking reactions due to the presence of the acidic site on the same catalyst as the metal site was the major cause of deactivation.

So far, what has been discussed were the results using Ni-MCF as the only catalyst. Figure 4.21 summarizes the product selectivities and phenol conversion from a sequential bed experiment featuring Ni-MCF in the upstream catalytic bed and zeolite HY in the second bed. The WHSV used based on the amount of Ni was still 5 hr^{-1} and the reactor temperature was set at 200°C. As shown, the sequential bed configuration was very successful in two important things: (1) phenol conversion was maintained at 100% for the duration of 15 hours; and, (2) the product stream was almost completely oxygen-free. The only oxygen containing molecule found in the outlet was that of a bicyclic, 1,1'-oxybis-cyclohexane at decreasing selectivities starting from 0.1%. Both cyclohexanol and cyclohexanone were not present in the product stream. Methylcyclopentane and benzene, though present, were formed in very small quantities.

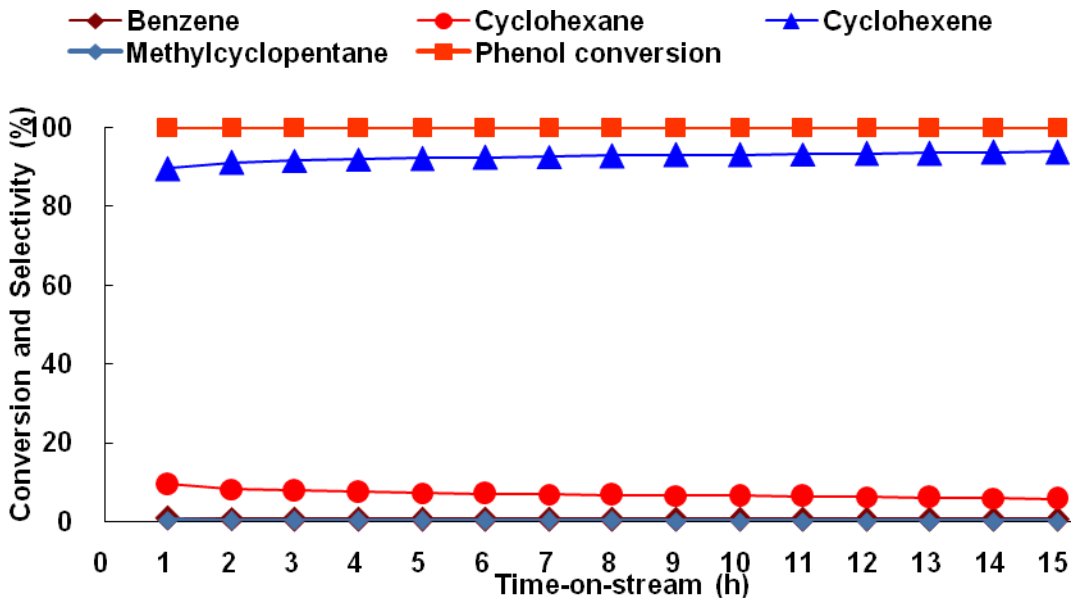

Figure 4.21 Ni-MCF : HY. Product selectivities of monocyclics produced from phenol conversion. Reaction conditions: temperature, 200°C; H_2 pressure, 0.78 MPa; catalyst loading, 100 mg; catalysts, Ni-MCF (Si/Ni = 12), HY (SiO_2/Al_2O_3 = 12); WHSV, 5 hr^{-1}; H_2O content, 10 wt%.

Figure 4.22 shows the activity and selectivity profile of a sequential catalyst bed configuration containing Ni-MCF followed by H-Al-MCF. Previous characterization results showed H-Al-MCF to have less acidic sites through NH_3-TPD as compared to zeolite HY. The main product was still cyclohex**ene**. However, H-Al-MCF-catalyzed run showed a different product profile than the HY catalyzed experiment. First, though the main product was still cyclohex**ene**, almost a negligible amount of cyclohexane was formed. Discounting the irregularities introduced by the pressure build-up fluctuations early in the run, a higher selectivity for cyclohex**ene** was reached in this set-up. Second, cyclohexanol still appeared in the product outlet suggesting that it was not completely consumed in the transformation reactions on the acid catalyst. This may be due to the smaller amount of acid sites available in H-Al-MCF, as compared to HY. Lastly,

cyclohexanone was absent in the product stream, suggesting its complete conversion to the more hydrogenated products.

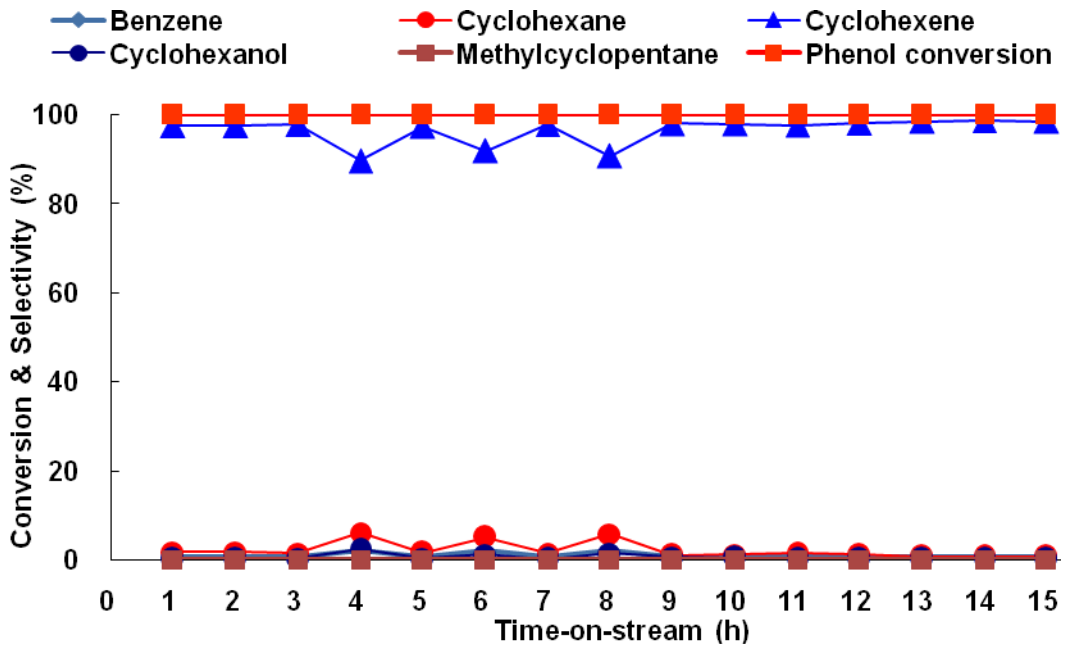

* Fluctuations due to pressure build-up and adjustment

Figure 4.22 Ni-MCF : H-Al-MCF. Product selectivities of monocyclics produced from phenol conversion. Reaction conditions: temperature, 200°C; H_2 pressure, 0.78 MPa; catalyst loading, 100 mg; catalysts, Ni-MCF (Si/Ni = 12), H-Al-MCF (SiO_2/Al_2O_3 = 12); WHSV, 5 hr^{-1}; H_2O content, 10 wt%.

Figure 4.23 shows a cartoon of the product generation in a sequential bed configuration. As previously mentioned, the only bicyclic product identified at the outlet in this sequential configuration was the 1,1'-oxybis-cyclohexane.

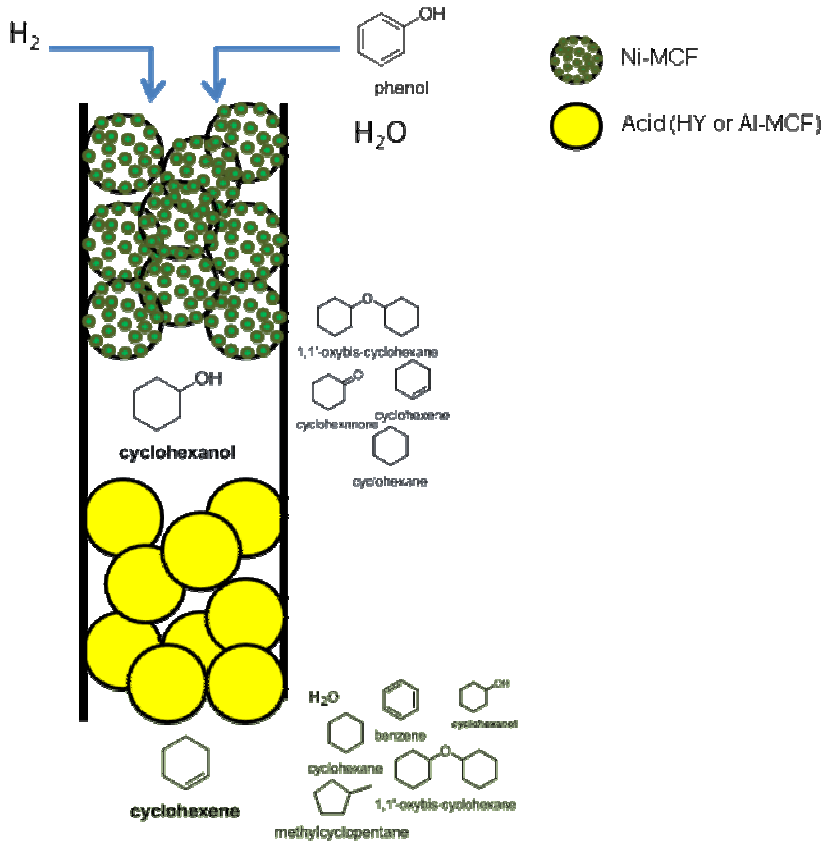

Figure 4.23 Schematic for the reaction pathway for a sequential Ni-MCF:HY or Ni-MCF:H-Al-MCF

4.3.3.2 Physically mixed catalysts

Cyclohexane was the main product formed in the HDO of phenol with 0.5 wt% Pt/Al_2O_3. In the previous experiments using Ni-MCF, cyclohexane comprised only a small fraction of the total products observed. However, by physically mixing the Ni-MCF and the acid catalysts (HY or H-Al-MCF), cyclohexane became the main product. Figures 4.24 and 4.25 show the composition of the outlet stream for each of the mixed bed experiments for Ni-MCF/HY and Ni-MCF/H-Al-MCF. As shown, phenol conversion was again at 100% conversion for the 15 hours time on stream. The main product was cyclohexane (>99% selectivity), with small amounts of methylcyclopentane.

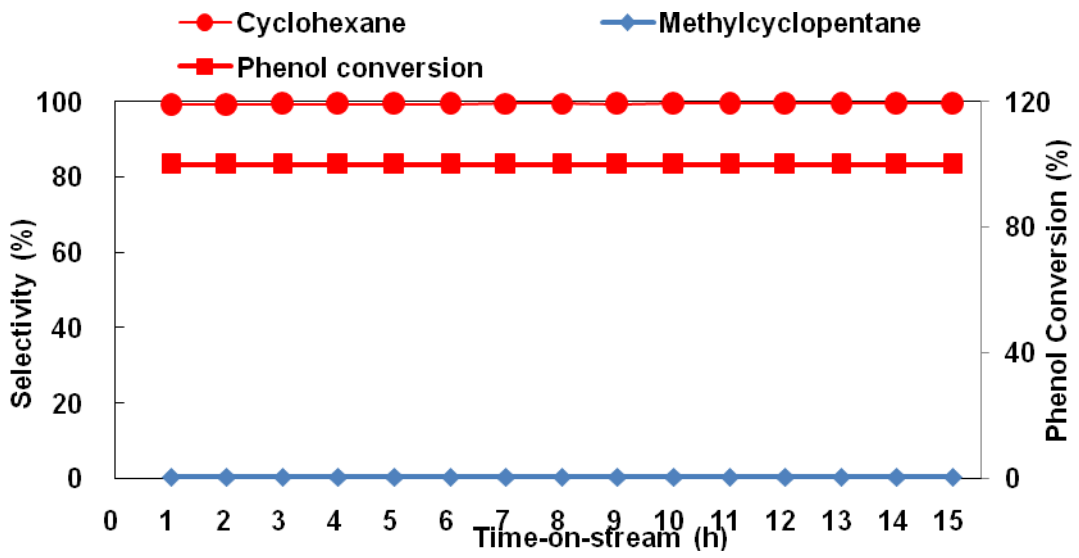

Figure 4.24 Ni-MCF/HY. Product selectivities of monocyclics produced from phenol conversion. Reaction conditions: temperature, 200°C; H_2 pressure, 0.78 MPa; catalyst loading, 100 mg; catalysts, Ni-MCF (Si/Ni = 12), HY (SiO_2/Al_2O_3 = 12); WHSV, 5 hr^{-1}; H_2O content, 10 wt%.

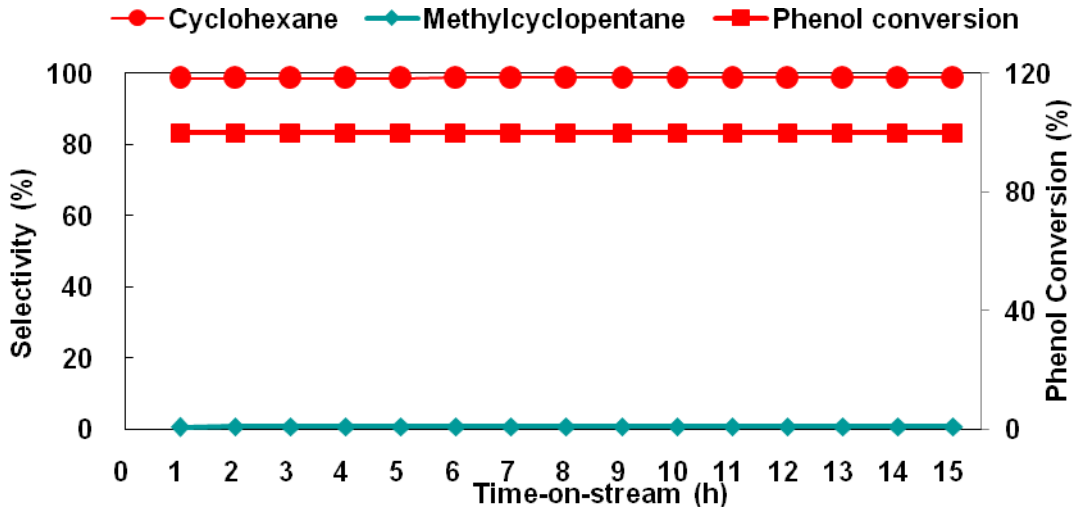

Figure 4.25 Ni-MCF/H-Al-MCF. Product selectivities of monocyclics produced from phenol conversion. Reaction conditions: temperature, 200°C; H_2 pressure, 0.78 MPa; catalyst loading, 100 mg; catalysts, Ni-MCF (Si/Ni = 12), H-Al-MCF (SiO_2/Al_2O_3 = 12); WHSV, 5 hr^{-1}; H_2O content, 10 wt%.

Aside from methylcyclopentane, some bicyclics and tricyclics comprise less than 1% of the product stream. Figure 4.26 shows the multi-ring components that were present in the product stream. The results shown in Figures 4.24 and 4.25 are significant in that the phenol conversion is maintained at 100% and stays at that level for the entire duration (15 hours) of the experiment. This is the first demonstration that using separate catalysts for the two functionalities (hydrogenation and acid catalysis), deactivation has been avoided.

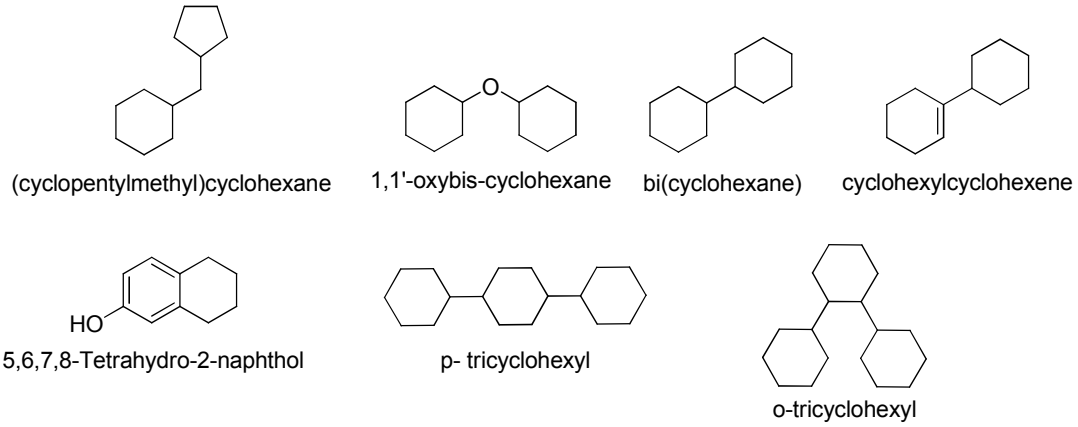

Figure 4.26 Identified bicyclic and tricyclic compounds

Figure 4.27 illustrates the probable reaction pathways occurring in a single packed bed with a physical mixture of the metal and acidic sites.

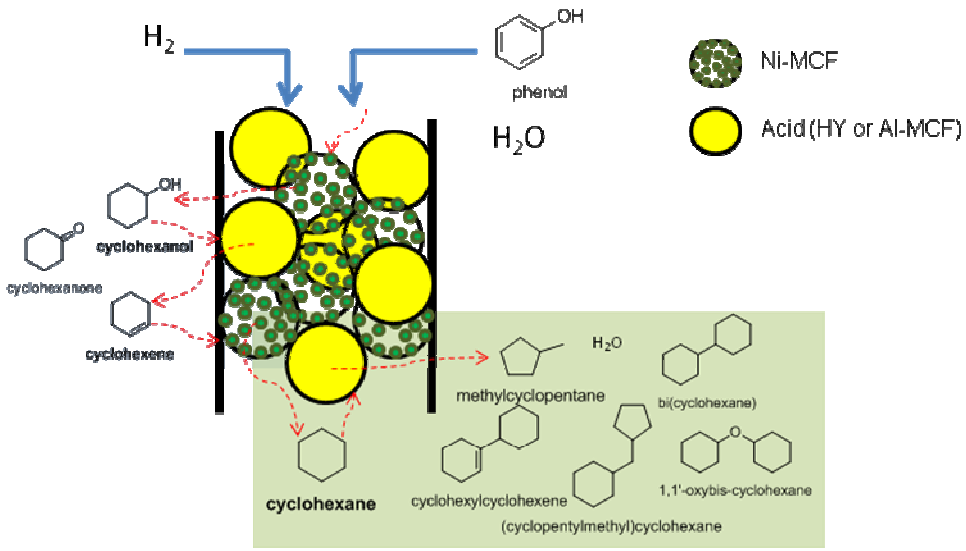

Figure 4.27 Schematic for the reaction pathway for a single bed with physically mixed catalysts, Ni-MCF/HY or Ni-MCF/H-AlMCF.

4.3.3.3 Wet-impregnated catalysts

Previously, it was shown that different configurations wherein the metal and acidic sites required for the hydrodeoxygenation/hydrogenation of phenol were on different supports were successful in producing a specific compound at high selectivity (>90%). As was hypothesized, separating the metal site from the acid site gave a more prolonged complete phenol conversion – much longer than was previously achieved in this group using 0.5 wt% Pt/HY.

In this section, bifunctional catalysts, made by wet impregnation of nickel nitrate onto HY and H-Al-MCF, were used in the HDO/hydrogenation of aqueous phenol. Figures 4.28 and 4.30 show the product distribution for Ni-Y and Ni-AlMCF, respectively. On the other hand, Figures 4.29 and 4.31 show the phenol conversion and selectivities of each group of product for the same catalysts.

For both wet-impregnated catalysts, complete phenol conversion was not reached. Ni-AlMCF showed a descending degree of conversion as time went by while the Ni-Y showed a plateau early on. Possible reasons for this include coking and sintering of the catalysts. Deactivation of acidic sites in zeolites due to the presence of phenol had already been reported [216, 223]. Pore blocking of the adsorbed phenol inside HMFI pores was suggested to be the reason for the deactivation of the zeolite towards n–heptane and methylcyclohexane transformation.

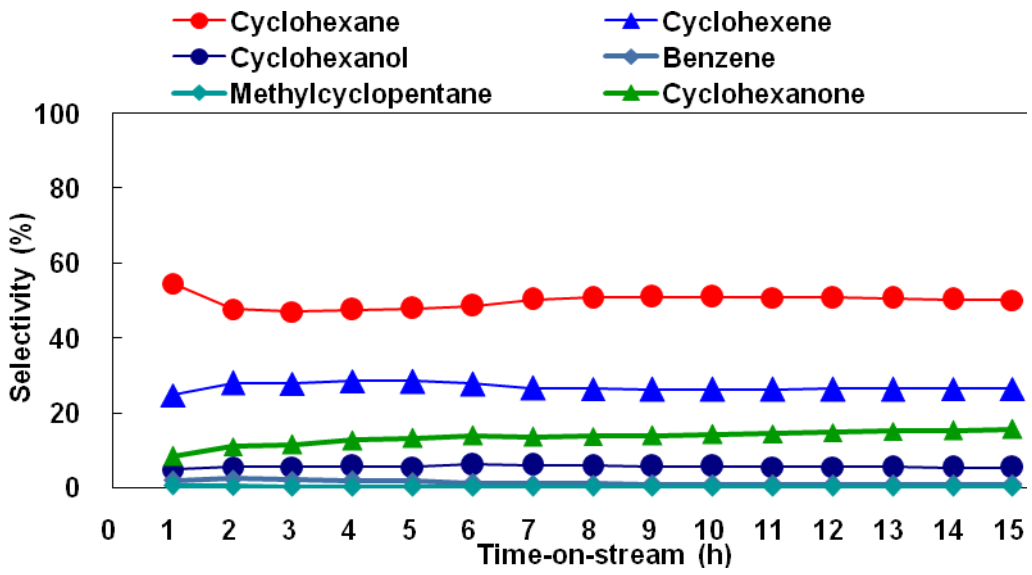

Figure 4.28 Ni-Y. Product selectivities of monocyclics produced from phenol conversion. Reaction conditions: temperature, 200°C; H_2 pressure, 0.78 MPa; catalyst loading, 100 mg; catalysts, Ni-Y (Si/Ni = 12, SiO_2/Al_2O_3 = 12); WHSV, 5 hr^{-1}; H_2O content, 10 wt%.

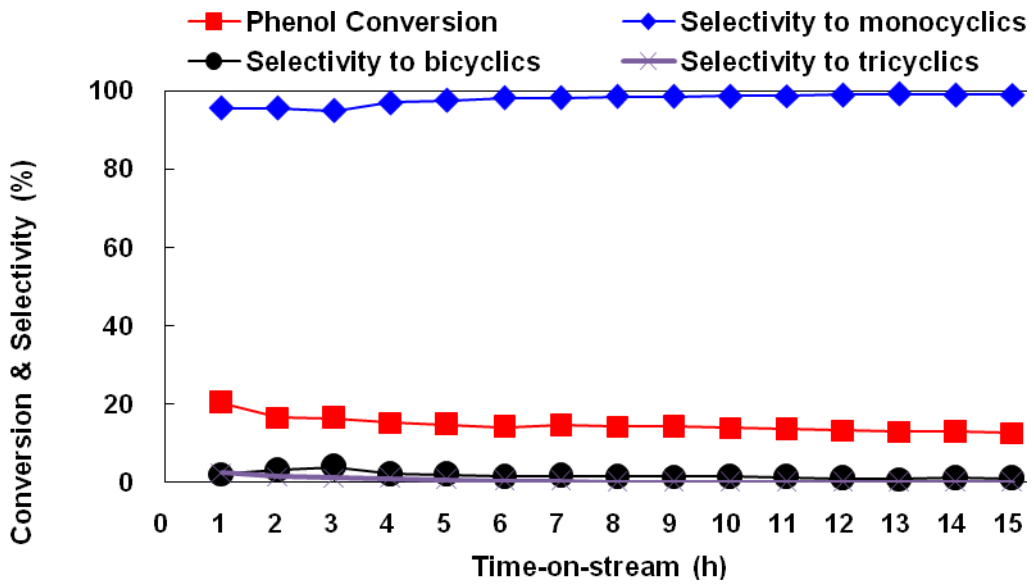

Figure 4.29 Ni-Y. Phenol conversion and selectivities of main group of compounds. Reaction conditions: temperature, 200°C; H_2 pressure, 0.78 MPa; catalyst loading, 100 mg; catalysts, Ni-Y (Si/Ni = 12, SiO_2/Al_2O_3 = 12); WHSV, 5 hr^{-1}; H_2O content, 10 wt%.

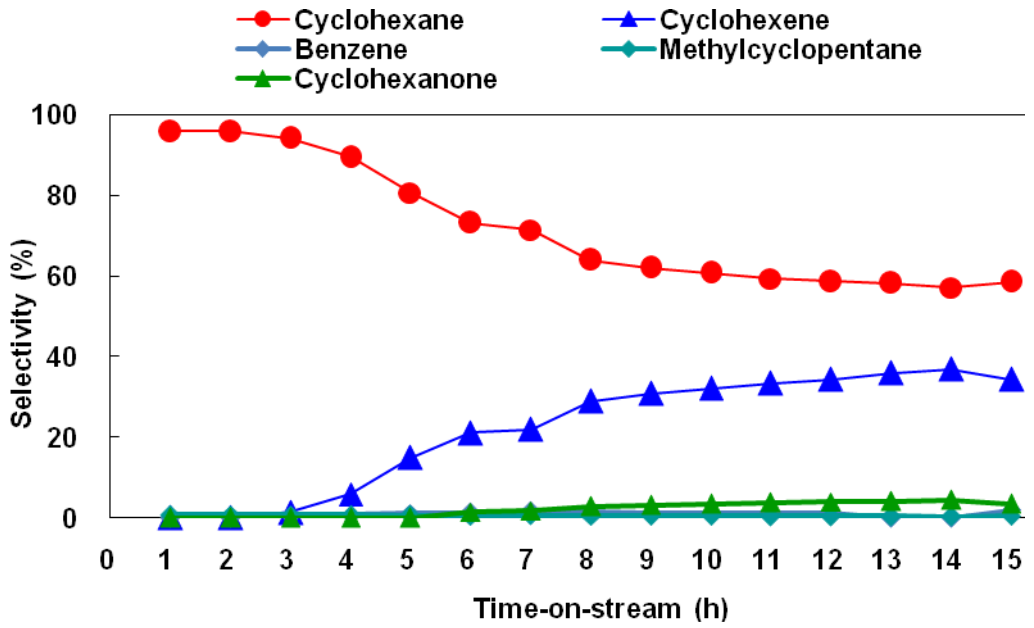

Figure 4.30 Ni-AlMCF. Product selectivities of monocyclics produced from phenol conversion. Reaction conditions: temperature, 200°C; H_2 pressure, 0.78 MPa; catalyst loading, 100 mg; catalysts, Ni-Y (Si/Ni = 12, SiO_2/Al_2O_3 = 12); WHSV, 5 hr^{-1}; H_2O content, 10 wt%.

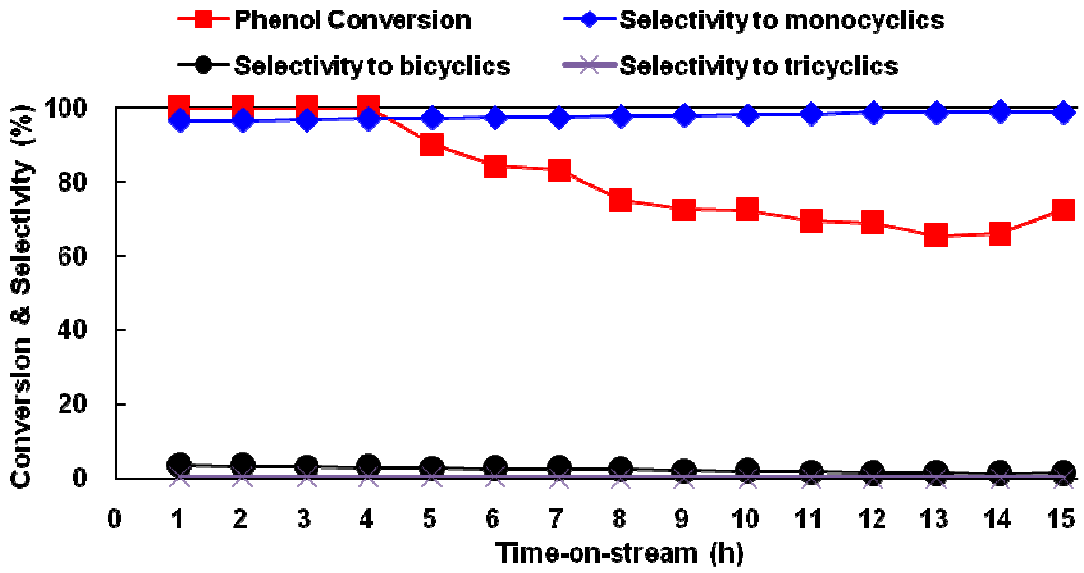

Figure 4.31 Ni-AlMCF. Phenol conversion and selectivities of main group of compounds. Reaction conditions: temperature, 200°C; H_2 pressure, 0.78 MPa; catalyst loading, 100 mg; catalysts, Ni-Y (Si/Ni = 12, SiO_2/Al_2O_3 = 12); WHSV, 5 hr^{-1}; H_2O content, 10 wt%.

Pore blockage may explain the trend shown by Ni-AlMCF wherein the phenol conversion was slowly decreasing [224]. It is interesting that this translated to a decrease in cyclohexane selectivity with an increase in cyclohex**ene** to a large extent and of cyclohexanone to a lesser degree (Figure 4.30). Cyclohexanol remained absent. It can thus be posited that there were enough acid sites to transform whatever cyclohexanol that was formed into cyclohex**ene**. However, nickel sites were increasingly getting less and less accessible thus translating to less phenol conversion[5], lower cyclohexane formation from cyclohex**ene** and slight increase in the amount of cyclohexanone that did not get converted.

[5] Experiments wherein aqueous phenol were fed into the reactor and allowed to pass through a bed of only acidic catalyst (either HY or H-AlMCF) were done. These did not show any phenol conversion through the GC analysis though TGA of the spent acid catalysts yielded the presence of carbonaceous compounds.

The low phenol conversion for Ni-Y and its steady value even at the start as well as that of the steady selectivities of the products do not suggest a gradual catalyst deactivation over time. Rather, it seemed to show an early on-set of deactivation that may be due to issues with accessibility of the nickel particles even at the beginning. Since the same reduction procedure was applied to all catalysts and considering that most of the Ni species in Ni-Y were reduced before that of Ni-AlMCF (which showed higher conversion) according to TPR (Figure 4.31), it can be assumed that most of the nickel species in Ni-Y should be already activated. It is interesting to understand the cause of this (concentration, dispersion, etc) as the result in Figure 4.29 suggests that Ni-Y can be tuned such that a stable phenol conversion may be achieved.

Considering the amount of carbonaceous deposits on the spent catalyst as measured by TGA, it can be seen from Table 4.5 that Ni-Y, by virtue of the stronger acidity of HY, had a higher ratio of higher temperature "coke" than Ni-AlMCF (B/A ratio 2.6 vs. 1.6). However, the more interesting part is if the incremental increase in the regions of coke were considered, the Ni-Y had almost 3x an increase compared to the Ni-AlMCF. Of course, the carbonaceous deposits being considered here were accumulation of the 15- hour run and most probably reflect the effect and not the probable cause of the low conversion exhibited by Ni-Y.

Table 4.4 TGA results of spent catalysts

	% Wt. Low Temperature	% Wt. High Temperature	% Wt. Lost due	Ratio of B/A

	Coke (A) (200°C to 360°C)	Coke (B) (360°C to 650°C)	to Organics	
HY	2.0	10.2	21.2	5.2
Ni-Y	5.8	14.9	24.7	2.6
H-Al-MCF	3.4	6.2	17.5	1.8
Ni-Al-MCF	5.4	8.8	18.2	1.6

Table 4. 5 Increase in coke content for spent acid catalyst in different configurations

	Δ (Low Temperature Coke)	Δ (High Temperature Coke)
HY	**-**	-
Ni-HY	194	46
H-Al-MCF	-	-
Ni-Al-MCF	59	42

4.3.3.4 Summary

Table 4.6 provides a quick summary of the results of the experiments discussed in the previous sections. This shows which configuration maximizes the production of a certain product. As was hypothesized, separation of the metal and acid active sites allowed a more sustained complete phenol conversion.

Table 4.6 Summary of reactions. Reaction conditions: temperature, 200°C; H_2 pressure, 0.79 MPa; catalysts, Ni-MCF, Ni-Y, NiH-Al-MCF, HY, H-Al-MCF

Catalyst(s)	**Major product**	**Selectivity to Major Product**		**Phenol Conversion**	
		after	after	after	after

		4 hours	15 hours	4 hours	15 hours
Ni-MCF	Cyclohexanol	82	91	100	100
HY	*no reaction*	-	-	-	-
H-Al-MCF	*no reaction*	-	-	-	-
Ni-Y	Cyclohex**ane**	48	50	15	13
Ni-Al-MCF	Cyclohex**ane**	89	55	100	73
Ni-MCF:HY	Cyclohex**ene**	92	94	100	100
Ni-MCF/HY	Cyclohex**ane**	99	99	100	100
Ni-MCF: H-Al-MCF	Cyclohex**ene**	92	98	100	100
Ni-MCF/H-Al-MCF	Cyclohex**ane**	99	99	100	100

4.4 CONCLUSION

This study probed the use of hydrothermally synthesized Ni-MCF in the hydrodeoxygenation/hydrogenation of aqueous phenol. Characterizations of this catalyst suggest the incorporation of the metal into the support, making it more recalcitrant to TPR and probably to sintering. EXAFS of a similarly synthesized catalyst on aluminosilicate showed that the NiO formed through the hydrothermal synthesis had a different bond distance and very different higher energy shell features compared to either the NiO reference material or the wet-impregnated version of the catalyst.

In using different combinations of the Ni-MCF with the acidic catalysts zeolite HY and H-Al-MCF, the selectivity to various monocyclic products in the hydrodeoxygenation/hydrogenation of aqueous phenol was successfully tuned. The initial hypothesis based on the understanding of the proposed mechanism that separation of the metal active site from the acid site would increase the sustained complete conversion of phenol was proven correct. Formation of bicyclics and tricyclics were inhibited for the most part. Ni-MCF, on its own, favored the formation of cyclohexanol at 100%

conversion for much longer hours than the previously reported system using Pt/HY [170]. In combination with a separate acid catalyst, the sequential bed catalyst configuration was capable of selectively forming cyclohex**ene** at selectivities higher than 98%. On the other hand, the physical mixture of the Ni-MCF and the acid catalyst in a single catalytic bed formed mainly cyclohexane at selectivities >99%. Additionally, aside from varying the catalyst configuration, control of the H_2/phenol ratio may also give another handle to control product selectivity.

Economically, the system designed in this study is very attractive since it is tunable, uses a non-precious, much cheaper metal (Pt vs. Ni), at a much lower reactor pressure than was previously used (> 80% reduction) and lastly, an almost 3x time-on-stream retained 100% phenol conversion.

4.4 RECOMMENDATIONS

This study was focused on understanding the effect of bifunctional catalysis on the hydrodeoxygenation/hydrogenation of phenol as a model bio-oil and the subsequent formation of the compounds in the previously suggested pathway. Effect of the catalyst configurations developed here on different bio-oil model compounds and/or their mixtures, or even actual bio-oil, would be of interest. Optimization of the catalyst concentration, metal dispersion and Si/Al ratio of the acid may be tackled for future studies. The preliminary experiments of varying catalyst amount at a constant feed flowrate (WHSV) hinted that an optimum metal loading may exist.

Another contribution of this study is the identification of systems which showed increased time on stream for complete phenol conversion and stable product selectivities.

However, longer time-on-stream experiments than 15 hours were not done. As longer experiments may shed light on the extent of the stability of the catalysts, these experiments may be worth pursuing for commercial applicability. Furthermore, no effort was done as yet on recycling these catalysts. This would be an important extension of this study.

Lastly, preliminary experiments showed that wet- impregnated catalysts had more sustained phenol conversion at higher H_2 pressures compared to the values reported at lower H_2 supplied. A similar study with Pt on different zeolite supports exhibited the same trends [224]. This can be an area of interest if a system that would be more compact in a large-scale set-up is of top priority and a specific catalyst loading can be optimized.

CHAPTER 5

CONCLUSIONS AND FUTURE WORK

5.1 SUMMARY AND CONCLUSIONS

The over-arching goal of this study was to probe the possibility of deriving alternative fuel or chemical feedstock from lignin. Considering the polymeric nature of lignin and its relatively much higher oxygen content than existing fossil fuel resources, the strategy employed in this endeavor involved (1) studying the depolymerization of lignin using high temperature base-catalyzed depolymerization, and (2) employing hydrodeoxygenation as a means to decrease the O/C ratio in the lignin-derived compounds.

The results of the research described in this thesis can be divided into three parts: (1) the base-catalyzed depolymerization of organosolv lignin; (2) batch hydrodeoxygenation of syringaldehyde in the presence of bulk and supported nickel phosphide; and, (3) continuous flow hydrodeoxygenation/hydrogenation of phenol utilizing the bifunctional catalyst system of metal-acid active sites.

5.1.1 Base-catalyzed depolymerization of organosolv lignin

As has been mentioned, lignin is the second most abundant natural polymer consisting of poly-aromatic units. It has three accepted starting monomers (syringyl, guaiacyl and p-coumaryl units) that can be linked together through radical-initiated dehydrogenative polymerizations occurring in plant cell walls. As a consequence, a variety of ether and C-C linkages form. These are the bonds that need to be broken simultaneously in order to yield lignin monomeric units.

In the base-catalyzed depolymerization investigated in this study, three different bases were used in a wide range of operating temperatures (165-350°C) using a 500-ml Monel Parr reactor. Water was used as a green, inexpensive solvent. The promise of separating the polar water from the non-polar products also added weight to this decision. Treatment of the starting lignin by NaOH and KOH bases showed completely solubilized reaction products up to 290°C. On the other hand, NH_4OH treated lignin increasingly gave solid residues as the reaction temperature was increased. It must be noted though that all experiments at 350°C yielded solids to which repolymerization reactions of the lignin fragments may be attributed to. Formation of carboxylic groups found in the ^{13}C NMR analysis of the whole product points to the occurrence of oxidation reactions as well as alkaline reactions. The nature of these experiments maybe similar to alkaline oxidative pulping reactions [63, 87] which typically uses much lower temperatures but much higher oxygen pressures. Molecular weight analysis of the acetylated evaporated products showed depolymerization compared to the acetylated starting material though the amount of identified and quantified monomer compounds through DCM extraction was at most only 6%.

An important insight gained in this study is the higher susceptibility of syringyl units than guaiacyl structures, thus giving an important criterion for the feed that may be more advantageously treated with this process if the repolymerization reactions can be addressed.

5.1.2 Batch hydrodeoxygenation of syringaldehyde

Syringaldehyde was one of the monomer units identified in the product of the BCD process. It is interesting as a lignin model compound because it contains three functional groups: (a) aldehydic; (b) phenolic; and, (c) methoxy. These are the main oxygen-containing functional groups present in most biomass-derived liquids [38]. These liquids are important intermediate products in the bioconversion processes. Removal of the oxygen-containing functionalities typically would require the presence of hydrogen and high temperature treatments. In this study, both bulk and supported catalysts were used. Because reduction is an important parameter for the formation of nickel phosphides, the capacity of the non-reduced bulk precursor compounds was also tested. The bulk catalysts (NiO, $Ni_3(PO_4)_2$ and $Ni_{12}P_5$) were shown to be capable of converting the aldehydic group of the starting material. $Ni_{12}P_5$ was found to catalyze the reaction to a greater extent as evidenced by the product profile. The methoxy group became de-methylated. On the other hand, the supported $Ni_{12}P_5$, Pt and Pd on alumina catalysts were more active than the bulk nickel catalysts. The slightly acidic alumina support was expected to have contributed to this higher activity. Ring-hydrogenated products were also formed in the presence of the supported catalysts. Another interesting class of products formed was the alkylated aromatics. Since there were no dedicated methyl group sources present, it is suggested that the methyls liberated from the action of the catalyst on the methoxy groups alkylated the aromatic ring. This is valuable for two reasons: (a) alkylated aromatics are valuable fuel components [141]; and (b) reinsertion of the methyl group into the compound increases carbon efficiency of the process. Supported $Ni_{12}P_5$ retained more of the alkylated aromatics among the supported catalysts.

Under the HDO conditions studied, $Ni_{12}P_5/Al_2O_3$, gave higher TOF values for syringaldehyde conversion than the Pt/Al_2O_3 and Pd/Al_2O_3.

5.1.3 Bifunctional aspects of phenol hydrodeoxygenation/hydrogenation

Aqueous phenol was used in this study as a lignin-derived model compound. Phenol is one of the most ubiquitous products, formed when processing whole biomass at high temperatures, present in amounts as high as 40% by weight of the resulting oil [118]. A previous study of phenol hydrodeoxygenation/hydrogenation in this group showed catalyst deactivation of Pt/HY after only 5 hours time-on-stream. Hypothesizing that coking catalyzed by the acidic zeolite was the main cause of metal deactivation, it was conceived that separation of the two active groups, metal and acid, would improve the system and would provide insight to the bifunctional catalysis occurring in the process. Testing this hypothesis led to the development of three systems capable of forming specific products at very high selectivities. Additionally, the objective of having a more robust catalyst system capable of longer retained activity for phenol conversion was achieved.

Ni supported on a purely silica support showed propensity to form cyclohexanol (>90%). A sequential catalyst system of Ni-MCF followed by the acid catalyst formed cyclohex**ene** (>98%)**,** in-line with what was proposed in the mechanism pathway. A single catalyst bed with a physical mixing of the two catalysts gave an almost pure stream (>99%) of cyclohexane. The latter was also the main product with a bifunctional catalyst, i.e., metal wet impregnated onto the acidic support. Whereas bifunctional catalyst showed severe carbon deactivation after only five hours run, separation of catalytic

activities (metal and acid sites) allowed not only better catalytic activity over a prolonged period, but it also provided an ability to tune the final products by sequencing these two activities.

5.2 SUGGESTIONS FOR FUTURE WORK

5.2.1 Catalytic upgrading of model compound mixtures

The work discussed in this dissertation applied hydrodeoxygenation on two model compounds that were lignin-derived: syringaldehyde and phenol. Through the batch experiments using syringaldehyde as feed in the presence of supported nickel phosphide, Pt and Pd catalysts, it was shown that the multi-functionality present in the syringaldehyde molecule as well as the multi-sited catalysts gave way to various products, both oxygenated and fully hydrogenated. Actual bio-oil is composed of varied compounds that may contain more than one functional group and it is thus not difficult to imagine that a myriad of products will be produced. Some of the more commonly identified compounds in pyrolytic bio-oil are presented below:

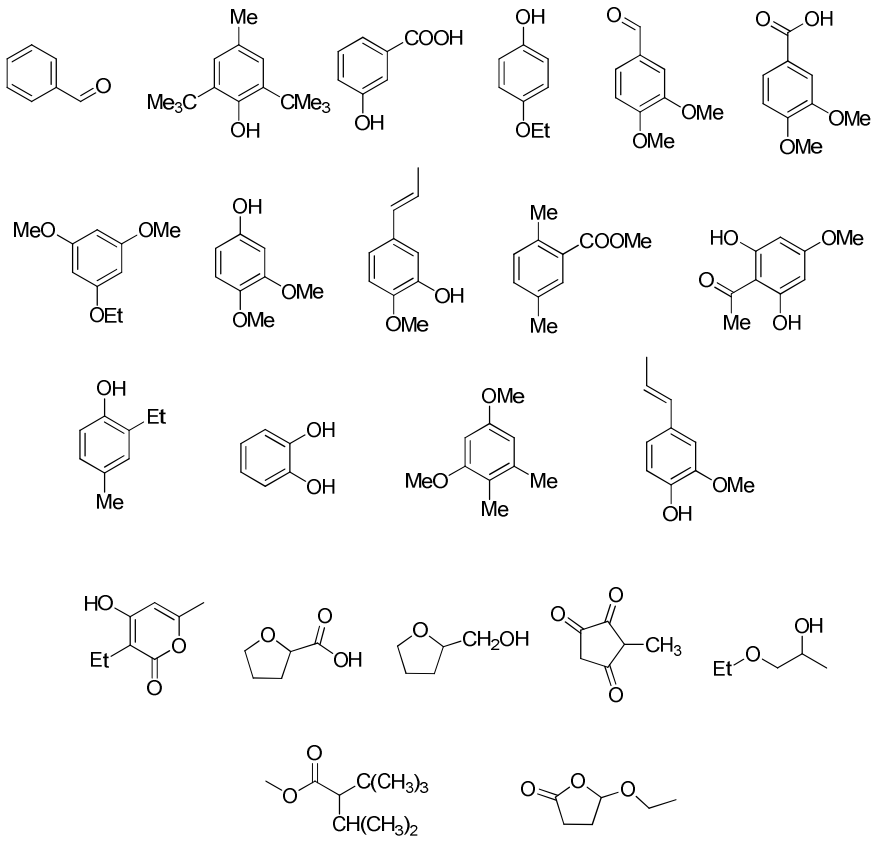

Figure 5.1 Typical structures of O-compounds in pyrolytic bio-oils. As cited by [38].

As shown, a larger percentage of the identified compounds were phenolic in nature, typically coming from the lignin fraction of biomass. However, the various substituents present in each of these compounds may affect the reactivity of the phenolic group and thus the selectivity of the products that can be formed. A systematic study of the effect of type of substituent in a single compound as opposed to the presence of other compounds which have different or similar substituents may give a better understanding of the performance of nickel phosphides and Ni-MCF:acid catalytic systems in actual HDO of pyrolysis oils. In the presence of actual biomass-derived liquid mixtures, it may not be practicable anymore to identify and quantify each of the products. Bulk elemental analysis, specifically C,H and O, may actually give a better index of the efficacy of the

HDO process. Lastly, longer time-on-stream studies, recyclability and deactivation of the catalysts need to be undertaken.

5.2.2 Use of H_2 atmosphere or hydrogen-donating solvents in direct biomass/lignin depolymerization

Formation of radical species during the lignin depolymerization conditions was suggested to have occurred, as previously discussed. Though formation of the radicals suggests fragmentation of the polymer, their inherently very high reactivity caused repolymerization reactions to occur, thus forming unwanted oligomeric chains. Stabilization of the radicals formed through the use of H_2 or hydrogen-donating solvent such as tetralin even during the depolymerization stage may impart better monomeric yields. A variation to this system may include the HDO-active catalysts which would then make the system a one-pot depolymerization-catalytic upgrading system.

5.2.3 Substitution of H_2 by CH_4 for alkylation

Methane is currently used as a fuel source for combustion. Steam reforming of methane for syn-gas generation and its subsequent use as feed for the Fischer-Tropsch process would yield higher molecular weight fuels. It has very stable C-H bonds that require very high temperatures to break, typically >500°C. However, these temperatures overlap with the ones that are also being used for pyrolysis. In view of this, its use as a substitute for H_2 may prove interesting.

Methane has been used to upgrade extra-heavy crude oil in the presence of water and was found to be effective in reducing crude viscosity (380°C, 11 MPa, 4 hrs, no catalyst) [225]. These authors found evidences of methyl incorporation through

deuterium studies. A similar principle may be applied to lignin or biomass in general. By incorporating an additional C-group, a better fuel stream may be produced.

Supported catalysts that showed capability of C-H activation, such as Pt, Ir and Ni may also be used [226-228]. The presence of these catalysts in this reaction may be beneficial in two ways: (1) better utilization of methane by producing higher hydrocarbons; and, (2) stabilization of bio-oil by using methane instead of H_2.

REFERENCES

1. *Smalley Institute Grand Challenges*. 2008 [cited 2011 Feb. 4].

2. *Key World Energy Statistics*. 2010, International Energy Agency: Paris, France.

3. Owen, N.A., O.R. Inderwildi, and D.A. King, *The status of conventional world oil reserves-Hype or cause for concern?* Energy Policy, 2010. **38**(8): p. 4743-4749.

4. *Annual Energy Review 2009*, U. EIA, Editor. 2010.

5. Deffeyes, K.S., *Beyond Oil*. 2005, New York: Hill and Wang.

6. Chen, W.Y. and R.N. Xu, *Clean coal technology development in China.* Energy Policy, 2010. **38**(5): p. 2123-2130.

7. *EPA Finalizes Regulations for the National Renewable Fuel Standard Program for 2010 and Beyond*, O.o.T.a.A. Quality, Editor. 2010, US EPA.

8. Hubbert, M.K., *Energy from Fossil Fuels.* Science, 1949. **109**: p. 103-109.

9. Hubbert, M.K., *Nuclear Energy and the Fossil Fuels*. 1956, Shell Development Company - Exploration and Poduction Research Division.

10. *Crude Oil: Uncertainty about Future Oil Supply Makes It Important to Develop a Strategy for Addressing a Peak and Decline in Oil Production*, U.G.A. Office, Editor. 2007: Washington, D.C.

11. Sissine, F., *Energy Independence and Security Act of 2007: A Summary of Major Provisions*, C.R. Service, Editor. 2007: Washington, D.C.

12. *Energy Independence and Security Act of 2007*. 2007, US GPO: USA.

13. Bowyer, J., R. Shmulsky, and J. Haygreen, *Forest Products and Wood Science: An Introduction*. 5th ed. 2007, Oxford, UK: Blackwell Publishing.

14. Sjöström, E., *Wood Chemistry*. 2nd ed. 1999, New York: Academic Press.

15. (2010) *Roadmap Background Information: Biofuels for Transport*.

16. Fargione, J.E., R.J. Plevin, and J.D. Hill, *The Ecological Impact of Biofuels.* Annual Review of Ecology, Evolution, and Systematics, 2010. **41**(1): p. 351-377.

17. Ragauskas, A.J., et al., *The path forward for biofuels and biomaterials.* Science, 2006. **311**(5760): p. 484-489.

18. Sims, R., et al., *From 1st- to 2nd- Generation Biofuel Technologies: An overview of current industry and R&D activities*. 2008, International Enery Agency: Paris, France.

19. *World Energy Outlook 2010 Executive Summary*. 2010, International Energy Agency: Paris, France.

20. *Sustainability of Biofuels: Future Research Opportunities*, USDOE and USDA, Editors. 2008.

21. Kamm, B., et al., *Lignocellulose-based Chemical Products and Product Family Trees*, in *Biorefineries - Industrial Processes and Products*, B. Kamm, P.R. Gruber, and M. Kamm, Editors. 2006, Wiley-VCH Verlag GmbH & Co. KGaA: Weinheim.

22. *Transport, Energy and CO2: Moving Towards Sustainability*. 2009, International Energy Agency: Paris, France.

23. Perlack, R., et al., *Biomass as Feedstock for a Bioenergy and Bioproducts Industry: The Technical Feasibility of a Billion-Ton Annual Supply*. 2005, Oak Ridge National Laboratory, US Department of Agriculture, US Department of Energy: Oak Ridge, TN.

24. Demirbas, M.F., *Biorefineries for biofuel upgrading: A critical review.* Applied Energy, 2009. **86**: p. S151-S161.

25. Huber, G.W. and J.A. Dumesic, *An overview of aqueous-phase catalytic processes for production of hydrogen and alkanes in a biorefinery.* Catalysis Today, 2006. **111**(1-2): p. 119-132.

26. *Top Value Added Chemicals from Biomass: Volume I - Results of Screening for Potential Candidates from Sugars and Synthesis Gas*, T. Werpy and G. Petersen, Editors. 2004, Pacific Northwest National Laboratory (PNNL) National Renewable Energy Laboratory (NREL).

27. Holladay, J., et al., *Top Value Added Chemicals from Biomass: Volume II - Results of Screenings for Potential Candidates from Biorefinery Lignin*. 2007, Pacific Northwest National Laboratory: USA.

28. *Biomass Feedstock Composition and Database*, National Renewable Energy Laboratory: Golden, Colorado.

29. Guerra, A., et al., *Comparative evaluation of three lignin isolation protocols for various wood species.* Journal of Agricultural and Food Chemistry, 2006. **54**(26): p. 9696-9705.

30. Guerra, A., et al., *Toward a better understanding of the lignin isolation process from wood.* Journal of Agricultural and Food Chemistry, 2006. **54**(16): p. 5939-5947.

31. Boerjan, W., J. Ralph, and M. Baucher, *Lignin biosynthesis.* Annual Review of Plant Biology, 2003. **54**: p. 519-546.

32. Ralph, J., et al., *Lignins: Natural polymers from oxidative coupling of 4-hydroxyphenylpropanoids.* Phytochemistry Reviews, 2004. **3**(1-2): p. 29-60.

33. Meister, J.J., *Modification of lignin.* Journal of Macromolecular Science-Polymer Reviews, 2002. **C42**(2): p. 235-289.

34. Hon, D. and N. Shiraishi, *Wood and Cellulosic Chemistry*. 2000, New York: Marcell and Decker.

35. Brunow, G., et al., *Oxidative Coupling of Phenols and the Biosynthesis of Lignin*, in *Lignin and Lignan Biosynthesis*. 1998, American Chemical Society. p. 131-147.

36. Lin, L. and C. Dence, eds. *Methods in Lignin Chemistry*. 1992, Springer-Verlag: New York.

37. Shevchenko, S.M. and G.W. Bailey, *Life after death: Lignin-humic relationships reexamined.* Critical Reviews in Environmental Science and Technology, 1996. **26**(2): p. 95-153.

38. Furimsky, E., *Catalytic hydrodeoxygenation.* Applied Catalysis a-General, 2000. **199**(2): p. 147-190.

39. Romero, Y., et al., *Hydrodeoxygenation of benzofuran and its oxygenated derivatives (2,3-dihydrobenzofuran and 2-ethylphenol) over NiMoP/Al_2O_3 catalyst.* Applied Catalysis a-General, 2009. **353**(1): p. 46-53.

40. Oasmaa, A. and E. Kuoppala, *Fast pyrolysis of forestry residue. 3. Storage stability of liquid fuel.* Energy & Fuels, 2003. **17**(4): p. 1075-1084.

41. Czernik, S. and A.V. Bridgwater, *Overview of applications of biomass fast pyrolysis oil.* Energy & Fuels, 2004. **18**(2): p. 590-598.

42. Kleinert, M. and T. Barth, *Towards a lignincellulosic biorefinery: Direct one-step conversion of lignin to hydrogen-enriched biofuel.* Energy & Fuels, 2008. **22**(2): p. 1371-1379.

43. Vispute, T.P., et al., *Renewable Chemical Commodity Feedstocks from Integrated Catalytic Processing of Pyrolysis Oils.* Science, 2010. **330**(6008): p. 1222-1227.

44. Zakzeski, J., et al., *The Catalytic Valorization of Lignin for the Production of Renewable Chemicals.* Chemical Reviews, 2010. **110**(6): p. 3552-3599.

45. Silverstein, R. and F. Webster, *Spectrometric Identification of Organic Compounds*. 1998, New York: John Wiley & Sons, Inc.

46. Robert, D., *Carbon-13 Nuclear Magnetic Resonance Spectroscopy*, in *Methods in Lignin Chemistry*, S. Lin and C. Dence, Editors. 1992, Springer-Verlag: Berlin.

47. Xia, Z., L. Akim, and D.S. Argyropoulos, *Quantitative 13C NMR Analysis of Lignins with Internal Standards.* Journal of Agricultural and Food Chemistry, 2001. **49**: p. 3573-3578.

48. Gosselink, R.J.A., et al., *Analytical protocols for characterisation of sulphur-free lignin.* Industrial Crops and Products, 2004. **19**(3): p. 271-281.

49. Maunu, S.L., *NMR studies of wood and wood products.* Progress in Nuclear Magnetic Resonance Spectroscopy, 2002. **40**(2): p. 151-174.

50. Glagovich, N. *NMR Spectroscopy: Nuclear Overhauser Effect*. 2009 Nov. 15, 2009 [cited 2010 Aug. 15].

51. Ralph, S.A., J. Ralph, and L.L. Landucci, *NMR Database of Lignin and Cell Wall Model Compounds*. 2004, USDA ARS.

52. Browning, B., *Methods of Wood Chemistry*. 1967, New York: Interscience Publishers.

53. Brauns, F.E., *Native Lignin1 I. Its Isolation and Methylation.* Journal of the American Chemical Society, 1939. **61**(8): p. 2120-2127.

54. Brunow, G., K. Lundquist, and G. Gellerstedt, *Lignin*, in *Analytical Methods in Wood Chemistry, Pulping and Papermaking*, E. Sjostrom and R. Alen, Editors. 1999, Springer-Verlag: Heidelberg.

55. TAPPI, T.A.o.t.P.a.P.I., *Acid-insoluble lignin in wood and pulp*.

56. Sievers, C., et al., *Quantitative solid state NMR analysis of residues from acid hydrolysis of loblolly pine wood.* Bioresource Technology, 2009. **100**(20): p. 4758-4765.

57. Vuorinen, T. and R. Alen, *Carbohydrates*, in *Analytical Methods in Wood Chemistry, Pulping and Papermaking*, E. Sjostrom and R. Alen, Editors. 1999, Springer-Verlag: Heidelberg.

58. Sun, R.C., et al., *Fractional isolation and partial characterization of non-starch polysaccharides and lignin from sago pith.* Industrial Crops and Products, 1999. **9**(3): p. 211-220.

59. Calimli, A. and A. Olcay, *SUPERCRITICAL DIOXANE EXTRACTION OF SPRUCE WOOD AND OF DIOXANE-LIGNIN AND COMPARISON OF THE EXTRACTS WITH THE PYROLYSIS PRODUCTS.* Separation Science and Technology, 1982. **17**(1): p. 183-197.

60. Fasching, M., et al., *A new and facile method for isolation of lignin from wood based on complete wood dissolution.* Holzforschung, 2008. **62**(1): p. 15-23.

61. Zhang, X.M., et al., *Separation and Structural Characterization of Lignin from Hybrid Poplar Based on Complete Dissolution in DMSO/LiCl.* Separation Science and Technology, 2010. **45**(16): p. 2497-2506.

62. Smook, G.A., *Handbook for Pulp & Paper Technologists*. 1992, Vancouver: Angus Wilde Publications.

63. Gierer, J., *Reactions of Lignin During Pulping - a Description and Comparison of Conventional Pulping Processes.* Svensk Papperstidning-Nordisk Cellulosa, 1970. **73**(18): p. 571-&.

64. Sundquist, J., *Organosolv pulping*, in *Chemical Pulping*, J. Gullichsen and C. Fogelholm, Editors. 1999, Fapet Oy: Helsinki, Finland.

65. Dence, C., *Reaction Principles in Pulp Bleaching*, in *Pulp Bleaching: Principles and Practice*, C. Dence and D. Reeve, Editors. 1996, TAPPI Press: Atlanta.

66. Gierer, J., *CHEMISTRY OF DELIGNIFICATION .1. GENERAL CONCEPT AND REACTIONS DURING PULPING.* Wood Science and Technology, 1985. **19**(4): p. 289-312.

67. Lapierre, C. and C. Rolando, *THIOACIDOLYSES OF PRE-METHYLATED LIGNIN SAMPLES FROM PINE COMPRESSION AND POPLAR WOODS.* Holzforschung, 1988. **42**(1): p. 1-4.

68. Akim, L., T. Feduline, and S. Shevchenko, *13C NMR of Lignins in Aqueous Alkali II. Ionization Effects on the Spectra of Technical Lignins.* Holzforshung, 1997. **51**(5): p. 419-427.

69. Thring, R.W., *ALKALINE-DEGRADATION OF ALCELL(R) LIGNIN.* Biomass & Bioenergy, 1994. **7**(1-6): p. 125-130.

70. Kadangode, S., *Lignin Conversion into Reformulated Hydrocarbon and Partially Oxygenated Gasoline Compositions*, in *Department of Chemical and Fuels Engineering*. 2001, University of Utah.

71. Shabtai, J.S., W.W. Zmierczak, and E. Chornet, *Process for conversion of lignin to reformulated hydrocarbon gasoline*. 1999, The University of Utah Research Foundation, USA . p. 32 pp.

72. Shabtai, J.S., W.W. Zmierczak, and E. Chornet, *Process for conversion of lignin to reformulated, partially oxygenated gasoline*. 2000, The University of Utah Research Foundation, USA . p. 25 pp.

73. Shabtai, J.S., et al., *Process for converting lignins into a high-octane blending component for gasoline*. 2003, USA . p. 20 pp., Cont.-in-part of U.S. Ser. No. 972,461.

74. Shabtai, J.S., et al., *Integrated alkali depolymerization-hydroprocessing of lignins for manufacture of high-octane alkylbenzene gasoline blending stocks*. 2003, USA . p. 19 pp.

75. Miller, J., et al., *Batch Microreactor Studies of Lignin Depolymerization by Bases. 1. Alcohol Solvents*. 2002, Sandia National Laboratories: Albuquerque, New Mexico.

76. Miller, J., et al., *Batch Microeactor Studies of Lignin Depolymerization by Bases. 2. Aqueous Solvents*. 2002, Sandia National Laboratories: Albuquerque, New Mexico and Livermore, California.

77. Marzialetti, T., et al., *Dilute acid hydrolysis of Loblolly pine: A comprehensive approach.* Industrial & Engineering Chemistry Research, 2008. **47**(19): p. 7131-7140.

78. Glasser, W.G., V. Dave, and C.E. Frazier, *MOLECULAR-WEIGHT DISTRIBUTION OF (SEMI-) COMMERCIAL LIGNIN DERIVATIVES.* Journal of Wood Chemistry and Technology, 1993. **13**(4): p. 545-559.

79. Capanema, E.A., M.Y. Balakshin, and J.F. Kadla, *A comprehensive approach for quantitative lignin characterization by NMR spectroscopy.* Journal of Agricultural and Food Chemistry, 2004. **52**(7): p. 1850-1860.

80. Holtman, K.M., et al., *Quantitative C-13 NMR characterization of milled wood lignins isolated by different milling techniques.* Journal of Wood Chemistry and Technology, 2006. **26**(1): p. 21-34.

81. Mitchell, T. and B. Costisella, *NMR--from spectra to structures: an experimental approach*. 2007: Springer.

82. Akim, L.G., T.G. Fedulina, and S.M. Shevchenko, *13C NMR of lignins in aqueous alkali. I. Ionization effect on the spectra of model compounds and milled wood lignins.* Holzforschung, 1996. **50**(Copyright (C) 2011 American Chemical Society (ACS). All Rights Reserved.): p. 237-244.

83. Sun, J.X., et al., *Inhomogeneities in the chemical structure of sugarcane bagasse lignin.* Journal of Agricultural and Food Chemistry, 2003. **51**(23): p. 6719-6725.

84. Hallac, B.B., Y.Q. Pu, and A.J. Ragauskas, *Chemical Transformations of Buddleja davidii Lignin during Ethanol Organosolv Pretreatment.* Energy & Fuels, 2010. **24**: p. 2723-2732.

85. Buckingham, A.D., T.P. Schaefer, and W.G. Schneider, *Solvent effects in nuclear magnetic resonance spectra.* J. Chem. Phys., 1960. **32**(Copyright (C) 2011 American Chemical Society (ACS). All Rights Reserved.): p. 1227-33.

86. Hansch, C., A. Leo, and R.W. Taft, *A survey of Hammett substituent constants and resonance and field parameters.* Chem. Rev., 1991. **91**(Copyright (C) 2011 American Chemical Society (ACS). All Rights Reserved.): p. 165-95.

87. Reitberger, T., et al., *Involvement of Oxygen-Derived Free Radicals in Chemical and Biochemical Degradation of Lignin*, in *Oxidative Delignification Chemistry*. 2001, American Chemical Society. p. 255-271.

88. Imsgard, F., *Autoxidation in Alkaline Media of Phenolic Compounds Related to Lignin*, in *Department of Organic Chemistry*. 1976, Royal Institute of Technology: Stockholm.

89. Ji, Y., E. Vanska, and A. van Heiningen, *New kinetics and mechanisms of oxygen delignification observed in a continuous stirred tank reactor.* Holzforschung, 2009. **63**(3): p. 264-271.

90. *Chemistry of delignification with oxygen, ozone and peroxides : symposium held at Raleigh, North Carolina, May 27-29, 1975 under the auspices of the School of Forest Resources of North Carolina State University*. 1980, Tokyo :: UNI Publishers.

91. Northey Robert, A., *A Review of Lignin Model Compound Reactions under Oxygen Bleaching Conditions*, in *Oxidative Delignification Chemistry*. 2001, American Chemical Society. p. 44-60.

92. Koda, K., et al., *Molecular weight-functional group relations in softwood residual kraft lignins.* Holzforschung, 2005. **59**(6): p. 612-619.

93. Cheng, S.N., et al., *Highly Efficient Liquefaction of Woody Biomass in Hot-Compressed Alcohol-Water Co-solvents.* Energy & Fuels, 2010. **24**: p. 4659-4667.

94. Demirbas, A., *Mechanisms of liquefaction and pyrolysis reactions of biomass.* Energy Conversion and Management, 2000. **41**(6): p. 633-646.

95. Fang, Z., et al., *Reaction chemistry and phase behavior of lignin in high-temperature and supercritical water.* Bioresource Technology, 2008. **99**(9): p. 3424-3430.

96. Marton, J., *Reactions in alkaline pulping*, in *Lignins: Occurrence, formation, structure and reactions*, K. Sarkanen and C. Ludwig, Editors. 1971, Wiley-Interscience: New York.

97. Capanema, E.A., et al., *Oxidative ammonolysis of technical lignins - Part 1. Kinetics of the reaction under isothermal condition at 130 degrees C.* Holzforschung, 2001. **55**(4): p. 397-404.

98. Capanema, E.A., et al., *Oxidative ammonolysis of technical lignins - Part 2. Effect of oxygen pressure.* Holzforschung, 2001. **55**(4): p. 405-412.

99. Capanema, E.A., et al., *Oxidative ammonolysis of technical lignins - Part 3. Effect of temperature on the reaction rate.* Holzforschung, 2002. **56**(4): p. 402-415.

100. Capanema, E.A., et al., *Oxidative ammonolysis of technical lignins. Part 4. Effects of the ammonium hydroxide concentration and pH.* Journal of Wood Chemistry and Technology, 2006. **26**(1): p. 95-109.

101. Baumberger, S., et al., *Molar mass determination of lignins by size-exclusion chromatography: towards standardisation of the method.* Holzforschung, 2007. **61**(4): p. 459-468.

102. Chen, F.G. and J. Li, *Aqueous gel permeation chromatographic methods for technical lignins.* Journal of Wood Chemistry and Technology, 2000. **20**(3): p. 265-276.

103. Connors, W.J., S. Sarkanen, and J.L. McCarthy, *GEL CHROMATOGRAPHY AND ASSOCIATION COMPLEXES OF LIGNIN.* Holzforschung, 1980. **34**(3): p. 80-85.

104. Guerra, A., et al., *On the propensity of lignin to associate: A size exclusion chromatography study with lignin derivatives isolated from different plant species.* Phytochemistry, 2007. **68**(20): p. 2570-2583.

105. *GPC/SEC Theory: Universal Calibration*. [cited 2011 1/22]; Available from: http://www.malvern.com/LabEng/technology/gel_permeation_chromatography_theory/universal_calibration_gpc_theory.htm.

106. Asgari, F. and D.S. Argyropoulos, *Fundamentals of oxygen delignification. Part II. Functional group formation elimination in residual kraft lignin.* Canadian Journal of Chemistry-Revue Canadienne De Chimie, 1998. **76**(11): p. 1606-1615.

107. Chen, H.T., M. Funaoka, and Y.Z. Lai, *Attempts to understand the nature of phenolic and etherified components of wood lignin.* Wood Sci. Technol., 1997. **31**(Copyright (C) 2011 American Chemical Society (ACS). All Rights Reserved.): p. 433-440.

108. El Hage, R., et al., *Characterization of milled wood lignin and ethanol organosolv lignin from miscanthus.* Polymer Degradation and Stability, 2009. **94**(10): p. 1632-1638.

109. Li, C.Q., et al., *The Behavior of free radicals in coal at temperatures up to 300 degrees C in various organic solvents, using in situ EPR spectroscopy.* Energy & Fuels, 2002. **16**(5): p. 1116-1120.

110. Hemmingsen, E., *At the base of Hubbert's Peak: Grounding the debate on petroleum scarcity.* Geoforum, 2010. **41**(4): p. 531-540.

111. Matutinovic, I., *Oil and the political economy of energy.* Energy Policy, 2009. **37**(11): p. 4251-4258.

112. Lynch, M.C., *Forecasting oil supply: theory and practice.* The Quarterly Review of Economics and Finance, 2002. **42**(2): p. 373-389.

113. Sorrell, S. and J. Speirs, *Hubbert's Legacy: A Review of Curve-Fitting Methods to Estimate Ultimately Recoverable Resources.* Natural Resources Research, 2010. **19**(3): p. 209-230.

114. *ENERGY 2020: A strategy for competitive, sustainable and secure energy - citizens' summary*. 2010, European Commission.

115. Huber, G.W., S. Iborra, and A. Corma, *Synthesis of transportation fuels from biomass: Chemistry, catalysts, and engineering.* Chemical Reviews, 2006. **106**(9): p. 4044-4098.

116. Puig-Arnavat, M., J.C. Bruno, and A. Coronas, *Review and analysis of biomass gasification models.* Renewable and Sustainable Energy Reviews, 2010. **14**(9): p. 2841-2851.

117. Valenzuela, M.B., C.W. Jones, and P.K. Agrawal, *Batch aqueous-phase reforming of woody biomass.* Energy & Fuels, 2006. **20**(4): p. 1744-1752.

118. Elliott, D.C., *Historical developments in hydroprocessing bio-oils.* Energy & Fuels, 2007. **21**(3): p. 1792-1815.

119. Laurent, E. and B. Delmon, *Influence of Oxygen-Containing, Nitrogen-Containing, and Sulfur-Containing-Compounds on the Hydrodeoxygenation of Phenols over Sulfided Como/Gamma-Al2o3 and Nimo/Gamma-Al2o3 Catalysts.* Industrial & Engineering Chemistry Research, 1993. **32**(11): p. 2516-2524.

120. Laurent, E. and B. Delmon, *Influence of Water in the Deactivation of a Sulfided Nimo Gamma-Al2o3 Catalyst During Hydrodeoxygenation.* Journal of Catalysis, 1994. **146**(1): p. 281-291.

121. Laurent, E. and B. Delmon, *STUDY OF THE HYDRODEOXYGENATION OF CARBONYL, CARBOXYLIC AND GUAIACYL GROUPS OVER SULFIDED COMO/GAMMA-AL2O3 AND NIMO/GAMMA-AL2O3 CATALYST .2. INFLUENCE OF WATER, AMMONIA AND HYDROGEN-SULFIDE.* Applied Catalysis a-General, 1994. **109**(1): p. 97-115.

122. Grange, P., et al., *Hydrotreatment of pyrolysis oils from biomass: Reactivity of the various categories of oxygenated compounds and preliminary techno-economical study.* Catalysis Today, 1996. **29**(1-4): p. 297-301.

123. Maggi, R. and B. Delmon, *A review of catalytic hydrotreating processes for the upgrading of liquids produced by flash pyrolysis*, in *Hydrotreatment and Hydrocracking of Oil Fractions*. 1997. p. 99-113.

124. Centeno, A., E. Laurent, and B. Delmon, *Influence of the Support of CoMo Sulfide Catalysts and of the Addition of Potassium and Platinum on the Catalytic Performances for the Hydrodeoxygenation of Carbonyl, Carboxyl, and Guaiacol-Type Molecules.* Journal of Catalysis, 1995. **154**(2): p. 288-298.

125. Laurent, E. and B. Delmon, *STUDY OF THE HYDRODEOXYGENATION OF CARBONYL, CARBOXYLIC AND GUAIACYL GROUPS OVER SULFIDED COMO/GAMMA-AL2O3 AND NIMO/GAMMA-AL2O3 CATALYSTS .1. CATALYTIC REACTION SCHEMES.* Applied Catalysis a-General, 1994. **109**(1): p. 77-96.

126. Wang, X.Q., P. Clark, and S.T. Oyama, *Synthesis, characterization, and hydrotreating activity of several iron group transition metal phosphides.* Journal of Catalysis, 2002. **208**(2): p. 321-331.

127. Oyama, S.T., et al., *Active phase of Ni2P/SiO2 in hydroprocessing reactions.* Journal of Catalysis, 2004. **221**(2): p. 263-273.

128. Ding, D.Y., et al., *Ni-Ni3P alloy catalyst for carbon nanostructures.* Chemical Physics Letters, 2003. **371**(3-4): p. 333-336.

129. Zhou, L., et al., *Spatial and electronic structure of the Ni3P surface.* Applied Surface Science, 2010. **256**(24): p. 7692-7695.

130. Zhao, H.Y., et al., *Hydrodeoxygenation of guaiacol as model compound for pyrolysis oil on transition metal phosphide hydroprocessing catalysts.* Applied Catalysis A: General, 2011. **391**(1-2): p. 305-310.

131. Oyama, S.T., *Novel catalysts for advanced hydroprocessing: transition metal phosphides.* Journal of Catalysis, 2003. **216**(1-2): p. 343-352.

132. Korányi, T.I., et al., *SBA-15-supported nickel phosphide hydrotreating catalysts.* Journal of Catalysis, 2008. **253**(1): p. 119-131.

133. Sawhill, S.J., et al., *Thiophene hydrodesulfurization over nickel phosphide catalysts: effect of the precursor composition and support.* Journal of Catalysis, 2005. **231**(2): p. 300-313.

134. Wang, H., et al., *Selective hydrogenation of cinnamaldehyde to hydrocinnamaldehyde over SiO2 supported nickel phosphide catalysts.* Catalysis Letters, 2008. **124**(3-4): p. 219-225.

135. Yang, S.F. and R. Prins, *New synthesis method for nickel phosphide hydrotreating catalysts.* Chemical Communications, 2005(33): p. 4178-4180.

136. Oyama, S.T., et al., *Effect of phosphorus content in nickel phosphide catalysts studied by XAFS and other techniques.* Journal of Catalysis, 2002. **210**(1): p. 207-217.

137. Berhault, G., et al., *In Situ XRD, XAS, and Magnetic Susceptibility Study of the Reduction of Ammonium Nickel Phosphate NiNH4PO4 center dot H2O into Nickel Phosphide.* Inorganic Chemistry, 2009. **48**(7): p. 2985-2992.

138. Carling, S.G., P. Day, and D. Visser, *CRYSTAL AND MAGNETIC-STRUCTURES OF LAYER TRANSITION-METAL PHOSPHATE HYDRATES.* Inorganic Chemistry, 1995. **34**(15): p. 3917-3927.

139. Mosciano, G., et al., *Organoleptic Characteristics of Flavor Materials.* Perfumer and Flavorist, 1994. **19**(3).

140. Altarawneh, M., et al., *Theoretical Study on the Thermodynamic Properties and Self-Decomposition of Methylbenzenediol Isomers.* Journal of Physical Chemistry A, 2010. **114**(43): p. 11751-11760.

141. Hileman, J.I., R.W. Stratton, and P.E. Donohoo, *Energy Content and Alternative Jet Fuel Viability.* Journal of Propulsion and Power, 2010. **26**(6): p. 1184-1195.

142. Oyama, S.T., et al., *In situ FTIR and XANES studies of thiophene hydrodesulfurization on Ni2P/MCM-41.* Journal of Catalysis, 2009. **268**(2): p. 209-222.

143. Natesakhawat, S., et al., *Deactivation characteristics of lanthanide-promoted sol-gel Ni/Al2O3 catalysts in propane steam reforming.* Journal of Catalysis, 2005. **234**(2): p. 496-508.

144. Ni, Y.H., et al., *Synthesis, characterization and properties of hollow nickel phosphide nanospheres.* Nanotechnology, 2006. **17**(19): p. 5013-5018.

145. Macedo, M.I.F., C.A. Bertran, and C.C. Osawa, *Kinetics of the gamma ->alpha-alumina phase transformation by quantitative X-ray diffraction.* Journal of Materials Science, 2007. **42**(8): p. 2830-2836.

146. Shu, Y.Y., Y.K. Lee, and S.T. Oyama, *Structure-sensitivity of hydrodesulfurization of 4,6-dimethyldibenzothiophene over silica-supported nickel phosphide catalysts.* Journal of Catalysis, 2005. **236**(1): p. 112-121.

147. Cho, K.S., et al., *Nickel Phosphide Catalysts Supported on SBA-15 for Hydrodesulfurization of 4,6-Dimethyldibenzothiophene.* Journal of the Japan Petroleum Institute, 2010. **53**(3): p. 173-177.

148. Oyama, S.T. and Y.K. Lee, *The active site of nickel phosphide catalysts for the hydrodesulfurization of 4,6-DMDBT.* Journal of Catalysis, 2008. **258**(2): p. 393-400.

149. Yin, H.W., J.X. Chen, and J.Y. Zhang, *Effects of calcination and reduction temperature on catalytic performance of Ni/TiO2 catalyst for hydrogenation of p-nitrophenol to p-animophenol.* Chinese Journal of Catalysis, 2007. **28**(5): p. 435-440.

150. Monti, D.A.M. and A. Baiker, *TEMPERATURE-PROGRAMMED REDUCTION - PARAMETRIC SENSITIVITY AND ESTIMATION OF KINETIC-PARAMETERS.* Journal of Catalysis, 1983. **83**(2): p. 323-335.

151. Jones, A. and B. McNicol, *Temperature-programmed reduction for solid materials characterization*. 1986, New York: Marcel Dekker Inc.

152. Bredenberg, J.B.S., et al., *HYDROGENOLYSIS AND HYDROCRACKING OF THE CARBON OXYGEN BOND .1. HYDROCRACKING OF SOME SIMPLE AROMATIC O-COMPOUNDS.* Journal of Catalysis, 1982. **77**(1): p. 242-247.

153. Vannice, M., *Kinetics of Catalytic Reactions*. 2005, New York, USA: Springer Science+Business Media Inc.

154. Srinivas, S.T. and P.K. Rao, *Direct Observation of Hydrogen Spillover on Carbon-Supported Platinum and Its Influence on the Hydrogenation of Benzene.* Journal of Catalysis, 1994. **148**(2): p. 470-477.

155. Centeno, A., R. Maggi, and B. Delmon, *Use of noble metals in hydrodeoxygenation reactions*, in *Hydrotreatment and Hydrocracking of Oil Fractions*, B. Delmon, G.F. Froment, and P. Grange, Editors. 1999. p. 77-84.

156. Du, H.B., et al., *The chemistry of selective ring-opening catalysts.* Applied Catalysis a-General, 2005. **294**(1): p. 1-21.

157. Chupin, J., et al., *Influence of the metal and of the support on the activity and stability of bifunctional catalysts for toluene hydrogenation.* Applied Catalysis a-General, 2001. **206**(1): p. 43-56.

158. Goacher, R.E., D. Jeremic, and E.R. Master, *Expanding the Library of Secondary Ions That Distinguish Lignin and Polysaccharides in Time-of-Flight Secondary Ion Mass Spectrometry Analysis of Wood.* Analytical Chemistry, 2010: p. null-null.

159. Ausavasukhi, A., T. Sooknoi, and D.E. Resasco, *Catalytic deoxygenation of benzaldehyde over gallium-modified ZSM-5 zeolite.* Journal of Catalysis, 2009. **268**(1): p. 68-78.

160. An, L., et al., *The influence of Ni loading on coke formation in steam reforming of acetic acid.* Renewable Energy, 2011. **36**(3): p. 930-935.

161. Tatsuta, K., et al., *The first total synthesis and structural determination of TMC-264.* Tetrahedron Letters, 2008. **49**(25): p. 4036-4039.

162. Ceylan, R. and J.B. Bredenberg, *HYDROGENOLYSIS AND HYDROCRACKING OF THE CARBON-OXYGEN BOND .2. THERMAL CLEAVAGE OF THE CARBON-OXYGEN BOND IN GUAIACOL.* Fuel, 1982. **61**(4): p. 377-382.

163. Vuori, A. and J.B. Bredenberg, *HYDROGENOLYSIS AND HYDROCRACKING OF THE CARBON-OXYGEN BOND .4. THERMAL AND CATALYTIC HYDROGENOLYSIS OF 4-PROPYLGUAIACOL.* Holzforschung, 1984. **38**(3): p. 133-140.

164. Vuori, A. and J.B. Bredenberg, *HYDROGENOLYSIS AND HYDROCRACKING OF THE CARBON-OXYGEN BOND .5. HYDROGENOLYSIS OF 4-PROPYLGUAIACOL BY SULFIDED COO-MOO3/GAMMA-AL2O3.* Holzforschung, 1984. **38**(5): p. 253-262.

165. Gutierrez, A., et al., *Hydrodeoxygenation of guaiacol on noble metal catalysts.* Catalysis Today, 2009. **147**(3-4): p. 239-246.

166. Viljava, T.R., R.S. Komulainen, and A.O.I. Krause, *Effect of H2S on the stability of CoMo/Al2O3 catalysts during hydrodeoxygenation.* Catalysis Today, 2000. **60**(1-2): p. 83-92.

167. Viljava, T.R., E.R.M. Saari, and A.O.I. Krause, *Simultaneous hydrodesulfurization and hydrodeoxygenation: interactions between mercapto and methoxy groups present in the same or in separate molecules.* Applied Catalysis a-General, 2001. **209**(1-2): p. 33-43.

168. Pinheiro, A., et al., *Impact of Oxygenated Compounds from Lignocellulosic Biomass Pyrolysis Oils on Gas Oil Hydrotreatment.* Energy & Fuels, 2009. **23**(1): p. 1007-1014.

169. Grenoble, D.C., *CHEMISTRY AND CATALYSIS OF THE TOLUENE HYDRODEALKYLATION REACTION .1. SPECIFIC ACTIVITIES AND SELECTIVITIES OF GROUP VIIB AND GROUP VIII METALS SUPPORTED ON ALUMINA.* Journal of Catalysis, 1979. **56**(1): p. 32-39.

170. Hong, D.Y., et al., *Hydrodeoxygenation and coupling of aqueous phenolics over bifunctional zeolite-supported metal catalysts.* Chemical Communications, 2010. **46**(7): p. 1038-1040.

171. Gayubo, A.G., et al., *Olefin Production by Catalytic Transformation of Crude Bio-Oil in a Two-Step Process.* Industrial & Engineering Chemistry Research, 2010. **49**(1): p. 123-131.

172. Ramires, E.C., et al., *Valorization of an Industrial Organosolv-Sugarcane Bagasse Lignin: Characterization and Use as a Matrix in Biobased Composites Reinforced With Sisal Fibers.* Biotechnology and Bioengineering, 2010. **107**(4): p. 612-621.

173. Valle, B., et al., *Selective Production of Aromatics by Crude Bio-oil Valorization with a Nickel-Modified HZSM-5 Zeolite Catalyst.* Energy & Fuels, 2010. **24**: p. 2060-2070.

174. Stocker, M., *Biofuels and Biomass-To-Liquid Fuels in the Biorefinery: Catalytic Conversion of Lignocellulosic Biomass using Porous Materials.* Angewandte Chemie-International Edition, 2008. **47**(48): p. 9200-9211.

175. Shin, E.J. and M.A. Keane, *Gas-phase hydrogenation/hydrogenolysis of phenol over supported nickel catalysts.* Industrial & Engineering Chemistry Research, 2000. **39**(4): p. 883-892.

176. Shin, E.J. and M.A. Keane, *Catalytic hydrogen treatment of aromatic alcohols.* Journal of Catalysis, 1998. **173**(2): p. 450-459.

177. *Cyclohexane (CX) Uses and Market Data*. 2010 [cited 2010 Oct. 29].

178. Hayase, S., et al., *Photopolymerization of cyclohexene oxide by the use of photodecomposable silyl peroxide - aluminum complex arylsilyl peroxide catalyst.* Macromolecules, 1986. **19**(4): p. 968-973.

179. Gal, Y.S., et al., *Polymerization of cyclohexene oxide by organoaluminum compounds.* Journal of Macromolecular Science-Pure and Applied Chemistry, 1993. **A30**(8): p. 531-540.

180. Fisher, W.B. and J.F. VanPeppen, *Cyclohexanol and Cyclohexanone*. Kirk-Othmer Encyclopedia of Chemical Technology. 2000: John Wiley & Sons, Inc.

181. Pina, G., C. Louis, and M.A. Keane, *Nickel particle size effects in catalytic hydrogenation and hydrodechlorination: phenolic transformations over nickel/silica.* Physical Chemistry Chemical Physics, 2003. **5**(9): p. 1924-1931.

182. Shin, E.J. and M.A. Keane, *Gas phase catalytic hydrodechlorination of chlorophenols using a supported nickel catalyst.* Applied Catalysis B-Environmental, 1998. **18**(3-4): p. 241-250.

183. Calvo, L., et al., *Hydrodechlorination of 4-chlorophenol in water with formic acid using a Pd/activated carbon catalyst.* Journal of Hazardous Materials, 2009. **161**(2-3): p. 842-847.

184. Minabe, M., et al., *HYDROGENATION OF 4-SUBSTITUTED BIPHENYLS.* Journal of Organic Chemistry, 1987. **52**(9): p. 1745-1748.

185. Molina, C.B., et al., *Pd-Al pillared clays as catalysts for the hydrodechlorination of 4-chlorophenol in aqueous phase.* Journal of Hazardous Materials, 2009. **172**(1): p. 214-223.

186. Yuan, G. and M.A. Keane, *Liquid phase catalytic hydrodechlorination of 2,4-dichlorophenol over carbon supported palladium: an evaluation of transport limitations.* Chemical Engineering Science, 2003. **58**(2): p. 257-267.

187. Zhao, C., et al., *Highly Selective Catalytic Conversion of Phenolic Bio-Oil to Alkanes.* Angewandte Chemie-International Edition, 2009. **48**(22): p. 3987-3990.

188. Zhao, C., et al., *Hydrodeoxygenation of bio-derived phenols to hydrocarbons using RANEY (R) Ni and Nafion/SiO2 catalysts.* Chemical Communications, 2010. **46**(3): p. 412-414.

189. Velu, S., et al., *Vapor phase hydrogenation of phenol over palladium supported on mesoporous CeO2 and ZrO2.* Applied Catalysis a-General, 2003. **245**(2): p. 317-331.

190. *Curent Primary and Scrap Metal Prices - London Metal Exchange*. 2011 [cited 2011 Jan. 24]; Available from: www.metalprices.com.

191. Mahata, N., et al., *Influence of the charge transfer capacity of alkali and alkaline earth metals as promoters in the hydrogenation of phenol over palladium and nickel catalysts.* Reaction Kinetics and Catalysis Letters, 2001. **72**(2): p. 297-302.

192. Lettow, J.S., et al., *Hexagonal to mesocellular foam phase transition in polymer-templated mesoporous silicas.* Langmuir, 2000. **16**(22): p. 8291-8295.

193. Liu, Y.M., et al., *Aluminum containing MCF silica as highly efficient solid acid catalyst for alcohol esterification.* Catalysis Letters, 2008. **125**(1-2): p. 62-68.

194. Ping, E.W., et al., *Highly dispersed palladium nanoparticles on ultra-porous silica mesocellular foam for the catalytic decarboxylation of stearic acid.* Microporous and Mesoporous Materials, 2010. **132**(1-2): p. 174-180.

195. Mile, B., et al., *TPR studies of the effects of preparation conditions on supported nickel catalysts.* Journal of Molecular Catalysis, 1990. **62**(2): p. 179-198.

196. Mile, B., et al., *THE LOCATION OF NICKEL-OXIDE AND NICKEL IN SILICA-SUPPORTED CATALYSTS - 2 FORMS OF NIO AND THE ASSIGNMENT OF TEMPERATURE-PROGRAMMED REDUCTION PROFILES.* Journal of Catalysis, 1988. **114**(2): p. 217-229.

197. Miguel-Garcia, I., et al., *H-2 assisted decomposition of cerium nitrate to ceria with enhanced catalytic properties.* Catalysis Communications, 2010. **11**(9): p. 848-852.

198. Marceau, E., et al., *Nickel(II) Nitrate vs. Acetate: Influence of the Precursor on the Structure and Reducibility of Ni/MCM-41 and Ni/Al-MCM-41 Catalysts.* Chemcatchem, 2010. **2**(4): p. 413-422.

199. Godelitsas, A., et al., *Characterisation of zeolitic materials with a HEU-type structure modified by transition metal elements: Definition of acid sites in nickel-loaded crystals in the light of experimental and quantum-chemical results.* Chemistry-a European Journal, 2001. **7**(17): p. 3705-3721.

200. Chen, J.X., et al., *An approach to preparing highly dispersed Ni2P/SiO2 catalyst.* Catalysis Communications, 2010. **11**(6): p. 571-575.

201. Tomiyama, S., et al., *Preparation of Ni/SiO2 catalyst with high thermal stability for CO2-reforming of CH4.* Applied Catalysis A: General, 2003. **241**(1-2): p. 349-361.

202. Burattin, P., M. Che, and C. Louis, *Characterization of the Ni(II) phase formed on silica upon deposition-precipitation.* Journal of Physical Chemistry B, 1997. **101**(36): p. 7060-7074.

203. Burattin, P., M. Che, and C. Louis, *Molecular approach to the mechanism of deposition - Precipitation of the Ni(II) phase on silica.* Journal of Physical Chemistry B, 1998. **102**(15): p. 2722-2732.

204. Boreave, A., A. Auroux, and C. Guimon, *Nature and strength of acid sites in HY zeolites: a multitechnical approach.* Microporous Materials, 1997. **11**(5-6): p. 275-291.

205. Topsoe, N.Y., K. Pedersen, and E.G. Derouane, *INFRARED AND TEMPERATURE-PROGRAMMED DESORPTION STUDY OF THE ACIDIC PROPERTIES OF ZSM-5-TYPE ZEOLITES.* Journal of Catalysis, 1981. **70**(1): p. 41-52.

206. Dussault, L., et al., *Influence of the metal nature (Ni, Cu, Mg) on the surface acid-base properties of mixed oxides elaborated from LDH.* Surface and Interface Analysis, 2006. **38**(4): p. 234-237.

207. Connell, G. and J.A. Dumesic, *THE GENERATION OF BRONSTED AND LEWIS ACID SITES ON THE SURFACE OF SILICA BY ADDITION OF DOPANT CATIONS.* Journal of Catalysis, 1987. **105**(2): p. 285-298.

208. Cardonamartinez, N. and J.A. Dumesic, *ACID STRENGTH OF SILICA-SUPPORTED OXIDE CATALYSTS STUDIED BY MICROCALORIMETRIC MEASUREMENTS OF PYRIDINE ADSORPTION.* Journal of Catalysis, 1991. **127**(2): p. 706-718.

209. Karthikeyan, D., et al., *Hydroisomerization of n-octane over bifunctional Ni-Pd/HY zeolite catalysts.* Industrial & Engineering Chemistry Research, 2008. **47**(17): p. 6538-6546.

210. Karthikeyan, D., et al., *Activity and selectivity for hydroisomerisation of n-decane over Ni impregnated Pd/H-mordenite catalysts.* Applied Catalysis a-General, 2008. **345**(1): p. 18-27.

211. Sagar, G.V., et al., *Dispersion and reactivity of copper catalysts supported on Al2O3-ZrO2.* Journal of Physical Chemistry B, 2006. **110**(28): p. 13881-13888.

212. Prinetto, F., et al., *Investigation of acid-base properties of catalysts obtained from layered double hydroxides.* Journal of Physical Chemistry B, 2000. **104**(47): p. 11117-11126.

213. Ennas, G., et al., *Sol-gel preparation and characterization of Ni-SiO2 nanocomposites.* Journal of Non-Crystalline Solids, 1998. **232**: p. 587-593.

214. Zheng, J., et al., *General and Facile Syntheses of Metal Silicate Porous Hollow Nanostructures.* Chemistry-an Asian Journal, 2010. **5**(6): p. 1439-1444.

215. Bezouhanova, C.P. and M.A. Alzihari, *CYCLOHEXANOL CONVERSION AS A TEST OF THE ACID-BASE PROPERTIES OF METAL-OXIDE CATALYSTS.* Catalysis Letters, 1991. **11**(2): p. 245-248.

216. Graca, I., et al., *Effect of phenol addition on the performances of H-Y zeolite during methylcyclohexane transformation.* Applied Catalysis a-General, 2009. **353**(1): p. 123-129.

217. Guisnet, M. and P. Magnoux, *FUNDAMENTAL DESCRIPTION OF DEACTIVATION AND REGENERATION OF ACID ZEOLITES*, in *Catalyst Deactivation 1994*, B. Delmon and G.F. Froment, Editors. 1994, Elsevier Science Publ B V: Amsterdam. p. 53-68.

218. Choudhary, V.R., et al., *Characterization of coke on H-gallosilicate (MFI) propane aromatization catalyst. Influence of coking conditions on nature and removal of coke.* Microporous and Mesoporous Materials, 1998. **21**(1-3): p. 91-101.

219. Sievers, C., et al., *Stages of aging and deactivation of zeolite LaX in isobutane/2-butene alkylation.* Journal of Catalysis, 2007. **246**(2): p. 315-324.

220. *London Metal Exchange Nickel Prices and News*. 2010 [cited 2010 Oct. 21]; Available from: http://www.metalprices.com/FreeSite/metals/nickelalloy/nickelalloy.asp.

221. *Platinum Prices London Metal Exchange*. 2010 Oct. 21]; Available from: http://www.metalprices.com/FreeSite/metals/pt/pt.asp.

222. Davis, M., et al., *National Hydrogen Energy Roadmap*. 2002, US Department of Energy: Washington.

223. Graça, I., et al., *Bio-oils and FCC feedstocks co-processing: Impact of phenolic molecules on FCC hydrocarbons transformation over MFI.* Fuel, 2011. **90**(2): p. 467-476.

224. Castano, P., et al., *Effect of the support on the kinetic and deactivation performance of Pt/support catalysts during coupled hydrogenation and ring-opening of pyrolysis gasoline.* Applied Catalysis a-General, 2007. **333**(2): p. 161-171.

225. Ovalles, C., et al., *Upgrading of extra-heavy crude oil by direct use of methane in the presence of water. Deuterium-labeled experiments and mechanistic considerations.* Fuel, 1995. **74**(Copyright (C) 2011 American Chemical Society (ACS). All Rights Reserved.): p. 1162-8.

226. Wei, J.M. and E. Iglesia, *Mechanism and site requirements for activation and chemical conversion of methane on supported Pt clusters and turnover rate comparisons among noble metals.* Journal of Physical Chemistry B, 2004. **108**(13): p. 4094-4103.

227. Wei, J.M. and E. Iglesia, *Isotopic and kinetic assessment of the mechanism of methane reforming and decomposition reactions on supported iridium catalysts.* Physical Chemistry Chemical Physics, 2004. **6**(13): p. 3754-3759.

228. Yamaguchi, A. and E. Iglesia, *Catalytic activation and reforming of methane on supported palladium clusters.* Journal of Catalysis, 2010. **274**(1): p. 52-63.